# CASPASE ISOFORMS IN INFLAMMASOME ACTIVATION

Zsofia Digby

Newnham College

Department of Veterinary Medicine

University of Cambridge

This dissertation is submitted for the degree of Doctor of Philosophy

February 2020

## Declaration and Statement of length

This thesis is the result of my own work and includes nothing which is the outcome of work done in collaboration except as declared in the Preface and specified in the text. It is not substantially the same as any that I have submitted, or, is being concurrently submitted for a degree or diploma or other qualification at the University of Cambridge or any other University or similar institution except as declared in the Preface and specified in the text. I further state that no substantial part of my thesis has already been submitted, or, is being concurrently submitted for any such degree, diploma or other qualification at the University of Cambridge or any other University or similar institution except as declared in the Preface and specified in the text. It does not exceed the prescribed word limit for the relevant Degree Committee.

This thesis does not exceed the word limit of 60,000 words (excluding tables, photographs, appendices and bibliography) set by the Degree Committee for the Faculties of Clinical Medicine and Veterinary Medicine.

**Zsofia Digby**

**February 2020**

**CASPASE ISOFORMS IN INFLAMMASOME FORMATION**

**Zsofia Digby**

## Summary

Inflammasomes are macromolecular signalling platforms composed of a receptor (for example NLRP3 or NLRC4), an adaptor (ASC) and effectors (caspases) that are thought to play critical roles in the host defence against microbial infections. Activation of inflammasomes leads to the processing of the pro-inflammatory cytokines pro-IL-1β and pro- IL-18 to their active form and cleavage of gasdermin D to induce pyroptosis. Caspase-1 is the main inflammatory caspase responsible for cytokine maturation and induction of cell death, while human caspase-4, -5 and the mouse orthologue caspase-11 play an essential role in cytosolic bacterial LPS recognition. The putative importance of inflammasomes suggest that their constituents should be conserved across different animal species, but there are major differences, particularly in the caspase repertoire, in both invertebrates and vertebrates. The dog (*Canis lupus familiaris*), for example, has a pseudogene for *NLRC4* and has a unique caspase-1/4/11 hybrid gene (CASP1-4/5/11) comprising the caspase-1 caspase recruitment domain (CARD) and the catalytic domain of caspase-4/5/11. Dogs produce bioactive IL-1β despite the apparent lack of the catalytically active domain of caspase-1, but how this occurs and whether inflammasome activation of CASP1-4/5/11 is required remains to be resolved.

In this study I characterised inflammasome function in dog macrophages (DH82 cell line) and mouse macrophages where a caspase 1/4/11 fusion protein that is functional equivalent to CASP1-4/5/11 (DogMo) had been generated by CRISPR/Cas9 gene editing. I used imaging (ASC and active caspase speck formation), cell death analysis and IL-β production as readouts before and after editing of key genes in inflammasome formation using CRISPR-Cas9 gene editing approaches.

The NLRP3 inflammasome is functional in dog macrophages, but the rate of inflammasome formation is lower compared to wild-type murine macrophages. This suggests that dog macrophages may be adapted to be tolerant to NLRP3 inflammasome activation only undergoing lytic cell death and IL-1β maturation when exposed to high concentrations of NLRP3 inflammasome activating ligands. DogMo cells retained full NLRP3 functionality.

Cytosolic LPS-induced non-canonical inflammasome activation induced IL-1β maturation and secretion without concomitant cell death induction in dog macrophages. No ASC speck formation or activated caspase speck was seen suggesting there are alternative pathways for cytosolic LPS recognition and the consequential IL-1β maturation. DogMo cells did not induce non-canonical inflammasome formation.

The NLRC4 inflammasome should not function in the dog and indeed DH82 cells infected with wild-type *S*. Typhimurium showed no ASC speck formation or active caspase recruitment and delayed cell death (compared to their wild-type mouse counterpart), but cleaved IL-1β was present in the supernatant. The processed IL-1β was smaller than the p17 fragment normally associated with cleavage by caspase-1. DogMo cells, which express NLRC4, did not process IL-1β as expected due to the lack of the catalytic domain of caspase-1 but still induced cell death albeit at a reduced level to wild-type mouse macrophages.

*S*. Typhimurium infection of CRISPR/Cas9 gene edited DH82 cells to remove CASP1-4/5/11 showed that cell death was independent of this caspase. Collectively, these data indicate that in dog cells processing of pro-IL-1β and cell death occurs by inflammasome-independent pathways. CRISPR/Cas9 gene editing of DH82 cells to remove the necroptotic cell death initiator RIP kinase 1 and apoptotic cell death initiator caspase-8 genes identified an essential role for RIPK1 in pro-IL-1β priming, and potentially, for caspase-8 in IL-1β maturation.

The characterisation of caspase functionality in dog and DogMo cells show marked differences despite their expression of a similar protein. The deficit in inflammasome functionality in the dog could point to an evolutionary adaptation to tolerate microorganisms associated with their lifestyle as an opportunistic scavenger to protect them against severe enteric infections from gut bacterial pathogens.

## Acknowledgments

First, I would like to thank Professor Clare Bryant for the opportunity to pursue my postdoctoral studies in her laboratory. I am grateful for her support and encouragement throughout the last three years. I would also like to thank all my colleagues for their help and support, especially, Dr. Panagiotis Tourlomousis, Dr. Steven Webster and most importantly Dr. Lee Hopkins who has been my mentor, dear friend, counsellor and personal entertainer throughout these years. I would also like to thank my peers for their scientific, never ending emotional support and friendship: Dr. Charlotte Macleod, Dr. Sam Katz, Dr. Milton Pereira, Rhiannon Wood, Myrto Vlazaki and Daniel Buhl.

I would like to thank Dr. Jonathan Powell and his group for their extensive collaboration. Particularly Dr. Rachel Hewitt for her scientific support, friendship and encouragement.

I am grateful to the Medical Research Council (MRC) for their financial support which made pursuing my postdoctoral studies possible.

At last, but not least, I am grateful to every member of the Department of Veterinary Medicine for creating such a fantastic, friendly and supporting environment. I have met some amazing people along the way.

I will be forever indebted to my parents who have supported me throughout my life. A very special thank you to my husband James who has been by my side during all the ups and downs of the last three years. Without his love and encouragement this PhD work would not have been possible. At last, I am grateful to all my friends and family, two and four legged, for their love and support.

# Table of Contents

## List of Abbreviations

| | |
|---|---|
| $AAA^+$ | ATPases associated with diverse cellular activities |
| AIM2 | Absence in melanoma 2 |
| ALR | AIM2-like receptor |
| ASC | Apoptosis-associated speck-like protein |
| Bid | BH3 interacting-domain death agonist |
| BIR | Baculovirus inhibitor repeats |
| BLAST | Basic local alignment search tool |
| BRCC3 | BRCA1/BRCA2-Containing Complex Subunit 3 |
| BSA | Bovine serum albumin |
| BTK | Bruton tyrosine kinase |
| CAPS | Cryopyrin-associated periodic syndrome |
| CARD | Caspase activation and recruitment domain |
| Cas1 | CRISPR-associated endonuclease 1 |
| CCP | Cambridge centre for proteomics |
| CED3 | Nematode cell death protein 3 |
| CFUs | Colony forming units |
| CIITA | MHC-II transactivator |
| CL | Cardiolipin |
| CLR | C-type lectin receptor |
| Cns2 | Conserved non-coding DNA sequences |
| CRISPR | Clustered regularly interspaced short palindromic repeats |
| crRNA | CRISPR RNA |
| DAMP | Damage-associated molecular pattern |
| DD | Death-fold domain |
| DED | Death-effector domain |
| DMEM | Dulbecco's modified eagle medium |
| DogMo | Dog-mouse |
| DPBS | Dulbecco's phosphate buffered saline |

| | |
|---|---|
| DSB | Double-stranded DNA break |
| ECL | Enhanced chemiluminescence |
| ENU | ethyl-N-nitrosourea |
| EST | Expressed sequence tag |
| FADD | FAS-associated death domain protein |
| FasL | Fas ligand |
| FCS | Foetal calf serum |
| FSC | Forward scatter |
| GBPs | Guanylate-binding proteins |
| GFP | Green fluorescent protein |
| GPA | Gentamicin protection assay |
| GSDM | Gasdermin |
| GSDMD | Gasdermin D |
| HDR | Homology-directed repair |
| HET-E | Plant het gene product involved in vegetative incompatibility |
| HIM | Homotypic interaction motif |
| HMGB1 | High mobility group box 1 |
| iBMDMs | Immortalised bone marrow-derived macrophages |
| ICE | IL-1-converting enzyme |
| ID | Intermediate domain |
| IECs | Intestinal epithelial cells |
| IFI16 | Gamma-interferon-inducible protein 16 |
| IKK | Iκβ kinase |
| IRAK1/4 | IL-1 receptor-associated kinase 1 and 4 |
| IRF3 | Interferon regulatory factor 3 |
| IRG | Immunity-related GTPase family member |
| KD | N-terminal kinase domain |
| LDH | Lactate dehydrogenase |
| LPS | Lipopolysaccharide |
| LRR | Leucine-rich repeats |
| LRRK2 | Leucine-rich repeat kinase 2 |

| | |
|---|---|
| Mal | MyD88 adaptor-like |
| MAPK | Mitogen-activated protein kinase |
| MDCK | Madin-darby canine kidney |
| MHCII | Major histocompatibility complex class II |
| MLKL | Mixed lineage kinase domain like pseudokinase |
| MNC | Mononuclear cell |
| MOI | Multiplicity of infection |
| MOMP | Mitochondrial outer membrane permeabilization |
| MUSCLE | Multiple sequence comparison by log-expectation |
| MyD88 | Myeloid differentiation primary response 88 |
| NAD | NACHT-associated domain |
| NADPH | Nicotinamide adenine dinucleotide phosphate-oxidase |
| NAIP | Neuronal apoptosis inhibitor protein |
| NBD | Nucleotide-binding domain |
| NF-κβ | Nuclear factor kappa-light-chain-enhancer of activated B cells |
| NGS | Normal goat serum |
| NIMA | Never in mitosis A |
| NLR | NOD-like receptor |
| NLRC4 | NAIP/nod-like receptor family caspase-activating and recruitment domain containing 4 |
| NLRP1 | Nuclotide-binding oligomerization domain, leucine rich repeat and pyrin domain containing protein 11 |
| NOD2 | Nucleotide-binding oligomerisation domain containing protein 2 |
| NS | Non-stimulated |
| OD | Optical density |
| OMV | Outer-membrane vesicles |
| PAM | Protospacer adjacent motif |
| PAMPs | Pathogen-associated molecular patterns |
| PBMCs | Peripheral blood mononuclear cells |
| PCV | Pathogen-containing vesicles |
| PFA | Paraformaldehyde |

| | |
|---|---|
| PJVK | Pejvakin |
| PKA | Protein kinase A |
| PKCδ | Protein kinase C delta |
| PR-3 | Proteinase-3 |
| Pro-IL-1β | Pro-interleukin 1β |
| PRR | Pathogen recognition receptor |
| PSSM | Position-specific scoring matrix |
| PTC | Pre-mature termination codon |
| PYD | Pyrin domain |
| PYK2 | Protein-tyrosine kinase 2 |
| RIP | Receptor interacting protein |
| RIPK3 | Receptor-interacting serine/threonine-protein kinase 3 |
| RLR | RIG-like receptor |
| RNP | Ribonucleoprotein |
| RT-PCR | Reverse transcriptase – polymerase chain reaction |
| SCV | *Salmonella*-containing vacuole |
| SEM | Standard error of means |
| Sip | *Salmonella* invasion protein |
| SPI | *Salmonella* pathogenicity island |
| SSC | Side scatter |
| STAND | Signal transduction ATPases with numerous domains |
| STAT | Signal transducer and activator of transcription |
| SYK | Spleen tyrosine kinase |
| T3SS | Type III secretion system |
| TAK1 | Transforming growth factor beta-activated kinase 1 (Tak1) |
| tBLASTn | Translated basic local alignment search tool nucleotide |
| TIR | Toll/interleukin-1 receptor |
| TLR | Toll-like receptor |
| TNF | Tumour necrosis factor |
| TNFR | Tumour necrosis factor receptor |
| TP-1 | Telomerase-associated protein 1 |

| | |
|---|---|
| tracrRNA | Trans-activating CRISPR RNA |
| TRADD | Tumour necrosis factor receptor type 1-associated death domain |
| TRAM | TRIF-related adaptor molecule |
| TRAPS | TNFR1 causing receptor-associated periodic syndrome |
| TRIF | TIR-domain-containing adapter-inducing interferon-β |
| TUNEL | Terminal deoxynucleotidyl transferase dUTP nick end labelling |

## List of Figures

## List of Tables

## List of Appendices

# Chapter 1.
# Introduction

## 1.1 Innate Immunity

Pathogenic microorganisms including bacteria, fungi, viruses and protozoans are capable of causing infection which can be detrimental to the host. To counteract this microbial threat, host species have evolved immune systems that function in the prevention and clearance of infection. In vertebrates, the immune system is comprised of both the innate and adaptive arms which provide non-specific and specific immunity to pathogens, respectively. In comparison, invertebrates and jawless fish are solely reliant on their innate immune system to combat infection. The innate arm provides rapid but non-clonal responses which are conserved in nature. Innate immunity effectively serves as a first line of defence and responds to pathogens and changes in cellular homeostasis to initiate responses in order to resolve infection and repair tissue damage. Moreover, innate immune responses (e.g. antigen presentation, cytokine release) are also required for the development of the adaptive immune response (e.g. B and T cell activation). The existence of an innate immune memory termed "trained immunity", has been proposed through transcriptional and epigenetic reprogramming of innate immune cells [1], [2]

## 1.2 Pattern Recognition Receptors

Innate immune responses are principally mediated via a group of germ-line encoded proteins called pattern recognition receptors (PRRs) which are able to detect both evolutionarily conserved structures associated with microorganisms termed pathogen associated molecular patterns (PAMPs) and host-derived endogenous ligands. PRRs can be found across the animal kingdom ranging from primitive organisms to higher vertebrates [3]. The concept of PRRs in innate immunity was first introduced by Charles Janeway [4]. This was proceeded by the discovery of the first innate signalling receptor (Toll) in *Drosophila Melanogaster* which was shown to be activated by the endogenous cytokine Spätzle, that is generated in response to microbial pathogens [3]. There is a large variation in the PRR repertoire found in different vertebrate species which

may have arisen as the consequence of differences in evolutionary pressures imparted during the development of the innate immune system.

PRRs can be conveniently divided into five distinct classes (Figure 1.2.1) based on their function, ligand specificity and cellular localisation [4], [5]. PRRs are expressed in a variety of immune cell sub-sets including macrophages, dendritic cells, monocytes, neutrophils and also non-immune cell types e.g. epithelial cells and fibroblasts [6]. Activated PRRs can induce signalling cascades resulting in pro-inflammatory responses which aim to eliminate invading pathogens and restore cellular homeostasis [7]. These cellular events include the production of a plethora of different cytokines and chemokines, as well as the induction of various forms of cell death [8]. Cytokine induced cell signalling can initiate particular responses following receptor binding on target cells in an autocrine, paracrine or endocrine fashion. The inflammatory roles afforded to cytokines include enhancing agent specific immune activation, memory development and the recruitment of other immune cell types (e.g. neutrophils) to ameliorate infection.

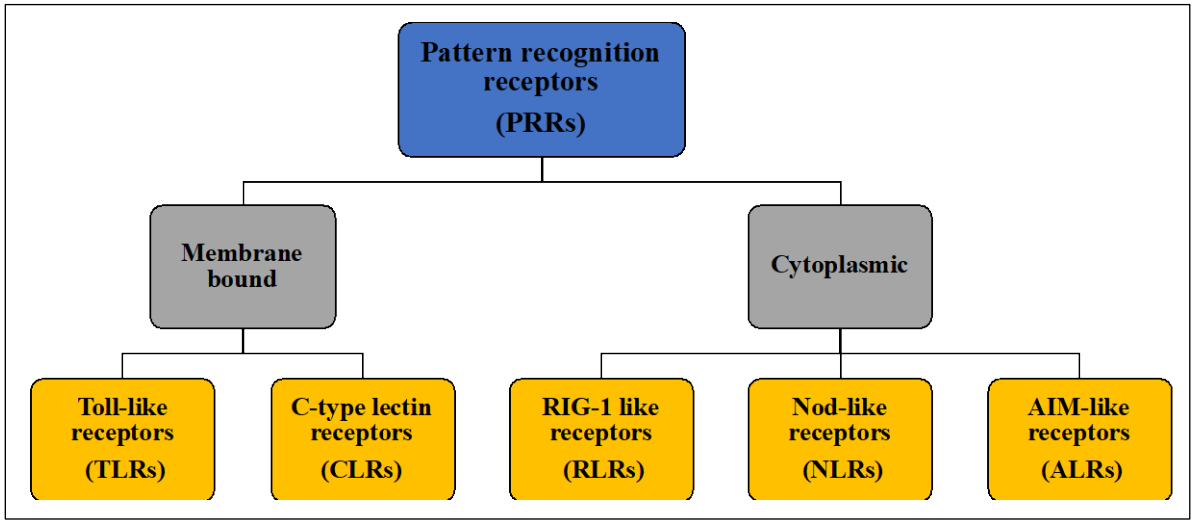


**Figure 1.2.1 Five distinct classes of PRRs.** PRRs comprise the Toll-like receptors (TLRs), C-type lectin receptors (CLRs), RIG-like receptors (RLRs), NOD-like receptors (NLRs), absent in melanoma 2 (AIM2)-like receptors (ALRs).

### 1.2.1 Toll-like Receptors

Toll-like receptors (TLRs) represent a family of transmembrane glycoproteins which sense invading pathogens through recognition of PAMPS. They also play a role in the detection of endogenous (host-derived) damage associated molecular patterns (DAMPs). To date, humans contain ten (TLR1-10), dogs contain nine functional TLRs (TLR1, 3-10) whereas mice express a complement of twelve (TLR1-9, 11-13) [9], [10]. Little is known however, about the effect of differences in TLRs on canine specific pathogen recognition and their associated downstream signalling pathways [11]. For example, dogs possess TLR2, -11 and -12 as pseudogenes, where the former is positioned upstream in tandem with its functional counterpart [9], while the canine TLR4 receptor is predicted to lack a transmembrane region [12].

TLR structure and function are highly conserved across the animal kingdom. They are expressed in both, immune (monocytes, dendritic cells, macrophages) and non-immune cells (fibroblasts, endothelial cells and epithelial cells). Human TLR1, -2, -4, -5, -6, -10 and -11 are expressed in the plasma membrane, while TLR3, -7, -8 and -9 are expressed in endosomal membranes. TLRs comprise a tripartite structure: an N-terminal leucine-rich repeat domain involved in ligand-sensing, a transmembrane spanning region and a cytoplasmic Toll/IL-1R (TIR) domain [13]. TIR domain homologues are found in plants which confer resistance against pathogens in plants [10]. Ligand binding results in the dimerization/stabilisation of pre-formed dimers of TLRs, leading to TIR domain interactions and the recruitment of compatible adaptor proteins; myeloid differentiation primary response 88 (MyD88), TIR-domain-containing adapter-inducing interferon-β (TRIF), MyD88 adaptor-like (Mal) or TRIF-related adaptor molecule (TRAM) [14], [15]. Activated TLRs promote transcription of pro-inflammatory receptors and cytokines via downstream signalling pathways mediated by their adaptor proteins. TLR1-2, 5-11 preferentially signal through MyD88/Mal adaptors activating nuclear factor kappa-light-chain-enhancer of activated B cells (NF-κβ) and interferon regulatory factor 3 (IRF3) transcriptions factors resulting in inflammatory gene transcription [16], [17]. TLR4 can signal via all adaptor proteins (MyD88/Mal/TRIF/TRAM) whilst TLR3 signals through adaptor TRIF activating the NF-κβ transcription factor and mitogen-activated protein kinases (MAPK) [16], [17]. Toll-like receptors exhibit high ligand specificity (Table 2.1.1). For example, TLR1 recognises triacyl lipoproteins

[18], TLR2 recognises peptidoglycans and signals in heterodimers with either TLR1 or TLR6 [19], while TLR4 recognises bacterial LPS [20]. Collectively, TLRs are crucial for host defence against a broad spectrum of pathogenic agents, while their inappropriate activation can lead to chronic inflammatory and auto-inflammatory disease in humans [21]. Thus far, efforts to link TLRs and auto-inflammatory phenotypes in other species, for example dogs, has proven controversial [22], [23].

| Toll-like receptor (TLR) | Ligand | Species |
|---|---|---|
| TLR1 | Triacylated lipoproteins | human, mouse |
| TLR2 | Triacylated lipoproteins | human, mouse |
| TLR3 | dsRNA | human, mouse |
| TLR4 | LPS | human, mouse |
| TLR5 | Bacterial flagellin | human, mouse |
| TLR6 | Diacetylated lipoproteins | human, mouse |
| TLR7 | Viral ssRNA | human, mouse |
| TLR8 | Viral ssRNA | human, mouse |
| TLR9 | Non-methylated CpG DNA motifs | human, mouse |
| TLR10 | Unknown | human |
| TLR11 | Bacterial flagellin | mouse |
| TLR12 | Unknown | mouse |
| TLR13 | Unknown | mouse |

**Table 1.2.1.1 List of functional Toll-like receptors (TLRs) found in humans and mice and their cognate ligands.**

### 1.2.2 Nod-like Receptors

The identification of plant R-genes responsible for species-specific resistance against plant pathogens [24], [25] and their subsequent sequence homology studies in humans led to the discovery of the first NLR protein [26]. As a group, the NLRs are members of the ATPases associated with diverse cellular activities ($AAA^+$) or signal transduction ATPases with numerous

domains (STAND) family [27]. NLRs provide an essential function in the recognition of intracellular pathogens and their consequent cellular disturbances [28]–[30]. NLRs are cytosolic proteins [31] which can be conveniently divided into four subfamilies based on the structure of their variable N-terminal region (Figure 1.2.2.1) [32]. Genes encoding NLR proteins appeared early in evolution as shown by the presence of NLR precursors in basal metazoans, such as sea urchins however, they are absent in nematodes and insects [33], [34]. NLR proteins typically comprise of three distinct domains: The N-terminal effector domain consists of either PYRIN (PYD), caspase activation and recruitment (CARD) or baculovirus inhibitor repeats (BIR). Their central nucleotide-binding domains (NBD), which can contain either NACHT (domain present in neuronal apoptosis inhibitor protein [NAIP], CIITA (major histocompatibility complex class II (MHC-II) transactivator), HET-E (plant het gene product involved in vegetative incompatibility), TP-1 (telomerase-associated protein 1) or NACHT-associated domain (NAD) [35]. NBD have been associated with functions including the regulation of signal transduction, but are also known to form homo- and heterotypic protein interactions [36]. These interactions mediate ATP-dependent proximity-induced self-oligomerisation which is essential for their activation and initiation of downstream signalling events [27]. The C-terminal domain consisting of leucine-rich repeats (LRRs) can play a role in ligand binding [6], [36].

To date, there are over 22 NLRs found in humans and 34 described in mice [6]. Although they are highly conserved among eukaryotic species, comparative genome studies have revealed several species-specific differences in NLR repertoires. For example, nucleotide-binding oligomerization domain, leucine rich repeat and pyrin domain containing protein 11 (NLRP11) appears to be primate specific [37], murine NAIPs have undergone expansion [38], NLRP4 is primate and rodent specific, while NLRP8 and -13 have been lost in rodents [37]. Zebrafish NLRs have undergone a large expansion and contain over 400 members within the family with some members being unique to teleost fish [39], [40]. Dogs lack *NAIP* genes and their *NLRC4* gene exists as a pseudogene [41]. There exists little evidence to explain how these species-specific differences have shaped the NLR-mediated innate immune responses to infection.

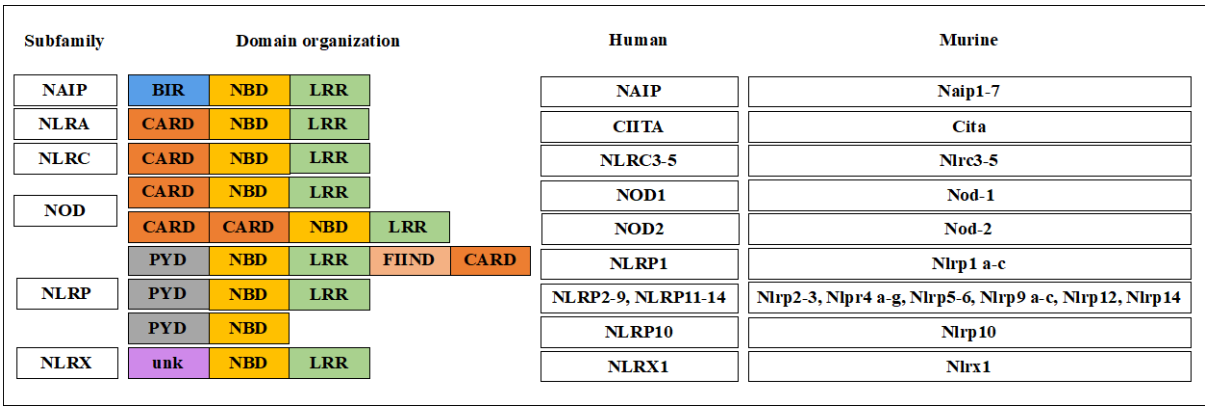


**Figure 1.2.2.1 NLR family members and their domain organisation.** Structurally NLRs comprise a variable amino-terminal death-fold domain (DD), caspase activation and recruitment domain (CARD), pyrin domain (PYD), baculovirus inhibitor repeats (BIRs), central nucleotide-binding domain (NBD) and a carboxyl-terminal leucine-rich repeat domains (LRRs).

An important consequence of NLR-mediated cytosolic recognition of PAMPs and DAMPs is the assembly of a cytosolic macromolecular protein complex called the inflammasome.

### 1.2.3 Inflammasomes

Inflammasomes act as a platform for inflammatory caspase activation leading to the processing of inflammatory cytokines pro-interleukin-1β (pro-IL-1β) and pro-IL-18 into their active forms through direct cleavage [42]. An additional consequence of inflammasome assembly is the induction of pyroptotic cell death and the release of the processed cytokines via the cleavage and activation of executioner protein Gasdermin D (GSDMD) which forms pores in membranes [43], [44].

The term inflammasome was first introduced in a study from 2002 which described the interaction of NLR's with the apoptosis-associated speck-like protein (ASC) via their PYD-PYD domains, which in turn facilitates recruitment of caspase-1 to ASC via a CARD-CARD interaction [42]. Upon sensing PAMPs and DAMPs, certain PRRs including NLRP3 [45], NAIP/nod-like receptor family caspase-activating and recruitment domain containing 4 (NLRC4) [46], hematopoietic expression interferon-inducible nature nuclear localization (HIN-200); absent in melanoma-2

(AIM-2) [47], PYRIN [48] and gamma-interferon-inducible protein 16 (IFI16) [49] oligomerize to form inflammasomes. Other NLRs, including human NLRP2 [50], NLRP7 [51] and mouse NLRP6 [52], NLRP9b [53] and NLRP12 [54] have also been proposed to form inflammasomes, although this has yet to be fully confirmed experimentally.

ASC, contains both a PYD and CARD domain and is essential for PYD containing receptors that do not comprise a CARD domain (e.g. NLRP3) to recruit caspase-1, while CARD containing receptors e.g. NLRC4 can recruit and activate pro-caspase-1 via homotypic interaction [55]. ASC activation and recruitment to the receptors induces oligomerisation of the ASC monomers [56] and has been shown to facilitate downstream signalling in response to PYD and also CARD containing receptor activation [57]. Condensed ASC effectively serves as a bridge between NLRs and the effector caspase proteins [57], [58]. There are species-specific differences with regards inflammasome composition which form part of the subject of this thesis.

Inflammasomes have been classified as either canonical or non-canonical. Assembly of a canonical inflammasome (Figure 1.2.3.1) results in caspase-1 activation [59], whereas non-canonical inflammasome formation (Figure 1.2.3.2) is mediated by caspase-11 in mice [60] and caspase-4, -5 in humans [61].

Depending on the type of insult, more than one NLR can be activated within a single cell forming an inflammasome which can contain the multiple NLRs and caspases [62]. After the assembly of the receptor complex, recruited ASC oligomerizes via the PYD domains forming a filamentous scaffold [58], [63]. Analysis of electron micrographs of purified NAIP5-NLRC4 inflammasomes from HEK293E cells showed that inflammasomes adopt an open wheel like structure displaying 11-12 spokes on their surface [64], [65]. ASC CARD domains remain exposed on the surface [63], which can then interact with pro-caspase-1 via CARD-CARD interactions. The ASC oligomeric complex [66] cluster can be visualised as a discrete cytoplasmic ASC speck [67], [68] with a diameter of approximately 1 micron. These protein-protein interactions result in the assembly of a platform where pro-caspase-1 can be recruited, leading to proximity induced dimerization and activation [58], which in turn leads to the processing and maturation of caspase-1 substrates.

GSDMD is a recently described human caspase-1/-4/-5 and mouse caspase-1/-11 protein substrate [43], [44]. GSDMD protein is highly conserved in mammals and is comprised of approximately 480 amino acids [69]. Following inflammatory caspase activation, GSDMD is cleaved into N- and C-terminal fragments. The N-terminal domain of approximately 30 kDa [43] binds with high affinity to phosphatidylserines and cardiolipins [70] of the plasma membrane causing pore formation which facilitates pro-inflammatory cytokine release and pyroptotic cell death [71]–[73]. Cleavage of the GSDMD linker region by human caspase-4 and -5 was also shown in mouse BMDMs [44]. Pores formed in the cell membrane by GSDMD-N fragment have a ring like structure [74] with an approx. 10-14nm inner diameter and comprises 16 symmetric protomers [75].

Inflammasome activation and formation is a tightly regulated process, however, gain of function or loss of function mutations in inflammasome genes can lead to inappropriate inflammasome activation. Dysregulated inflammatory responses can then lead to the development of auto-inflammatory or autoimmune diseases. Some of the many auto-inflammatory diseases include gain-of-function mutations in the NLRP3 gene causing cryopyrin-associated periodic syndrome (CAPS) [76] or in the NOD2 receptor causing Blau syndrome [77].

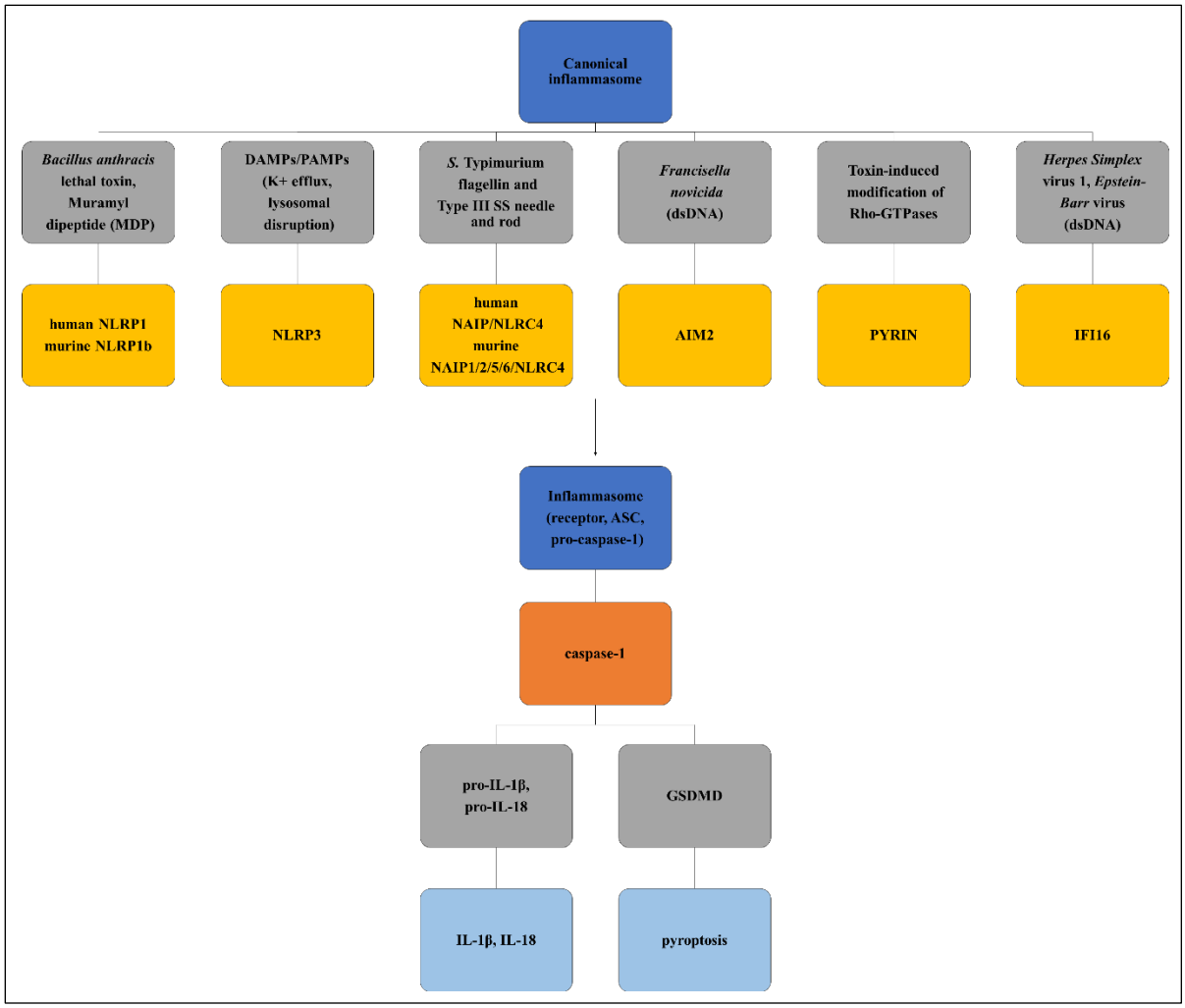


**Figure 1.2.3.1 A subset of PRRs can form canonical inflammasomes.** PRR activation upon ligand recognition promotes the recruitment of the adaptor protein ASC. Polymerised ASC acts as a scaffold facilitating the recruitment of pro-inflammatory caspase-1 to the inflammasome. Activated caspase-1 cleaves inflammatory cytokines pro-IL-1β and pro-IL-18 into their active forms. It also drives pyroptotic cell death by cleavage of GSDMD.

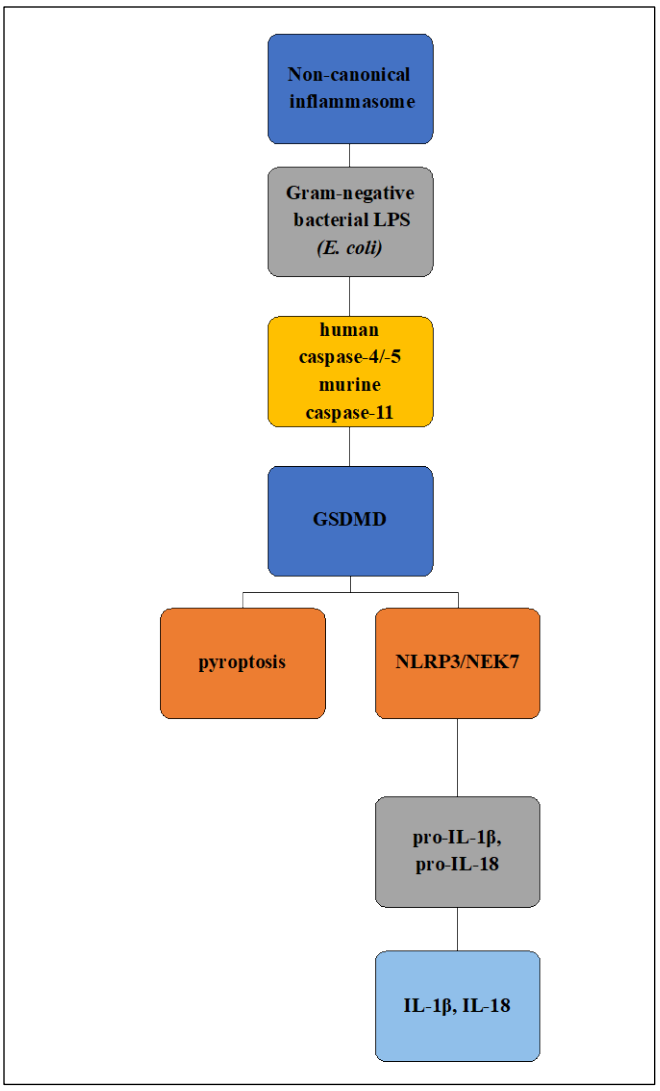


**Figure 1.2.3.2 Schematic of non-canonical inflammasome formation mediated by human caspase-4, -5 and its murine homologue caspase-11.** Gram-negative bacterial LPS is directly recognised by human caspase-4, -5 and murine caspase-11. This results in their oligomerisation, subsequent activation and non-canonical inflammasome formation. Caspase-4/5/11 cleaves GSDMD which in turn drives pyroptotic cell death. GSDMD cleavage subsequently activates non-canonical NLRP3 inflammasome activation driving the maturation of inflammatory cytokines.

### 1.2.4 NLRP3

NLRP3, also known as cryopyrin or NALP3, was first shown to be activated in response to ATP and bacterial toxins (nigericin and maitotoxin) and that it also assembles into an inflammasome following its activation [78]. The NLRP3 inflammasome is the most well studied and different activation mechanisms have been proposed to explain the molecular events that underly its assembly. It has been proposed that NLRP3 acts as a general sensor for perturbations in cell homeostasis [79], [80]. These include increase in intracellular calcium [81] and reduction in levels of intracellular potassium [82]. Moreover, increase of extracellular potassium and the inhibition of potassium efflux [83] has been shown to inhibit NLRP3 inflammasome formation. Activating signals also include extracellular ATP [82], uric acid crystals [84], bacterial pore forming toxins [82], [85], Gram-positive (e.g. *Staphylococcus* aureus) [86] and Gram-negative bacteria (e.g. *S.* Typhimurium) [62], [87], viruses [88], fungal [89] and protozoan infections [90]. These activators can induce mitochondrial membrane disruption [82], lysosomal rupture [91], cathepsin B release [92], mitochondrial-associated dysfunction [93], cardiolipin translocation of the mitochondria [94] and oxidised mitochondrial DNA release [95]. Despite the expression of NLRP3 in many other species, its' precise function and importance in controlling pathogenesis remains not fully understood. Recent research investigating the role of NLRP3 in other species suggests similar roles to that observed in humans and mice. For example, NLRP3 was shown *in vitro* to play an important role in swine PBMCs response to classical swine fever virus [96] and *in vivo* in Cherry Valley Duck immune responses to challenge with avian pathogenic *E. coli* [97].

The sequence of events leading to the activation of the canonical NLRP3 inflammasome (Figure 1.2.4.1) consists of two distinct stages [98]. The first step involves ligand priming of the TLR, when TLRs via the MyD88 pathway [99], nucleotide-binding oligomerisation domain containing protein 2 (NOD2) or TNFR1/2 activation [100] induces NF-κB transcription factor [98] and MAPK activation [101], resulting in the upregulation of NLRP3 and pro-IL-1β expression. Schroder *et al*. suggested that the priming step also induces post-translational modifications in NLRP3 receptors, as a short-period of pre-incubation with LPS did not alter NLRP3 expression levels, but did augment inflammasome activation [102]. The second, activation step is initiated upon NLR ligand binding in an ATP-dependent manner, which is followed by NLRP3-oligomerisation and ASC recruitment. Several molecules have been shown to regulate the transcriptional and translational induction and modification of the NLRP3 receptor.

BRCA1/BRCA2-Containing Complex Subunit 3 (BRCC3) mediated deubiquitylation of NLRP3 has been suggested to be preconditional to NLRP3 inflammasome activation [103]. Among others, FAS-associated death domain protein (FADD) and caspase-8 have been shown to regulate priming and induction of NLRP3 expression [104], whilst MyD88, IL-1 receptor-associated kinase 1 and 4 (IRAK1/4) and TRIF regulate transcriptional and post-transcriptional NLRP3 induction and activation [105], [106]. The role of never in mitosis A (NIMA)-related kinase family member NEK7 as an NLRP3 inflammasome regulator has been reported in three independent studies [107]–[109]. The NEK7 catalytic domain has been shown to directly bind the LRR domain of NLRP3 to control NLRP3 oligomerization, and subsequent ASC-speck formation and caspase-1 activation [107], [108]. Additional post-translational modifications by spleen tyrosine kinase (SYK) [110], protein-tyrosine kinase 2 (PYK2) [111] and bruton tyrosine kinase (BTK) [112] were shown to positively regulate NLRP3 inflammasome formation. In contrast, phosphorylation by protein kinase A (PKA) [113], nitrosylation [114] and autophagy [115] appear to negatively regulate the NLRP3 inflammasome. Although, NLRP3 was first discovered as the underlying driver in the pathogenesis of familial cold auto-inflammatory and Muckle-Wells syndromes [76], its role in excessive inflammation has been linked to numerous other inflammatory diseases including gout [116], diabetes [117], cancer [118], atherosclerosis [119] and arthritis [120].

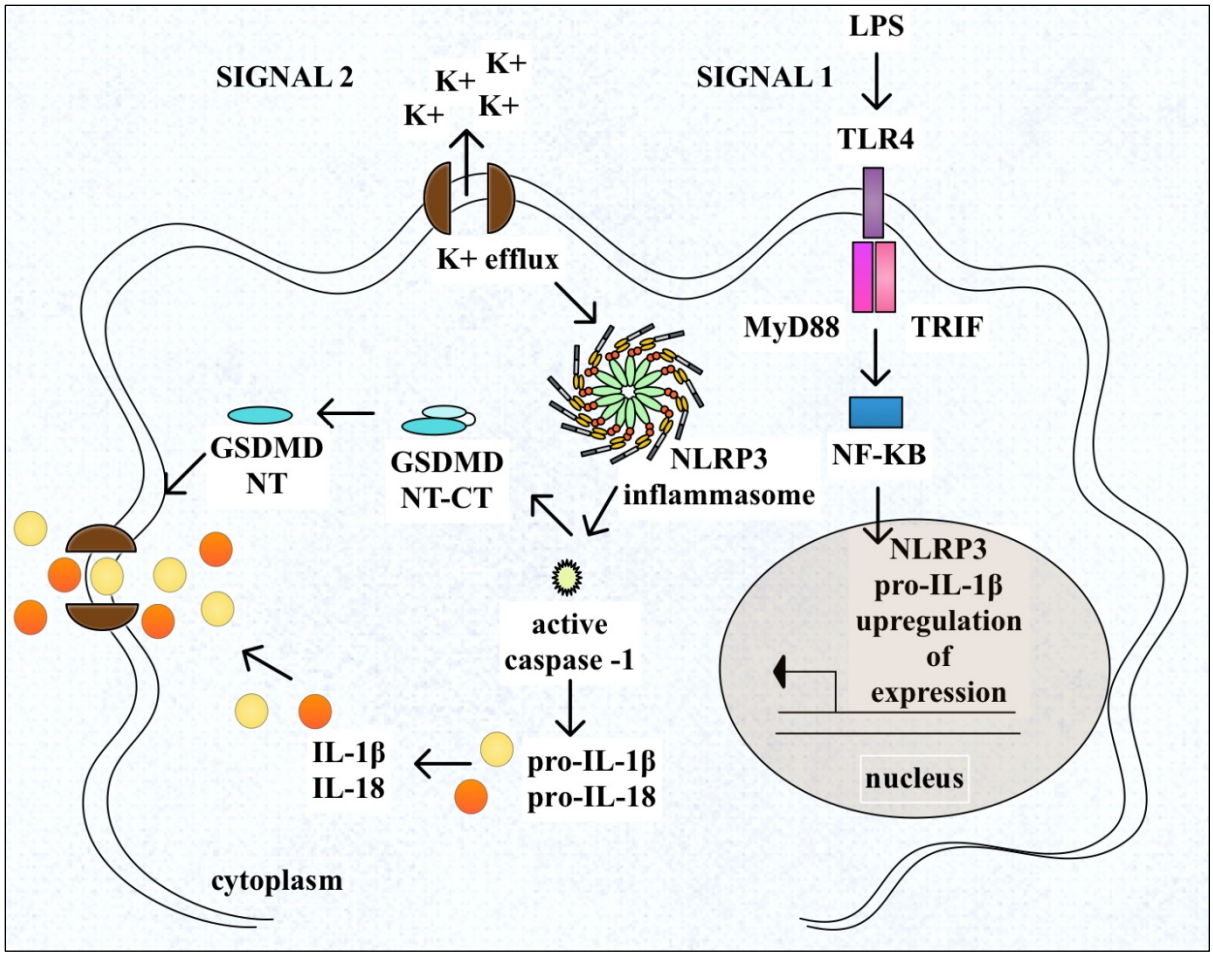


**Figure 1.2.4.1 The NLRP3 inflammasome.** NLRP3 inflammasome formation involves a two-step activation system. Signal 1 induces protein expression of pro-inflammatory cytokines and inflammasome components. Ligand sensing acts as signal 2 resulting in NLRP3 oligomerisation, ASC and inflammatory pro-caspase-1 recruitment. Active caspase-1 drives cytokine maturation and GSDMD cleavage. The active N-terminal fragment of GSDMD induces pore formation in the plasma membrane leading to pyroptotic cell death.

### 1.2.5 NLRC4

NLRC4 was originally named IL-1-converting enzyme (ICE)-protease-activating factor due to its role in caspase-1 activation [121], [122]. It contains a C-terminal LRR, a central NACHT and an N-terminal CARD domain, which can bind directly to pro-caspase-1 via homotypic CARD interactions [121]. NLRC4 has been shown to be crucial in immune responses against intracellular

pathogens such as *S.* Typhimurium [123], *Shigella flexneri, Pseudomonas aureginosa* and *Legionella pneumophila* [124]. Unlike NLRP3, NLRC4 is constitutively expressed in macrophages and dendritic cells and therefore does not require transcriptional priming [121], [125]. In a resting cell, NLRC4 exists in an auto-inhibited state via LRRs and NBD cis interactions [126]. Upon ligand detection, protein kinase C delta (PKCδ) or leucine-rich repeat kinase 2 (LRRK2) [127] mediated phosphorylation of NLRC4 on S533 [128], [129] driving self-oligomerisation, adapter ASC recruitment and inflammasome formation [130]. The NLRC4 family contains the NAIPs which act as sensor molecules upstream of NLRC4 [131], and their direct interaction with bacterial ligands provide specific ligand recognition of PAMPs translocated to the host cytosol by the bacterial type III secretion systems (T3SS) [55], [132]. Upon ligand binding, NAIP and NLRC4 hetero-oligomerize and form the NAIP/NLRC4 inflammasome [64]. Further studies have revealed that flagellin, T3SS rod and needle proteins are also capable of NLRC4-mediated caspase-1 activation. Specifically, murine NAIP1 recognises T3SS needle proteins e.g. Prgl and SSaG [133], NAIP2 recognises T3SS rod proteins e.g. PrgJ, while NAIP5/6 recognises flagellin [46]. Human NAIP [38] recognises the needle component of the T3SS, similarly to murine NAIP1 [46]. Bacterial ligand binding occurs via NAIPs' HD1-WHD-HD2 domain regions [131], which results in the exposure of the catalytic surface of the receptor. These conformational changes allow NLRC4 receptor binding which then undergoes structural changes at the WHD domain region [134]. This facilitates the recruitment and self-oligomerization of additional NLRC4 receptors, and ultimately the formation of NAIP/NLRC4 inflammasomes (Figure 1.2.5.1) [46].

The mouse genome contains multiple NAIP genes, while humans encode only a single gene equivalent. Alternative splicing of human NAIP however has been suggested in primary human macrophages [135]. NAIP/NLRC4 receptors are highly conserved across mammalian species. There is, however, evidence for species-specific differences e.g. zebrafish lack NAIP/NLRC4 orthologues but inflammasome-like complexes have been shown to assemble in zebrafish neutrophils in response to *S.* Typhimurium flagellin [136]. NAIP orthologues are present in frogs [137], while dogs and pigs lack functional *NAIP*/*NLRC4* genes [41], [138]. Specifically, dogs lack NAIPs and their *NLRC4* gene has been rendered inactive due to multiple deleterious mutations [41]. The very same mutations can also be found in wolves. Interestingly this not the case for

felidae, another member of the carnivora order, where the respective NLRC4 gene does not contain premature stop codons [41]. The functional consequences of these differences in species-specific pathogen recognition and subsequent clearance have yet to be fully elucidated.

Within the NAIP/NLRC4 inflammasome a single NAIP receptor can be found in association with multiple NLRC4 receptors [134] and arranged in a wheel-like structure [139]. NLRC4 can recruit pro-caspase-1 directly via CARD-CARD interactions [121], or indirectly via ASC adapter protein [140] to form the canonical NLRC4 inflammasome. NLRC4 inflammasome mediated pyroptosis and GSDMD cleavage happen independently from ASC [123], but IL-1β and IL-18 maturation is greatly enhanced when ASC is recruited to the complex [140], [141]. The NLRC4 inflammasome can cooperate with NLRP3 to augment the inflammatory responses resulting in the recruitment of both, caspase-1 and caspase-8 to the assembled complex. Within the inflammasome active caspase-1 drives IL-1β and IL-18 maturation, while recruited caspase-8 modulates their processing [55], [62].

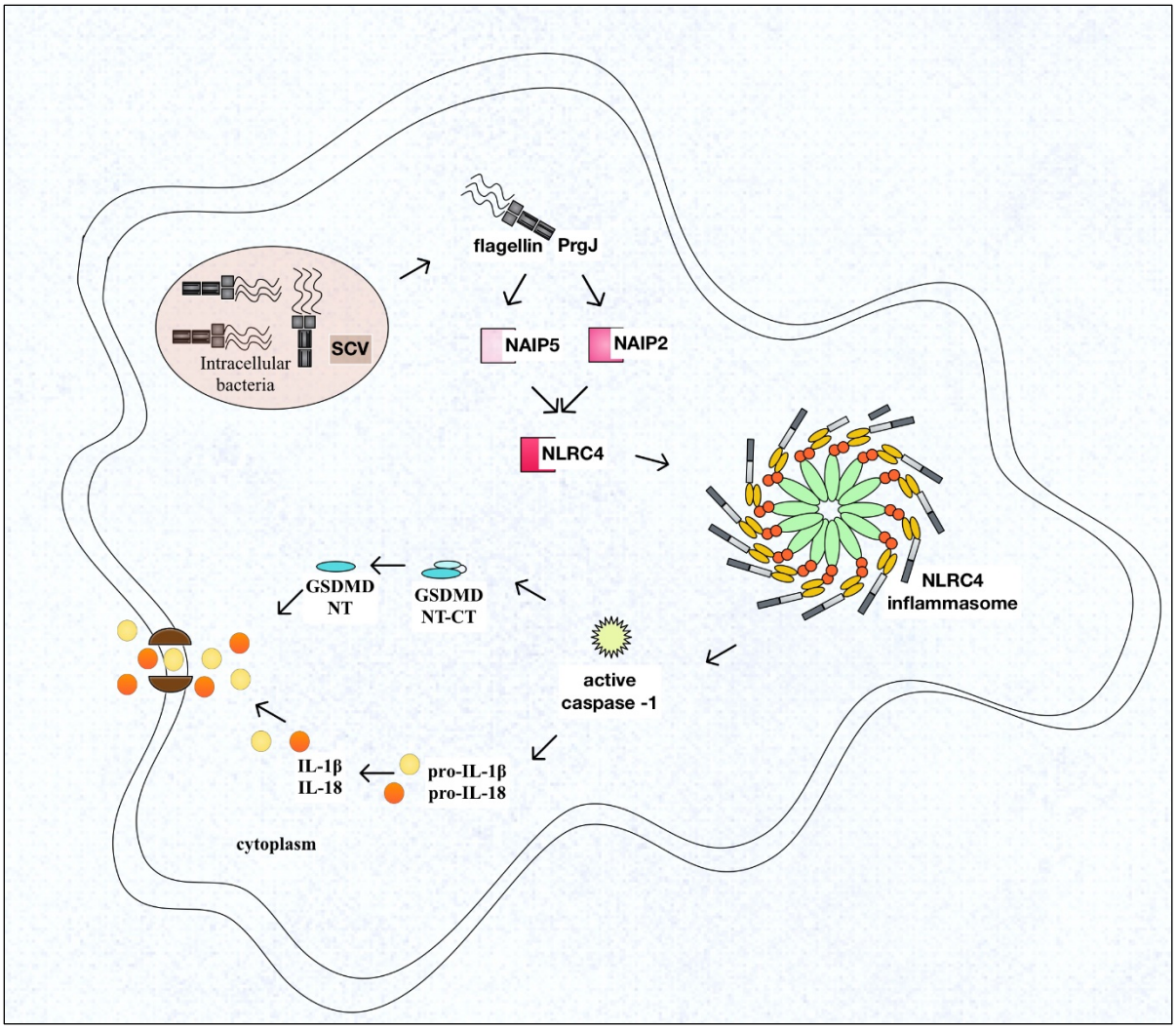


**Figure 1.2.5.1 The NLRC4 inflammasome.** Flagellin and type III SS components are directly recognised by NAIP sensor proteins. Ligand bound NAIPs engage with multiple NLRC4 receptors resulting in their activation and oligomerisation. NLRC4 subsequently recruits ASC and pro-caspase-1 resulting in NLRC4 inflammasome assembly. Activated caspase-1 drives pro-inflammatory cytokines IL-1β and IL-18 maturation and induces pyroptotic cell death via GSDMD-NT.

### 1.2.6 Caspases

Caspases are evolutionary conserved cysteine-aspartic acid proteases [142] that play an essential role in programmed cell death (apoptosis and pyroptosis) and cytokine maturation [143]. Caspase-

1, originally named IL-1β-converting enzyme was the first of the caspases to be identified and was shown to exist in an inactive zymogen form within the cytosol [144], [145]. The N-terminal domain can either contain a CARD (caspase-1, -2, -4, -5, -9, -11, -12) or DED pro-domain (caspase-8, 10) which enable homotypic protein-protein interactions. The C-terminal domain consists of a smaller and larger subunit (p10 and p20, respectively) which together contain residues essential for catalytic activity with the small and large subunits linked together with an inter-subunit linker region [146]. Close proximity of multiple pro-caspases induces their auto-proteolytic cleavage (pro-domain linker and inter-subunit linker) [147] leading to the generation and heterodimerization of p10 and p20 subunits and their subsequent activation. Caspases can be divided into two major groups based on their function. To date there are five known mammalian pro-inflammatory (caspase-1, 4, 5, 11, 12) and seven pro-apoptotic (caspase-2, 3, 6, 7, 8, 9, 10) caspases [148]. Pro-apoptotic caspases can be further categorised into initiator (caspase-2, -8, -9 and -10) and effector (caspase-3, -6, and -7) caspases based on their function [149]. In contrast, caspase-14 has been suggested to have a role in proliferation and differentiation, it appears to have no apoptotic or inflammatory function [150]. Activated inflammatory caspases cleave after aspartic residues in the precursor forms of IL-1β and IL-18 converting them into their biologically active forms [142]. Activated caspase 1/11/4/5 also execute pyroptotic cell death by cleaving GSDMD [43], [44], [151].

Caspases contain a somewhat variable substrate recognition motif which enables functional complexity and also redundancy in their substrates and therefore functions [142]. Mammalian inflammatory genes are present in a so-called inflammatory gene cluster. Early on during mammalian evolution the amplification of the caspase-1 gene resulted in the appearance of additional inflammatory caspases. Gene amplification and selective gene loss can give rise to caspases redundant in their function and also caspases gaining different or even entirely new functions in different species. In humans, there are 14 proteins containing a C14 peptidase domain. With the exception of caspase-12, which has been reported to inhibit inflammation in mice [152] the proteolytic activity of all other caspases has been shown [153]. Interestingly, the human equivalent of inflammatory caspases-1 and -4 are fused together forming a hybrid gene in dogs and cats [154]. Human caspase-12 gene produces a truncated protein after the CARD domain [153] generating a catalytically inactive enzyme. Genes encoding inflammatory caspase-12 in dogs and

cats contain multiple splice variants resulting in the expression of either one or two CARD domains. In contrast to human caspase-12, canine caspase-12 was shown to be capable of autocatalytic processing in an *E. coli* overexpression system [41].

#### 1.2.6.1 Caspase-1

The elucidation of the Nematode cell death protein 3's (CED3) essential role in cell death [155], [156] led to the discovery and characterisation of its mammalian homologue ICE, later termed caspase-1 [144]. Caspase-1 activation requires ASC polymerisation [157] and subsequent inflammasome formation [123]. Mature caspase-1 cleaves the pro-inflammatory cytokines IL-1β and IL-18 at aspartic acid resides Asp116-117 and Asp35-Asn36, respectively [144]. Caspase-1 is the main inflammatory caspase recruited to the canonical NLRP3 and NLRC4 inflammasomes in inducing cell death and cytokine maturation. It also has a crucial role in cytokine processing downstream of the non-canonical caspase-11 inflammasome induced NLRP3 inflammasome [158], [159]. The function of human and mouse inflammatory caspases have been extensively researched, while there is little known about their function in other species. The canine caspase-1 family locus contains only two C14 peptidase domain containing genes, namely caspase-12 and the hybrid caspase-1-4/5/11. Dogs, as well as cats have lost the 3'terminal of caspase-1 and the 5'terminal of caspase-4 genes [154]. The first three exons of the hybrid gene resemble the first three exons of human and murine caspase-1, while exons 4 to 10 shows high similarity to exons 2 to 8 of the human caspase-4 and murine caspase-11, respectively [154]. These proteins show the typical domain organization of caspases, that is, an N-terminal pro-domain, a C-terminal catalytically active caspase domain and cleavage sites [154]. Alternative splicing can produce two isoforms by facultative inclusion of the exon 4, which results in the presence of two tandem CARD domains [154]. There is, however, little information about the functional consequences of the caspase-1/4/11 gene fusion.

#### 1.2.6.2 Caspase-11, -4 and -5

Caspase-11 was discovered based on its high sequence similarity (46%) to caspase-1 [160]. Early *in vivo* experiments carried out using *caspase-1*$^{-/-}$ and *caspase-11*$^{-/-}$ mice suggested redundant roles of these caspases in resistance to lethal sepsis [161], [162]. Later on, *caspase-1*$^{-/-}$ mice proved to

be also deficient for caspase-11 due to a passenger mutation present in 129-embryonic stem cells used to generate caspase-1 knock-out mice [60]. Subsequent experiments showed that *caspase-1*$^{-/-}$ mice were susceptible to LPS induced lethal sepsis, while *caspase-11*$^{-/-}$ mice proved to be resistant [60]. These results suggested the existence of two different pathways mediated by these caspases. Activated caspase-11 alone, within cells, cannot cleave pro-IL-1β and pro-IL-18 [163]. Further experiments showed that the induction of pyroptotic cell death does not require the presence of either NLRP3, adapter protein ASC [60] or caspase-1. In contrast to the induction of cell death, inflammatory cytokines pro-IL-1β and IL-18 maturation relies on the activation of caspase-1 via the NLRP3 inflammasome [60].

Caspase-11 was shown to form a so-called non-canonical inflammasome (Figure 1.2.6.2.1) in response to e.g. *E. coli* [60], *Shigella Flexneri* [164] and *S.* Typhimurium [165] leading to pyroptotic cell death and pro-IL-1β maturation. The non-canonical caspase-11 inflammasome can restrict the replication and promote the clearance of cytosolic bacteria (e.g. enteropathogenic *E. coli*) *in vivo* [166], [167]. Ligand recognition is mediated via a TLR4 and NLR-independent manner where the CARD domain of murine capase-11 and human caspase-4, -5 is thought to directly bind and form a complex with the lipid A moiety of intracellular LPS [61], [163], [168].

Similar to canonical inflammasome formation, activation of the non-canonical caspase-11 inflammasome involves a two-step procedure. In resting cells caspase-11 is not constitutively expressed and therefore, the first step is the transcriptional priming of caspase-11 via the activation of NF-κβ and signal transducer and activator of transcription (STAT) transcriptional factors by TLR agonists and IFNs [169]. The TLR2 agonist Pam3CSK4 activates caspase-11 expression via MyD88, the TLR3 agonist polyI:C via TRIF/IRF3 and TLR4 agonist extracellular LPS via MyD88/TRIF pathways [164], [168], [170]. The second step involves intracellular LPS recognition and subsequent caspase-11 dimerization and activation [171]. Activated caspase-11 induces pyroptotic cell death by directly cleaving pyroptosis executioner GSDMD protein [43], [44].

Caspase-11 can only recognise bacterial LPS, however, once it has gained access into the cytosol. Different mechanisms have been proposed to explain how LPS enters the cytosol e.g. via outer-

membrane vesicles (OMV) secreted by Gram-negative bacteria [172] which have been shown to facilitate pathogen-host interactions and bacterial survival. OMVs contain a variety of molecules, including LPS, phospholipids, peptidoglycan and nucleic acids (DNA and RNA) [173] and are important in the delivery of extracellular LPS into the cytosol of BMDMs [174]. Released OMVs are taken up by host cell via clarithin-mediated endocytosis where LPS can be released from early endosomes and present for detection in the cytosol [174]. Guanylate-binding proteins (GBPs) [175], [176] and immunity-related GTPase family member (IRG) have also been implicated in enhancing the release of LPS from OMVs and Gram-negative bacteria [177]–[179]. IRGs are important in the recognition and association of self-derived vesicles, while GBPs (e.g. GBP2) bind and rupture vesicles lacking IRGs (e.g. bacterium-derived vesicles) [180]. Mice deficient for GBPs showed increased survival and reduced levels of IL-1β and IL-18 in the serum, compared to their wild-type siblings following injection with *E. coli*-derived purified OMVs [181]. While *in vitro* experiments carried out on BMDMs deficient for GBPs showed reduced caspase-11 activation and pyroptosis in response to *Legionella pneumophila* infection [177]. Pathogen-containing vesicles (PCVs) generated by the host cell membrane have also been implicated in LPS introduction to the cytosol [178].

Primates carry two orthologues of the murine caspase-11, namely caspase-4 and caspase-5. Human caspase-4 is constitutively expressed in myeloid and epithelial cells [61], [167], while caspase-5 requires transcriptional priming [182]. The murine caspase-11 orthologue human caspase-4 and -5 have also been shown to activate the non-canonical inflammasome in human monocytes [61], [183]. A recent study, however, suggested differential roles for human caspase-4 and caspase-5. Caspase-5 activity was essential for *Pseudomonas aureginosa* OMV induced inflammasome formation, while caspase-4 induced inflammasome activation occurred in response to *Pseudomonas aureginosa* LPS that was not associated with OMVs in human THP-1 monocytes [184]. LPS-induced inflammasome formation can be activated in a single step in human primary monocytes. Two distinct mechanisms have been proposed for this so far although both pathways rely on TLR4. One proposed TLR4-mediated LPS internalisation and subsequent caspase-5 activation [183]. The other pathway relies on TLR4/TRIF-mediated complex II formation containing RIPK1/caspase-8/FADD upstream of this alternative NLRP3 activation [185]. These

results support the presence of species-specific differences in pathogenic extracellular and intracellular recognition pathways.

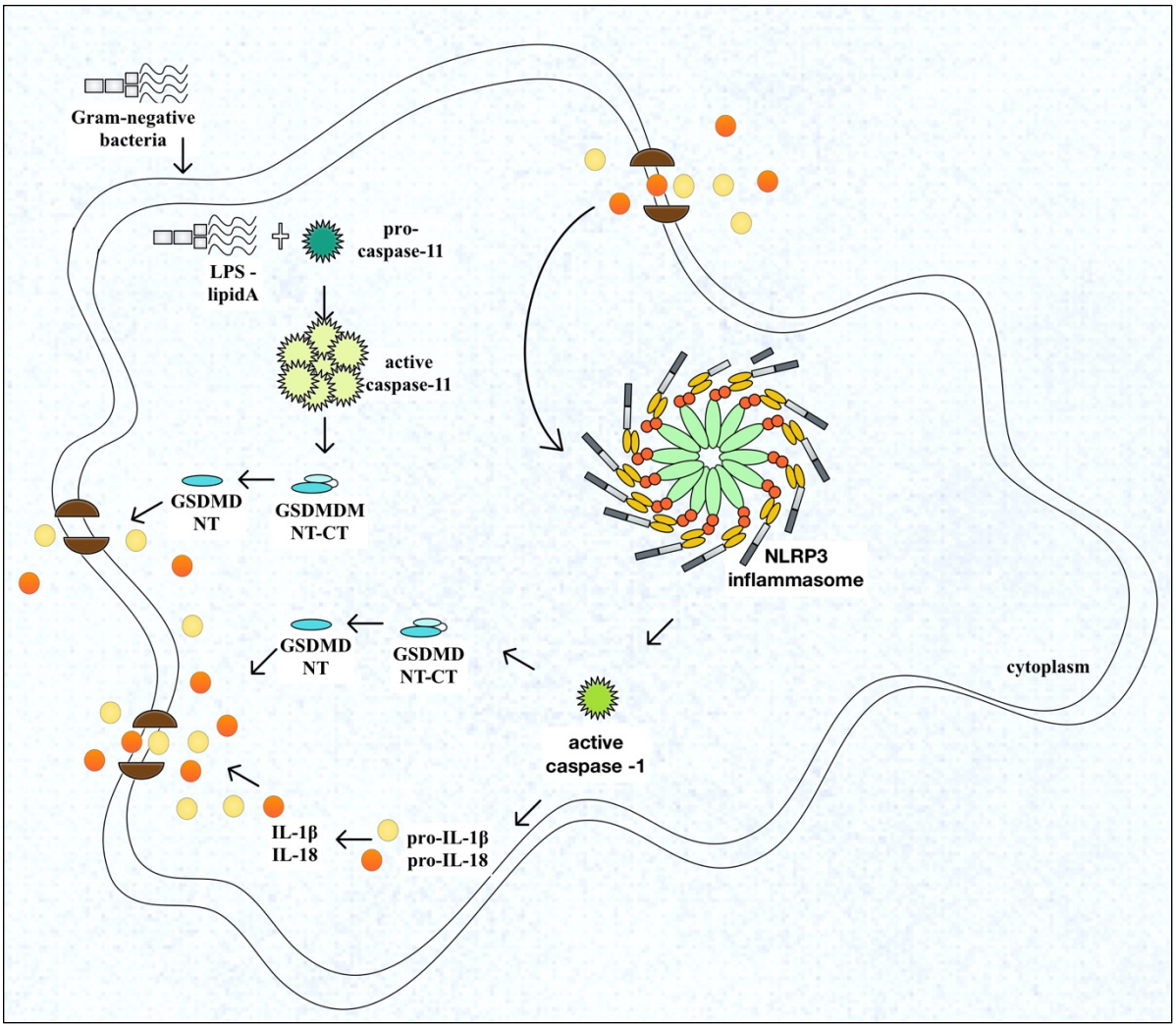


**Figure 1.2.6.2.1 The non-canonical inflammasome.** Cytosolic LPS is recognised and directly binds to the CARD domain of caspase-11. This interaction induces the oligomerisation, proximity induced auto-proteolysis and activation of pro-caspase-11. Activated caspase-11 drives pyroptosis by cleaving executioner GSDMD protein and pro-inflammatory cytokine maturation by caspase-1 via the downstream activation of the NLRP3 inflammasome.

### 1.2.6.3 Caspase-8

The role of caspase-8 in driving extrinsic apoptosis and regulating necroptosis [186]–[188] in response to death receptor activation or mitochondrial damage [189] is well documented (Figure 1.2.6.3.1). Caspase-8 consists of a pro-domain containing two tandem DED domains and a CARD domain consisting of a small and a large catalytic subunit. Caspase-8 deletion is embryonic lethal in mice [188]. Accompanying loss of receptor-interacting serine/threonine-protein kinase 3 (RIPK3) however rescues the lethality phenotype [187], [190]. These results suggested a role for caspase-8 in inhibiting necroptotic cell death and provided evidence on crosstalk between distinct cell death pathways. When pro-apoptotic signals (TNFα) bind to their death receptors (TNFR) in the plasma membrane, it induces death receptor trimerization. The resulting conformational change of the cytoplasmic portion exposes the death-domain (DD) [191], [192] of the receptor which enables the recruitment of the FADD [193], tumour necrosis factor receptor type 1-associated death domain protein (TRADD) and RIPK1 via homotypic DD-DD interactions [194], [195]. The resulting protein assembly is referred to as Complex I.

Depending on the type of posttranslational modification, RIPK1 can either initiate cell survival or induce apoptotic (complex IIa) or necroptotic (complex IIb) cell death pathways. Linear ubiquitination of RIPK1 drives transforming growth factor beta-activated kinase 1 (TAK1)/ Iκβ kinase (IKK) dependent transcriptional activation of NF-κβ transcription factor [196], [197]. Activation of NF-κβ drives cytokine and pro-survival protein transcription [198]. Post-translational modifications (e.g. phosphorylation) of RIPK1 are important to limit RIPK1/caspase-8/FADD association [199], therefore promoting cell survival.

Upon cell death induction, complex I dissociates from the death receptor which enables RIPK1/FADD complex to recruit pro-caspase-8 via homotypic death-effector domain (DED) interactions assembling complex IIa, therefore inducing apoptosis [200], [201]. Proximity induced auto-proteolysis and dimerization results in the activation of pro-caspase-8 [202], [203]. Catalytically active caspase-8 (p18 subunit) can directly cleave and activate effector caspases (e.g. caspase-3) [204] or indirectly via BH3 interacting-domain death agonist (Bid) which stimulates mitochondrial outer membrane permeabilization (MOMP) resulting in cytochrome c release [205].

In apoptotic-deficient cells, TNFR activation induces complex IIb formation, thereby initiating necroptotic cell death [206] which requires the kinase activity of RIPK1, RIPK3 and mixed lineage kinase domain like pseudokinase (MLKL) [207]–[210]. Recent studies have showed that the NLRP3 inflammasome in murine BMDMs, murine and human dendritic cells lacking either GSDMD or proteolytically active caspase-1 were able to recruit and activate pro-caspase-8 within the ASC complex [211]–[213]. Furthermore, activated caspase-8 induced a so called secondary pyroptosis and delayed IL-1β release [213]. Caspase-8 can induce apoptotic cell death in murine macrophage and dendritic cells lacking functional caspase-1 or GSDMD [214], [215]. Recent research suggests that besides driving apoptosis and regulating necroptosis, caspase-8 can substitute for caspase-1 and drive lytic cell death and cytokine maturation. Caspase-8 has been shown to process IL-1β in HEK293T cells [216], mouse BMDCs [217] and BMDMs [218]. It has also been shown to be recruited to the NLRC4 inflammasome in *S.* Typhimurium infected wild-type murine BMDMs in an ASC-dependent manner [140]. Where caspase-8 has been suggested to interact with ASC via DED-PYD interactions resulting in caspase-8 filament formation and subsequent ASC activation [219]. *S.* Typhimurium induced cell death and pro-IL-18 processing was shown to be caspase-8 independent, while it was shown to regulate IL-1β processing and expression [140]. Other studies also highlighted the essential role of caspase-8 in the priming of inflammatory cytokine expression [104], [220] and some suggested caspase-8 mediated pro-IL-1β processing [216], [221], [222]. Purified caspase-8 is able to cleave recombinant mouse GSDMD *in vitro* and also drive rapid cell death that is morphologically similar to pyroptosis [216], [223]–[225]. The efficiency of caspase-8 in cleaving GSDMD, however, was considerably lower than that observed for caspase-1 [223].

These results suggest that in the absence of functional inflammatory caspases, caspase-8 can function as a substitute inflammatory caspase in addition to its' defined roles in regulating necroptosis and driving apoptosis. Depending on the type of insult, caspase-8 can drive an inflammatory type of cell death in the form of secondary pyroptosis and inflammatory cytokine maturation.

These experiments suggest that components of the inflammasome complex can have highly redundant roles. While each recruited effector protein has a preferential function, in their absence

other members can substitute for these functions in order to drive effective innate immune responses against invading pathogens.

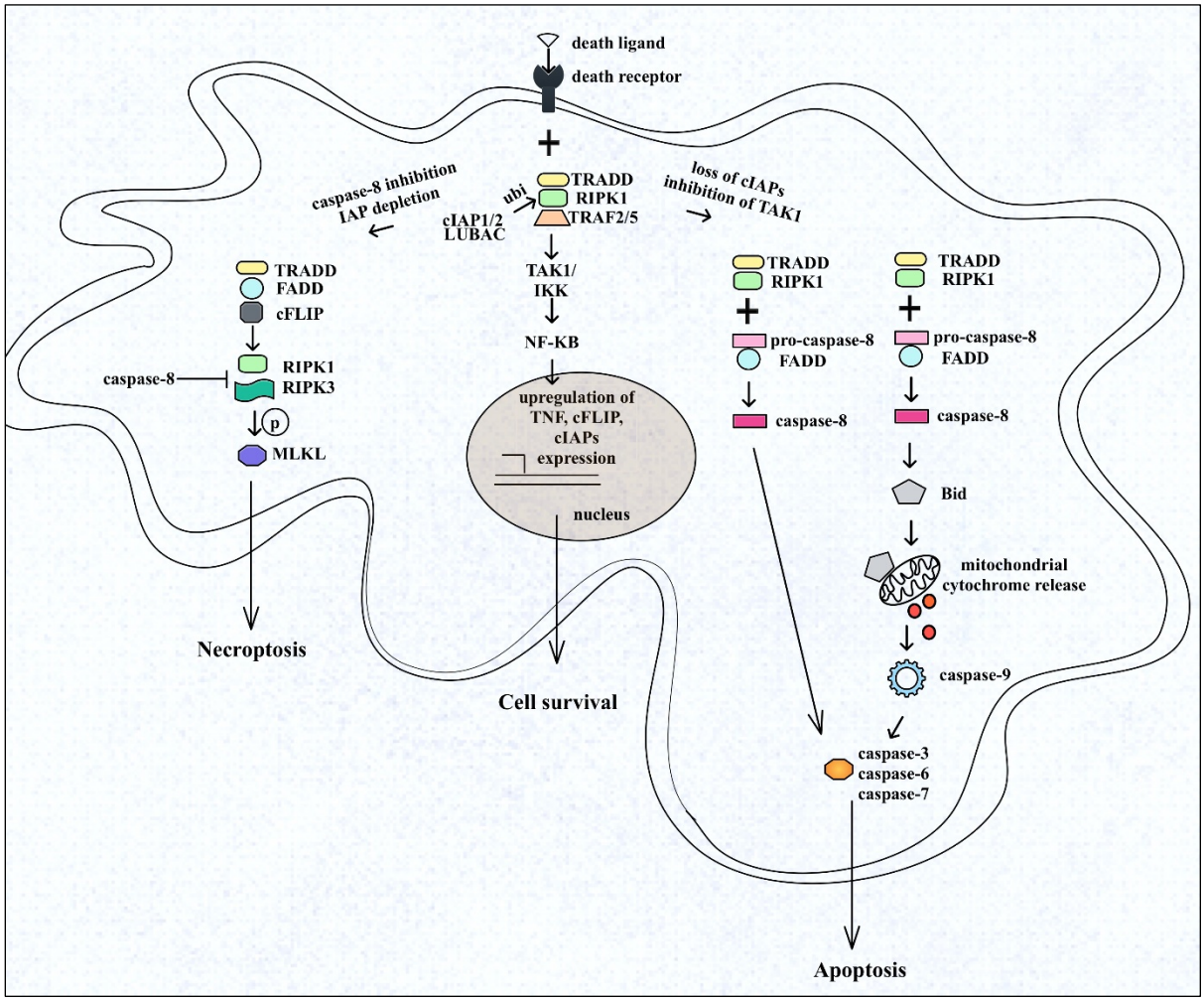


**Figure 1.2.6.3.1 Caspase-8 role in initiating apoptosis and inhibiting necroptosis.** Cells undergo apoptotic cell death when death ligands bind (e.g. TNF) to death receptors (e.g. TNFR) or cells sense cellular stress (e.g. mitochondrial dysfunction). This results in the recruitment of adaptor proteins (TRADD, FADD) and activation of initiator caspase-8. Active caspase-8 can then directly activate executioner caspases-3, -6 and -7 or indirectly via caspase-9. Cleaved Bid protein relocates to the mitochondrial membrane and causes cytochrome c release via membrane permeabilization and subsequent activation of pro-caspase-9. Activated caspase-9 can then directly cleave the executioner caspases -3, -6 and -7.

### 1.2.7 Gasdermins

Gasdermin (GSDM) proteins are expressed in a variety of cell types (e.g. macrophages, neutrophils, dendritic cells) and tissues (skin, gastrointestinal track) [226]. Members of the GSDM family include human GSDMA (murine GSDMA1-3), GSDMB (absent in mice), GSDMC (murine GSDMC1-4), GSDMD, GSDME and Pejvakin (PJVK) [227], [228]. With the exception of PJVK, all of the identified members of the GSDM family contain an N-terminal fragment and exhibit pore-forming activity [75], [229]. Gasdermins have a conserved two domain arrangement, where the C-terminal autoinhibitory domain binds to the catalytic N-terminal domain which are bridged together via a linker loop [75], [230]. Gasdermins require proteolytic cleavage within the linker region for the activation and release of the ~30 kDa N-terminal domain [70], [75], [231]. GSDMD was identified as a caspase-1, -11 substrate by two independent studies; a whole genome CRISPR screen of macrophages and a mouse ENU mutagenesis based forward genetic screen [43], [44]. GSDME (also known as DFNA5) was also shown to be cleaved by apoptotic caspase-3, resulting in an N-terminal fragment with pore forming attributes similar to its GSDMD counterpart [232]. Activated human inflammatory caspase-1, -4 and -5 can cleave GSDMD at 275-Asp position and murine caspase-1 and -11 at 276-Asp [43], [44], [71]. The N-terminal fragment preferentially binds to the cardiolipin (CL), phosphatidylserine, and phosphoinositol residues in the cell membrane [70], [74], [231] and mitochondrial membrane [233] thereby forming pores of varying sizes between 10-20 nm in diameter [70], [72], [234]. This suggests that passive release of IL-1β and IL-18 and DAMPs (cytochrome c, cathepsin B) can occur prior to cell lysis upon pore formation [235], [236]. An additional role for GSDMD is a purported bactericidal activity by direct binding to target lipids (namely cardiolipin) in the bacterial cell wall [70]. Mouse BMDMs stimulated with bacterial peptidoglycan, mouse BMDCs in response to oxidized phospholipid oxPAPc and mouse neutrophils following acute *S.* typhimurium challenge secrete IL-1β without concurrent pyroptosis [236]–[238]. Cells lacking GSDMD released reduced levels of IL-1β [236], [238]. These observations suggest that cell death and cytokine release may be decoupled where cell fate may be determined by a threshold of GSDMD pores formed within a membrane.

Gasdermin orthologue proteins can be found in other species for example in zebrafish [239] which contains two gasdermin pore-forming domains (*gsdmea and gsdmeb*). *In vivo* challenge of

zebrafish embryos with mycobacterial DNA suggest *gsdmeb* gene to be an orthologue of mammalian GSDMD [239]. GSDMD has been annotated in several other species including dogs, horses and pigs. Little is known, however, about whether their functions in the context of pathogen clearance are homologous to their human and mouse counterparts.

### 1.3 Innate Immunity induced cell death mechanisms

Following infection, PAMPs can be recognised by a multitude of PRRs. Their activation result in the induction of different signalling pathways that can lead to the production of chemokines, cytokines and the induction of programmed cell death [8]. Programmed cell death is important in both, physiological (organ development, tissue homeostasis) and pathological processes [240]. It plays a crucial role in removing unwanted, damaged and potentially harmful cells. It also disrupts pathogens' replicative niche while alerting neighbouring cells leading to pathogenic clearance [8]. Programmed cell death (Figure 1.3.1) can occur through caspase-dependent (for example, apoptosis, pyroptosis) and caspase-independent (for example, necroptosis and autophagy) mechanisms.

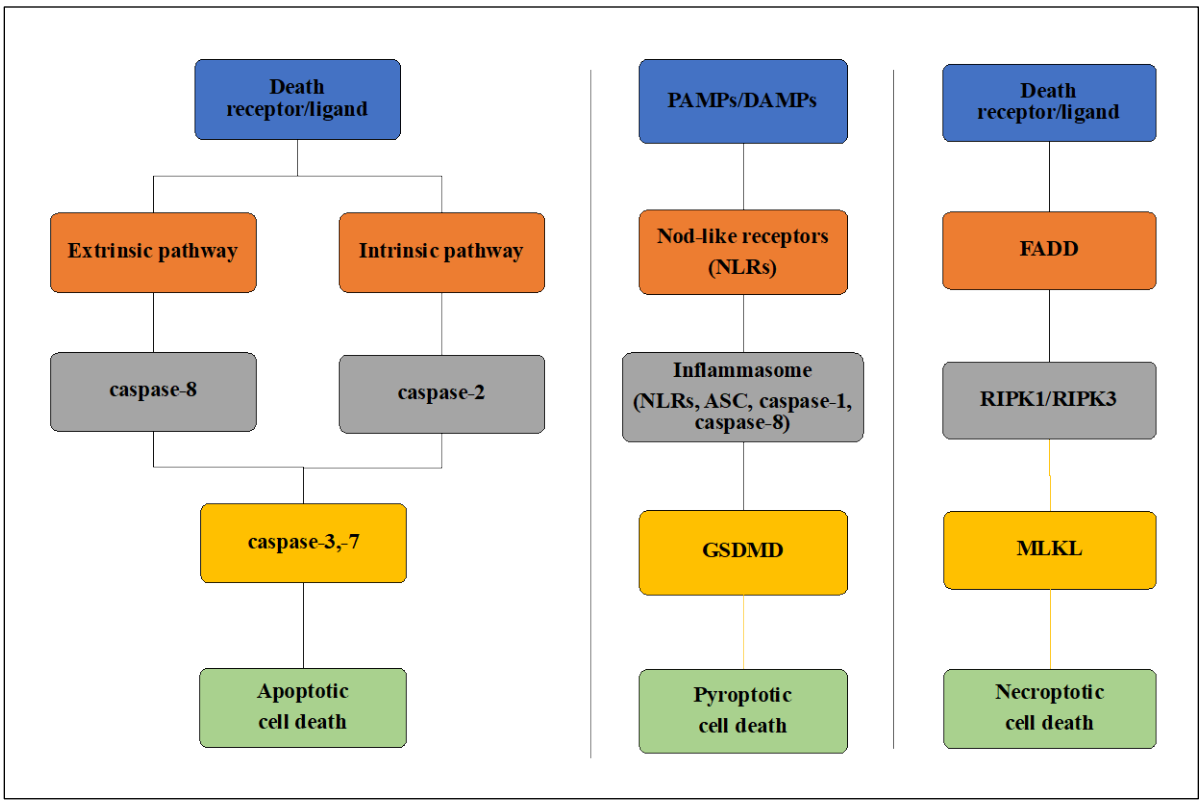


**Figure 1.3.1 Programmed cell death pathways.** Schematic diagrams showing the major steps involved in the apoptotic, pyroptotic and necroptotic cell death pathways. (A) Cells undergo apoptotic cell death when death ligands bind to death receptors or cells sense cellular stress (e.g. mitochondrial dysfunction). This results in the recruitment of adaptor proteins and activation of initiator caspases-2 and -8. Cleaved caspases can then directly activate executioner caspases 3- and -7. (B) Cells undergo pyroptotic cell death when intracellular NLRs along with adaptor protein ASC form inflammasomes. Within the inflammasome pro-caspase-1 is recruited and cleaved into its active form. Active caspase-1 then drives pyroptotic cell death by cleaving GSDMD. (C) Cells undergo necroptotic cell death when death ligand binds to death receptors under caspase-deficient conditions. This trigger the formation of necrosome containing FADD, RIPK1 and RIPK3 proteins which drives the phosphorylation and activation of executioner protein MLKL.

Apoptosis was first described by Kerr *et al*. [241] and is a caspase-dependent cell death mechanism [242]. Apoptotic cell death can be triggered by intrinsic and extrinsic signals, either when pro-survival factors are depleted, cellular stress sensors are activated or by death-inducing ligands

binding to their receptors [243]. While apoptosis plays an essential role in embryonic development [244], it is also important in pathogenesis [245]. Cells undergoing apoptosis exhibit a characteristic set of morphological features (Figure 1.3.2). Apoptotic cells undergo shrinkage [246], [247], their plasma membranes bleb and cells are packaged into membrane-enveloped fragments known as apoptotic bodies [243]. Chromatin within apoptotic cells condenses and terminal deoxynucleotidyl transferase dUTP nick end labelling (TUNEL) staining reveals high levels of DNA damage [248]. Apoptotic cells do not release their cellular contents into the milieu and their apoptotic bodies are readily cleared by phagocytic cells [249], [250]. Apoptosis was, therefore, thought to be immunologically silent triggering little or no inflammation [251] although whether this process is truly immunologically silent is currently the topic of some debate.

Besides apoptosis, programmed necrosis includes additional forms of regulated cell death processes, e.g. necroptosis and pyroptosis. Programmed necrosis is a lytic, pro-inflammatory form of cell death. It is characterised by swelling and subsequent membrane and organelle rupturing [252]. The loss of membrane integrity results in the release of cellular contents thereby triggering inflammatory responses [253]. Pyroptosis was initially identified as a caspase-dependent form of apoptosis [242], [254]. Pyroptosis is typically induced by inflammatory caspases which cause the affected cells to display membrane vesicles, followed by cell swelling [255]. This results in pore formation in their plasma membranes through which inflammatory cytokines (e.g. IL-1β, IL-18) and cytoplasmic contents (e.g. LDH) are released into the extracellular milieu [246]. Like apoptosis, cells undergoing pyroptosis display DNA damage [256], the extent of which is less than what occurs during apoptosis (Figure 1.3.2). Phagocytes including macrophages [254], dendritic cells [257] and monocytes [183] can undergo pyroptotic cell death. The cell rupture results in the release of intracellular pathogens, while the secreted cytokines and chemokines recruit other type of immune cells (neutrophils) to facilitate pathogenic clearance [8]. Necroptosis was first reported as a Fas ligand (FasL), tumour necrosis factor (TNF) or TNF-related apoptosis inducing ligand when primary murine macrophage cells are stimulated with pan-caspase inhibitor Z-VAD-FMK [258], [259]. Cells undergo necroptotic cell death in response to rapid, severe insults (oxidative stress) [260] and in response to pathogenic infections (murine cytomegalovirus) [261]. Necroptosis associated morphology resembles that of its pyroptotic counterpart. Cells undergoing necroptosis (Figure 1.3.2) swell and rupture, resulting in the release of DAMPS (e.g. HMGB1 (High mobility

group box 1) which is normally chromatin associated)) triggering inflammatory responses [253]. RIPK1 has been shown to play a fundamental role in regulating cellular responses and determining cell fate [262], [263]. RIPK1 has a tripartite domain organisation. It consists of an N-terminal kinase domain (KD), a central intermediate domain (ID) including a receptor interacting protein (RIP) homotypic interaction motif (HIM) and a C-terminal DD [186], [264], [265]. Activated RIPK1 kinase domain has been shown to function in promoting cell death via necroptotic or apoptotic cell death pathways [190], [266]. Interaction with FADD and caspase-8 can induce RIPK1-dependent apoptosis [267], while binding and phosphorylation of RIPK3 mediates necroptotic cell death pathway [268]. The kinase [200], [269] and intermediate domains have been shown to be essential in mediating cell death responses [270], while the death domain is important in mediating RIPK1 dimerization and subsequent activation [265]. The DD is also crucial in mediating TNFR activation-induced cytokine expression via the NF-κβ transcription factor [270], [271] and MAPK signalling pathway [272], entirely independently of its kinase activity.

| Morphology | Apoptosis | Necroptosis | Pyroptosis |
|---|---|---|---|
| Cell markers | Bcl-2<br>Membrane asymmetry (Annexin V)<br>DNA damage (TUNEL)<br>cytochrome-c release | RIPK1<br>RIPK3<br>MLKL | GSDMD<br>ASC<br>caspase-11 (mouse)<br>caspase-4/-5 (human) |
| Cell lysis | ✗ | ✓ | ✓ |
| Cell swelling | ✗ | ✓ | ✓ |
| Membrane rupturing | ✗ | ✓ | ✓ |
| Membrane blebbing | ✓ | ✗ | ✗ |
| Pore formation | ✗ | ✗ | ✓ |
| Chromatin condensation | ✓ | ✓ | ✓ |
| DNA fragmentation | ✓ | ✓ | ✓ |
| DNA damage | ✗ | ✓ | ✓ |
| Inflammation | ✗ | ✓ | ✓ |

**Figure 1.3.2 Cell markers and morphological features characteristic of apoptotic, necroptotic and pyroptotic forms of cell death.** Image adapted from Labbe & Saleh, 2011.

Programmed cell death mechanisms and autophagy work synergistically to contribute to the effective innate immune responses against invading pathogens. It is not inconceivable that multiple cell death mechanisms can be activated simultaneously in order to increase the magnitude of the innate immune responses. Perhaps the presence of multiple death pathways can also compensate for one another if one or more of these pathways prove to be defective.

### 1.4 *S.* Typhimurium

*Salmonella* is a Gram-negative, motile, pathogenic bacterium. Epidemiological studies have revealed that the majority of *Salmonella*-related foodborne disease related deaths are caused by non-typhoidal *Salmonella enterica* infections with more than 200 million worldwide cases of disease reported each year [273]. The genus *Salmonella* comprises two distinct species, *Salmonella enterica* and *Salmonella bongori*. The former can be subdivided into a further six subspecies and another, 50+ serogroups and 2400 *serovars* based on their O somatic and H flagellar antigens, respectively. *Salmonella enterica serovars* can cause enteric fever (typhoidal) or diarrhoea (non-typhoidal). Depending on the immune status of the host, the latter can cause gastroenteritis in immunocompetent and bacteraemia in immunocompromised individuals [274]. *Salmonella* Pathogenicity Islands (SPIs) encode virulence factors which are important in their pathogenicity [275]. There are twelve SPIs: 1-6, 9, 11-14 and 16, but virulence factors are mainly associated with T3SS 1 and 2. Expression of SPIs is tightly regulated and can rapidly respond to environmental changes [276], [277]. SPI1 and SPI2 form molecular syringes which enable the injection of effector proteins into the host cytosol following entry into the cell. SPI-1 produces the bacterial proteins (*Salmonella* invasion protein (Sip) B, C and D)) which are essential in host cell adhesion and invasion [278]. The T3SS is responsible for the expression of secretory system components, effector proteins, chaperones and transcriptional regulators. *Salmonella* effector proteins trigger host cytoskeletal rearrangement [279] followed by micropinocytic uptake [280] in epithelial cells. *Salmonella* initially resides in the host phagosomal compartments creating '*Salmonella*-containing vacuole' (SCV) and induces SPI-2 T3SS-2 expression [281]. *Salmonella* has evolved numerous different strategies to avoid host cell defence mechanisms. These include prevention of SCV fusion with lysosomes, attenuation of superoxide production via the distraction

of the nicotinamide adenine dinucleotide phosphate-oxidase (NADPH) assembly [282] and neutralisation of host antimicrobial peptides [283].

### 1.4.1 *S.* Typhimurium and Innate Immunity

*Salmonella* infection in mice and humans occurs via consumption of contaminated food so the resident innate immune system of the gastrointestinal tract is especially important in these infections. There are two distinct steps involved in *Salmonella* pathogenesis, namely adhesion to the intestinal epithelial cells (IECs) and the subsequent invasion and colonisation of the intestinal lumen [284]. *Salmonellae* are recognised by an array of intra- and extracellular receptors. These receptors can initiate distinct signalling pathways in order to limit *Salmonellae* replication, drive their clearance and to alert neighbouring immune cells. TLRs resident in the plasma- and endosomal membranes are the first pattern-recognition receptors to detect *Salmonellae*. Mice lacking TLR4 infected with *S.* Typhimurium show reduced survival rate and higher bacterial burden compared to their wild-type counterpart [285]. This underlines the particular importance for TLR4 in early cytokine production and controlling bacterial burden of *S.* Typhimurium *in vivo* [286]. While *S.* Typhimurium flagellin recognition by TLR5 in gut enterocytes induces inflammatory cytokine IL-8 expression via NF-κβ signalling [287], it is not required for controlling systemic *S.* Typhimurium infection in mice [288]. Intracellularly, NLRC4 has been shown to be important to regulate *S.* Typhimurium early in infection. Using *in vivo* mouse models, IEC-specific activation of NLRC4 inflammasome induced caspase-1, caspase-8 and GSDMD-dependent pyroptotic cell death and intrinsic IEC expulsion from the epithelial layer provide protection against intestinal *S.* Typhimurium invasion [289]. NLRC4 inflammasome activation following *Salmonella* infection results in inflammatory cytokine maturation and release via pyroptosis. While *S.* Typhimurium can also activate the formation of the NLRP3 inflammasome which was shown to play redundant roles to NLRC4 in a mouse model of lethal, but not in sub-lethal, *S.* Typhimurium infection [62], [141]. Mice lacking both NLRP3 and NLRC4 receptors showed higher bacterial burden in their mesenteric lymph nodes, spleen and liver compared to wild-type mice in lethal infection models [141]. Inflammasome activation results in the activation of inflammatory caspase-1 which has been shown to be a crucial mediator of the host immune response against *S.* Typhimurium, providing resistance during the intestinal and systemic phase of

infection [290]. *In vivo* experiments carried out using *caspase-1*$^{-/-}$ mice showed increased bacterial burden systemically and afflicted mice succumbed to lethal infection earlier compared to their wild-type siblings [291]. Mice lacking either IL-1β or IL-18 exhibited enhanced susceptibility to *S.* Typhimurium infection [290]. Inflammasome assembly showed the simultaneous recruitment of caspase-1, caspase-8 and NLRP3 downstream of the NLRC4 receptor to the ASC-speck in *S.* Typhimurium infected macrophages [62], [292]. Caspase-1 induced pyroptotic cell death disrupts the replicative niche of *S.* Typhimurium while also initiating its clearance by neutrophils [293], [294]. Upon SCV lysis the released cytosolic LPS is recognised by murine caspase-11 and its human homologue caspase-4 [60], [295]. Mice *in vivo* models have suggested that caspase-11 may be important in restricting intracellular *S.* Typhimurium replication in the intestinal epithelium [167].

### 1.4.2 *S.* Typhimurium infection in different species

A wide range of different animal species are susceptible to salmonellosis depending upon the type of *Salmonella*. These species include reptiles (e.g. turtle), amphibians (frogs), poultry (e.g. chicken), rodents (e.g. mice), farm animals (e.g. cows, sheep and pigs), dogs, cats and horses [296]–[298]. Similar to humans, the primary route is mainly via the consumption of contaminated food or water. Although *Salmonella enterica* subspecies *enterica* contains over 2400 serovars, salmonellosis in humans and domestic animals is caused by a relatively small number of serovars. For example *Salmonella enterica* serotype Enteritidis and *Salmonella enterica* serotype Typhimurium can infect a wide range of different species, however, host-specific serovars have also been identified. For example, fowl typhoid and pullorum diseases are caused by *Salmonella enterica* serovar Gallinarum and Pullorum, respectively [299]. Salmonellosis in cattle is mainly associated with serovar Dublin [300], [301], while in pigs disease is predominantly caused by *Salmonella enterica* servovar Cholerasuis [302]. *S.* Typhimurium infections of calves mimics the pathology of gastroenteritis characterised in humans [303]. Interestingly, pigs can acquire infection via the intranasal route, causing pneumonia in the majority of cases [304]. *Salmonella enterica* serovar Abortus ovis is an ovine-restricted serovar. Although the infection spreads mainly via the oral-faecal route, conjunctival and vaginal routes have also been proposed [305]. The existence of different infection routes identified in different species makes *Salmonella* an interesting pathogen.

Little is known, however, about whether the mechanism of infection and the signalling pathways induced following *Salmonella* recognition are homologous in different host species.

Subclinical infections and active carriage of *Salmonella* serovars have been reported in domestic animals with clinical salmonellosis mainly occurring in young or immunocompromised individuals [306]. In subclinical infections, bacteria are largely constrained to the gastrointestinal tract of the infected animal with faecal excretion of bacteria sometimes reported for months or even for years [307]. *Salmonella* pathogenesis and virulence varies between different host species. Interestingly, *Salmonella* species can cause enteritis and diarrhoea in cats and dogs. However a large number of asymptomatic *Salmonella* infections have been reported in both species [308], [309]. For example, examination of faeces taken from healthy dogs showed that 23% of the samples were indicative of a subclinical *Salmonella* infection with *S.* Typhimurium being one of the most commonly isolated serovars [310], [311]. *Salmonella* pathogenesis has predominantly been studied in human and rodent systems. There are, however, major species-specific differences in pattern recognition receptors and in inflammasome components. Understanding the consequences of these differences is paramount to better understand pathogen recognition and how the bacteria are controlled by the host. The work in this thesis will investigate the consequence of the inflammasome and caspase repertoire in the dog and its functional role in the sensing of *S.* Typhimurium.

### 1.5 Aims

Inflammasomes are macromolecular signalling complexes that play a fundamental role in host defence against microbial infections. However, inflammasomes have also been implicated in numerous inflammatory disorders described in humans, and therefore represent a viable target for therapeutic intervention. There exists major differences in the pattern recognition receptor and caspase repertoires found in different animal species. One of the model species used in the area of anti-inflammatory research is the dog (*Canis Lupus Familiaris*). Surprisingly, inflammasome machinery alongside their activation and function remain to be fully characterised in the dog.

In this thesis I aim to investigate the functional consequences that arise as a result of the major differences in the inflammasome associated repertoire that exists in the dog. The main objectives are as follows:

a) To perform Multiple Sequence Comparison by Log-Expectation analysis of amino acid sequences of the main inflammasome components present in the dog, mouse and human genome and identify their catalytic sites.
b) To confirm by immunoblotting the expression of the main inflammasome components in the immortalised dog macrophage cell line, DH82.
c) To characterise inflammasome responses in the dog using a combination of imaging (ASC and active caspase speck formation), cell death analysis and IL-β detection in the DH82 cell line in response to well described sterile inflammatory ligands and infectious whole bacteria using *Salmonella enterica serovar* Typhimurium (*S.* Typhimurium).
d) To confirm inflammatory responses of DH82 macrophages to sterile ligands and *S.* Typhimurium infection in canine primary mononuclear cells (MNCs) isolated from whole blood.
e) To optimise electroporation conditions and parameters for CRISPR-Cas9 gene editing in the DH82 cell line.
f) To identify one, key components of cell death response induced by sterile inflammatory ligands and following *S.* Typhimurium infection in DH82 cells by editing key genes associated with pyroptotic, necroptotic and apoptotic pathways using the optimised CRISPR-Cas9 methodology arising from (e) and two, assess the functional consequences of targeted gene disruption.
g) To characterise primary murine bone marrow derived macrophages (BMDMs) harbouring a functional equivalent to the CASP-1/4/5/11 gene found in the dog.
h) To generate a phylogenetic tree for the comparative analysis of putative and confirmed caspases of different animal species, including the dog.

# Chapter 2.
# Materials and Methods

## 2.1 Cell culture

Murine immortalised bone-marrow derived macrophages (iBMDMs), a kind gift from Professor Kate Fitzgerald (University of Massachusetts Medical School, USA) and the canine malignant histiocytic macrophage-like cell line, DH82 (ATCC CRL-10389) were maintained in DMEM-complete medium (DMEM+) (Dulbecco's Modified Eagle Medium (DMEM) (Sigma-Aldrich, D6546), 10% Foetal Calf Serum (FCS) (Thermo Fisher Scientific, 16000044), 5 mM L-glutamine (Sigma-Aldrich, G3126), 100 µg/ml streptomycin and 100 units/ml of penicillin (Sigma-Aldrich, P4333) at 37°C, 5% $CO_2$. Primary mouse BMDMs were isolated by Dr Panagiotis Tourlomousis (Department of Veterinary Medicine, University of Cambridge, UK) from wild type C57BL/6 mice obtained from Charles River, UK. Dog-Mouse (DogMo) chimeric primary BMDMs were a gift from Vishva Dixit (Genentech, USA). Primary BMDMs were maintained in primary complete medium (10% FCS, 20 mM L-glutamine, 100 µg/ml streptomycin and 100 units/ml penicillin, 20% L929 conditioned medium). L292 conditioning medium was prepared by culturing the L929 mouse fibroblast cell line for up to two weeks in RPMI medium supplemented with 10% FCS and 2mM L-glutamine. Saturated L929 supernatant was harvested and then clarified using a 0.22 µm filter (Millipore). For bacterial infection studies, cell cultures and bacteria were prepared in antibiotic-free medium (DMEM-).

## 2.2 Mononuclear cell isolation from canine blood

Peripheral blood mononuclear cells (PBMCs) were derived from residual blood samples taken from dogs admitted to the Queen's Veterinary School Hospital (Department of Veterinary Medicine, University of Cambridge) for venous blood sampling and testing (Table 2.2.1). Histopaque-1077 density gradient medium (Sigma-Aldrich, H8889) was carefully introduced via the central hole to the insert of a SepMate$^{TM}$ mononuclear cell (MNC) isolation tube (Stem Cell Technologies, 85415). Blood samples acquired from different dogs (see Table 2.2.1) were pooled and the samples were immediately diluted in an equivalent volume of wash buffer (Dulbecco's phosphate buffered saline (DPBS) (Sigma-Aldrich, D8537) plus 2% FCS, 0.22 µm filtered). The

diluted blood was then used to overlay the density gradient medium in the SepMate$^{TM}$ tube. Samples were centrifuged at 1200 x g for 10 minutes at room temperature with the centrifuge break on. The top layer above the insert containing MNCs was decanted off with a single, quick inversion and subsequently washed two times with wash buffer. The cells were pelleted in between washes by centrifugation at 300 x g for 8 minutes. Following the final wash, the pelleted cells were resuspended in primary cell culture DMEM medium, using 10 ml medium / 3 ml of undiluted blood sample. The cells were seeded in 10 $cm^2$ Petri-dishes and differentiated as described in 2.3 Preparation of primary bone marrow derived macrophages.

| Identifier | Veterinarian | Breed | Age | Reason for blood test |
|---|---|---|---|---|
| 1379 2901 | Mott | Whippet | 9 years | Chemo monitoring |
| 1379 3501 | Catton | Retriever | 12 years | Monitoring of treatment for anal sac adenocarcinoma |
| 1379 4801 | Shelton | Cocker Spaniel | Unknown | Monitoring of immune-mediated haemolytic anaemia |
| 1379 5301 | Peckham | Staffordshire Bull Terrier | 11 years | Chemo monitoring |
| 1379 5401 | Russel | Labradoodle | 12 years | Screening |
| 1379 6201 | Matthews | Greyhound | 6 years | Chemo monitoring |
| 1386 0901 | Teparitcharov | Pug | 5 years | Protein-losing enteropathy |
| 1386 1301 | Akhter | Cacapoo | 4 years | Immune Mediated Thrombocytopenia re-check |
| 1386 3601 | Rice | Staffordshire Bull Terrier | 8 years | Screening |
| 1393 5602 | Gadsby | Staffordshire Bull Terrier | Unknown | Acute hepatitis |
| 1393 8601 | Ayliffe | Bullmastiff | 7 years | Vomiting and diarrhoea |
| 1393 9901 | Floto | Labradoodle | 3 years | Hypoadrenocorticism |
| 1394 1801 | Rose | Springer Spaniel | 8 years | Chemo monitoring |
| 1394 3201 | Wilkin | X-Breed | 9 years | Post liver biopsy monitoring |

**Table 2.2.1 List of patients whose blood was used in experiments (including information of the breed, their age and reason for phlebotomy).**

### 2.3 Preparation of primary bone marrow derived macrophages

Mice were euthanised by cervical dislocation and sterilised by immersion in 70% ethanol. Fur and skin were removed, and the legs were separated from the body at the hip joint. The legs were placed into fresh cold DMEM medium and maintained on ice until further processing. In a sterile

tissue culture hood, the legs were placed into Petri-dishes containing 10 ml of cold DMEM medium and all soft tissue was removed. The tibia and femur bones were separated by cutting the knee ligaments using a scalpel. The ends of each bone were subsequently removed to generate an opening for retrieval of the bone marrow. In order to harvest the bone marrow, each bone was repeatedly flushed out with DMEM medium using a 25-gauge needle and 20 ml syringe. Cells were transferred to a 50 ml falcon tube and centrifuged at 1000 rpm for 5 minutes. Pelleted cells were then plated out into sterile petri-dishes for differentiation into macrophages. Alternatively, cells were re-suspended in freezing medium (90% FCS and 10% DMSO (Sigma Aldrich, D8418-100ML)) and stored at -80°C for 24 hours, then transferred to -150°C for long term storage. During the process of reviving frozen primary bone marrow macrophages, cells were placed in a 37°C water bath until they were completely thawed. Cells were re-suspended in 8ml of fresh primary cell culture DMEM medium and centrifuged at 1000 rpm for 5 minutes. Pelleted cells from each vial were re-suspended in 30 ml of fresh primary cell culture DMEM medium and transferred into Petri-dishes, 10 ml/dish. Cells were cultured for 3 days at 37°C in 5% $CO_2$. On day 3, an additional 10 ml of primary cell culture DMEM medium was added to the cells prior to incubation for a further 3 days at 37°C in 5% $CO_2$ atmospheric conditions. On day 7 cell culture medium was removed from each dish and was replaced with 10 ml fresh primary cell culture DMEM medium. Cells were gently scraped off and were transferred into a 50 ml conical tube. The same process was repeated for each dish and cells from the same genotype were pooled. Cells were pelleted at 1000 rpm for 5 minutes. Cells used for gentamicin protection assays were re-suspended in 10 ml of fresh primary $DMEM^-$ medium, whereas macrophages used for nigericin and cytosolic LPS ligand stimulations were re-suspended in 10 ml of primary DMEM+ medium. Cells were enumerated using the trypan blue exclusion method and were plated on flat bottom 96-well cell culture plates at the desired cell concentration.

### 2.4 Culturing of *S.* Typhimurium and growth curves

Frozen glycerol stocks of wild-type *Salmonella* Typhimurium *(S.* Typhimurium) strain SL1344 and SL1344 mutant strains *ΔFliC/FliB*, *ΔPrgJ*, *ΔFliC/FliB/PrgJ* (generated by Dr John Wright, Department of Veterinary Medicine, University of Cambridge) were thawed and streaked onto each of two LB agar plates (Sigma-Aldrich, L2897-1KG) and incubated for 24 hours at 37°C.

Three single colony forming units (CFUs) were emulsified in 5 ml fresh LB agar broth (Sigma-Aldrich, L3022-1KG) and incubated for 17.5 hours at 37°C in a shaking incubator at 200 rpm. After incubation, 500 µl of inoculum was transferred into 5 ml fresh LB agar broth and incubated for an additional 2 hours at 37°C in a shaking incubator at 200 rpm. Bacteria were then pelleted at 3,500 x g for 10 minutes at room temperature and re-suspended in 1 ml of DMEM-. The optical density (OD) was measured at 600 nm and the inoculum was diluted in 15 ml fresh LB agar broth to obtain OD 0.01. This value represented the 0-hour time-point. A dilution series of the inoculum was prepared and plated in triplicate onto LB agar plates. Plates were incubated at 37°C overnight and CFU were enumerated the following morning. The inoculum was subsequently returned to the shaking incubator at 37°C, 200 rpm. Thereafter, ODs were measured, and serial dilutions of the inoculum were prepared hourly for a total duration of eight hours.

### 2.5 Infection of BMDMs with *S.* Typhimurium

Murine immortalised wild-type, *Nlrc4*$^{-/-}$, *caspase-1*$^{-/-}$*caspase-11*$^{-/-}$ iBMDMs and primary wild-type and DogMo BMDMs, DH82 and blood-derived primary macrophage cells were seeded in 96-well flat-bottomed plates at a concentration of either $1x10^6$ or $5x10^5$ cells/ml in DMEM- and incubated overnight at 37°C in 5% $CO_2$. Cells were infected with either stationary phase *S.* Typhimurium wild-type strain SL1344 and mutant strains *ΔFliC/FliB*, *ΔPrgJ* or *ΔFliC/FliB/PrgJ* (as described in Section 2.4 culturing of *Salmonella* Typhimurium and growth curves) for 1 hour with multiplicity of infection (MOI) 1, 10 or 50. The culture supernatant was subsequently removed and stored at -80°C for further analysis (1-hour time-point). In experiments using the mutant bacterial strains, the inocula were centrifuged onto the adherent macrophages at 500 x g for 10 minutes. To ensure the correct number of bacteria were used for infection, ten-fold serial dilutions of each MOI of SL1344, *ΔFliC/FliB*, *ΔPrgJ*, *ΔFliC/FliB/PrgJ* were prepared in sterile DPBS. Thereafter, 50 µl from the appropriate dilution was spread out on to each of two LB agar plates and incubated overnight at 37°C. MOIs were then calculated the following day based on the number of CFU counted. For 2-hour time-point infections, cell culture medium containing bacteria was replaced with DMEM$^-$ cell culture medium supplemented with gentamicin (Thermo Fisher, 15750060) at 50 µg/ml final concentration. Cells were further incubated for one hour at 37°C in

5% $CO_2$ (during which time the high concentration of gentamicin kills remaining extracellular bacteria). The supernatant was then removed and stored at -80°C until required (2-hour time-point). For the 6- and 24-hour time-points, 50 µg/ml gentamicin was replaced with fresh DMEM-cell culture medium containing gentamicin at a final concentration of 10µg/ml. Percentage of cell lysis induced as consequence of bacterial infection was measured at each time-point using the CytoTox 96® Non-Radioactive Cytotoxicity Assay (Promega, G1780) according to the manufacturer's instructions. This assay measures the extracellular release of the stable, cytosolic enzyme lactate dehydrogenase (LDH) present in cells in a coupled enzymatic reaction where the amount of converted end product linearly correlates with the amount of LDH released into the supernatant. In this assay, 50 µl of substrate reagent was added to 50 µl of cell culture supernatant in 96-well flat-bottom plates (Corning, CLS3599) and incubated for up to 30 minutes in the dark. To stop the reaction, 25 µl of stop solution was added to each well and the absorbance was read at 490 nm wavelength using either the PHERAstar (BMG, Labtech) or CLARIOstar Microplate Reader (BMG, Labtech). Wavelength correction was set to subtract 570 nm readings from 490 nm wavelength readings, which allows for the correction of optical imperfection in plates.

Experiments involving primary canine mononuclear cells (MNCs) could only be performed once due to the limited number of samples sourced from the Queen's Veterinary School Hospital. Therefore, results obtained from these experiments should be interpreted with a degree of caution. Furthermore, residual blood samples were taken from patients who had undergone chemotherapy or suffer from autoimmune disease (Table 2.2.1). One can assume that these factors may introduce heterogeneity in the observed cellular responses to ligand stimulation. Furthermore, the blood samples were collected from multiple different breeds and therefore genetic influence cannot be eliminated. Therefore, my results can only be taken as an indication of what the responses of primary canine MNCs are like post infection with *S.* Typhimurium.

### 2.6 Inflammasome activators and inhibitors

Murine, canine iBMDMs and primary cells were seeded at either $5x10^5$ or $6x10^6$ cells/ml in a 96-well flat-bottomed plate (200 µl/well) overnight at 37°C, 5% $CO_2$. Adherent cells were primed with either ultrapure *E.coli* lipopolysaccharide (LPS) (InvivoGen, tlrl-3pelps) at a final

concentration of 200 ng/ml for 3 hours or Pam3CSK4 (Pam3) (InvivoGen, tlrl-pms) at a final concentration of 10 µg/ml for 4 hours at 37°C, 5% $CO_2$. Cells were then stimulated with either nigericin (Sigma-Aldrich, N7143-5MG) ranging from 10 µM to 200 µM final concentration for 1 hour. For non-canonical inflammasome activation, cells were incubated with ultrapure LPS at 1 µg/ml or 5 µg/ml final concentration in the presence of FuGENE HD transfection reagent (Promega, E2311) for 16 hours at 37°C, 5% $CO_2$. LPS and transfection reagent were pre-incubated for 15 minutes at room temperature prior to addition to the cells. For inhibitor experiments, cells were pre-incubated with either pan-caspase Z-VAD-FMK (R&D Systems, FMK001) at a final concentration of 10 µM or caspase-8 Z-IETD-FMK (R&D Systems, FMK007) at a final concentration of 10 µM (Table 2.6.1). Culture medium was supplemented with inhibitors during both priming and ligand stimulation steps.

| Activator /Inhibitor | Stock concentration | Working concentration | Receptor/ Target | Supplier |
|---|---|---|---|---|
| cLPS | 5 mg/ml | 1µg/ml and 5 µg/ml | Caspase-11 | InvivoGen |
| LPS | 5 mg/ml | 200 ng/ml | TLR4 | InvivoGen |
| Nigericin | 10 mM | 10-, 20-, 50-, 100-, 150-, 200 µM | NLPR3 | Sigma-Aldrich |
| Pam3 | 1 mg/ml | 10 µg/ml | TLR1/2 | InvivoGen |
| Z-IETD-FMK | 20 mM | 10 µM | Caspase-8 | R&D Systems |
| Z-VAD-FMK | 20 mM | 10 µM | Pan-caspase | R&D Systems |

**Table 2.6.1 List of activators and inhibitors used in cell stimulation experiments.** Information includes stock concentration, working concentrations, receptor/target proteins and supplier.

Experiments involving primary canine mononuclear cells (MNCs) could only be performed once due to the limited number of samples sourced from the Queen's Veterinary School Hospital. Therefore, results obtained from these experiments should be interpreted with a degree of caution. Furthermore, residual blood samples were taken from patients who had undergone chemotherapy or suffer from autoimmune disease (Table 2.2.1). One can assume that these factors may introduce heterogeneity in the observed cellular responses to ligand stimulation. Furthermore, the blood samples were collected from multiple different breeds and therefore genetic influence cannot be eliminated. Therefore, my results can only be taken as an indication of what the responses of

primary canine MNCs are like in response to sterile inflammatory ligands and post infection with *S.* Typhimurium.

### 2.7 Sample preparation for immunofluorescent staining and imaging

Murine and canine iBMDMs and primary macrophages were seeded at a density of $2x10^5$ cells/well on an 8-well chamber slide (ThermoFisher, 154534) and incubated overnight at 37ºC, 5% $CO_2$. Following ligand stimulation, cells were incubated with either FAM FLICA caspase-1 (Bio-Rad, ICT097), caspase-8 (Bio-Rad, ICT099) or poly-caspase (Bio-Rad, ICT0091) diluted 1:300 in culture medium for 30 minutes at 37°C. Post stimulation, cells were washed three times with DPBS and subsequently fixed in 4% paraformaldehyde (PFA)/DPBS (Thermo Fisher Scientific, 28908) for 15 minutes at room temperature in the dark. Fixed cells were washed twice with DPBS and then incubated in blocking buffer (DPBS containing 0.01% saponin (Sigma-Aldrich, 47036-50G-F) and 10% normal goat serum (NGS) (Dako, X0907) for 1 hour at 37°C. After blocking, cells were incubated with anti-ASC (AL177) pAb (Adipogen, AG-25B-0006-C100) diluted 1:500 in blocking reagent for 50 minutes at 37°C. Each well was washed three times with pre-warmed DPBS prior to incubation with goat-anti-rabbit-IgG-AlexaFluor$^{488}$ (Invitrogen, A11034) or -AlexaFluor$^{568}$ (Invitrogen, A11036) for 40 minutes at 37°C. All secondary antibodies were diluted 1:1000 in DBPS prior to use. Following primary and secondary antibody staining, cells were stained with nuclear Hoechst 33342 (Invitrogen, H3570) labelling solution for 10 minutes at room temperature at a final concentration of 5 µg/ml (Table 2.7.1). Cells were then mounted in VECTASHIELD Antifade Mounting Medium (H-1000, Vector) and kept at 4°C in the dark until required for imaging. Immuno-labelled cells were imaged using an Inverted Fluorescence Microscope (Leica DM IRM).

| Reagent | Host | Catalogue number | Manufacturer | Stock concentration | Dilution | Conjugate |
|---|---|---|---|---|---|---|
| Anti-ASC pAb (clone AL177) | rabbit | AG-25B-006-C100 | AdipoGen Life Sciences | 1mg/ml | 1:500 | HRP |
| FAM FLICA™ caspase-1 kit | N/A | ICT097 | Bio-Rad | N/A | 1:300 | Alexa Fluor 488nm |
| FAM FLICA™ caspase-8 kit | N/A | ICT099 | Bio-Rad | N/A | 1:300 | Alexa Fluor 488nm |
| FAM FLICA™ poly caspase kit | N/A | ICT091 | Bio-Rad | N/A | 1:300 | Alexa Fluor 488nm |
| Goat anti-rabbit IgG | goat | A11034 | Invitrogen | 2 mg/ml | 1:500 | Alexa Fluor 488nm |
| Goat anti-rabbit IgG | goat | A11036 | Invitrogen | 2 mg/ml | 1:500 | Alexa Fluor 568nm |
| Hoechst 33342 anti-nucleus | N/A | H3570 | Invitrogen | 10 mg/ml | 1:2000 | Alexa Fluor 405nm |

**Table 2.7.1 List of reagents used for immunofluorescence staining of cells.** Information includes host animal, catalogue number, supplier, stock concentration, dilutions used and conjugate.

### 2.8 Cytokine measurement using ELISA

Mouse IL-1β and canine IL-1β released into cell culture supernatant was measured using Mouse IL-1β ELISA Set BD OptEIA™ (BD Biosciences, 559603) and Canine IL-1β/IL-1F2 DuoSet (R&D Systems, DY3747) respectively, as described in the manufacturer's instructions. Capture antibody (40 µl/well) was added to each triplicate well of a 96-well half area high protein binding microplate (Grenier Bio-One, 675061). For mouse IL-1β, capture antibody was diluted 1:250 in coating buffer (7.13g $NaHCO_3$ + 1.59g $Na_2CO_3$ in 1 litre of MilliQ water, pH adjusted to 9.5 with 10N NaOH). Canine IL-1β capture antibody was diluted 1:180 in reagent diluent comprising 1% BSA (Bovine Serum Albumin, Fisher Scientific, BP9702-100) in DPBS, pH 7.2-7.4, 0.22 µm filtered). Plates were sealed and incubated overnight at 4°C (mouse IL-1β) or room temperature (canine IL-1β). Thereafter, the wells were aspirated and washed three times with ELISA wash buffer (DPBS + 0.05% Tween-20 (Promega, H5151)). Following the final wash, each plate was inverted and blotted on paper towels in order to remove any residual wash buffer. Plates were blocked in species-specific reagent diluent (180 µl/well) for two hours at room temperature. Mouse

reagent diluent consisted of 10% FCS in DPBS 0.22µm filtered, while canine consisted of DPBS alone. After blocking, the washing step was repeated, during which time the appropriate dilutions of samples and standards were prepared in the same type of culture medium as the supernatant. Forty microliters of standard or sample was added/well and incubated for an additional two hours at room temperature. The washing step was repeated (mouse IL-1β five times, canine IL-1β three times) and detection antibody (40 µl/well) diluted in reagent diluent (mouse IL-1β 1:500, canine IL-1β 1:180) was added to each well. Mouse IL-1β plates were incubated for one hour, whilst canine IL-1β plates were incubated for a period of two hours, both at room temperature. The washing step was repeated (mouse IL-1β five times, canine IL-1β three times) and Streptavidin-HRP (40 µl/well) diluted in reagent diluent (mouse IL-1β 1:250, canine IL-1β 1:200) was added to each well and incubated at room temperature. Mouse IL-1β plates were subsequently incubated for 30 minutes, whereas canine IL-1β plates were incubated for 20 minutes in the dark at room temperature. The washing step was repeated (mouse IL-1β seven times, canine IL-1β three times) and BD TMB Substrate Reagent (Fisher Scientific, BD555214) (40 µl/well) was added. Mouse and canine IL-1β plates were incubated in the dark at room temperature for 30 minutes and 20 minutes, respectively. Stop solution (20 µl/well) was added to each plate and the absorbance was read at 450 nm wavelength using either a PHERAstar or CLARIOstar Microplate Reader (BMG, Labtech). Wavelength correction was set to subtract 570nm readings from 450 nm wavelength readings which allows for correction of optical imperfection in the ELISA plates.

### 2.9 Total protein extraction of cell lysates

Supernatants were aspirated from macrophages cultured in 6-well flat bottom plates (Corning, CLS3516) and replaced with 1 ml of fresh DMEM medium. Cells were gently scraped and then pelleted by centrifugation at 1000 rpm for 5 minutes. Thereafter, the medium was removed and the cell pellet was disrupted in 40 µl of ice-cold RIPA solution (150 mM NaCl, 10 mM Tris-HCl, 5 mM EDTA, 1% Triton-X100, 10 mM NaF, 1 mM $NaVO_4$, 20 mM PMSF) supplemented with Protease Inhibitor Cocktail (Sigma-Aldrich, P8340-5ML) (1:100 dilution) and incubated for 30 minutes on ice. Lysed cells were centrifuged at 14,000 rpm for 15 minutes at 4ºC. Supernatants containing protein were transferred into a new 1.5 ml Eppendorf tube and the protein concentration

was determined using the Pierce™ BCA Protein Assay Kit (Thermo Fisher, 23227), following the manufacturer's instructions. Briefly, 5 µl of each cell lysate was diluted 1:10 in RIPA solution and serial dilutions were prepared for each sample (1:20, 1:40, 1:80). In addition, serial dilutions of standard protein (Bovine Serum Albumin (BSA)) were prepared at final concentrations of 2000 µg/µl, 1000 µg/µl, 500 µg/µl, 250 µg/µl, 125 µg/µl, 62.5 µg/µl and 31.25 µg/µl. 5 µl of each sample and standard was transferred in triplicate to a 96-well flat bottom plate and 95 µl of working solution (A:49 parts – B:1 part) was added to each well. The assay was incubated for up to 30 minutes at room temperature and the absorbance was measured on a PHERAstar Microplate Reader (BMG, Labtech). Actual protein concentrations were calculated using the measurements based on standard curve generated in Microsoft Excel. Standardised amounts of each cell lysate were then prepared for immunoblotting by incubating the appropriate volume of sample with Pierce™ Lane Marker (5x) Reducing Sample Buffer (Thermo Fisher, 39000) on a hot block for 10 minutes at 100°C. Following denaturation, the lysates were placed on ice and then briefly centrifuged to pool the sample prior to storage at -80°C until required. Alternatively, cell lysates were prepared by replacing supernatants from cells cultured in 96-well flat-bottomed plates with 30µl of ice-cold 0.5% Triton-X100/DPBS per well. Plates were then stored at -20°C to facilitate passive lysis of the cells. When required, plates containing lysed cells were thawed and triplicate wells were pooled. Thereafter, 64 µl of each pooled sample was transferred into a new 1.5 ml Eppendorf tube and mixed with 16 µl of Pierce™ Lane Marker (5x) Reducing Sample Buffer prior to heating at 100°C for 10 minutes. After denaturation lysates were cooled briefly on ice followed by centrifugation and analysis by western blot.

### 2.10 Total protein extraction from cell culture supernatants

Cell culture supernatants were transferred into a 15 ml falcon tube and centrifuged at 1000 rpm for 5 minutes in order to remove dead cells. Clarified supernatants were transferred to a fresh 15 ml falcon tube and 1 x volume of ice-cold methanol and 0.25 x volume of chloroform were added to each sample and vortexed briefly for 20 seconds. Samples were then centrifuged at 16,000 x g for 12 minutes at 4°C. After centrifugation, upper and lower phases were aspirated to leave only the intermediate phase containing the precipitated protein. The protein layer was carefully aspirated and centrifuged for 10 minutes at 4°C. Protein pellets were washed twice in 500 µl of ice-cold

methanol. In between washes the resuspended pellets were centrifuged at 16,000 x g for 5 minutes at 4°C. After the final wash, all of the methanol was carefully removed, and the pellets were allowed to dry. Pellets were re-suspended in 40 µl of Laemmli 2 x concentrate sample buffer (Sigma Aldrich, S3401-10VL) and heated at 100°C for 10 minutes and stored at -80°C until required. Alternatively, protein from supernatants derived from cells cultured in 96-well plates were prepared by transferring 100 µl of supernatant from each replicate into fresh 1.5 ml Eppendorf tubes. 400 µl of ice-cold methanol was then added to each sample and briefly vortexed before a further 100 µl of chloroform was added to the tube. After brief vortexing, 300 µl of $ddH_20$ was added to each sample and then centrifuged at 14,000 x g for 2 minutes. The top, aqueous layer was pipetted off and protein residing in the interphase layer was collected and transferred to a fresh 1.5 ml Eppendorf tube. 400 µl of ice-cold methanol was then added and the samples were vortexed briefly prior to centrifugation at 14,000 x g for 3 minutes. Methanol was then carefully aspirated, and the pellet was allowed to air-dry at room temperature. Samples were re-suspended in 40 µl of Laemmli 2× Concentrate Sample Buffer and heated at 100ºC for 10 minutes. Thereafter, the denatured protein samples were cooled on ice, briefly spun down and stored at -80ºC until further analysis.

### 2.11 Western blotting

Denatured proteins were resolved by SDS-PAGE using 12% tris-glycine polyacrylamide gels (see recipe in Table 2.11.1) in conjunction with the Bio-Rad Mini-Protean Tetra electrophoresis apparatus. Sample volume loaded per well ranged between 20 and 40 µl. Colour pre-stained broad range protein markers (Cell Signalling, 14208) were included on each gel. Electrophoresis was carried out at 100 V until the dye front had migrated to the bottom of the resolving gel.

| Reagent | Working concentration | Manufacturer | Catalogue number | Volume |
|---|---|---|---|---|
| 12% resolving gel | | | | |
| Acrylamide | 40% | Sigma | A6050 | 1.5 ml |
| Milli-Q water | N/A | N/A | N/A | 2.15 ml |
| Tris-HCl pH8.8 | 1.5 M | Sigma | T9503-5KG | 1.25 ml |
| SDS | 10% | Sigma | L3771-100G | 50 µl |
| Ammonium-persulfate | 10% | Sigma | A3678-25G | 50 µl |
| TEMED | N/A | Sigma | T9281-25ml | 2 µl |
| 5% stacking gel | | | | |
| Acrylamide | 40% | Sigma | A6050 | 250 µl |
| Milli-Q water | N/A | N/A | N/A | 1.45 ml |
| Tris-HCl pH8.8 | 1 M | Sigma | T9503-5KG | 250 µl |
| SDS | 10% | Sigma | L3771-100G | 20 µl |
| Ammonium-persulfate | 10% | Sigma | A3678-25G | 20 µl |
| TEMED | N/A | Sigma | T9281-25ml | 2 µl |

**Table 2.11.1 SDS-PAGE resolving gel recipe.** Information includes working concentration, supplier, catalogue number and volume.

Resolved proteins were transferred to nitrocellulose membranes pre-soaked in transfer buffer by wet transfer overnight at 56 mA. Following transfer, each nitrocellulose membrane was washed once in TBS-T (1x TBS (50mM Tris-HCl and 150mM NaCl (Sigma Aldrich, S5886-1KG) in (Milli-Q $H_2O$ and 0.1% Tween-20) and subsequently blocked in 50 ml of 5% milk in TBS-T for 1 hour at room temperature. Each membrane was transferred to a 50 ml Falcon tube and washed twice in TBS-T for 5 minutes/wash. Primary antibodies were diluted in 1% milk-TBS-T and were incubated with the membranes for two hours on a rotary mixer (Table 2.11.2). Membranes were washed five times in TBS-T for 5 minutes/wash and secondary antibody prepared in 1% milk/TBS-T was added (Table 2.11.3). Membranes were incubated for an additional 2 hours on a rotary mixer. Thereafter, the membranes were washed with TBST (5 x 5 minutes) prior to detection of proteins by enhanced chemiluminescence (ECL). Western Lightning Plus-ECL Substrate (Perkin Elmer, NEL103E001EA) was prepared in 1:1 ratio according to the manufacturer's instructions and 750 µl of the working reagent was added to each membrane and incubated for 4 minutes at room temperature. Protein bands were visualised using a GeneGnome chemiluminescence imager (Syngene, GeneGnome XRQ).

| Antibody | Host | Catalogue number | Manufacturer | Stock concentration | Working Dilution | Conjugate |
|---|---|---|---|---|---|---|
| Anti-ASC (AL177) | rabbit polyclonal | AG-25B-006-C100 | AdipoGen Life Sciences | 1 mg/ml | 1:500 | - |
| Anti-canine IL-1β | goat polyclonal | AF3747 | R&D Systems | 0.2 mg/ml | 1:500 | - |
| Anti-caspase-1 p10 (M-20) | rabbit polyclonal | sc-514 | Santa Cruz Biotechnology | 100 µg/ml | 1:500 | - |
| Anti-caspase-11 (17D9) | rat monoclonal | sc-56038 | Santa Cruz Biotechnology | 200 µg/ml | 1:500 | - |
| Anti-DDDDK tag (M2) | mouse monoclonal | ab49763 | Abcam | 100 µg/ml | 1:1000 | HRP |
| Anti-GSDMD | rabbit polyclonal | STJ112203 | St. John's Laboratory | | 1:1000 | - |
| Anti-GSDMDC1 (64-Y) | mouse monoclonal | sc-81868 | Santa Cruz Biotechnology | 100 µg/ml | 1:100 | - |
| Recombinant anti-GSDMD (EPR19828) | rabbit monoclonal | ab209845 | Abcam | 100 µl at 0.588 mg/ml | 1:500 | - |

**Table 2.11.2 List of primary antibodies used in western-blotting experiments.**

| Antibody | Host | Catalogue number | Manufacturer | Original concentration | Dilution | Conjugate |
|---|---|---|---|---|---|---|
| goat anti-rabbit IgG-HRP | goat | sc-2054 | Santa Cruz Biotechnology | 400 µg/ml | 1:2000 | HRP |
| goat anti-rat IgG-HRP | goat | NB-7115 | Novus Biologicals | 1 mg/ml | 1:1000 | HRP |
| mouse anti-rabbit IgG-HRP | mouse | sc-2357 | Santa Cruz Biotechnology | 400 µg/ml | 1:200 | HRP |
| mouse IgGκ BP-HRP | mouse | sc-516102 | Santa Cruz Biotechnology | 400 µg/ml | 1:2000 | HRP |

**Table 2.11.3 List of secondary antibodies used in western-blotting experiments.**

## 2.12 Generation of CRISPR edited cell lines

Schematic representation of the workflow for CRISPR-Cas9 gene editing and for Illumina MiSeq library preparation can be found in Figures 2.12.1 and 2.12.2, respectively.

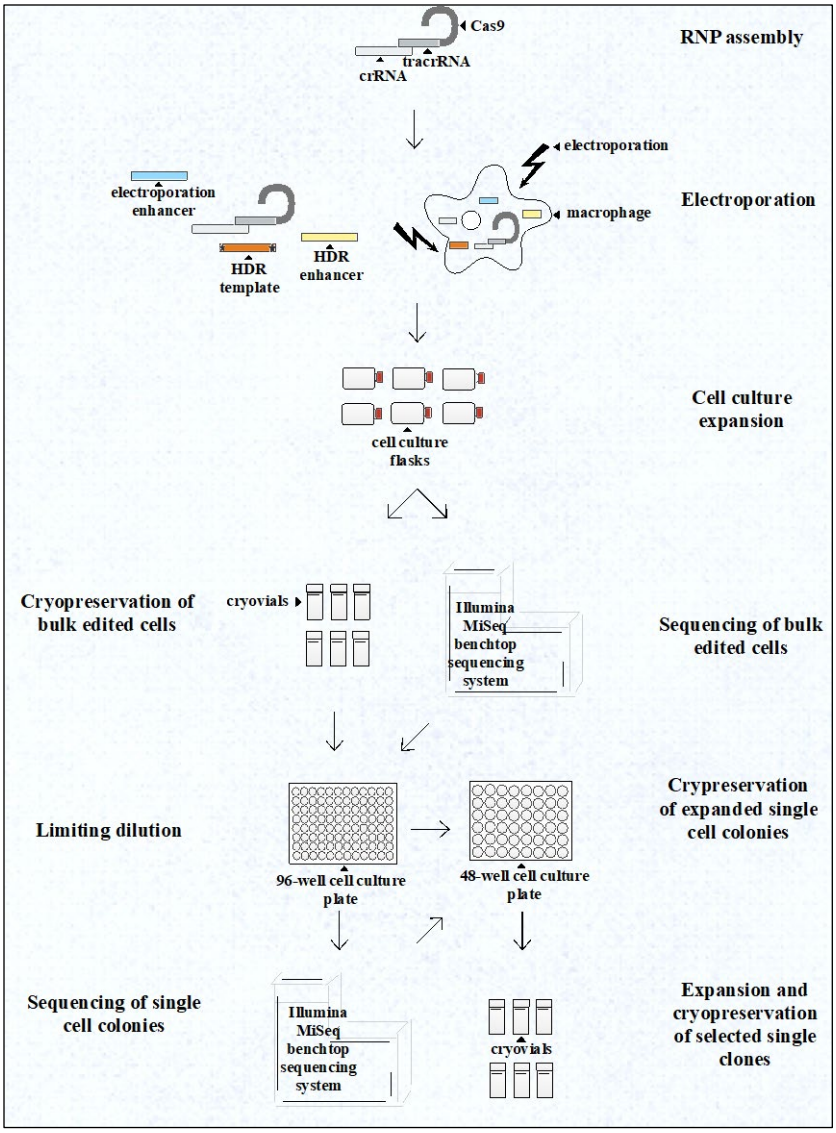


**Figure 2.12.1 Workflow showing the major steps taken to perform gene editing using CRISPR-Cas9 technology.** The first step involves RNP complex assembly consisting of target sequence specific crRNAs, tracrRNAs and recombinant Cas9 proteins. Assembled RNP complexes were then electroporated into wild-type DH82 cells. Following recovery, a large proportion of the bulk edited cells were frozen down and the remainder were retained for further analysis. This included Illumina MiSeq library preparation and sequencing to identify mutations and limiting dilution to obtain single cell colonies. Single cell colonies were divided in two, one half was frozen down and the other half was prepared for sequence analysis. Based on the sequencing results, appropriate single cell colonies were revived, expanded and cryopreserved.

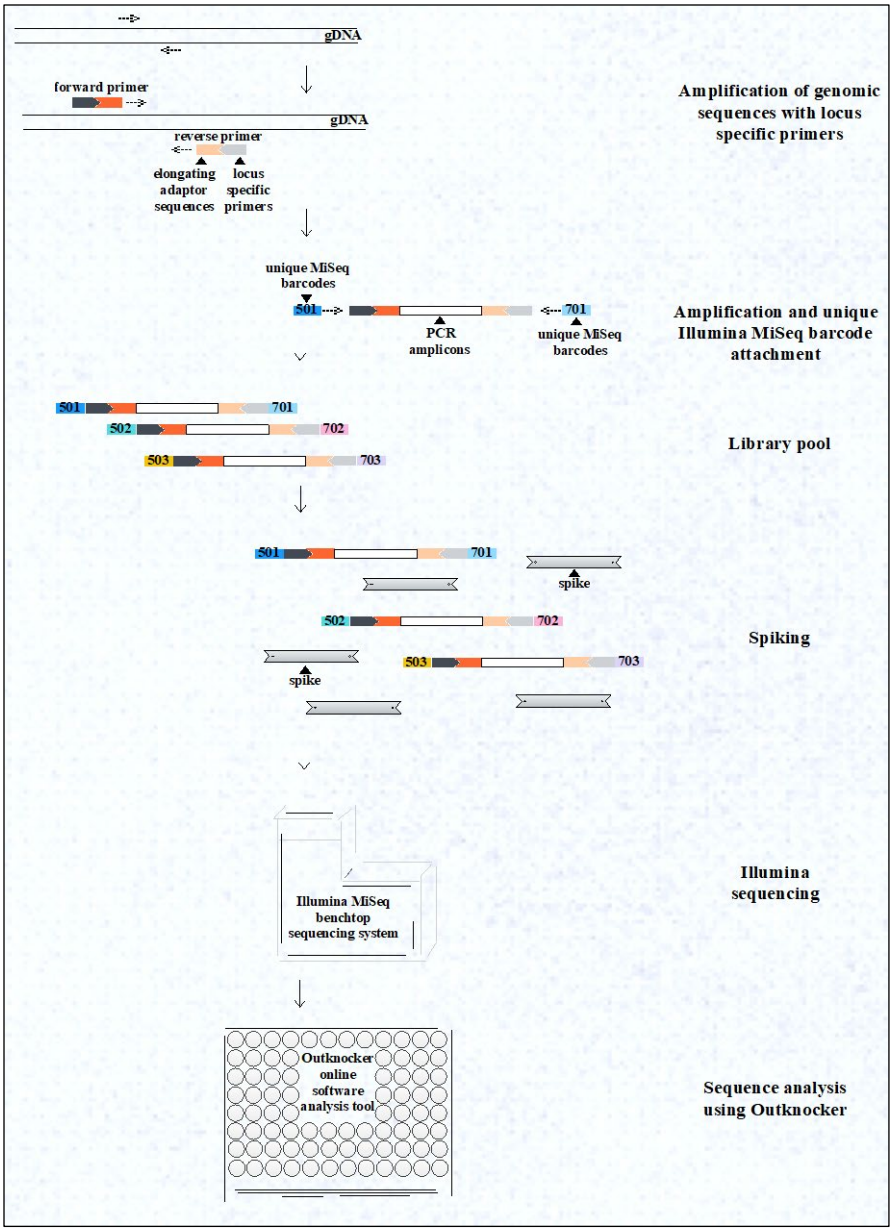


**Figure 2.12.2 Schematic representation of the workflow for Illumina Miseq library preparation.** Following genomic DNA extraction, first level MiSeq PCR was preformed using locus-specific primers including elongated adapter sequences. During second level MiSeq PCR, Illumina unique adaptor sequences were attached to the first level MiSeq amplicons. Up to 96 samples carrying unique identifiers were pooled and spiked with PhiX sequencing control prior to sequencing. Illumina MiSeq sequencing results were then analysed using the OutKnocker online analysis tool [312] to identify mutations that had been induced.

### 2.12.1 Nucleofection Optimisation

Adherent DH82 macrophages were harvested and centrifuged at 1000 rpm for 5 minutes prior to resuspension in DMEM+. Optimisation of conditions for nucleofection was carried out using the Amaxa Cell Line Optimization Nucleofector Kit (Lonza, VC0-1001N) as described in the manufacturer's instructions. Resuspended cells were enumerated, and two cell suspension aliquots were prepared, each containing the number of cells required for 9 sample conditions ($1.6x10^6$ cells/sample). Each cell preparation was centrifuged for 5 minutes at 1,000 rpm and the supernatant was discarded. One of the cell pellets was re-suspended in 900 µl of Solution L (100 µl/sample) including electroporation supplement and the other in 900 µl of Solution V (100 µl/sample) including electroporation supplement. 800 µl of each suspension aliquot was transferred into a sterile 1.5 ml Eppendorf tube and 16 µg pmaxGFP vector (2 µg/sample) was added to the mix. The two remaining 100 µl aliquots of cell suspension without GFP vector were kept and used later as negative controls. 100 µl of cell suspension aliquot was transferred into a sterile electroporation cuvette and the appropriate electroporation program was run. Immediately after electroporation, 500 µl of pre-warmed DMEM+ was added to the cuvette and cells were transferred into 6-well culture plates containing 1.5 ml pre-warmed DMEM+ medium. The wash step of each cuvette was repeated with another 500 µl of DMEM+ medium to ensure all of the electroporated cells were collected. Electroporation was repeated for both solutions for each program (Table 2.12.1.1). Electroporated cells were incubated at 37ºC in 5% $CO_2$. The following day, electroporated cells were harvested and re-suspended in FACS buffer (1% BSA in DPBS). GFP expression for each sample was analysed 24-hour post-electroporation. Intact cells were gated by plotting the forward scatter signal (FSC) on the x axis versus the side scatter signal on the y axis (SSC). Cells were excited with a 488-laser and GFP positive cells were gated by plotting GFP intensity on the x axis versus cell count on the y axis.

| Program | Solution L | Solution V | pmaxGFP |
|---|---|---|---|
| 1 | A-020 | A-020 | + |
| 2 | T-020 | T-020 | + |
| 3 | T-030 | T-030 | + |
| 4 | X-001 | X-001 | + |
| 5 | X-005 | X-005 | + |
| 6 | L-029 | L-029 | + |
| 7 | D-023 | D-023 | + |
| 8 | - | - | + |
| 9 | T020 | T020 | - |

**Table 2.12.1.1 Nucleofection optimization conditions.**

### 2.12.2 crRNA, HDR template and Miseq PCR primer design

crRNAs for gene knock-outs were designed to bind near the catalytic sites and identified catalytic residues of each gene of interest. For gene-tagging, crRNAs were designed to be immediately upstream of, or up to, 60 nucleotides from the stop codon of the targeted genes (Table 2.12.2.1). The crRNA designs were performed using Benchling online research platform (https://benchling.com) and crRNA sequences were confirmed using IDT's Custom Alt-R® CRISPR-Cas9 guide RNA tool (https://eu.idtdna.com/site/order/designtool/index/CRISPR_CUSTOM). crRNAs and tracrRNAs (IDT, 1072534) were synthesised at 10 nmol and 100 nmol concentrations, respectively, both in lyophilized forms. crRNAs and tracrRNA were reconstituted in IDTE (IDT, 11-01-02-02) to 200 μM final concentration and were stored long term at -20°C. Homology-directed repair (HDR) templates were designed to include DDDDK-tag sequence immediately upstream of stop codons and were purchased as single stranded ultramer DNA oligonucleotides (https://eu.idtdna.com/site/order/oligoentry/index/ultra). The phosphate backbone of the first and last ten oligos of each HDR template were substituted with a phosphorothioate bond. This chemical modification increases the resistance of the inter-nucleotide linkage between oligos to endonucleolytic degradation. Pam sites (NGG sequence) of crRNAs were also mutated to prevent nucleolytic cleavage of HDRs by Cas9 endonuclease. Codons overlapping pam sites were altered so that the change in Pam sites would not affect codons encoding amino acid sequences. If pam site mutation resulted in a change in amino acid, a codon encoding a different amino acid within the same classification characterised by their side-chains was chosen (Table 2.12.2.2). HDR

templates were obtained at 4 nmol concentration in dry form. Upon arrival, HDR templates were re-suspended in IDTE buffer (IDT, 11-01-02-02) to 200 μM final concentration. For first level Miseq PCR, locus-specific primers were designed based on the canine reference genome (CanFam3.1) available on the Ensembl Genome Browser (https://www.ensembl.org/index.html), using Primer-blast online primer finding tool (https://www.ncbi.nlm.nih.gov/tools/primer-blast/). Genomic amplicons were designed to be a minimum of 175 base pairs and a maximum of 270 base pairs in length, with nuclease target sites and DDDDK-tag sequences positioned preferably in the centre. First level MiSeq PCR primers were also elongated with 5' adaptor sequences that are required for the second level PCR [313] (Table 2.12.2.3). PAGE purified first level MiSeq primers were ordered at 100 μM stock concentration from Sigma-Aldrich and were reconstituted in UltraPure™ DNase/RNase-Free Distilled Water (Thermo Fisher, AM9916) upon arrival, according to the manufacturer's instructions and were stored at -20°C. First level MiSeq primers were used at 10 μM final working concentration and primer melting temperatures were determined using the NEB online melting temperature calculator (https://tmcalculator.neb.com/#!/main). Universal, 96-well barcode primer dilutions for second level MiSeq PCRs were prepared by combining 8 unique forward and 12 unique reverse primers in a 96-well plate format at a final concentration of 5 μM per primer [313].

| | |
|---|---|
| Caspase-1/4/11 crRNA sequence 1 | CAACCTCAAGGACAAACCGA |
| Caspase-1/4/11 crRNA sequence 2 | GCATCCTGAATGGAATCTGT |
| Caspase-8 crRNA sequence 1 | TTTTATTCAGGCTTGTCAAG |
| Caspase-8 crRNA sequence 2 | CCTACCGAAACCCCATGGAG |
| Caspase-15 crRNA sequence 1 | TTTATCATCCAGGCCTGTAG |
| Caspase-15 crRNA sequence 2 | ATCATCCAGGCCTGTAGAGG |
| Caspase-15 crRNA sequence 3 | AGGCCTGTAGAGGAGGTAAG |
| GSDMD crRNA sequence 1 | GTGTACACTCTATGCCTGTC |
| GSDMD crRNA sequence 2 | ACTGCTGTTATGCCTGAGCG |
| GSDMD crRNA sequence 3 | TGAGCGAGGACCCCTGTTA |
| RIPK1 crRNA sequence 1 | TAATTATGGAGACCATTGAA |
| RIPK1 crRNA sequence 2 | TGGAGAAGGCGTAATACACA |

**Table 2.12.2.1 List of crRNAs design for gene knock-out and gene tagging experiments. A minimum of two crRNAs were designed for each gene of interest.**

| |
|---|
| HDR template for GSDMD crRNA sequence 1<br>C*C*C*C*A*G*G*T*G*T*GCTGGGAGCCAGAGGCCCGGGACCACACGTGTACACTCTATGCC<br>TGTCTAGCACTGCTGTTATGCCTGAGCGAGGACCCCTGTGACTACAAAGACGATGACGACAA<br>GTAGGGCTGACCGGCTCTGCCCGCCAGCGTGCT*G*G*G*C*A*G*C*T*C*T |
| |
| HDR template for GSDMD crRNA sequence 2<br>C*C*C*C*A*G*G*T*G*T*GCTGGGAGCCAGAGGCCCGGGACCACACGTGTACACTCTATGCC<br>TGTCTGGCACTGCTGTTATGCCTGAGCGAAGACCCCTGTGACTACAAAGACGATGACGACAA<br>GTAGGGCTGACCGGCTCTGCCCGCCAGCGTGCT*G*G*G*C*A*G*C*T*C*T |
| |
| HDR template for GSDMD crRNA sequence 3<br>C*C*C*C*A*G*G*T*G*T*GCTGGGAGCCAGAGGCCCGGGACCACACGTGTACACTCTATGCC<br>TGTCTGGCACTGCTGTTATGCCTGAGCGAGGACCCCTGTGACTACAAAGACGATGACGACAA<br>GTAGGCCTGACCGGCTCTGCCCGCCAGCGTGCT*G*G*G*C*A*G*C*T*C*T |

**Table 2.12.2.2 List of HDR templates for gene tagging experiments.** Phosphorothioate modified nucleotides increasing resistance against endonuclease degradation are marked with a star symbol.

| |
|---|
| Caspase-1/4/11 PCR 1 forward primer<br>**ACACTCTTTCCCTACACGACGCTCTTCCGATCT**CGCCCAGAGCATAAGTCCTC |
| |
| Caspase-1/4/11 PCR 1 reverse primer<br>**TGACTGGAGTTCAGACGTGTGCTCTTCCGATCT**TCATGGCCTTTGGGGTTTCT |
| |
| Caspase-8 PCR 1 forward primer crRNA 1<br>**ACACTCTTTCCCTACACGACGCTCTTCCGATCT**CTATGGCTCTGATGGGCAGG |
| |
| Caspase-8 PCR 1 reverse primer crRNA 1<br>**TGACTGGAGTTCAGACGTGTGCTCTTCCGATCT**GCTGACTTTCTGCTGGGGAT |
| |
| Caspase-8 PCR 1 forward primer crRNA 2<br>**ACACTCTTTCCCTACACGACGCTCTTCCGATCT**GCTGACTTTCTGCTGGGGAT |
| |
| Caspase-8 PCR 1 reverse primer crRNA 2<br>**TGACTGGAGTTCAGACGTGTGCTCTTCCGATCT**AGAGGGGGTAAGTGCTCACA |
| |
| Caspase-15 PCR 1 forward primer<br>**ACACTCTTTCCCTACACGACGCTCTTCCGATCT**TGGCTGTTGCCTCATTACCC |
| |
| Caspase-15 PCR 1 reverse primer<br>**TGACTGGAGTTCAGACGTGTGCTCTTCCGATCT**ATGTTTCGGGGATGCCTGAG |
| |
| GSDMD PCR 1 forward primer<br>**ACACTCTTTCCCTACACGACGCTCTTCCGATCT**GTGTGCTGGGAGCCAGAG |
| |
| GSDMD PCR 1 reverse primer<br>**TGACTGGAGTTCAGACGTGTGCTCTTCCGATCT**CAGCCAGGTGGGCATGAG |
| |
| RIPK1 PCR 1 forward primer<br>**ACACTCTTTCCCTACACGACGCTCTTCCGATCT**ACAGTTGCTTTGGCCTGTTTG |
| |
| RIPK1 PCR 1 reverse primer<br>**TGACTGGAGTTCAGACGTGTGCTCTTCCGATCT**ACCTTAATGTGAAAGTCATCATCG |
| |

**Table 2.12.2.3 List of first level MiSeq PCR designs for gene knock-out and gene tagging experiments.** Underlined sections are the locus-specific sequences, while nucleotides highlighted in bold are the 5' adaptor sequences required for the second level MiSeq PCR.

### 2.12.3 Electroporation of DH82 cell line

Equimolar amounts of tracr- and crRNAs were mixed in clear PCR tubes at three different concentrations (100, 200 and 400 pmoles) and heated at 95˚C in a BIO-RAD T100™ thermocycler for 5 minutes. Prior to Cas9-crRNA-tracrRNA ternary complex assembly, crRNA-tracrRNA duplexes were allowed to cool to room temperature. Ribonucleoprotein (RNP) assembly reaction was performed on duplexes by adding an equimolar concentration of Cas9 endonuclease protein (IDT, 1074182) to the complex. Reactions were mixed and incubated at 21˚C in a BIO-RAD T100 thermocycler for 15 minutes. RNP complex was then supplemented with equimolar concentration of Alt-R® Cas9 electroporation enhancer (IDT, 1075916). For endogenous gene tagging, HDR template was also added to the RNP complex. Electroporation enhancer is a Cas9 specific carrier DNA sequence which has been optimised to work with the Amaxa Nucleofector 2b (Lonza, AAB-1001) to increase transfection efficiency thereby enhancing the rate of genome editing. For endogenous gene tagging, Alt-R® HDR Enhancer (IDT, 1081072) was added at a final concentration between 20 to 30 µM to cell culture medium following electroporation and the cells were incubated in the presence of HDR enhancer for 24 hours at 37°C, 5% $CO_2$. Thereafter, cell culture medium containing HDR enhancer was replaced with fresh medium and further incubated overnight at 37°C, 5% $CO_2$. This small molecule compound is used to improve rates for homology-directed repair, therefore increasing the efficiency for endogenous gene tagging. In the meantime, DH82 cells were harvested and enumerated using trypan blue exclusion (Thermo Fisher Scientific, 15250061) with a target cell number of $1.6x10^6$ cells/condition. Cells were transferred into 50 ml falcon tubes (Sigma Aldrich, CLS430829-500EA) and centrifuged at 1000 rpm for 5 minutes. After centrifugation, the supernatant was carefully removed and the cells were re-suspended in 100 µl of Nucleofector Solution V containing electroporation supplement (Lonza, VCA-1003). 10 µl of RNP was introduced to a sterile 1.5 ml Eppendorf tube and 100 µl of cell/buffer suspension was added to the mix. The nucleofection buffer-cell-RNP mix was then transferred directly into an electroporation cuvette and a single electroporation was performed in an Amaxa Nucleofector 2b (Lonza, AAB-1001) using the X-005 program following the manufacturer's instructions. After electroporation, the cell suspensions were transferred into 6-well cell culture plates containing 2 ml of pre-warmed DMEM+ culture medium and the cells were allowed to recover for 24 hours at 37˚C in 5% $CO_2$. The following day cells were harvested by gentle scraping and transferred into

T75 flasks containing DMEM+ medium. Cells were cultured at 37˚C in 5% $CO_2$, until 80% confluency was attained. During splitting of bulk populations one third of the harvested cells was further cultured until 60% confluency and collected for genomic DNA extraction. The remaining two thirds of the cells were frozen down in triplicates in freezing medium.

### 2.12.4 Preparation of DNA from bulk edited cell populations and single cell colonies

DNA extraction of bulk edited cell populations was performed using the PureLink™ Genomic DNA Mini Kit (ThermoFischer Scientific, K1820-01). A minimum of $1x10^6$ cells were transferred to a fresh 1.5 ml Eppendorf tube and centrifuged at 1000 rpm for 5 minutes. Pelleted cells were then re-suspended in 200 µl of DPBS and 20µl of proteinase K followed by 20 µl of RNAse A was added to the cell suspension. Samples were mixed by vortexing and then incubated at room temperature for 2 minutes. Thereafter, 200 µl of Genomic Lysis Buffer was added to the mix and vortexed until the solution became homogenous. Samples were then incubated in a 55°C water bath for 10 minutes prior to the addition of 200 µl of 100% ethanol to each sample and briefly vortexed. Lysates were transferred into spin columns and centrifuged at 10,000 x g for 1 minute. Spin columns were washed twice, first with 500 µl of Wash Buffer 1, centrifuged at 10,000 x g for 1 minute. A second wash was performed with 500 µl of Wash Buffer 2 containing ethanol. Subsequently, the columns were centrifuged at maximum speed for 3 minutes and transferred into fresh 1.5 ml Eppendorf tubes. 30 µl of Elution Buffer was added and samples were incubated for 1 minute prior to centrifugation at maximum speed for one minute. DNA was eluted twice in 25 µl of UltraPure™ DNase/RNase-Free Distilled Water (Thermo Fisher, AM9916) resulting in a total volume of 25 µl in order to maximise DNA yield. Eluted DNA was then stored at -20°C until required. DNA extraction of single cell colonies was performed by first removing supernatant from cells followed by the addition of 20 µl of direct lysis buffer (1 mM $CaCl_2$ (Sigma Aldrich, C3381-500G), 3 mM $MgCl_2$ (Sigma Aldrich,M2670-500G), 1 mM EDTA/10 mM Tris (pH 7.5) (Fisher Scientific, BP2477-500), 1 % Triton X-100, 0.2 mg/mL proteinase K (Thermo Fisher, AM2548)) to each well. Proteinase K was added fresh, immediately prior to lysis. Cells were gently re-suspended and transferred into a 96-well PCR plate. Cell/lysate mix were then incubated for 10 minutes at 65°C followed by 15 minutes at 95°C on a BIO-RAD T100$^{TM}$ Thermocycler. Cell

lysates directly used for first level MiSeq PCR reactions either immediately after lysis or alternatively samples could be stored at -20°C until required.

### 2.12.5 Miseq PCR preparations and reactions

For the analysis of bulk populations, genomic DNA was dispensed at two different concentrations (250- and 500 ng) into a 96-well PCR plate. For single cell colonies, 1 µl of each cell lysate was used. The PCR protocol for locus-specific amplification was performed as follows: 10 µl of 2X Phusion HF Buffer (ThermoFisher F531L), 1 µl of 10 µM of each, forward- and reverse primers and DNase/RNase-free distilled water to make a total of 20 µl reaction/sample. Each well was thoroughly re-suspended, and samples were run on a BIO-RAD T100$^{TM}$ thermocycler (Table 2.12.5.1).

(A)

| | | | |
|---|---|---|---|
| Step 1 | 98°C | 30 seconds | 30 repeats |
| Step 2 | 98°C | 10 seconds | |
| Step 3 | 64°C | 15 seconds | |
| Step 4 | 72°C | 15 seconds | |
| Step 5 | 72°C | 60 seconds | |
| Step 6 | 10° | HOLD | |

(B)

| | | | |
|---|---|---|---|
| Step 1 | 98°C | 30 seconds | 30 repeats |
| Step 2 | 98°C | 10 seconds | |
| Step 3 | 65°C | 15 seconds | |
| Step 4 | 72°C | 15 seconds | |
| Step 5 | 72°C | 60 seconds | |
| Step 6 | 10° | HOLD | |

(C)

| | | | |
|---|---|---|---|
| Step 1 | 98°C | 30 seconds | 30 repeats |
| Step 2 | 98°C | 10 seconds | |
| Step 3 | 66°C | 15 seconds | |
| Step 4 | 72°C | 15 seconds | |
| Step 5 | 72°C | 60 seconds | |
| Step 6 | 10° | HOLD | |

**Table 2.12.5.1 First level MiSeq PCR conditions.** (A) includes conditions used for caspase-8 crRNA 2, (B) conditions used for caspase-15 crRNA 1, -2 and GSDMD crRNA1, -2, -3, (C) conditions used for the hybrid caspase-1/4/11 crRNA 1, -2 and caspase-8 crRNA 1 and RIPK1 crRNA 1, -2.

Following first level MiSeq PCR, amplicons generated from bulk cell populations were assayed for correct size by PAGE. Briefly, DNA was mixed with Gel Loading Dye (Thermo Fisher, #F350) and resolved on a 3% agarose gel (BIO-RAD, #1613030). A lane containing DNA ladder (Bioline, #H5-417-105) was included on all gels. The second MiSeq PCR was performed as follows; 10 µl

of 2X Phusion HF Buffer (ThermoFisher F531L), 7µl of DNase/RNase-free distilled water, 1 µl of amplicon from first level Miseq PCR for each amplicon and 2 µl of universal 96-well Miseq barcode primers [313] (Table 2.12.5.2) were added to each sample. Samples were mixed thoroughly and were run on a BIO-RAD$^{TM}$ thermocycler (Table 2.12.5.3).

| | |
|---|---|
| A701 | ATCACGAC |
| A702 | ACAGTGGT |
| A703 | CAGATCCA |
| A704 | ACAAACGG |
| A705 | ACCCAGCA |
| A706 | AACCCCTC |
| A707 | CCCAACCT |
| A708 | CACCACAC |
| A709 | GAAACCCA |
| A710 | TGTGACCA |
| A711 | AGGGTCAA |
| A712 | AGGAGTGG |
| A501 | TGAACCTT |
| A502 | TGCTAAGT |
| A503 | TGTTCTCT |
| A504 | TAAGACAC |
| A505 | CTAATCGA |
| A506 | CTAGAACA |
| A507 | TAAGTTCC |
| A508 | TAGACCTA |

**Table 2.12.5.2 List of unique MiSeq sequencing barcodes for second level PCR.** 96 unique primers were produced by plating barcodes A701-A712 horizontally (A1-A12) and barcodes A501-A508 vertically (A1-H1) on a 96-well plate.

| | | | |
|---|---|---|---|
| Step 1 | 98°C | 30 seconds | |
| Step 2 | 98°C | 10 seconds | 30 repeats |
| Step 3 | 63°C | 15 seconds | |
| Step 4 | 72°C | 15 seconds | |
| Step 5 | 72°C | 60 seconds | |
| Step 6 | 10° | HOLD | |

**Table 2.12.5.3 Second level MiSeq PCR conditions.**

### 2.12.6 Miseq library preparations

2 µl each of the second level MiSeq PCR products were pooled in a 1.5 ml Eppendorf tube and mixed thoroughly by pipetting up and down. Thereafter, 0.7x volume of Agencourt AmPure XP beads (Beckman Coulter, #A63880) was added to the library pool and incubated for 15 minutes at room temperature, then placed on a magnetic stand for five minutes. The supernatant was carefully removed, and the library pool was washed with 500 µL of 70% EtOH for 30 seconds by re-suspending completely. The Eppendorf tube containing the library was placed back onto a magnetic stand and incubated for another 5 minutes. The ethanol was subsequently removed, and the washing step was repeated. Following the second wash, the bead pellet was allowed to air dry for 10 minutes with the lid of the Eppendorf tube left open at room temperature. The dried bead pellet was re-suspended in 35 µl of Elution Buffer (Qiagen, #19086) and incubated for 2 minutes at room temperature and then placed back onto the magnetic stand for another 5 minutes. After complete separation of the beads the supernatant was carefully removed and transferred into a fresh Eppendorf tube. Following elution, the DNA concentration was determined using Qubit™ dsDNA BR Assay Kit (Qubit, #Q32853) following the manufacturer's instructions. Working solution (BR buffer:200 parts – BR reagent:1 part) was prepared for two standards and samples. For standards, 190 µl was aliquoted into a 0.5 ml clear PCR tube, whereas for samples, 199 µl of working solution was used and 10µl of each standard and 1µl of sample were added to the appropriate PCR tubes. Samples were vortexed and incubated for two minutes at room temperature. DNA concentrations were read on a Qubit Fluorometer by measuring the standards first. The library pool was then diluted in a final volume of 300 µl of DNase/RNase-free distilled water to yield a 4 nM final concentration. The library concentration was further determined using NEBNext® Library Quant Kit for Illumina® (NEB, #E7630S) according to the manufacturer's instructions. Library dilution (1:1000) was prepared in 1x dilution buffer (10x dilution buffer diluted in nuclease-free water), then two further ten-fold serial dilutions were prepared in 1x dilution buffer (1:10,000 and 1: 100,000). QPCR assays for standards (10-, 1-, 0.1-, 0.01pM concentrations) and library were set up using master mix (100 µl primer mix, 1.5 ml master mix and 20 µl ROS normalisation dye). 4 µl of DNA standard/sample dilution was added to 16 µl master mix. A no template DNA control was also included (4 µl of library dilution buffer was added to 16 µl of master mix.) The qPCR plate was sealed and centrifuged for 2 minutes at 2500

rpm and ran using Applied Biosystems 7500 machine (Table 2.12.6.1). Actual library concentration was determined using the Ct values obtained from qPCR, analysed using NEBiocalculator qPCR Library Quantification (https://nebiocalculator.neb.com/#!/qPCRlibQnt) online tool, generating a standard curve using the Ct values obtained for the 4 standards. When necessary, library concentrations based on the Ct values were adjusted to obtain the actual 4 nM final concentration. The library was then further diluted to 20 pM concentration by adding 5 µl of 0.2 N NaOH buffer and 900 µl of HT1 (Illumina MiSeq Reagent Nano Kit v2 300-cycles, #MS-103-1001) buffer to 5 µl of 4 nM library. The 20 pM library was further diluted in HT1 buffer to obtain a 12 pM final concentration. A final volume of 600 µl of 12 pM library supplemented with 12.5 pM PhiX Sequencing Control v3 spikes (Illumina, #FC-110-3001) was loaded into the MiSeq benchtop sequencing systems (Illumina).

| | | | |
|---|---|---|---|
| Step 1 | 95°C | 60 seconds | |
| Step 2 | 98°C | 15 seconds | 30 repeats |
| Step 3 | 63°C | 45 seconds | |

**Table 2.12.6.1 QPCR assay conditions.**

### 2.12.7 Limiting dilution of bulk edited cell populations

Frozen vials of bulk edited populations were thawed and grown to 60% confluency in DMEM+ medium. Cells were then gently scraped and centrifuged at 1000 rpm for 5 minutes. Cell number was calculated using trypan blue exclusion method and the cells were diluted to a density of 10 cells/ml. 20% of the DMEM+ culture medium was replaced with DH82 conditional medium. A total volume of 100 µl of cell suspension was added to each well of a flat-bottom 96-well cell culture plate. To increase the number of single cell colonies, up to 10 plates were plated for single cell cloning. Cells were incubated for one week at 37°C in 5% CO2. At the end of the first week, 100 µl of DMEM+ medium was added to each well and cells were incubated for an additional 7 days at 37°C in 5% CO2. Thereafter, each well was assessed for colonies originating from a single cell. Cells in selected wells were washed once with 100 µl of pre-warmed DPBS, then trypsinized

with 50 µl of 1x trypsin solution for 5 minutes at 37°C in 5% $CO_2$. After 5 minutes, trypsin was deactivated with 150 µl of pre-warmed DMEM+. Cells were gently pipetted up and down for a total of 5 times. Resulting cell suspensions were divided: 80 µl of cell suspension/well was dispensed across two 48-well cell culture plates and 40 µl of cell suspension/well into a flat-bottom 96-well cell culture plate. Cells in 48-well plates were left to adhere overnight then 80 µl of filtered freezing medium was added to each well. Plates were then sealed, wrapped in bubble wrap, placed into a polystyrene box and transferred into -80°C freezer overnight. The next day, plates were transferred to a -150°C freezer and stored until further analysis. Cells in 96-well plates were further cultured until 60% confluency after which DNA extraction and MiSeq library preparation were performed for subsequent single cell clone sequencing analysis as discussed previously.

### 2.12.8 Revival and expansion of single cell colonies

48-well cell culture plates containing single cell colonies were thawed at 37°C in 5% $CO_2$ and 1 ml of DMEM+ medium was added to each well. Cells were allowed to settle for a minimum of four hours at 37°C in 5% $CO_2$, prior to replacing the medium with 1 ml of fresh DMEM+ medium. Single cell colonies were left to recover for 48 hours at 37°C in 5% $CO_2$, followed by trypsinisation and were then transferred into T25 cell culture flasks. Cells were grown to 80% confluency at 37°C in 5% $CO_2$ and then harvested and transferred into T75 cell culture flasks. Upon reaching 80% confluency the cells were frozen down (in triplicates) in freezing medium.

### 2.12.9 Analysis of sequencing output fastq files

Sequences were analysed using the OutKnocker online analysis tool (http://www.outknocker.org/outknocker2.htm). Under Analyse Sequencing Data tab, crRNA sequences were added in capital letters into the Nuclease Target Site box in the same orientation as the reference genome, including Pam motifs. Up to 96 extracted fastq files were uploaded by using Select FASTQ files tab and evaluation of the results was executed by START ANALYSIS button. Under the Results tab, each clone is represented by a pie chart. The caspase-1/4/11 hybrid gene was utilised to illustrate the data output generated by the OutKnocker software for bulk-edited and single cell colonies (Figures 2.12.9.1 and 2.12.9.2, respectively). The size of the pie

chart relates to the number of amplicon reads for each clone and the area and colour of the pie chart sections demonstrate the relative abundance and type of indels identified based on sequence analysis. Colours in the shade of red represents frameshift insertions and deletions, while the colour blue denotes in-frame indels and grey colour label no indel events.

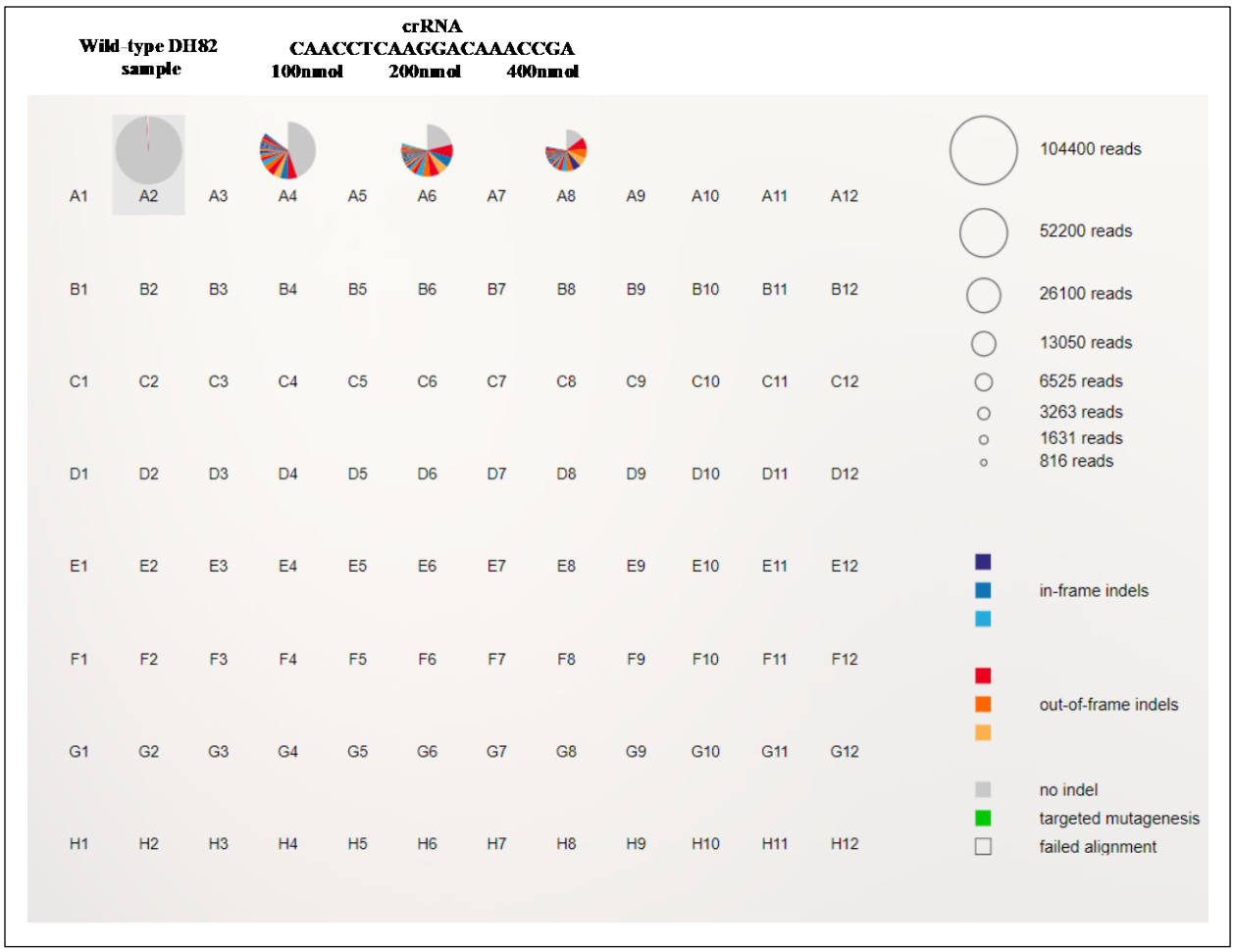


**Figure 2.12.9.1 Sequencing analysis of bulk-edited DH82 cell populations for indels induced by CAACCTCAAGGACAAACCGA crRNA for the canine caspase-1/4/11 hybrid gene.** DH82 cells were electroporated with RNP complexes prepared at three different concentrations (100, 200 and 400 nmol). crRNA was designed to be proximal to the catalytic site of the canine hybrid gene. Genotyping using Illumina MiSeq sequencing revealed that electroporated only wild-type cells displayed no genome modification, while Cas9-edited cells showed a mixture of in-frame and out-of-frame mutations. The size of each pie chart corresponds to the number of reads that were analysed for each sample (see legend in top right corner). Pie areas in the shade of red represents out-of-frame, areas in the shade of blue represents in-frame insertions and deletions, grey areas represent no indel calls (see legend in bottom right corner) while empty wedges show sequences that failed alignment.

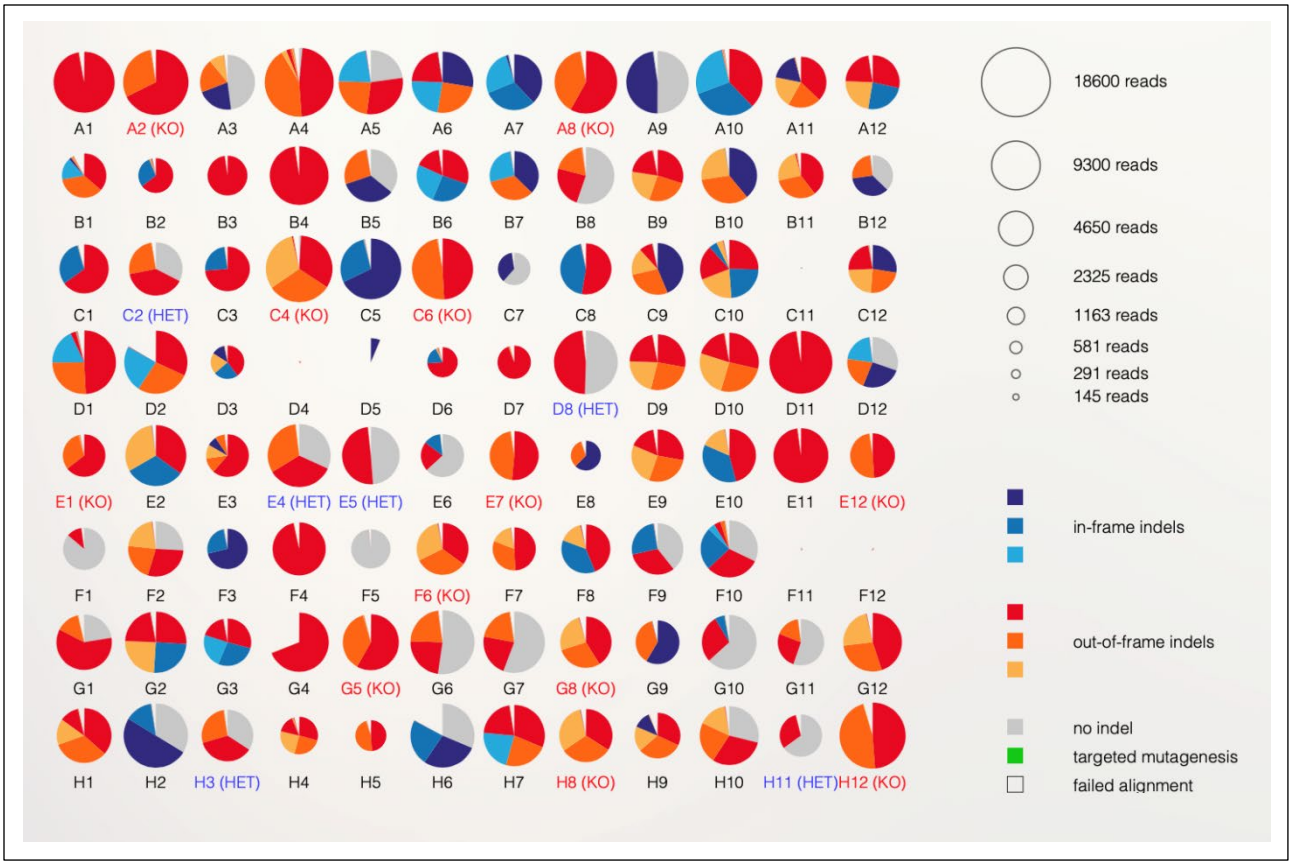


**Figure 2.12.9.2 OutKnocker analysis of 96 DH82 single cell colonies electroporated with CRISPR crRNA targeting the canine caspase-1/4/11 hybrid gene.** DH82 cells were electroporated with CRISPR crRNA GCATCCTGAATGGAATCTGT to target the canine hybrid caspase-1/4/11 gene. Following limiting dilution, up to 96 single cell colonies were selected and genotyped using Illumina MiSeq sequencing. Sequencing results were analysed using OutKnocker online analysis tool. Each pie chart represents a single colony, whereas the size of each pie chart corresponds to the number of reads that were analysed for each colony (see legend in top right corner). Pie areas in the shade of red represents out-of-frame, areas in the shade of blue represents in-frame insertions and deletions, while grey areas represent no indel calls (see legend in bottom right corner). Colony positions in red letters highlight knock-out colonies, while blue letters highlight heterozygous colonies for the canine caspase-1/4/11 hybrid gene.

Individual clones were selected by clicking on those pie charts displaying frameshift mutations. The sequences of selected clones aligned to the reference genome can be found at the bottom of

the results page. The letter size of the amplicon bases linearly correlates with the relative abundance of that specific base. Nucleotides with reduced confidence are illustrated with smaller letters to that of other bases. Bases outlined in red indicate mismatches to the reference genome. The caspase-1/4/11 hybrid gene was used to illustrate the data output for the list of different indels identified by the OutKnocker software for bulk-edited and single cell colonies (Figures 2.12.9.3 and 2.12.9.4, respectively).

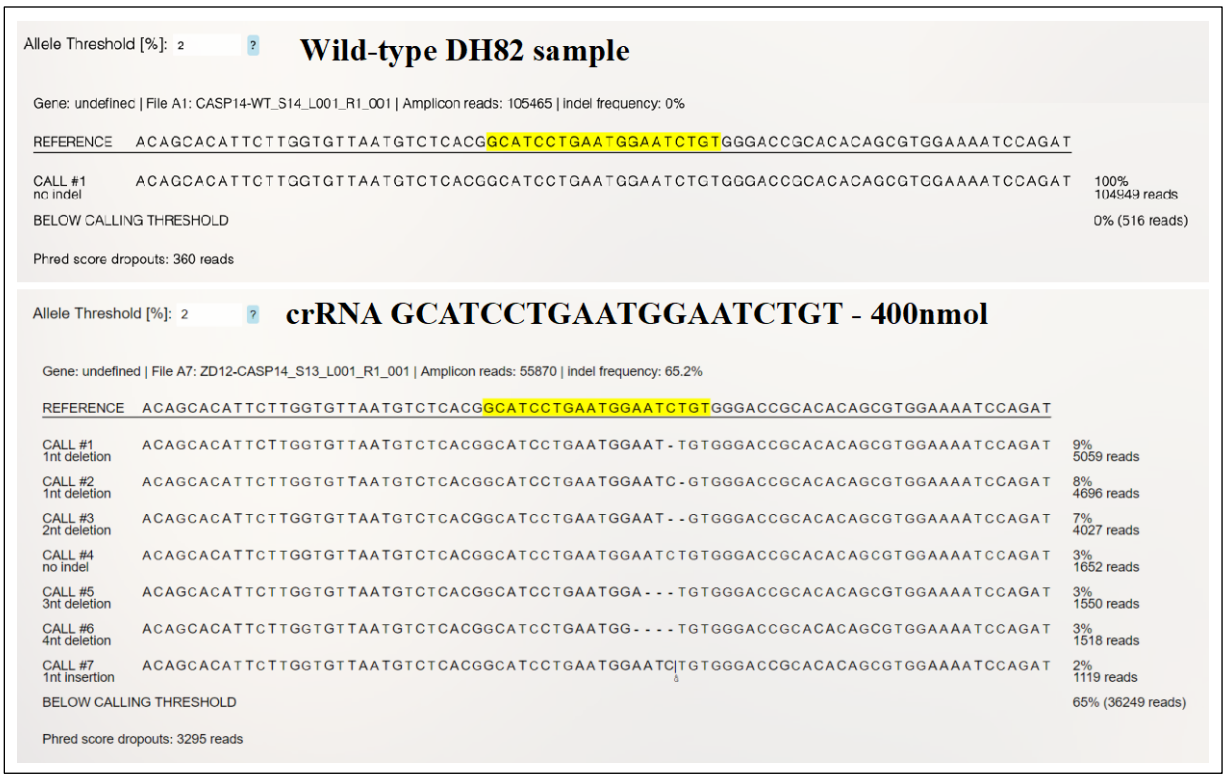


**Figure 2.12.9.3 List of different indels identified in bulk-edited DH82 cell populations by sequence analysis using GCATCCTGAATGGAATCTGT crRNA for the canine caspase-1/4/11 hybrid gene.** DH82 cells were electroporated with RNP complexes prepared at three different concentrations (100, 200 and 400 nmol). crRNA was designed to be near the catalytic site of the canine hybrid gene. Electroporated only wild-type DH82 cells yielded amplicon reads that matched exclusively the wild-type sequence, while Cas9 edited cells yielded amplicon reads that contained a mixture of in-frame and out-of-frame mutations. These results are indicative of the type, position, percentage and number of reads associated with each mutation present in the bulk edited population. The underscored nucleotide sequence represents the wild-type reference sequence, while nucleotides highlighted in yellow show CRISPR crRNA target site. Information including total percentage and total number of reads corresponding to each identified indel are shown underneath the reference sequence. Nucleotides shown in smaller font sizes are less confident calls based on the sequencing data, while nucleotides replaced with hyphens represents the position of nucleotides deleted by CRISPR Cas9. The software also provides information on the percentage and total number of reads that could not be aligned to the reference sequence and the number of reads that were excluded from analysis (Phred score dropouts).

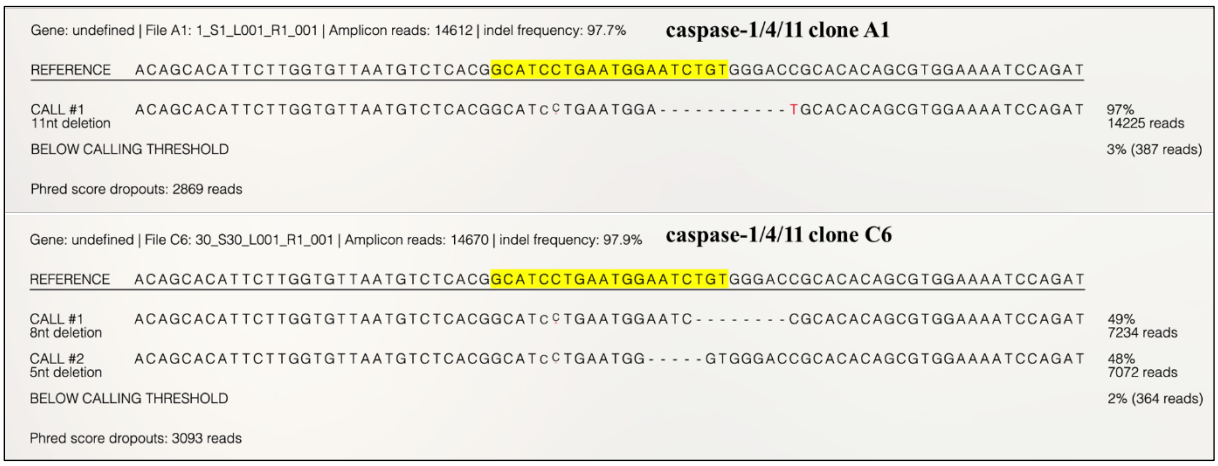


**Figure 2.12.9.4 Illumina MiSeq sequencing of caspase-1/4/11 identified out-of-frame indel mutations for colonies A1 and C6 are depicted near the catalytic site in exon 6.** DH82 cells were electroporated with CRISPR crRNA GCATCCTGAATGGAATCTGT to target the canine hybrid caspase-1/4/11 gene near the catalytic site. Following limiting dilution, up to 96 single cell colonies were selected and genotyped using Illumina MiSeq sequencing. Information displayed by the analysis software includes the file name, number of amplicon reads and indel frequency. The underscored nucleotide sequence represents the wild-type reference sequence, while nucleotides highlighted in yellow show CRISPR crRNA target sites. Information including total percentage and total number of reads corresponding to each identified indel are shown underneath the reference sequence. Nucleotides shown in smaller font sizes are less confident calls based on the sequencing data, while nucleotides replaced with hyphens represents the position of nucleotides deleted by CRISPR Cas9. The software also provides information on the percentage and total number of reads that could not be aligned to the reference sequence and the number of reads that were excluded from analysis (Phred score dropouts).

## 2.13 Genotyping of DogMo cells provided by Vishva Dixit, Genentech Research Institute

DNA extraction of murine DogMo and wild-type primary BMDMs were carried out on a minimum of $1x10^6$ cells/genotype using PureLink™ Genomic DNA Mini Kit (ThermoFischer Scientific, K1820-01). PCR protocol for locus-specific amplification was performed as follows, 10 µl of 2X Phusion HF Buffer (ThermoFisher F531L), 1 µl of 10 µM of each primer (Table 2.13.1) and

DNase/RNase-free distilled water to make a total of 20 µl reaction/sample. The contents of each well was thoroughly re-suspended, and samples were run on a BIO-RAD T100$^{TM}$ thermocycler (Table 2.13.2). Following PCR, amplicons generated were assayed for correct size by PAGE. 5µl of amplicons from each sample were resolved on a 1% agarose gel supplemented with 5x GelPilot DNA Loading Dye, 5x (Qiagen, #151047521). DNA ladder (New England BioLabs, #N0551G) was included on each gel and gel electrophoresis was performed at 100V for 40 minutes.

| | |
|---|---|
| Primer 1 (5'-3') | TTCTGTGTCATAGCCAAGTTC |
| Primer 1 (5'-3') | ATACTGTCTGTGTCCTTCTCA |
| Primer 1 (5'-3') | ACGAGTGGTTGTATTCATTATTG |

**Table 2.13.1 List of primer designs for confirmation of DogMo and wild-type genotypes.**

| | | | |
|---|---|---|---|
| Step 1 | 94°C | 4 minutes | |
| Step 2 | 94°C | 1 minute | 30 repeats |
| Step 3 | 60°C | 30 seconds | |
| Step 4 | 72°C | 1 minute | |
| Step 5 | 72°C | 10 minutes | |
| Step 6 | 4°C | HOLD | |

**Table 2.13.2 Genotyping assay conditions.**

## 2.14 Phylogenetic tree building of mammalian caspases

For this work the NCBI reference sequence was used for the catalytic domain of caspase-1 isoform alpha precursor (NP001244047). This sequence was used for Position Specific Iterated (PSI) – Basic Local Alignment Search Tool (BLAST) (https://blast.ncbi.nlm.nih.gov/Blast.cgi?CMD=Web&PAGE=Proteins&PROGRAM=blastp&RUN_PSIBLAST=on) against the human protein reference database (protein_refseq) and downloaded sequences for caspases (1-10, 12 and 14). Multiple Sequence Comparison by Log-Expectation (MUSCLE) (https://www.ebi.ac.uk/Tools/msa/muscle/) was used to generate a multiple sequence alignment of the human caspases and to identify the first and last fully conserved

residues. Using this identified conserved sequence, a Position-Specific Scoring Matrix (PSSM) was constructed using PSI-BLAST against the human reference protein database. Two iterations of PSI-BLAST were run with the default selected sequences to maximise the number of identifiable sequences with caspase catalytic domains. Sequences for each caspase displaying 100% coverage to the query sequence were used to generate the PSSM. The human PSSM was uploaded and the PSI-BLAST was run against different mammalian species (Table 2.14.1). Putative and confirmed caspases were identified based on their query cover, percentage of alignment and e-values. Preparation of identified putative and confirmed caspase protein sequences for phylogenetic tree building was carried out using UGENE bioinformatics toolkit (http://ugene.net). Protein sequences were aligned using ClustalW within the UGENE software. Identified misalignments were manually reviewed and first positions containing gaps at the start and at the end of the sequences were deleted and each column containing any sequence gaps were also removed. Once satisfied with the sequence alignment, a neighbour-joining phylogenetic tree was built using the PHYLIP phylogenetics package. Neighbour-joining allows a fast analysis generating a single possible phylogenetic tree to investigate sequence homology and therefore establish relationships. It also allows the assessment of confidence levels by bootstrapping where the higher the number displayed on each part of the tree means more confident grouping within the branch. The generated phylogenetic tree was displayed using FigTree graphical viewer of phylogenetic trees (http://tree.bio.ed.ac.uk/software/figtree/)

| **Common name** | **Scientific name** | **Ensembl taxon ID** |
|---|---|---|
| Cat | *Felis catus* | 9685 |
| Chimpanzee | *Pan troglodytes* | 9598 |
| Dog | *Canis lupus familiaris* | 9615 |
| Human | *Homo sapiens* | 9606 |
| Mouse | *Mus musculus* | 10090 |
| Pig | *Sus scrofa* | 9823 |
| Platypus | *Ornithorhynchus anatinus* | 9258 |
| Tasmanian devil | *Sarcophilus harrisii* | 9305 |

**Figure 2.14.1 List of mammalian species investigated in caspase sequence analysis.**

## 2.15 Statistical analysis

The work described in Chapter 3 and Chapter 4 of this thesis was focused on the characterisation of inflammatory responses in the dog using a canine immortalised macrophage-like cell line, DH82. Responses to the chosen panel of ligands have previously been established in the murine equivalent. I therefore used these immortalised murine cells as internal experimental controls to ensure that the experimental results I obtained for the DH82 cells were reliable. However, there are a number of additional differences (including PRR and caspase repertoire) that exist between the two species which could potentially drive or influence the observed phenotypic differences. Consequently, I chose not to perform statistical analysis but instead compare and contrast the overall trends observed between the murine and canine macrophages.

In Chapter 5 I aimed to identify genes driving the DH82 cell lytic responses and IL-1β release following *S.* Typhimurium infection. In these experiments the objective was to prevent cell lysis and therefore abrogate IL-1β release. The observed difference between the genetically altered cell lines were either negligible or pronounced but due to time limitations, only a small proportion of recovered clones were characterised. Therefore, statistical analysis would not have yielded any valuable information but instead highlight variation within the selected clones.

The primary aim of the work described in Chapter 6 of this thesis was to characterise Dog-Mouse (DogMo) primary bone marrow derived macrophages containing the hybrid caspase-1/4/11 fusion gene. However, due to the limited number of available frozen primary DogMo BMDMs, only a maximum of two independent experiments could be performed for each selected ligand. Consequently, statistical analysis therefore could not be performed on the limited datasets.

Statistical analysis could be performed for each individual experiment where at least three independent experiments are available using the latest version of Prism software (currently version 8.4.2, GraphPad). Depending on the number of experimental groups, the data type and the number of qualitative variables, statistical difference could be determined using either one-way analysis of variance (ordinary one-way ANOVA) with Tukey's multiple comparison post-test or unpaired t-test. The mean values of the triplicate wells within each independent experiment would be

calculated and the resulting three mean values would then be used for statistical analysis. For experiments using sterile ligands, cell line responses for each concentration would be compared separately while for infection assays the values for the different cell lines would be compared for each infection time-point. A p-value below 0.05 would be considered to be significant.

# Chapter 3

# Characterisation of the DH82 cell line responses to well characterised inflammasome activators

## 3.1 Introduction

Inflammasomes play a critical role in the defence against microbial infections [314]. Their assembly results in the activation of inflammatory caspases, which leads to the processing and maturation of the pro-inflammatory cytokines, pro-IL-1β and pro-IL-18 [6] and initiation of pyroptosis via GSDMD cleavage [43], [44] and subsequent membrane pore formation. Understanding mechanisms regulating inflammasome activation and regulation is an intense area of research and studies are predominantly carried out in rodent and human systems. Much less is known about inflammasomes in other species. Genomic and proteomic analysis of different species has identified significant differences in key genes that regulate innate immunity that raises questions about fundamental aspects of inflammasome evolution and its role in host immunity. Bioinformatics analysis of canine inflammatory caspases, for example, reveals that caspase-1 and canine caspase-4/11 equivalent has formed a fusion gene product whose function remains undetermined. In this chapter, I will describe the characterisation of putative canine inflammasome responses to a range of sterile insults in a canine cell line (DH82) and primary canine peripheral blood mononuclear cells (PBMCs).

The canine DH82 macrophage-like cell line has been primarily used to investigate pathological disorders [315] and pathogenic infections [316]–[319] in the context of veterinary science. Ensembl genome browser (https://www.ensembl.org/index.html) contains reference genomes, including genes (ENSG) and their transcript (ENST) sequences for multiple species, including the dog (CanFam3.1). Many genes important in inflammatory responses in mice and humans are also annotated in the dog. This includes NLRP3 (ENSCAF00000010686), IL-1β (ENSCAF00000007249) and GSDMD (ENSCAF00000001301). There are, however, remarkable differences between some of the genes involved in inflammatory responses. Comparative genomic sequence analysis has shown that the *NAIP* gene is absent and the *NLRC4* gene contains multiple premature stop-codons in the dog genome [41]. Genomic sequence analysis has further shown that

the dog caspase-1 gene has lost its 3' end sequences, while the adjacent gene caspase-4 has lost its 5'end regions [154]. This results in the expression of a hybrid gene, encoding the N-terminal CARD domain of caspase-1 and the C-terminal caspase domain of caspase-11 genes [154] (Figure 3.1.1). Reverse transcription polymerase chain reaction (RT-PCR) analysis of PBMCs showed alternative mRNA splicing of the gene, producing two alternative transcripts [154]. The smaller transcript consists of the CARD domain similar of the human and mouse caspase-1 genes and the caspase domain similar of the human caspase-4/-5 and murine caspase-11 genes. By contrast, the larger transcript includes the CARD domain similar of the human caspase-4/-5 and murine caspase-11 genes, resulting in two tandem CARD domains (Figure 3.1.1).

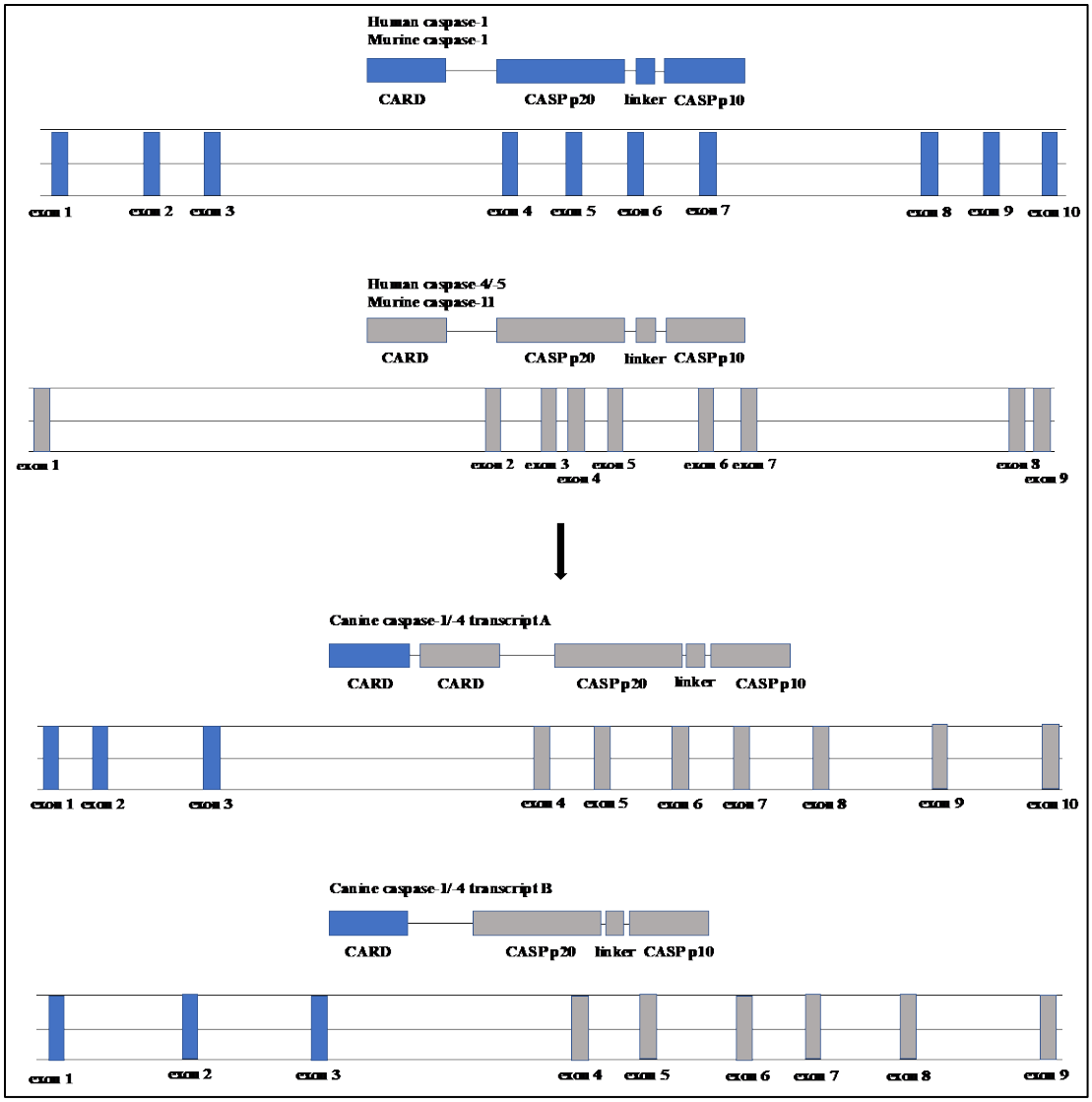


**Figure 3.1.1 Domain organisation of the dog caspase-1/4/11 hybrid protein.** The gene encoding the canine hybrid protein can produce two alternative transcripts. (Transcript A) The larger transcript contains two tandem CARDs and a caspase domain. The first CARD domain shows high sequence homology to the CARD domain of human and murine caspase-1. While the second CARD domain shows high sequence similarities to the CARD domain of human caspase-4/-5 and murine caspase-11. The caspase domain shows high similarities to the caspase domain of human caspase-4/-5 and murine caspase-11. (Transcript B) By contrast, the shorter transcript excludes the second CARD domain, resulting in a gene sequence consisting of a CARD domain similar to human and murine caspase-1 and the caspase domain similar to human caspase-4/-5 and murine caspase-11.

Species-specific differences in caspases are present in both invertebrate and vertebrate species, but the functional consequence of these differences is unclear in the host response to infections and inflammatory stimuli. Here, I have performed multiple sequence alignment (MUSLCE) analysis of transcripts of the main inflammatory genes found in the human, mouse and dog genomes to assess the similarities in catalytic residues essential for function and therefore protein activity. I have also characterised a canine histiocytic macrophage-like DH82 cell line and its responses to well characterised inflammatory activators in a series of *in vitro* experiments. Canonical activation of the NLRP3 inflammasome was carried out using nigericin bacterial toxin, while non-canonical NLRP3 inflammasome was activated using cytosolic LPS. Inflammasome activity was determined by measuring cell lysis (relative LDH release), ASC speck formation, fluorescent caspase probe localisation and the production and maturation of IL-1β. Morphological changes induced by these activators were also monitored by live cell imaging using bright-field microscopy.

### 3.2 Investigation of the dog hybrid caspase-1/4/11 gene using multiple sequence comparison by log-expectation (MUSCLE) analysis of its transcripts and mass spectrometry analysis of its protein expression

Previous genomic analysis has shown the gene sequence organisation of the caspase-1/4/11 hybrid gene and the production of its two alternatively spliced mRNA transcripts [154]. Gene expression however at the protein level has not yet been shown. While the caspase-1 gene is constitutively expressed in cells [160], human caspase-5 [182] and murine caspase-11 [160] expression requires priming. To investigate whether the canine caspase-1/4/11 hybrid gene is expressed at the protein level and whether the expression requires priming, mass spectrometry analysis of full protein extracts was performed by the Cambridge Centre for Proteomics (CCP) Core Facility. Extracted proteins from DH82 cells were prepared without any treatment (medium only) (Figure 3.2.1A) or after LPS priming (200 ng/ml for 3 hours) (Figure 3.2.1B) and submitted for analysis. SDS/PAGE gel electrophoresis of each sample (12 µg) was run and gels were stained with Coomassie colloidal stain. Bands between the 32 kDa and 58 kDa molecular weight markers corresponding to the predicted protein sizes of the canine caspase fusion protein were cut out and mass spectrometry was performed.

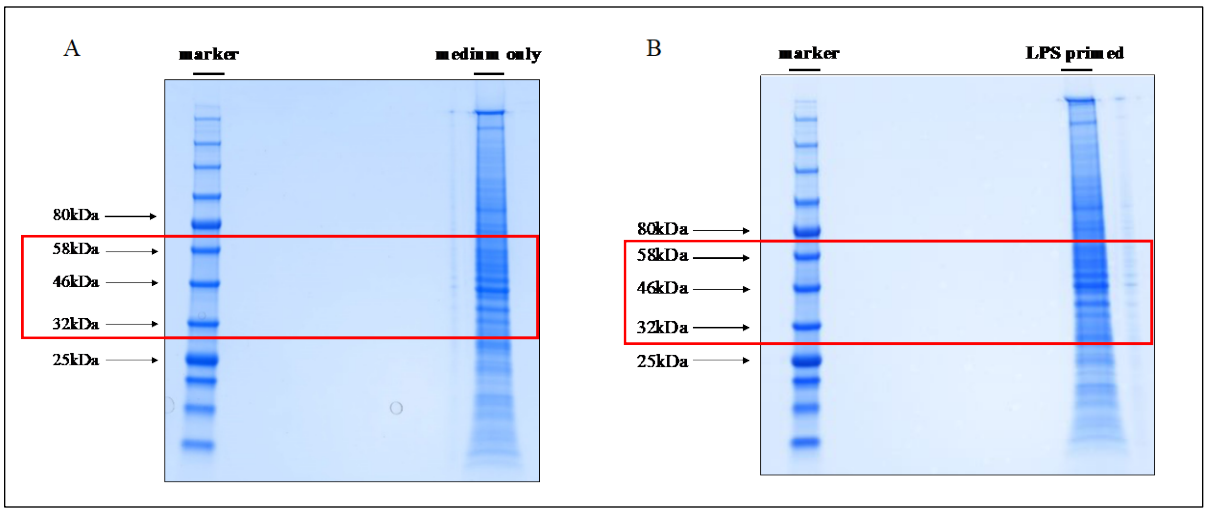


**Figure 3.2.1 Gel image of full protein extractions from non-stimulated (medium only) and LPS primed DH82 cell lysates.** Medium only (A) and LPS primed (B) samples were cut out between the 32 kDa and 58 kDa molecular weight markers (area marked with red rectangles) and prepared for mass spectrometry analysis by the Cambridge Centre for Proteomics (CCP) Core Facility.

Analysis of mass spectrometry results using Mascot database showed the expression of the hybrid gene at the protein level in DH82 cells (Figure 3.2.2). The hybrid gene is constitutively expressed for the reason that the protein was detected in the non-stimulated (medium only) (Figure 3.2.2A), as well as the LPS primed samples (Figure 3.2.2B). The hybrid gene consisting of the 5'end of caspase-1 including the promoter region explains the constitutive expression of the protein [154]. Unfortunately, the analysis could not differentiate between the two transcripts as regions common to both were detected by mass spectrometry (Figure 3.2.2).

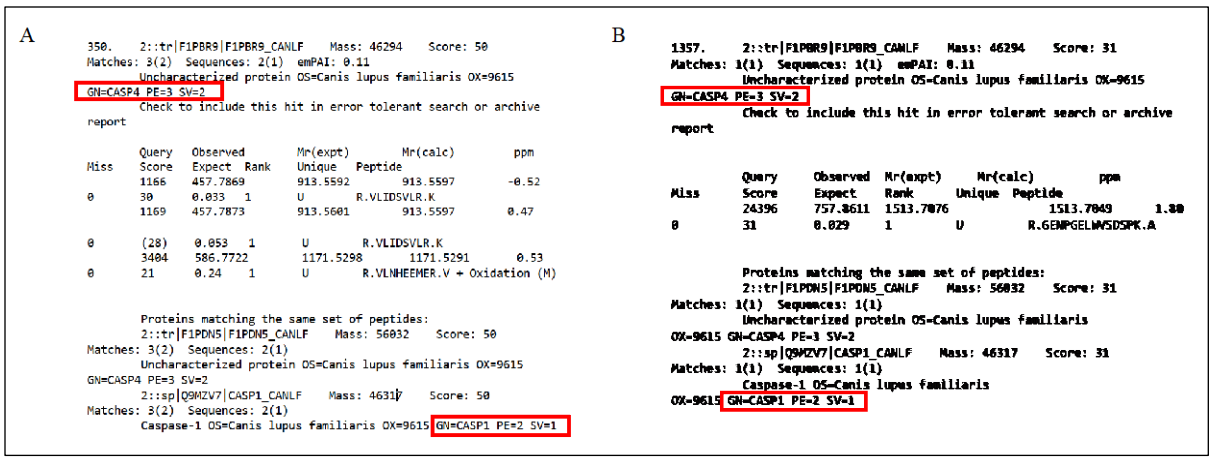


**Figure 3.2.2 Mass spectrometry analysis shows constitutive expression of the dog caspase-1/4/11 hybrid gene.** Mass spectrometry analysis of full protein extracts from (A) non-stimulated (medium only) and (B) LPS primed DH82 cell lysates showed constitutive expression of the hybrid gene. This detection method could not distinguish between the two transcripts as only amino acids common to both were detected. Proteins matching the same peptide sequence are highlighted in red rectangles.

Multiple sequence alignment analysis of the dog fusion gene (ENSCAFG00000014860, ENSCAFT00000036213.3, ENSCAFT00000023587.3), human caspase-4 (ENSG00000196954, ENST00000393150.7) and mouse caspase-11 (ENSMUSG00000033538, ENSMUST00000027012.13) indicated high similarities in the caspase domains. The caspase family signature peptide QACRG (highlighted in red rectangle) including the catalytic residue (258-Cys) responsible for enzymatic activity and autocatalysis [320]–[322] is present and conserved in the dog (Figure 3.2.3). These results suggested that the canine caspase-1/4/11 hybrid protein is functional in the dog.


**Figure 3.2.3 Multiple sequence alignment of transcripts of the dog fusion protein, human caspase-4 and mouse caspase-11 suggests catalytically active canine hybrid protein.** Protein sequences in the caspase domain showed high degrees of similarity between mouse caspase-11, human caspase-4 and canine hybrid protein larger (dog1) and smaller transcripts (dog2). The catalytic residue at 258-Cys position appeared to be conserved. This suggested that the dog fusion protein possesses enzymatic activity and is capable of autocatalysis.

### 3.3 Investigation of the inflammasome regulator ASC and executor of pyroptosis GSDMD transcripts using multiple sequence comparison by log-expectation (MUSCLE) analysis of transcript sequences and western blot analysis of their protein expression

One hallmark of inflammasome activation is the recruitment of the universal adapter protein ASC to the activated receptors [42]. Heteromeric aggregation of the ASC serves as a scaffold leading to caspase recruitment, activation and subsequent cytokine processing [57], [323]. The gene encoding ASC has not yet been annotated in the dog genome. Using Basic Local Alignment Search Tool (BLAST) analysis of human ASC protein sequence (ENSG00000103490, ENST00000247470.10) against the dog genome indicated that the gene has not yet been annotated as a whole (https://www.ensembl.org/Canis_familiaris/Tools/Blast/Results?db=core;tl=mUzCEkqzMWFnc6wi-5421405). The presence of a short intermediate exon containing flexible residues can make it difficult for automated gene prediction. The human ASC protein sequence (ENSG00000103490, ENST00000247470.10) therefore was searched in translated BLAST nucleotide (tBLASTn) (https://blast.ncbi.nlm.nih.gov/Blast.cgi?PROGRAM=tblastn&PAGE_TYPE=BlastSearch&LINK_LOC=blasthome) against the canine Expressed Sequence Tag (EST) database (Figure 3.3.1). MUSCLE analysis of the predicted ASC (GR890948.1 and DN347564.1) protein sequence against the human (ENSG00000103490, ENST00000247470.10) and murine (ENSMUSG00000030793, ENSMUST00000033056.4) ASC amino acid sequences suggested the expression of functional ASC protein in the dog (Figure 3.3.1). Targeted mutagenesis of the human ASC protein identified a number of residues to be important in heteromeric aggregation [324]. The majority of these residues (highlighted with red rectangles in Figure 3.3.1) appeared to be conserved between mouse, human and dog ASC amino acid sequences.

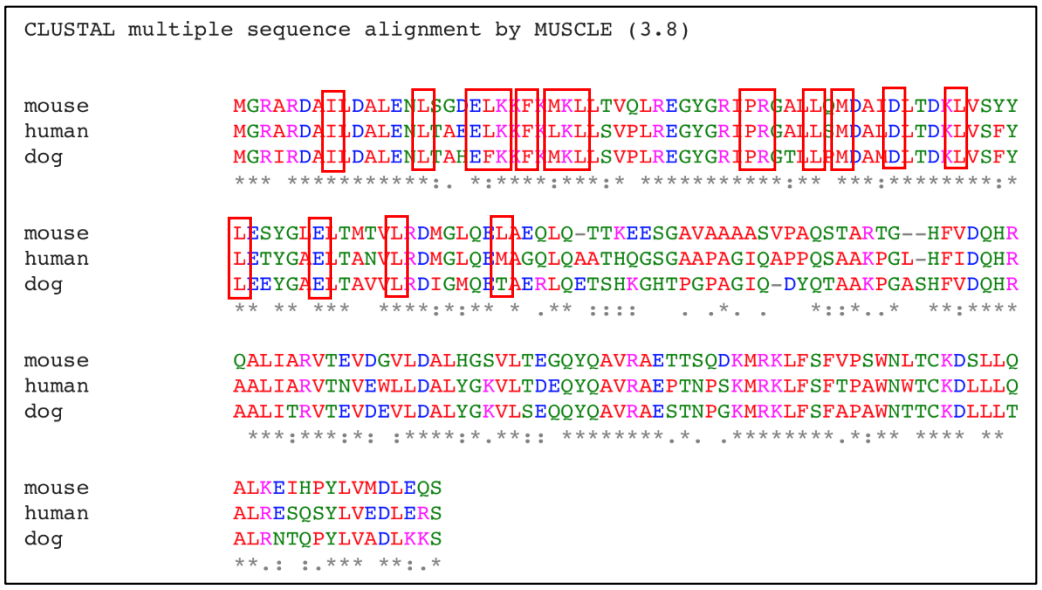


**Figure 3.3.1 Translated Basic Local Alignment Search Tool nucleotide (tBLASTn) and Multiple Sequence Comparison by Log Expectation (MUSCLE) analysis of human ASC protein sequence against the dog genome identified a not yet annotated gene encoding ASC (GR890948.1 and DN347564.1) in the dog.** The identified dog ASC showed high sequence similarities to the murine (ENSMUSG00000030793, ENSMUST00000033056.4) and human ASC (ENSG00000103490, ENST00000247470.10) amino acid sequences. The majority of the residues found to be important in PYD filament formation (highlighted in red rectangles) are conserved among human, mouse and dog sequences.

Western blotting analysis of cell lysates against ASC protein extracted from murine immortalised wild-type (Figure 3.3.2A and D), *Asc*$^{-/-}$ (Figure 3.3.2C) and canine DH82 (Figure 3.3. B and E) macrophages were carried out as described in Materials and Methods sections 2.9 and 2.11. Two-fold protein dilution from each cell line was run and blotted against ASC using primary and HRP-conjugated secondary antibodies. Primary ASC antibody includes a synthetic peptide sequence which corresponds to amino acids in the N-terminal PYD domain of human ASC. This similarity could result in cross reaction of the primary ASC antibody with the dog ASC protein. As expected, ASC protein in lysates of murine wild-type cells was detected at the 22 kDa [67] marker (Figure 3.3.2A) while using secondary antibody only (Figure 3.3.2D) resulted in no protein detection, showing the specificity of the primary antibody. As a further control to secondary antibody only

staining, analysis of lysates from *Asc*$^{-/-}$ cells failed to show any ASC protein (Figure 3.3.2C). The secondary antibody only control for the DH82 cell lysates (Figure 3.3.2E) showed no protein detection, suggesting that any bands detected with the primary antibody was sequence specific. Based on the tBLASTn results (Figure 3.3.1) dog ASC also has an expected size of 22 kDa. The presence of multiple bands was identified, including a strong band just under the 46 kDa marker. This band can possibly be dimerized ASC protein which could potentially be the result of poor reduction of intra- and intermolecular disulphide bonds (Figure 3.3.2B) during sample preparation.

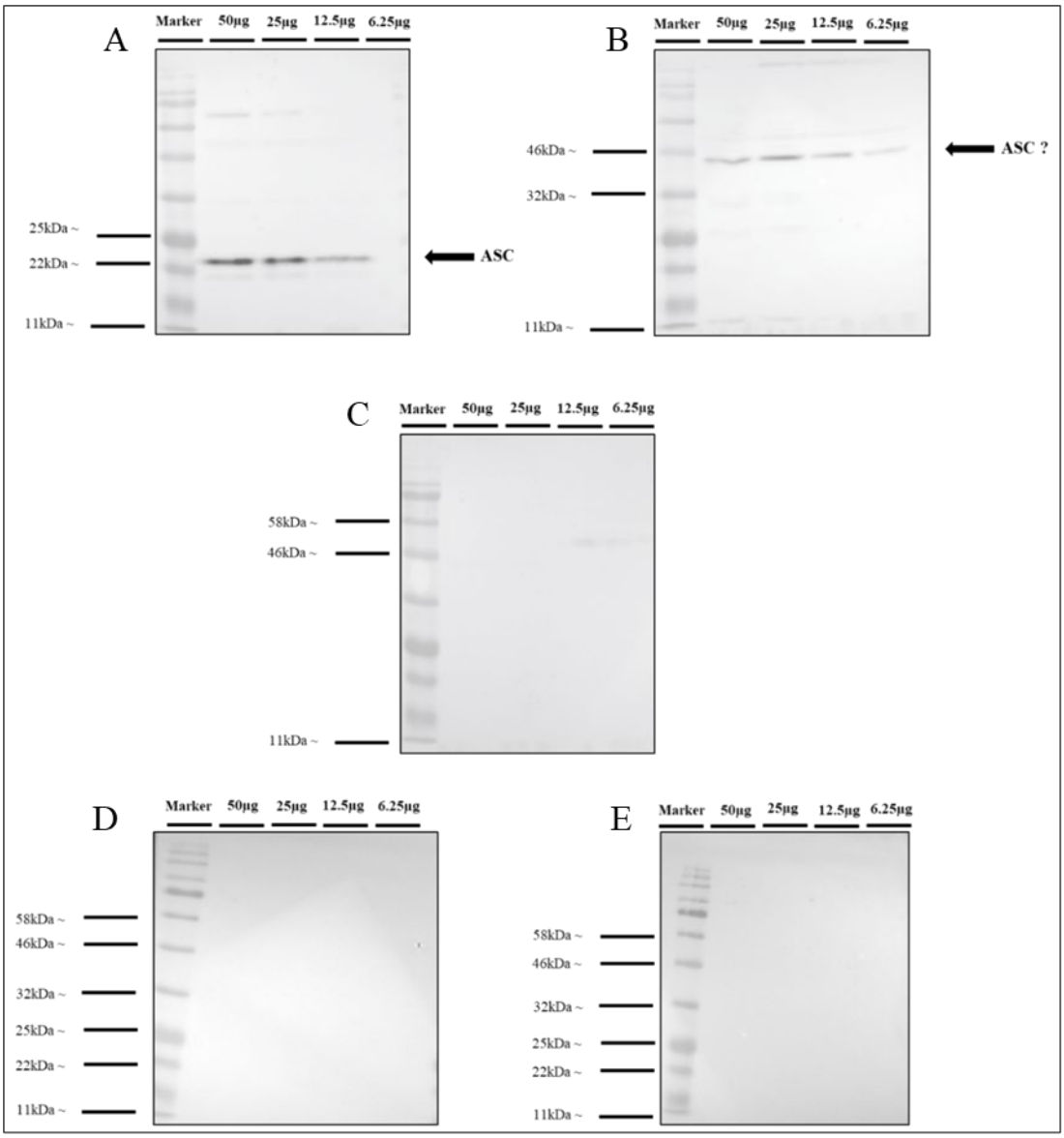


**Figure 3.3.2 Western blotting analysis of full protein extracts of immortalised murine wild-type, *Asc*$^{-/-}$ and DH82 cell lysates using primary anti-ASC and HRP-conjugated secondary antibodies.** Two-fold serial dilution of full protein extracts were run for each cell line and blotted against ASC protein. (A) Murine ASC was detected at the expected 22 kDa size. (B) Multiple bands were detected in the cell lysate of DH82 cells, including a strong band just under the 46 kDa marker. (C) ASC could not be detected in full protein extracts of murine *Asc*$^{-/-}$ cells. (D-E) Secondary antibody controls showed no unspecific antibody binding in cell lysates from either (D) wild-type or (E) DH82 cells. Representative immunoblots are from three independent experiments.

Inflammasome formation and caspase activation drives maturation of inflammatory cytokines and their release due to pyroptotic cell death [42]. Members of the gasdermin protein family are important inflammatory caspase substrates, including the pyroptosis executioner protein GSDMD [228]. Genome wide CRISPR-Cas9 screens of murine BMDMs [44] and ethyl-N-nitrosourea-mutagenized (ENU) mice [43] screens identified GSDMD as a human caspase-1/-4/-5 and murine caspase-1/-11 substrate. GSDMD cleavage by activated inflammatory caspases removes the inhibitory C-terminal domain, generating an active, effector N-terminal domain [44]. The active N-terminal domain has been shown to bind to cardiolipin, phosphatidylserine and phosphatidylinositol phosphates in the cell membrane causing pore formation that leads to pyroptotic cell death and the release of inflammatory cytokines [70], [72], [75]. The gene encoding GSDMD has been annotated in the dog genome. MUSCLE analysis of dog GSDMD (ENSCAFG00000001301, ENSCAFT00000038192.2) against human (ENSG00000104518, ENST00000262580.9) and murine (ENSMUSG00000022575, ENSMUST00000023238.5) protein sequences showed high similarities (Figure 3.3.3). Sequence analysis showed that the catalytic site (275-Asp) for caspase-1, caspase-4 and caspase-11 cleavage (marked with red rectangle) is conserved [44], suggesting functional GSDMD in the dog (Figure 3.3.3).


**Figure 3.3.3 Multiple sequence comparison by log-expectation (MUSCLE) analysis of dog against human and murine GSDMD amino acid sequences identified caspase-1 and caspase-4 cleavage site to be conserved.** Transcript analysis of dog (ENSCAFG00000001301, ENSCAFT00000038192.2), human (ENSG00000104518, ENST00000262580.9) and murine (ENSMUSG00000022575, ENSMUST00000023238.5) protein sequences encoding GSDMD showed high similarities between all three species with the catalytic residue (highlighted in red rectangle) in the caspase-1, caspase-4 and caspase-11 cleavage site being conserved.

Caspase activation and subsequent GSDMD cleavage results in the generation of an active N-terminal domain responsible for the execution of pyroptotic cell death [70], [72], [75]. Western blotting analysis of *S.* Typhimurium infected DH82 cell lysates were carried out in order to investigate GSDMD cleavage. DH82 cells were infected with wild-type *S*. Typhimurium bacteria at an MOI of 1 for 24 hours as described in Materials and Methods section 2.5. Total cellular lysate protein extracts were prepared, subjected to SDS-PAGE and immune blotted with primary and HRP-conjugated secondary antibodies as described in Materials and Methods sections 2.9 and 2.11. There is a deficit in available anti-sera for canine research, therefore I utilised three different primary antibodies that are commercially available and were raised against murine (Saint John's and Abcam) or human (Santa Cruz) GSDMD protein. Western-blot analysis of cell lysates from DH82 cells infected with wild-type *S*. Typhimurium failed to detect any protein bands when a murine specific primary antibody from Abcam was used (Figure 3.3.4B). The remaining antisera from St John's and Santa Cruz detected multiple protein bands (Figure 3.3.4A and C), none of which were in the region expected for the full length (~50 kDa) or N-terminal cleaved domain (~30 kDa) forms of GSDMD. Furthermore, secondary antibody only controls for the Saint John's (Figure 3.3.4D) and Santa Cruz (Figure 3.3.4E) antibodies, detected the same bands, suggesting non-specific binding. These results unfortunately prevented further analysis of GSDMD processing in canine macrophages by immunoblot.

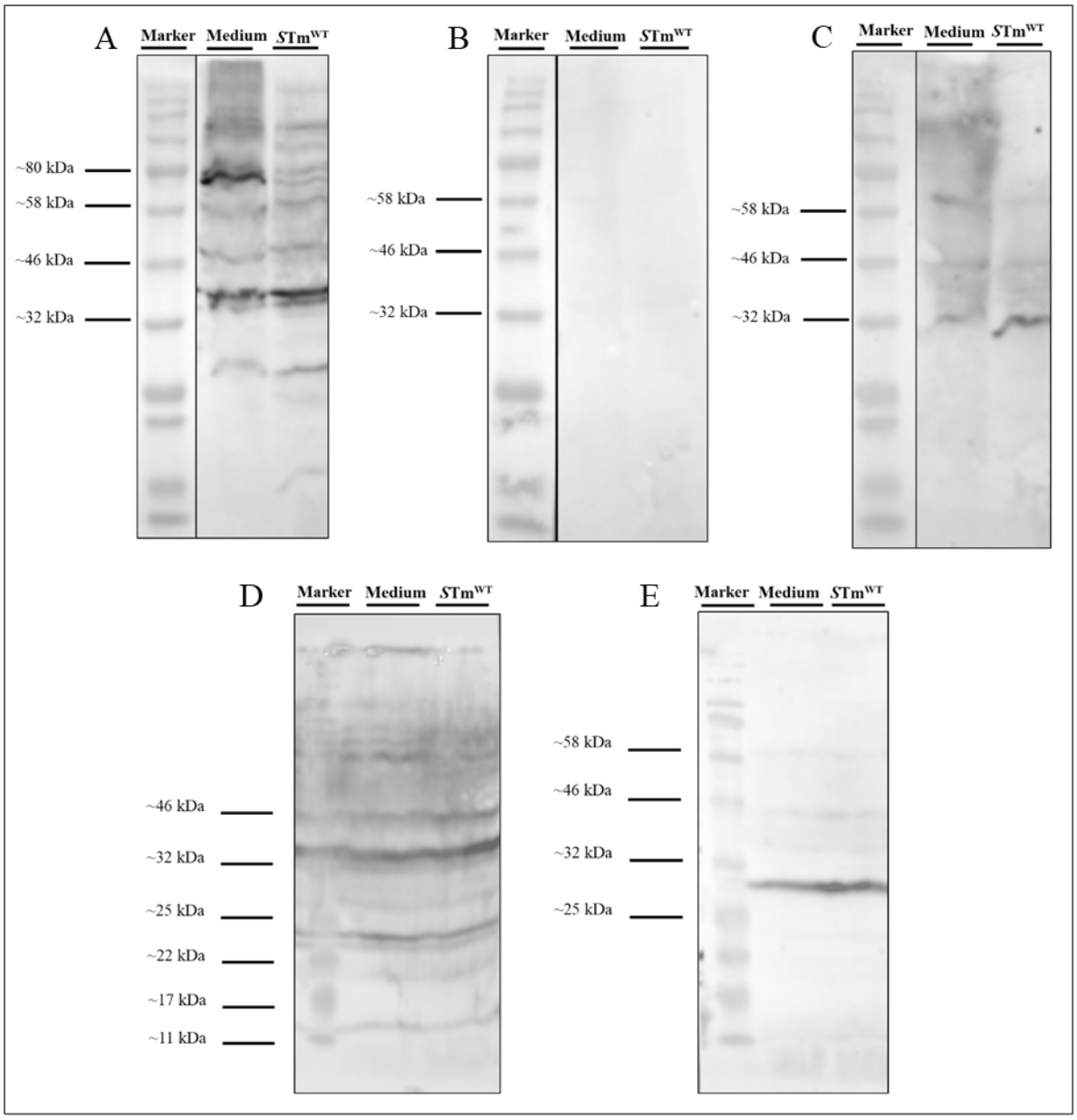


**Figure 3.3.4 Immuno blotting of GSDMD protein from DH82 cell lysates infected with *S.* Typhimurium with an MOI of 1 for 24 hours.** Three different primary antibodies were used, two raised against murine GSDMD; one from Saint John's (A) and one from Abcam (B). The third antibody was raised against human GSDMD from Santa Cruz (C). While Abcam antibody failed to detect any protein bands (B), bands detected with Saint John's (A) and Santa Cruz (C) antibodies suggested non-specific binding based on the results obtained with HRP-conjugated secondary antibody only staining (D and E). Representative immunoblots are from two independent experiments.

### 3.4 Multiple sequence comparison by log-expectation (MUSCLE) analysis of the dog, human and mouse NLRP3 and IL-1β sequences

NLRP3 forms inflammasome complexes [78] in response to a wide range of stimuli [83], [325]. Upon canonical NLRP3 activation, NLRP3 recruits ASC and activates pro-caspase-1 within the complex. Although NLRP3 activation can occur also downstream of the non-canonical caspase-11 inflammasome activation [60], [158], [326]. Multiple sequence alignment of canine (ENSCAFG00000010686, ENSCAFT170023), human (ENSG00000162711, ENST00000336119.7) and mouse (ENSMUSG00000032691, ENSMUST00000101148.8) NLRP3 protein sequences showed high level of homology suggesting conserved function throughout different species. Residues (amino acids: 15-Glu, 23-Lys, 24-Lys, 27-Met, 43-Arg, 64-Glu and 82-Asp) which have been associated with roles in nucleation of the ASC aggregates [323] based on mutagenesis studies appeared to be conserved (Figure 3.4.1). Sequence alignment analysis suggested that dogs have functional NLRP3 capable of ASC aggregate nucleation.

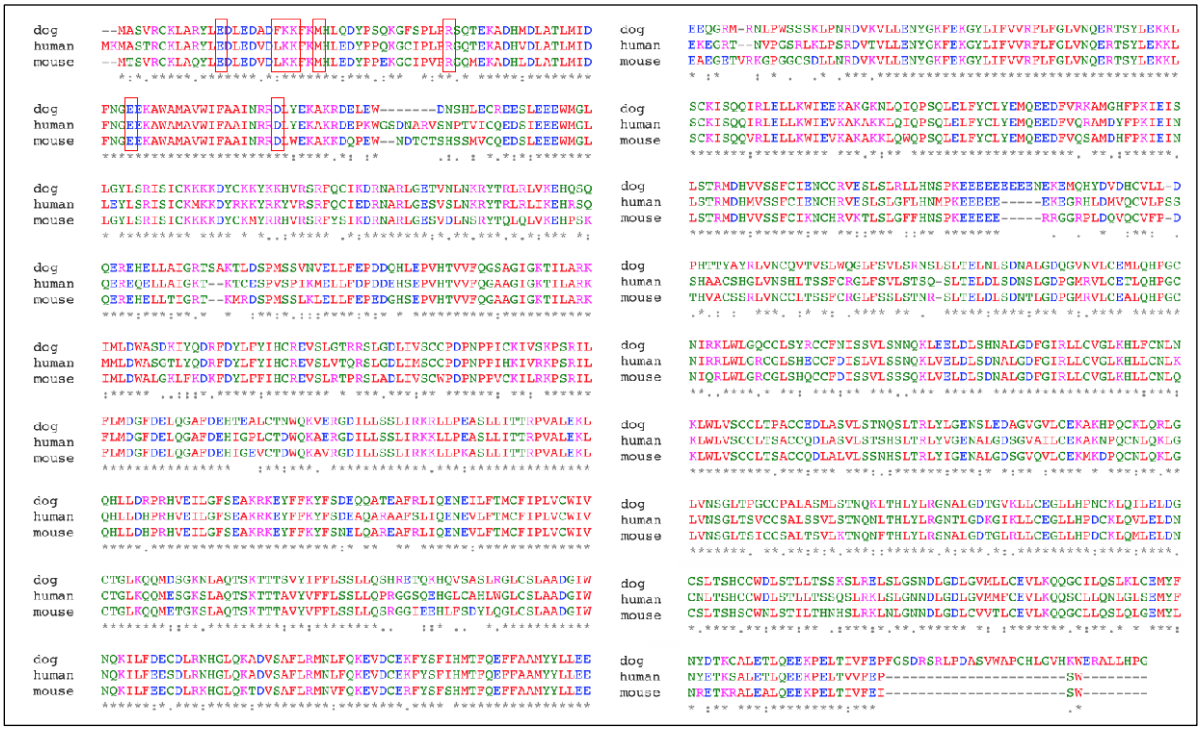

**Figure 3.4.1 Multiple sequence alignment analysis of dog, human and mouse NLRP3 amino acid sequences suggest an NLRP3 homologue is present in the dog.** Protein sequence alignment shows high similarity between the dog (ENSCAFG00000010686, ENSCAFT170023), human (ENSG00000162711, ENST00000336119.7) and mouse (ENSMUSG00000032691, ENSMUST00000101148.8) NLRP3. Amino acid residues (highlighted in red rectangles) associated with nucleation of ASC aggregates can be found, therefore appear to be conserved in the dogs.

In addition to NLRP3 I also performed multiple sequence alignment analysis of the dog (ENSCAFG00000007249, ENSCAFT00000011613.3), human (ENSG00000125538, ENST00000263341.6) and mouse (ENSMUSG00000027398, ENSMUST00000028881.13) IL-1β protein as this is a critical inflammatory mediator and substrate of active caspase-1 produced as a consequence of NLRP3 activation. Importantly, the sequence analysis demonstrated a high degree of sequence similarities between species, which like NLRP3 suggested conserved function in different mammalian species. Amino acid residues 27-Asp and 116-Asp functioning as caspase-1 and caspase-1/-8 cleavage sites [327], respectively can also be found in the dog (Figure 3.4.2).

These results suggested potential pro-IL-1β cleavage and maturation by the activated canine hybrid caspase-1/4/11 protein.

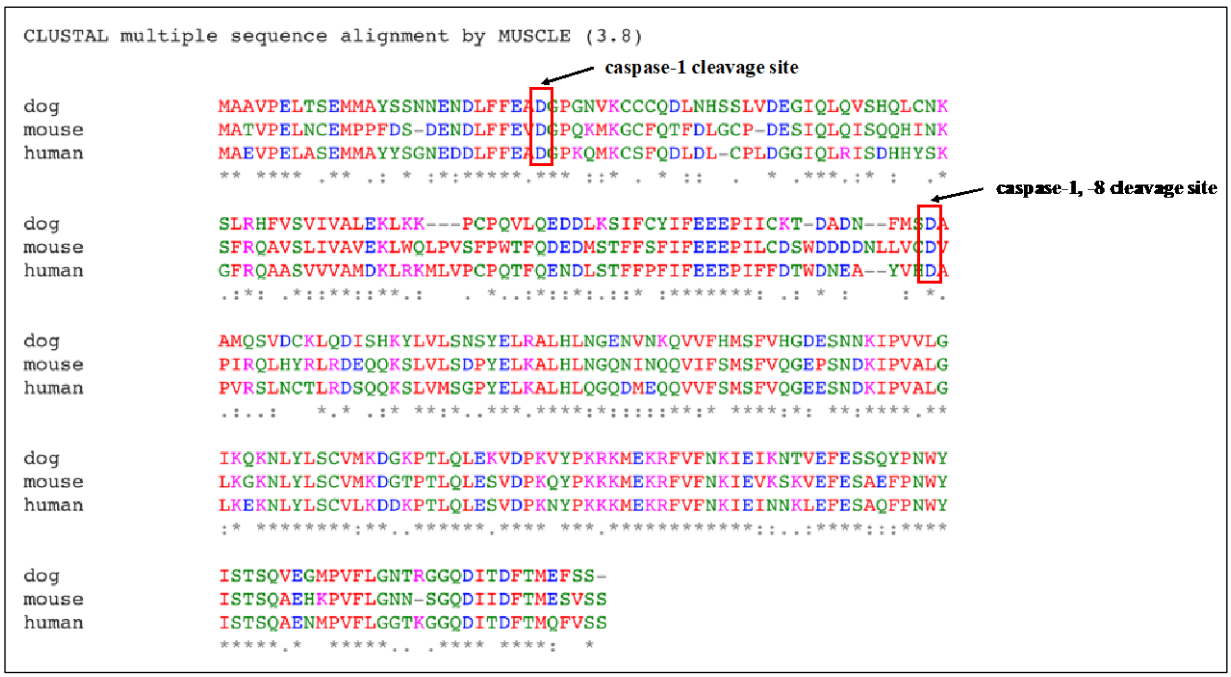


**Figure 3.4.2 Sequence alignment analysis of the dog, human and mouse IL-1β amino acid sequences shows conserved caspase-1 and caspase-8 cleavage sites.** Sequence alignment shows high degree of similarities between the dog (ENSCAFG00000007249, ENSCAFT00000011613.3), human (ENSG00000125538, ENST00000263341.6) and mouse (ENSMUSG00000027398, ENSMUST00000028881.13) IL-1β protein sequences with catalytic residues (highlighted in red rectangle) acting as caspase-1, caspase-8 cleavage sites being conserved across the three species.

### 3.5 Canonical NLPR3 inflammasome activation in DH82 cells using nigericin bacterial toxin

NLRP3 inflammasome activation requires two distinct steps. First is priming with TLR ligands leading to upregulation of inflammatory genes, including NLRP3 itself, pro-IL-1β and pro-IL-18 [98], [328]. While the second step results in the activation of the NLRP3 inflammasome [329],

[330]. The NLRP3 inflammasome responds to a wide range of stimuli, including the efflux of potassium [82], [85], generation of mitochondrial ROS [331], [332] and cathepsin B activity [333], [334]. Upon activation, NLPR3 oligomerises with pro-caspase-1 and ASC inflammasome components [42], [140]. Activation of caspase-1 results in the cleavage and maturation of inflammatory cytokines and GSDMD resulting in pyroptotic cell death [44].

To characterise NLRP3 inflammasome activation in canine DH82 macrophages I compared DH82 responses with well characterised wild-type and *caspase-1*$^{-/-}$*caspase-11*$^{-/-}$ murine immortalised BMDMs in response to the canonical NLPR3 inflammasome activator, nigericin bacterial toxin. The aim of this experiment was to assess the functionality of canine NLRP3 and the hybrid caspase-1/4/11 proteins. In all experiments, cells were primed with ultrapure LPS (200 ng/ml for 3 hours) to drive expression of inflammasome constituents and then stimulated with increasing concentration of nigericin bacterial toxin (20-200 μM for 1 hour) as described in Materials and Methods section 2.6. Extracellular LPS has been shown to induce NLRP3 and IL-1β expression via TLR4/MyD88 and NF-κβ signalling pathways in mouse BMDMs [98]. Nigericin is a bacterial toxin derived from Streptomyces hygroscopicus [335]. Being a potassium ionophore, it decreases intracellular levels of potassium which has been shown to be essential for NLRP3 inflammasome activation [82], [85]. Percentage of cell lysis induced was determined by directly measuring the relative amount of LDH released into the supernatant. LDH is a stable cytosolic enzyme, that is released upon cell lysis which can be found in animals, plants and bacteria and is therefore a good indicator of cell death as a consequence of membrane rupture and cell lysis [336]. Secretion of the inflammatory cytokine, IL-1β into the supernatant was measured by ELISA method and its cleavage was confirmed using western blotting to differentiate between pro-IL-1β which could be released into the supernatant upon cell lysis independent of caspase maturation.

First, I used methanol vehicle control following LPS priming to eliminate any cell lysis contributed by the solvent (Figure 3.5.1A). Methanol induced a small percentage of cell lysis in wild-type murine cells, while DH82 cells showed no response. I, therefore, concluded that the observed DH82 cell lysis was a direct consequence of nigericin treatment (Figure 3.5.1).

Murine bone marrow derived macrophages lacking functional caspase-1 do not process pro-IL-1β and cannot induce pyroptosis in response to NLRP3 inflammasome activators [337]. As expected, LPS priming did not induce cell death in *caspase-1*$^{-/-}$*caspase-11*$^{-/-}$ cells, while 20 μM final concentration of nigericin was sufficient to activate inflammasome formation and cell lysis in wild-type cells (Figure 3.5.1B). In contrast, lytic responses of DH82 cells were refractory to nigericin treatment at 20 μM final concentration, resembling responses exhibited by *caspase-1*$^{-/-}$*caspase-11*$^{-/-}$ cells (Figure 3.5.1B).

To investigate if higher concentrations of nigericin could stimulate cell lysis of DH82 cells I used increasing concentration of nigericin (Figure 3.5.1B) as described in Materials and Methods section 2.6. Treatment with elevated concentrations of nigericin induced a corresponding increase in cell lysis of DH82 and *caspase-1*$^{-/-}$*caspase-11*$^{-/-}$ cells (Figure 3.5.1B). Treatment with 200 μM final concentration of nigericin resulted in equivalent cell lysis responses in DH82 and *caspase-1*$^{-/-}$*caspase-11*$^{-/-}$ murine cells (Figure 3.5.1B) and therefore suggested an inflammasome independent toxicity issue at this high dose. Thus, my data suggested that although canine cells have conserved NLRP3 and a caspase-1/4/11 hybrid gene that was expected to be functional, canine cells appeared to be refractory to NLRP3 induced cell death.

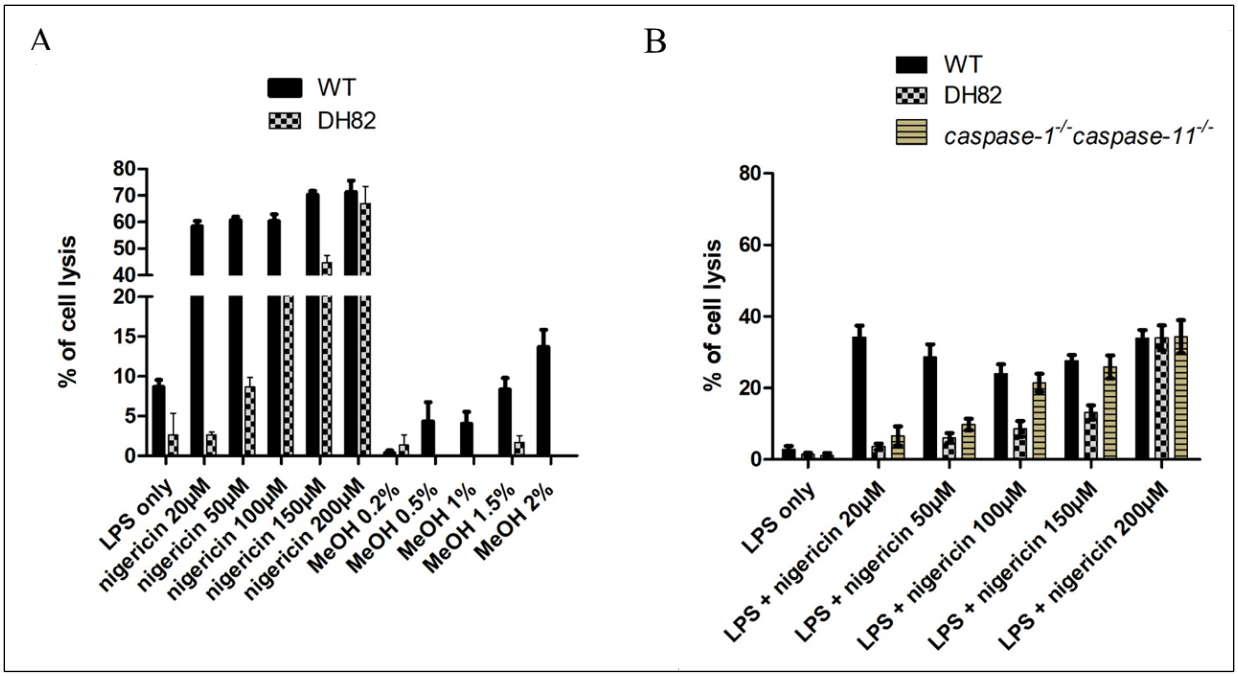


**Figure 3.5.1 High dose of nigericin drives NLRP3 independent cell lysis in DH82 cells.** (A) Murine immortalised wild-type and DH82 cells were primed with LPS then stimulated with increasing concentration of nigericin, along with the equivalent concentration of methanol solvent. Nigericin induced cell lysis was assessed by directly measuring LDH release into the supernatant. Results are representative of a single experiment where error bars represent the standard error of means (SEM) of triplicate wells. (B) Murine immortalised wild-type, *caspase-1*$^{-/-}$*caspase-11*$^{-/-}$ and DH82 cells were primed with LPS then stimulated with increasing concentration of nigericin. Nigericin induced cell lysis was assessed by directly measuring LDH release into the supernatant. Data shown is pooled from three independent experiments. Error bars represent the standard error of means (SEM) of triplicate wells.

The amount of IL-1β released into the supernatant of nigericin stimulated immortalised murine wild-type and canine DH82 macrophages were also determined as described in Materials and Methods section 2.8. DH82 cells secreted increasing amount of IL-1β in response to increasing concentration of nigericin (Figure 3.5.2). The priming of cells via TLRs happens independently of inflammasome activation [98], in which case cell lysis would result in the release of unprocessed pro-IL-1β. On the contrary, wild-type cells showed higher IL-1β release in response to stimulation with lower concentrations of nigericin, while stimulation with high concentration of nigericin

resulted in the lowest amount of IL-1β release. This is presumably due to the rapid toxicity issue I demonstrated in Figure 3.5.1 above and is a reflection that rapid cell lysis did not allow sufficient time for IL-1β expression (Figure 3.5.2). In contrast and in agreement with the cell lysis data above, canine production of IL-1β was refractory to low dose nigericin but significant IL-1β was detected at high doses of nigericin and correlated with my cell lysis data. This suggested that although the lysis may not be inflammasome specific in these cells, the lysis was associated with IL-1β release.

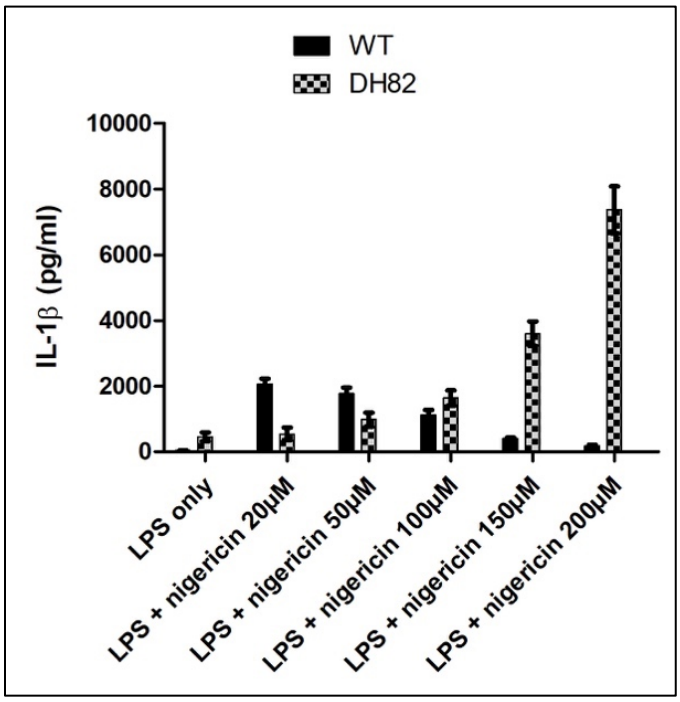


**Figure 3.5.2 The amount of IL-1β released into the supernatant of nigericin stimulated DH82 cells is proportional to the nigericin concentration used.** Murine wild-type and canine DH82 cells were primed with LPS (200 ng/ml for 3 hours) then stimulated with nigericin bacterial toxin in an increasing concentration (20-200 μM). IL-1β release into the supernatant was quantified using canine and murine specific ELISA detection method. Data shown is pooled from three independent experiments. Error bars represent the standard error of means (SEM) of triplicate wells.

Cleavage of the pre-form of IL-1β is a common read-out of inflammasome activation [42], [290], [338]. The ELISA kit used to measure canine IL-1β in the supernatant has only been validated to

recognise the full-length form of the protein. Therefore, western blot analysis was carried out to assess IL-1β cleavage. DH82 cells were primed with LPS (200 ng/ml for 3 hours) and stimulated with nigericin at 200 μM final concentration to maximise the amount of cell lysis induced as described in Materials and Methods section 2.6. Following protein precipitation of the supernatant, immunoblotting against canine IL-1β was performed (Figure 3.5.3) as described in Materials and Methods sections 2.10 and 2.11. Immunoblotting of precipitated protein from LPS and nigericin stimulated DH82 macrophages revealed significant amounts of pro-IL-1β (~33 kDa) and a small fraction of that appeared to be cleaved (~17 kDa) (Figure 3.5.3). These results suggested that inflammatory cytokine expression can be upregulated in the presence of TLR ligands. It also suggested, that the inflammasome can be activated in DH82 cells in response to nigericin to result in IL-1β cleavage, but the presence of significant pro-IL-1β would suggest that the ELISA results are largely based upon detection of this unprocessed form, possibly released as a consequence of the cell lysis I previously observed.

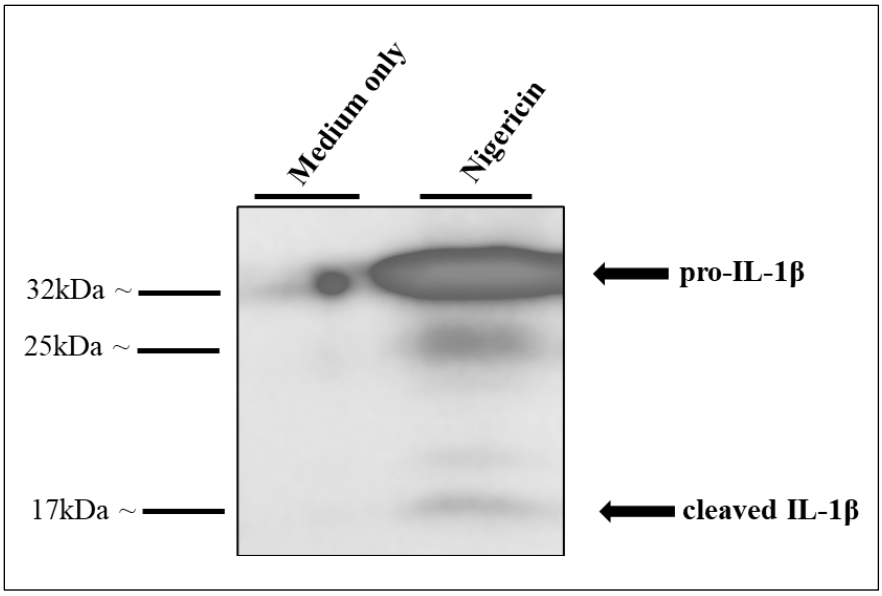


**Figure 3.5.3 Western blot analysis of the supernatant reveals small degree of IL-1β cleavage in nigericin stimulated DH82 cells.** DH82 cells were primed with LPS (200 ng/ml for 3 hours), following stimulation with nigericin (200 μM for 1 hour). Total protein was precipitated from the supernatant and IL-1β cleavage was investigated using western blotting. A large amount of pro-IL-1β was released into the supernatant, and a small fraction was in its mature form. Representative immunoblot is from three independent experiments.

Another hallmark of inflammasome activation is ASC aggregate formation [57], [58] and caspase recruitment [42], [140], [145] which can be immunofluorescently labelled and visualised as an ASC-speck within the cytosol of cells [339]. In this experiment, DH82 cells were primed with LPS (200 ng/ml for 3 hours) and stimulated with nigericin (20 μM) for 1 hour as described in Materials and Methods section 2.6. Prior fixation, cells were stained for active caspases using FLICA reagent and cytosolic ASC as described in Materials and Methods section 2.7. FLICA is an immunofluorescent labelled caspase inhibitor that covalently binds to active caspases. Non-stimulated cells were stained with poly-caspase stain, which binds to a sequence conserved in all caspases (Figure 3.5.4). As expected, non-stimulated (NS) cells did not show ASC-speck formation or caspase activation (Figure 3.5.4). In contrast, DH82 cells stimulated with nigericin at low concentrations, which I previously demonstrated did not result in inflammasome activation (20 μM) as characterised by IL-1β release and lytic cell death surprisingly displayed low level

ASC-speck formation and activate caspase recruitment of caspase-8 and presumably the hybrid caspase-1/4/11 to the specks (Figure 3.5.4). These results suggested that NLRP3 inflammasome can be activated causing recruitment, but presumably not activation, of caspases by low dose nigericin. This hypothesis was also in agreement with my previous data analysing cell lysis and IL-1β release in canine macrophages.

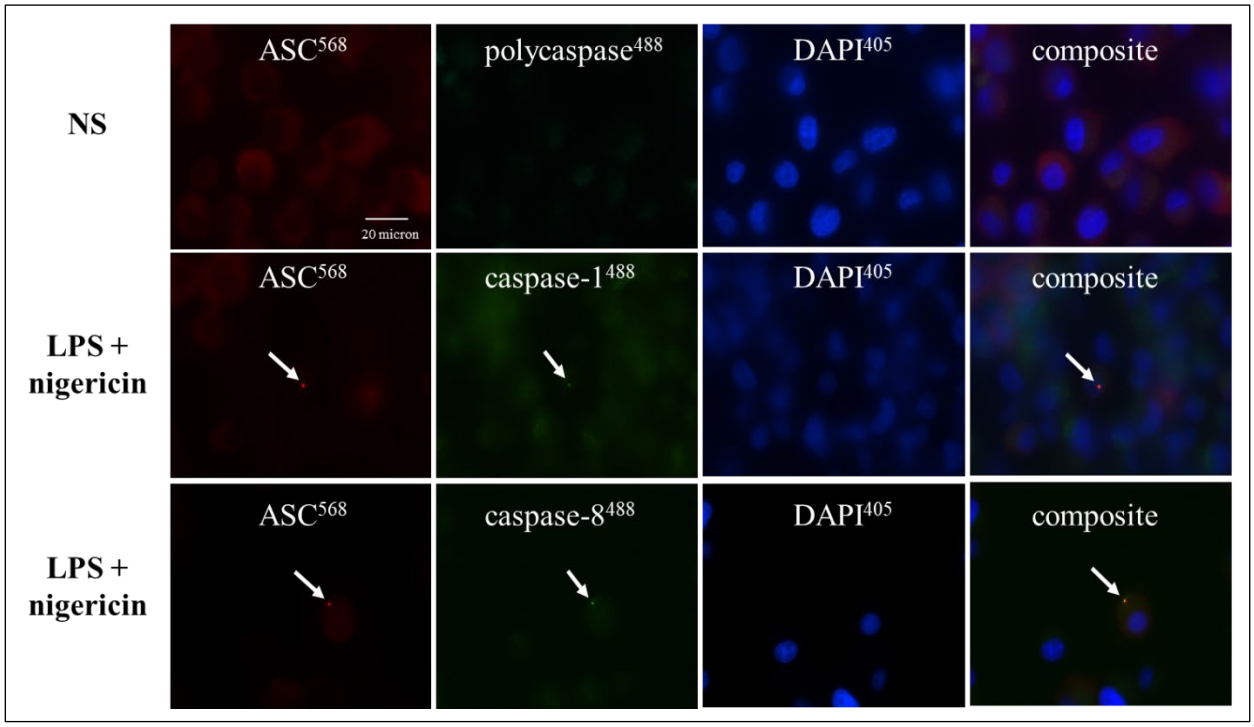


**Figure 3.5.4 NLRP3 activation induces ASC speck formation and both, hybrid caspase-1/4/11 and caspase-8 recruitment.** DH82 cells were primed with LPS (200 ng/ml) and stimulated with nigericin bacterial toxin (20 μM for one hour). Non-stimulated (NS) cells were left in cell culture medium. Live cells were stained for activated caspases (poly-caspase, caspase-1 or caspase-8). Following fixation cells were stained for cytoplasmic ASC and nuclei using DAPI staining. Representative immunofluorescent images are from three independent experiments.

Cells undergoing pyroptosis can be characterised by a number of phenotypic and morphological features, including DNA damage [256], pore formation [246] and cell swelling [255] as a consequence of osmotic shock that ultimately results in cell lysis which can be visualised as a so called 'popping' event [255]. These events can be visualised by bright-field microscopy without

the need of any staining. To assess the morphological changes induced by nigericin, DH82 cells were primed with LPS (200 ng/ml) and were stimulated with nigericin (200 μM for 1 hour). Bright-field images using a confocal microscope were taken every two minutes of the same focal point during the hour incubation. Representative images can be found in Figure 3.5.5, which shows DH82 cell swelling and rupturing. This morphology can be attributed to pyroptotic cell death or it could be a non-specific result of the nigericin ionophobic nature. Cells undergoing other types of lytic cell death, like necroptosis can also display similar morphology [253].

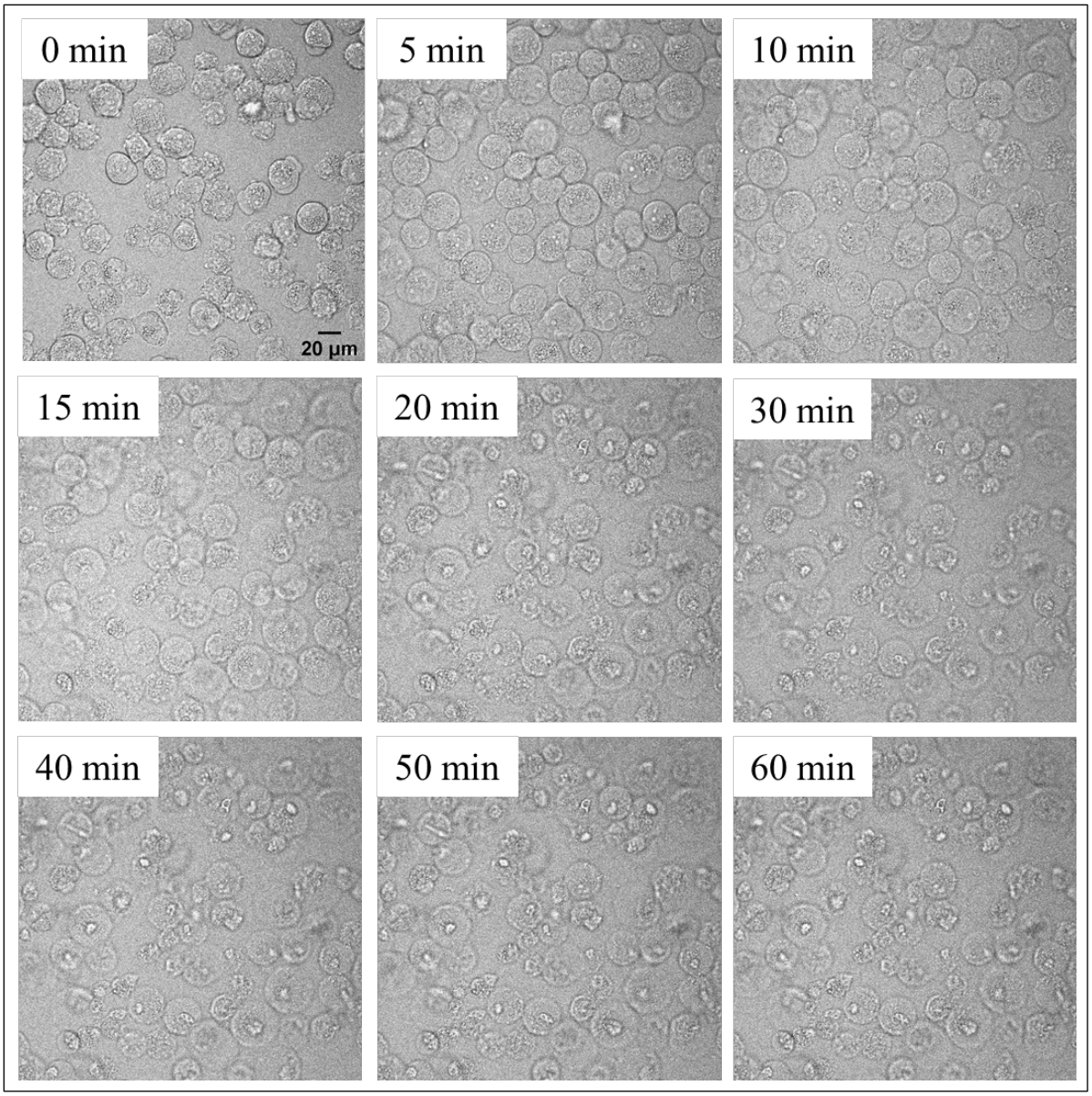


**Figure 3.5.5 Confocal imaging of LPS primed and nigericin stimulated DH82 cells shows characteristics of pyroptotic cell death.** DH82 cells were primed with LPS (200 ng/ml) and stimulated with nigericin (200 µM for one hour). Bright field images were taken throughout the hour incubation on a confocal microscope. Cells displayed substantial swelling and rupturing. Representative images of the different morphological stages observed are shown above. Representative bright-field images are from a single experiment.

DH82 cells have been derived from a ten-year-old golden retriever with malignant histiocytosis [340]. To confirm that the lytic phenotype observed in DH82 cells (Figure 3.5.1) was not a consequence of being a cancerous cell line, I repeated the nigericin stimulation experiment using primary canine PBMCs isolated from patients attending the phlebotomy clinic at the Clinical Pathology Laboratory, Department of Veterinary Medicine, University of Cambridge (Table 2.2.1) as described in Materials and Methods sections 2.3 and 2.6. Due to extremely low sample availability, an experiment using only one concentration of nigericin could be performed. Percentage of cell lysis induced was determined by the amount of LDH release, while IL-1β secretion into the supernatant by using canine specific ELISA method as described in Materials and Methods section 2.8 (Figure 3.5.6). The amount of cell lysis induced and IL-1β was released into the supernatant were comparable between the DH82 cell line and blood PBMCs (Figure 3.5.6). This suggested, that the immortalised DH82 cell line responses can be directly related to how primary cells respond.

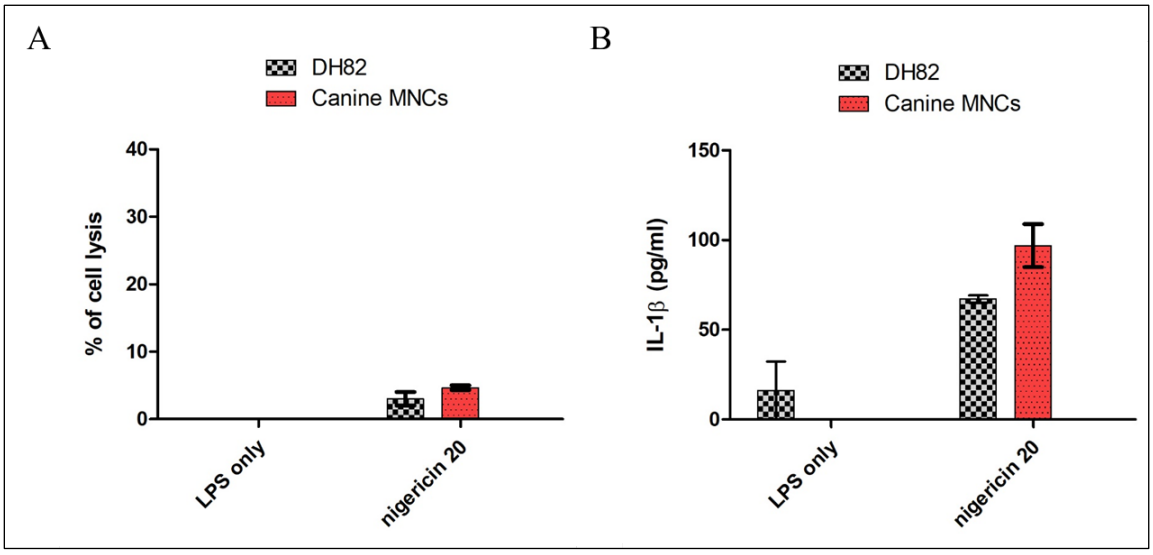


**Figure 3.5.6 DH82 and primary PBMC cells show similar cell lysis and IL-1β release responses following nigericin stimulation.** DH82 and primary blood MNCs were primed with LPS (200ng/ml) and stimulated with nigericin (20 µM for 1 hour). (A) Cell lysis was measured by the relative amount of LDH released into the supernatant, while (B) IL-1β was quantified using ELISA method. Data shown is from a single experiment. Error bars represent the standard error of means (SEM) of triplicate wells.

### 3.6 Activation of the non-canonical inflammasome formation in DH82 cells

Analogous to canonical NLRP3 inflammasome regulation, the first step in the activation of non-canonical inflammasome formation is priming. TLR ligands (e.g. LPS) bind to TLRs (e.g. TLR4) [341] and induce transcriptional translation of several inflammatory genes, including caspase-11, NLRP3, pro-IL-1β and pro-IL-18 via the NF-κβ and IRF3 signalling pathways [98], [164], [328]. Followed by activation when the CARD domain of the murine caspase-11 [61] and human caspase-4/-5 [61], [342] recognise and directly bind the lipid A moiety of the LPS in the cytosol [163], [168]. This interaction results in proximity induced activation and autoproteolysis of caspase-4/-5/-11 leading to pyroptosis [60] and, eventually, NLRP3 [158] and caspase-1 dependent IL-β processing and release [60], [71], [163], [168]. GSDMD cleavage by inflammatory caspase-1/-4/-5/-11 releases the N-terminal active fragment [43], [44], [229], [230] which then binds to cardiolipin of the cell membrane and the mitochondria to induce pore formation leading to pyroptotic cell death [70], [72], [74], [75] and mitochondrial damage to promote mitochondrial apoptotic pathway [233].

My previous bioinformatic analysis suggested the presence of the LPS binding CARD domain of caspase-4 in the canine hybrid caspase-1/4/11 protein. I therefore investigated whether this hybrid caspase could respond to intracellular LPS. Alternative splicing of the hybrid mRNA can produce two transcripts [154]. While the smaller transcript consists of a single CARD similar to that of human and murine caspase-1, the larger transcript contains two tandem CARDs with the second CARD similar to that of caspase-4/-11 [154] (Figure 3.1.1). Mass spectrometry analysis could not specifically identify which transcript is expressed in DH82 cells (Figure 3.2.1), therefore functional analysis was employed *in vitro*.

Non-canonical inflammasome activation was performed as described in Materials and Methods section *2.6.* wild-type murine, *caspase-1*$^{-/-}$*caspase-11*$^{-/-}$ and canine DH82 macrophages were primed with Pam3CSK4 (10 μg/ml for 4 hours), a TLR1/2 ligand [343], driving caspase-11, NLRP3 and IL-1β expression via the NF-κβ [344] signalling pathway. Cytosolic LPS delivery was then performed using different concentrations of LPS (5-, 10- or 20 μg/ml) in conjunction with FuGENE®HD (Promega) transfection reagent for 16 hours.

In order to determine the contribution of the well documented cytotoxic effects of transfection reagents, I first performed an experiment to test the toxicity of each reagent in isolation (Figure 3.6.1A). Individually, none of the reagents induced notable amount of cell lysis in either murine wild-type or dog DH82 cells (Figure 3.6.1A). Any cell lysis induced in subsequent experiments can be attributed to the effect of cytosolic LPS. TLR1/2 activation by Pam3CSK4 and TLR4 activation by extracellular LPS induced IL-1β release into the supernatant of DH82 cells, but not wild-type murine cells, without concurrent LDH release (Figure 3.6.1B). Cytosolic delivery of LPS was required to drive IL-1β release in wild-type cells (Figure 3.6.1B), but DH82 cells did not release LDH or IL-1β in response to cytosolic LPS alone. This suggested the expression of the shorter transcript of the hybrid caspase1/11, consisting of the single CARD from caspase-1 is dominant in DH82 cells and therefore non-responsive to cytosolic LPS [154] (Figure 3.1.1).

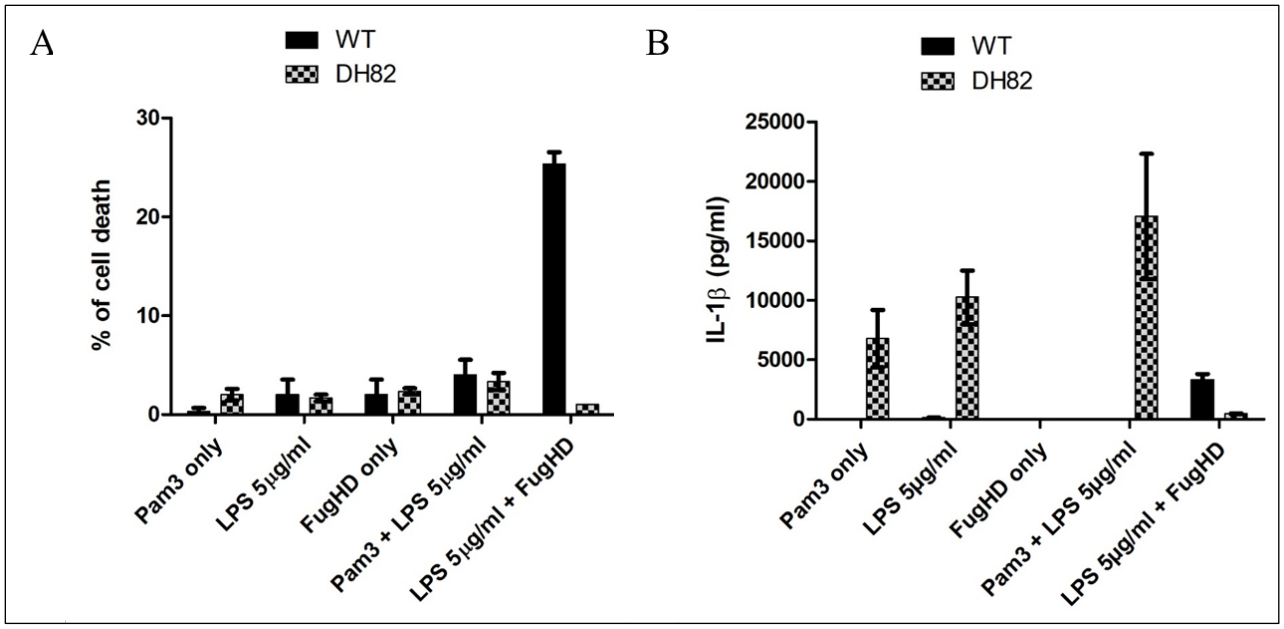


**Figure 3.6.1 Priming of TLR1/2 and TLR4 is sufficient to drive IL-1β release in DH82 cells.** Wild-type murine and canine DH82 cells were stimulated individually with ligands and reagents used to activate the non-canonical inflammasome formation. (A) Percentage of cell lysis induced was determined by measuring LDH, while (B) IL-1β release was measured using ELISA method. Data shown is pooled from three independent experiments. Error bars represent the standard error of means (SEM) of triplicate wells.

To further investigate the apparent resistance to intracellular LPS activation of the non-canonical inflammasome in canine cells, I investigated whether higher concentrations of LPS could induce non canonical inflammasome activation. To test this hypothesis, immortalised murine wild-type, *caspase-1*$^{-/-}$*caspase-11*$^{-/-}$ and canine DH82 cells were primed with Pam3CSK4 (10 µg/ml for 4 hours) and stimulated with increasing concentrations of transfected LPS (5-, 10- and 20 µg/ml) for 16 hours (Figure 3.6.2). As expected, the delivery of cytosolic LPS induced LDH release in wild-type murine macrophages [60], but not in *caspase-1*$^{-/-}$*caspase-11*$^{-/-}$ cells [60]. DH82 cells failed to release LDH to cytosolic LPS even at the highest concentration (Figure 3.6.2A) resembling the phenotype of *caspase-1*$^{-/-}$*caspase-11*$^{-/-}$ murine macrophages in terms of their cell lytic response (Figure 3.6.2A). Wild-type murine cells only released IL-1β with transfected LPS, in contrast, the

priming step of DH82 cells was sufficient for IL-1β secretion and occurred in the absence of LDH release (Figure 3.6.2 B).

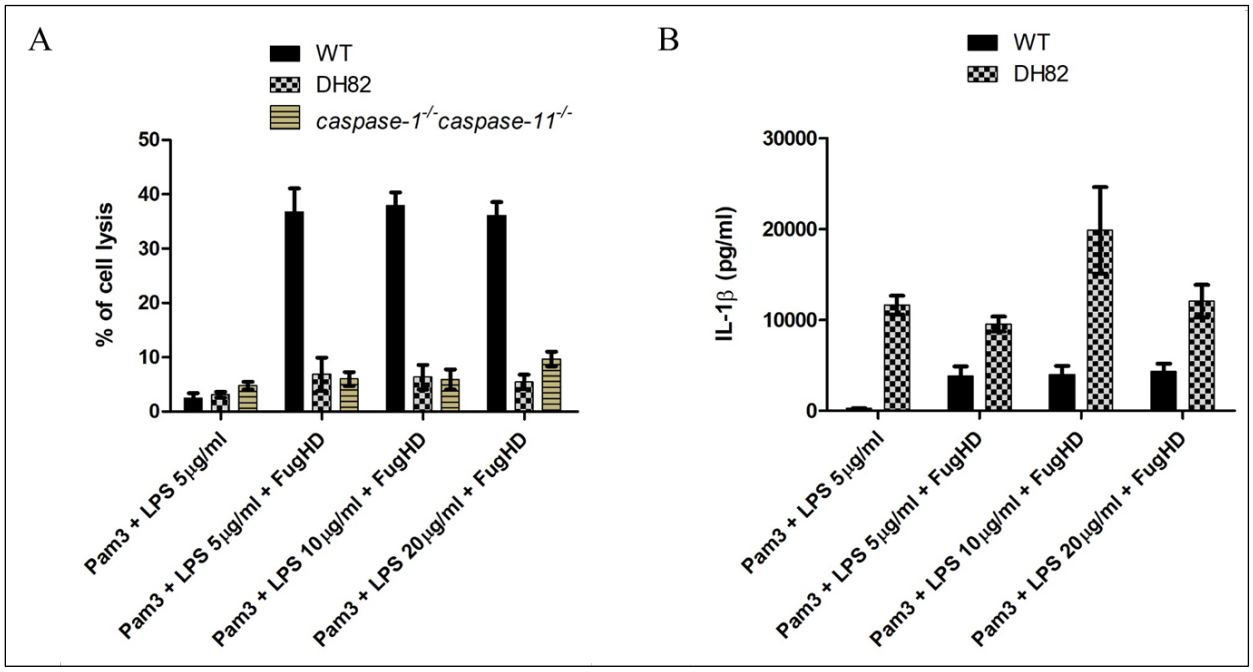


**Figure 3.6.2 Canine macrophages do not activate non-canonical inflammasome death responses and priming alone induces IL-1β release into the supernatant in the absence of cell lysis.** Murine wild-type, *caspase-1*$^{-/-}$*caspase-11*$^{-/-}$ and canine DH82 cells were primed with Pam3CSK4 (10 µg/ml for 4 hours) then stimulated with either LPS (5 µg/ml) alone or in conjunction with FuGENE®HD transfection reagent. (A) Percentage of cell lysis induced was determined by measuring LDH release into the supernatant, while (B) IL-1β release was measured using ELISA method. Data shown is pooled from three independent experiments. Error bars represent the standard error of means (SEM) of triplicate wells.

To investigate IL-1β processing in the supernatant, protein precipitation and subsequent immunoblotting analysis was carried out on supernatants from non-stimulated (medium only), Pam3CSK3 (10 µg/ml for 4 hours) only, un-primed transfected LPS (5 µg/ml for 16 hours) and Pam3CSK4 (10 µg/ml for 4 hours) primed, transfected LPS (5 µg/ml for 16 hours) stimulated DH82 cells (Figure 3.6.3). With the exception of the medium only sample, all other stimulations

resulted in the expression and secretion of pro-IL-1β (Figure 3.6.3). However, cleavage was only observed in cells primed with Pam3CSK4 (Figure 3.6.3). These results suggested an alternative IL-1β activation pathway dependent on receptors TLR1 and 2 (Figure 3.6.3).

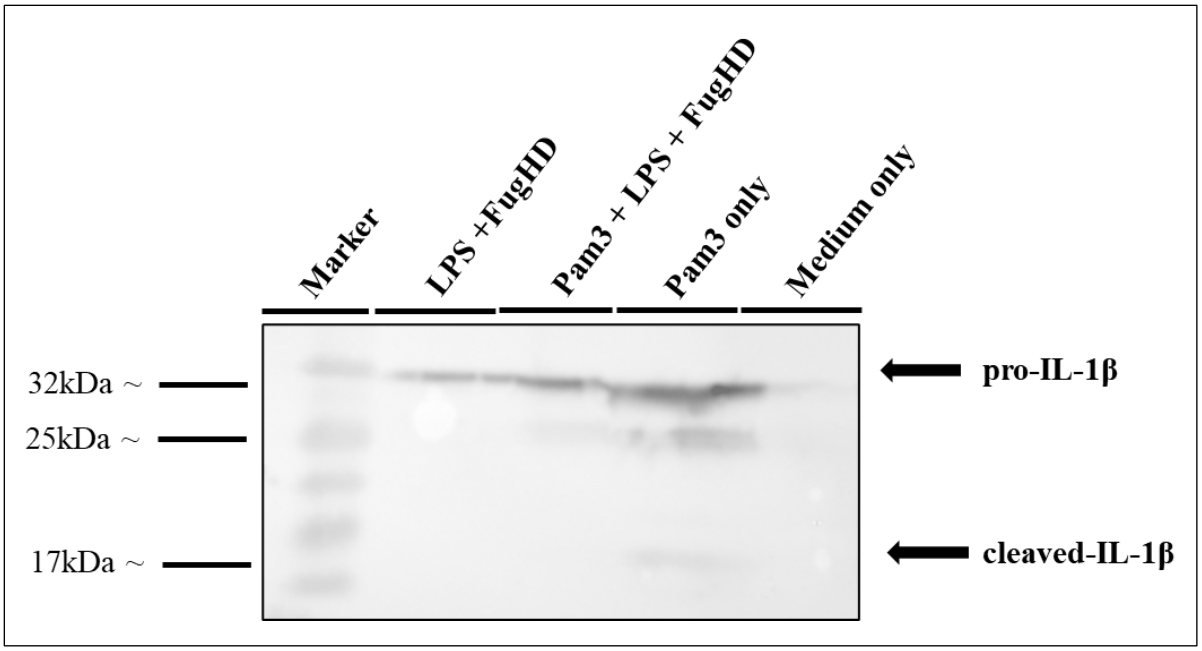


**Figure 3.6.3 Priming only is sufficient to drive IL-1β secretion and cleavage in DH82 cells.** Full protein precipitation of supernatants from DH82 cells primed with Pam3CSK4 (10 µg/ml for 4 hours), transfected LPS (5 µg/ml for 16 hours) and Pam3CSK4 (10 µg/ml for 4 hours), LPS transfected (5 µg/ml for 16 hours). Samples were immune blotted against canine specific IL-1β. Representative immunofluorescent image is from two independent experiments.

ASC speck formation and caspase recruitment were also assessed in DH82 cells following Pam3CSK4 (10 µg/ml for 4 hours) and transfected LPS (5 µg/ml for 16 hours). Prior to fixation, cells were stained for the presence of active caspases (FAM-FLICA). After fixation cells were stained for cytosolic ASC. Non-stimulated cells were stained with poly-caspase stain, while stimulated cells were either stained for active caspase-1 or caspase-8. Cells stimulated with cytosolic LPS did not display ASC-speck formation or activated caspase recruitment (Figure 3.6.4). These results further pointed in the direction of an IL-1β processing pathway independent of inflammasome formation. While also providing further evidence that the canine hybrid caspase-

1/4/11 protein is incapable of recognising cytoplasmic LPS, suggesting the expression of the shorter transcript.

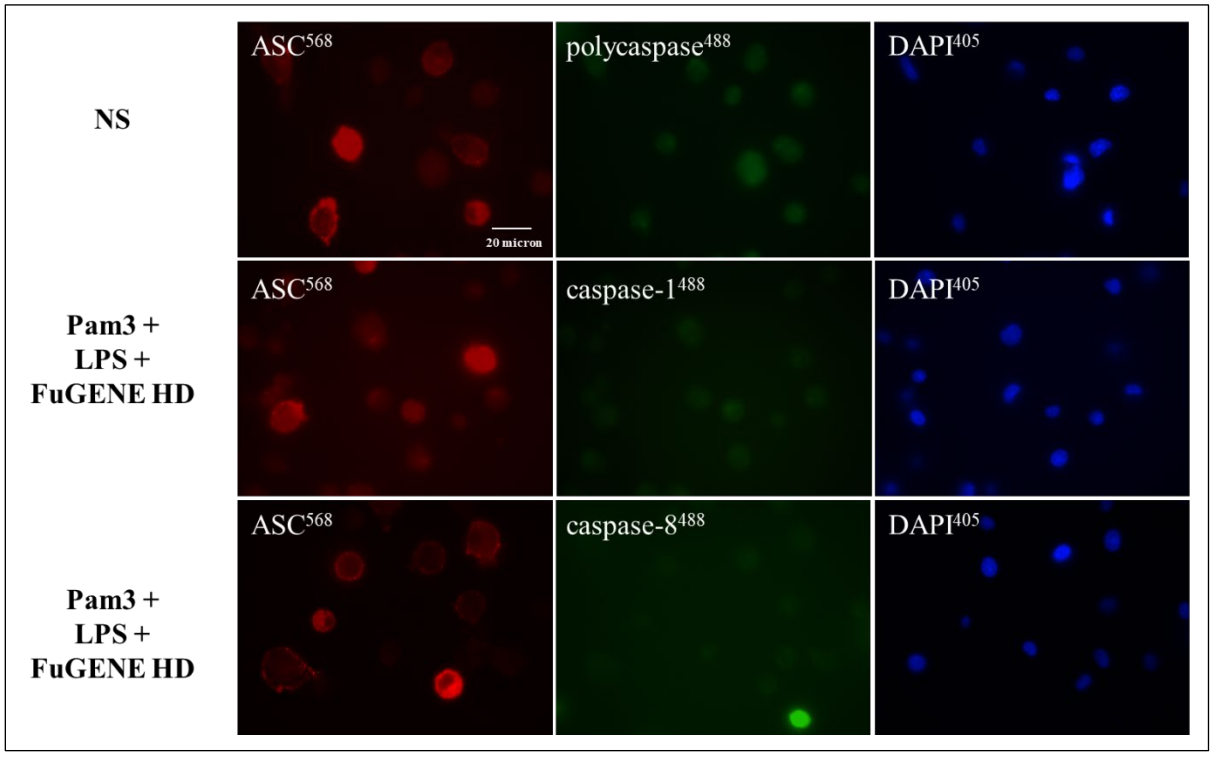


**Figure 3.6.4 Non-canonical inflammasome activation of DH82 cells fail to induce ASC-speck formation and activated caspase recruitment.** DH82 cells were primed with Pam3CSK4 (10 µg/ml for 4 hours) and transfected with LPS (5 µg/ml for 16 hours). Prior fixation, cells were stained for activated caspase-1 or caspase-8. After fixation cells were stained for cytosolic ASC. Non-stimulated cells were left in medium and were stained for cytoplasmic ASC and activated caspases. Representative immunofluorescent images are from three independent experiments.

To investigate any substantial morphological changes occurring in response to non-canonical inflammasome activation, DH82 cells were primed with Pam3CSK4 (10 µg/ml for 4 hours), following LPS transfection (5 µg/ml) for 16 hours. Morphological changes were recorded using confocal microscopy, where bright field images were taken every 10 minutes of the 16-hour incubation. Representative images are shown in Figure 3.6.5. No obvious or gross morphological changes were observed, even after 16-hours cells (Figure 3.6.5).

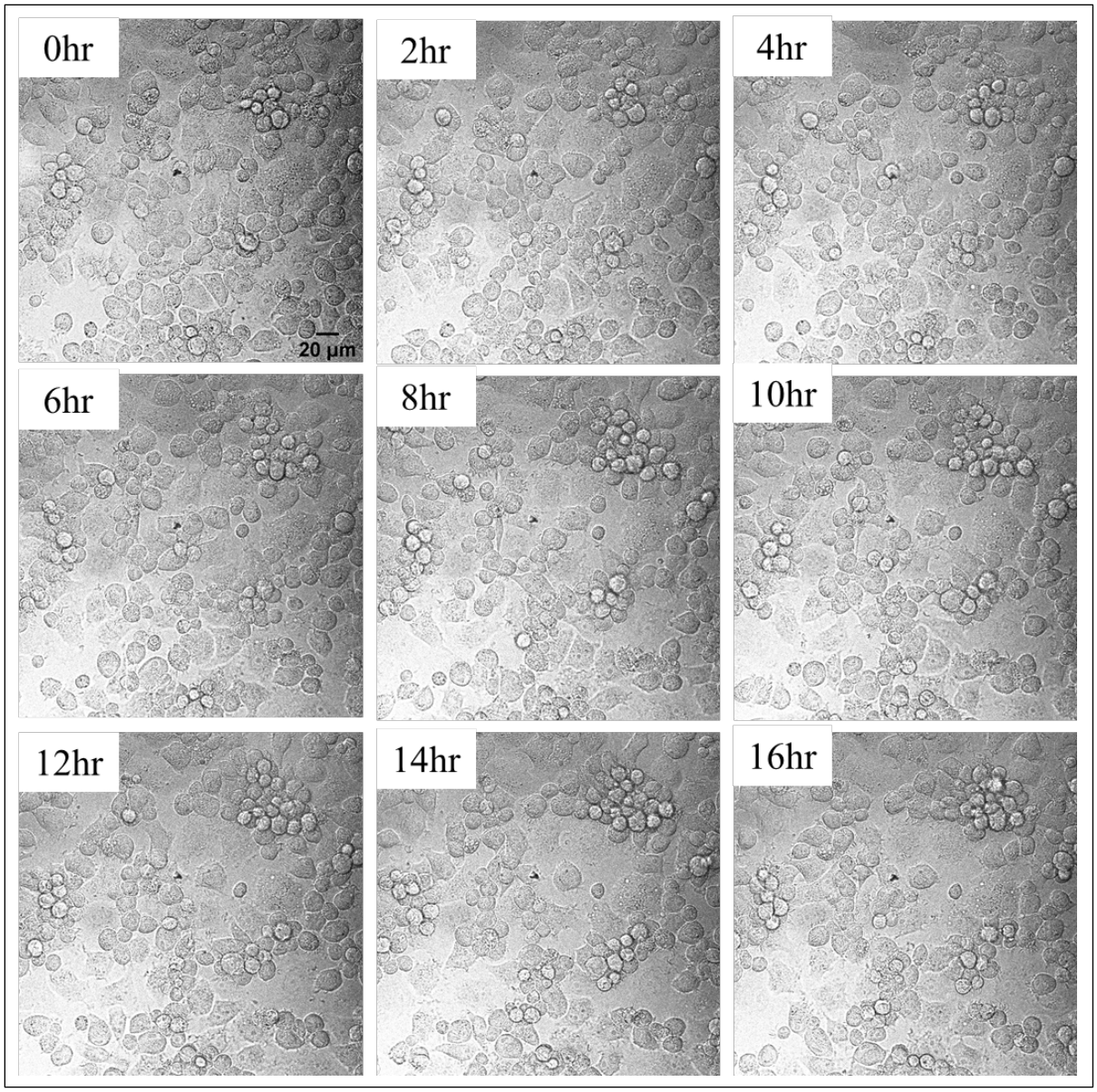


**Figure 3.6.5 DH82 cells failed to show any distinct morphological changes in response to the non-canonical inflammasome activator, cytosolic LPS.** DH82 cells were primed with Pam3CSK4 (10 µg/ml for 4 hours) and transfected LPS (5 µg/ml) for 16 hours. Bright field images were taken every 10 minutes during the 16 hours incubation on a confocal microscope. Representative bright-field images are from a single experiment.

The effect of the non-canonical inflammasome activator intracellular LPS was also assessed on primary canine PBMCs isolated from patients attending the phlebotomy clinic at the Clinical

Pathology Laboratory, Department of Veterinary Medicine, University of Cambridge (Table 2.2.1) as described in Materials and Methods sections 2.3 and 2.6. Due to the limited access and volume of samples, only a single experiment could be performed (Figure 3.6.6). Primary PBMCs and DH82 cells were primed with Pam3CSK4 (10 μg/ml for 4 hours) or FuGENE®HD transfection reagent alone and also Pam3CSK4 primed followed by LPS transfection (5 μg/ml) (Figure 3.6.6). Percentage of cell lysis induced was determined by the relative amount of LDH release (Figure 3.6.6A), while IL-1β in the supernatant using canine specific ELISA method (Figure 3.6.6B). Canine primary cells mimicked the LDH and IL-1β responses of the DH82 cells. Regardless of the treatment no LDH release was observed, but Pam3CSK4 priming along was sufficient for IL-β release into the supernatant (Figure 3.6.6).

Experiments involving primary canine mononuclear cells (MNCs) could only be performed once due to the limited number of samples sourced from the Queen's Veterinary School Hospital. Therefore, results obtained from these experiments should be interpreted with a degree of caution. Furthermore, residual blood samples were taken from patients who had undergone chemotherapy or suffer from autoimmune disease (Table 2.2.1). One can assume that these factors may introduce heterogeneity in the observed cellular responses to ligand stimulation. Furthermore, the blood samples were collected from multiple different breeds and therefore genetic influence cannot be eliminated. Therefore, my results can only be taken as an indication of what the responses of primary canine MNCs are like in response to sterile inflammatory ligands and post infection with *S.* Typhimurium.

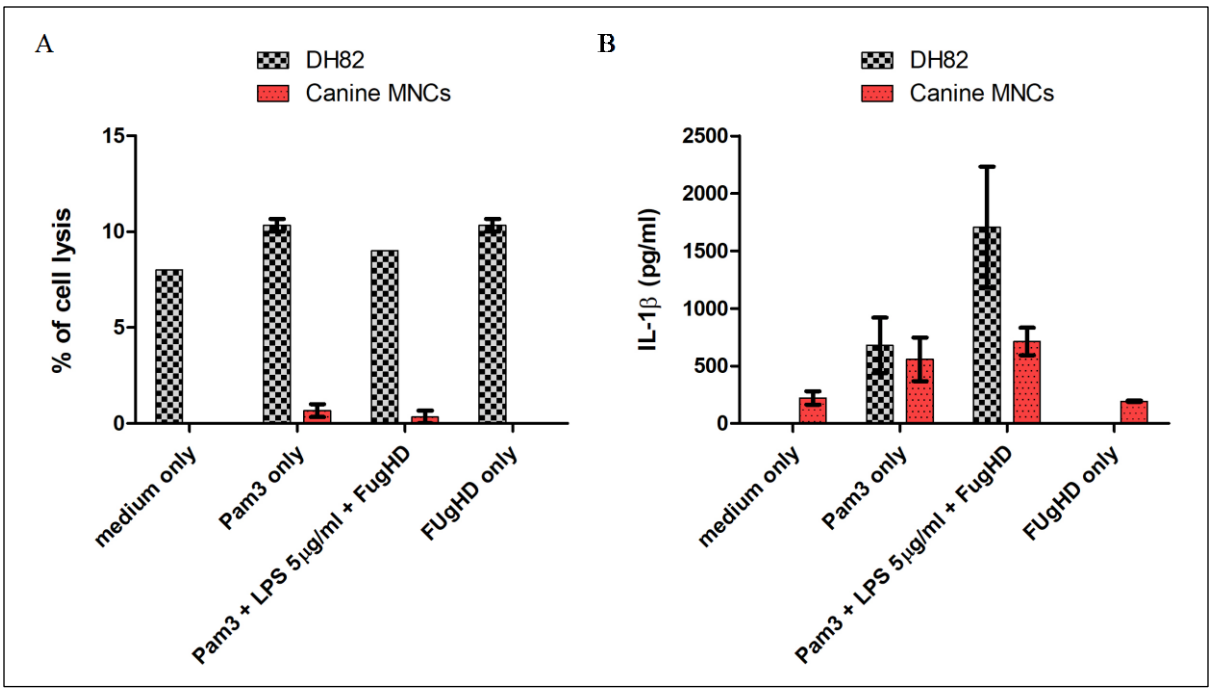


**Figure 3.6.6 Pam3CSK4 priming alone induced IL-1β secretion in canine blood PBMCs.** DH82 and primary blood PBMCs were primed with Pam3CSK4 (10 µg/ml for 4 hours) or transfection reagent alone and Pam3CSK4 (10 µg/ml for 4 hours) primed followed by LPS transfection (5 µg/ml) for 16 hours. (A) Percentage of cell lysis induced was determined by measuring LDH release into the supernatant, while (B) IL-1β release was measured using ELISA method. Data shown is from a single experiment. Error bars represent the standard error of means (SEM) of triplicate wells.

TLR dependent IL-1β release has been reported previously [185], [345], [346]. Gaidt *et al*., has shown an NLRP3, ASC and caspase-1 dependent IL-1β secretion and maturation in LPS primed human and porcine monocytes. They have shown a RIPK1/FADD/caspase-8 dependent pathway upstream of NLRP3 activation. They have named it 'alternative inflammasome' activation given its independency of potassium concentration and the lack of pyroptosome formation [185]. Caspase-8 involvement has been suggested in the priming [347] and activation [104] of NLPR3 inflammasome while it has been shown to directly cleave IL-1β using HEK293T and Raw264.7 cells [216]. It is tempting to speculate that DH82 cells might engage in a similar, TLR/caspase-8 dependent inflammasome activation.

## 3.7 Discussion

Genomic analysis showed the presence of a caspase-1/4/11 fusion in the canine genome [154]. The genes encoding these proteins are located next to each other in the human and mouse genomes. Dogs have lost the 3'end of caspase-1 and the 5'end of caspase-4 (Figure 3.1.1). Mass spectrometry analysis of DH82 cell lysates have demonstrated the constitutive expression of the canine hybrid caspase-1/4/11 gene at the protein level (Figure 3.2.2). Multiple sequence comparison by log-expectation (MUSCLE) analysis has also shown the presence of the catalytic residue (258-Cys) suggesting the presence of a functional protein (Figure 3.2.3).

MUSCLE analysis of further genes also involved in inflammasome formation and function have been investigated. Amino acids sequence analysis of canine NLRP3, GSDMD and IL-1β against the human and mouse sequences showed conservation across these species. Residues suggested to play important roles in ASC nucleation are conserved in canine NLRP3, suggesting the presence of a functional protein (Figure 3.4.1). Analysis of GSDMD protein sequences identified the conserved caspase-1 cleavage site to be present in the dog (Figure 3.3.3). Although western blotting analysis of dog GSDMD using human and mouse antibodies did not work probably because of a lack of antibody cross reactivity (Figure 3.3.4), sequence analysis suggested the presence of a functional GSDMD (Figure 3.3.3). Sequence analysis of IL-1β showed the presence of the caspase-1 and caspase-8 cleavage sites in the dog (Figure 3.4.2). The presence of the adapter protein ASC has also been identified in the dog genome, but it has not yet been annotated as a single gene (Figure 3.3.1). Sequence comparison has identified both, the PYD and CARD domains with the residues important for filament nucleation being present in the identified sequences (Figure 3.3.1). Western blotting analysis using an ASC antibody that cross reacts with human and mouse ASC proteins, showed the possible presence of ASC at the protein level in DH82 cell lysates (Figure 3.3.2). These results suggested the presence of functional inflammatory proteins in the dog and their responses have been investigated in the second part of this chapter.

DH82 cell responses to known inflammatory activators were determined by measuring cell lysis (LDH release and live cell imaging), ASC speck formation, fluorescent caspase probe localisation and the production of IL-1β. Canonical activation of the NLRP3 inflammasome using nigericin

bacterial toxin resulted in low level of ASC-speck formation and activated caspase-1 and caspase-8 recruitment (Figure 3.5.4). To induce cell lysis and IL-1β release, DH82 cells required high concentration of the nigericin ligand, while they showed complete resistance to concentrations widely established in human and mouse cells (Figures 3.5.1 and 3.5.2). Based on the results obtained using murine *caspase-1*$^{-/-}$*caspase11*$^{-/-}$ cells, the nigericin-induced cell lysis was most likely NLRP3-independent (Figure 3.5.1). The presence of bioactive IL-1β suggested a low level inflammasome activation or production of IL-1β induced by priming to LPS (Figure 3.5.3). Live cell imaging of nigericin stimulated DH82 cells suggested the induction of a lytic form of cell death (Figure 3.5.5 20'). The observed nigericin resistance to inducing cell lysis has also been validated in canine PBMCs, representing primary cell responses (Figure 3.5.6).

Non-canonical NLRP3 inflammasome activation and cytosolic recognition by caspase-11 were also investigated. While transfection of LPS did not induce cell lysis in DH82 cells, large amount of bioactive IL-1β were present in cell supernatants (Figure 3.6.2). TLR priming events led to the release of processed IL-1β without concomitant cell lysis (Figure 3.6.3). This phenomenon has been reported in human monocytes, where TLR4 activation leads to IL-1β maturation with cell surviving [87], [185]. The lack of ASC speck formation and activated caspase recruitment observed in DH82 cells gives further evidence for potential TLR mediated inflammasome formation (Figure 3.6.4). Live cell imaging of TLR primed and LPS transfected DH82 cells also showed no obvious morphological changes throughout the treatment (Figure 3.6.5). IL-1β release and the lack of cell lysis have also been investigated using canine PBMCs, showing similar results to those observed in DH82 cells (Figure 3.6.6). Overall this suggests that canines have evolved refractory inflammasome responses to stimuli activating NLRP3 and raises important questions about the role of inflammasomes in innate immunity and host defence in other species such as humans.

# Chapter 4

# Characterisation of the DH82 cell line responses to *S.* Typhimurium infection

## 4.1 Introduction

The NLRC4 inflammasome responds to evolutionarily conserved bacterial components of the T3SS [124], [348] (PrgI and PrgJ) and flagellin to initiate immune responses to clear bacterial infections [46]. Detection of these ligands requires NAIPs that have been identified as the intracellular sensor proteins that enable NLRC4 receptors activation and subsequent responses [46], [133], [135]. Upon ligand binding, NAIP recruits NLRC4 proteins [349] into an inflammasome complex leading to caspase-1 activation. Active caspase-1 mediates inflammatory cytokine maturation [350] and initiation of pyroptotic cell death by GSDMD cleavage [43], [44]. It has been shown that NLRP3, ASC, caspase-1 and caspase-8 can all be recruited to the NLRC4 inflammasome [62]. ASC may be dispensable for caspase-1 recruitment because NLRC4 contains a CARD domain [121], its presence within the inflammasome however enhances cytokine processing [351]. This could be due to the presence of additional CARD domains recruiting additional caspase-1 proteins to the inflammasome complex.

Genomic sequence analysis has shown that domesticated dogs and other species of the canine family entirely lack the *NAIP* genes and their *NLRC4* gene contains two premature stop codons making it a non-functional, pseudogene [41]. I therefore investigated the consequences of this genotype and the role of the canine caspase-1/4/11 hybrid protein in DH82 cells in a series of *in vitro* infection assays using *Salmonella enterica* serovar Typhimurium – a well characterised bacterial pathogen that activates the NLRC4 inflammasome.

In this chapter I monitored inflammasome activity by measuring cell lysis (relative LDH release) and the production and cleavage of IL-1β. Morphological changes induced by these activators were also monitored by live cell imaging using bright-field microscopy.

## 4.2 *S.* Typhimurium infection of DH82 macrophages

Gentamicin protection assays (GPA) were used to investigate the inflammatory responses induced in DH82 cells by *S.* Typhimurium. During this assay, canine DH82 and murine iBMDMs were infected with different *S.* Typhimurium strains (SL1344 wild-type, *ΔFliC/ΔFliB, ΔPrgJ, ΔFliC/ΔFliB/ΔPrgJ*) as described in Materials and Methods section 2.5.

Prior to infection experiments, growth curves for each *S.* Typhimurium strain were determined to ensure the uniformity of multiplicity of infection (MOI) used in this work (Figure 4.2.1). Optical density (OD) was measured and colony forming units (CFUs) were calculated after every hour for a total of 10 hours (Figure 4.2.1) as described in Materials and Methods section 2.4. To assess the number of CFUs at the incubation time-point used in infection assays, CFUs were also enumerated after the 17.5 + 2 hours culturing time-point (Figure 4.2.1B). Comparison of the ODs and CFUs showed that the wild-type *S.* Typhimurium strain displayed reduced growth kinetics compared to the mutants (Figure 4.2.1). This can be the result of reduced energy requirements as a consequence of not expressing large and complex proteins. I therefore used equal CFU's from wild-type and mutant strains based upon my growth kinetic analysis in subsequent assays.

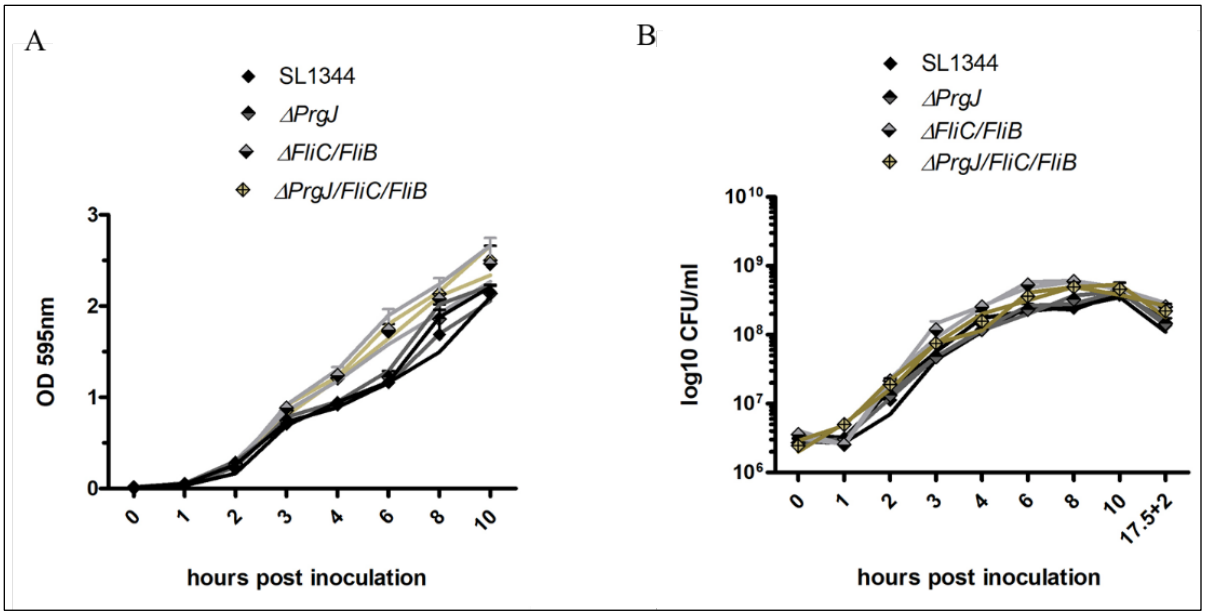


**Figure 4.2.1 Wild-type *S.* Typhimurium growth has reduced kinetics compared to mutant strains.** (A) OD of *S.* Typhimurium inoculums was measured each hour for up to 10 hours as described in Materials and Methods section 2.4. (B) CFUs of *S.* Typhimurium inoculums were numerated each hour up to 10 hours incubation and at 17.5 + 2 hours culturing time-point as described in Materials and Methods section 2.4. Data shown is pooled from two independent experiments. Error bars represent the standard error of means (SEM) of triplicate wells.

A consequence of NLCR4 activation by *S.* Typhimurium infection is the rapid induction of caspase-1 dependent host cell pyroptosis [62], [123]. In the bioinformatics analysis there was no canine *NAIP* genes and premature stop codons are present in the *NLRC4* gene [41], so I hypothesised that canine macrophages would be resistant to *S.* Typhimurium induced cell death. To investigate this I compared the inflammasome responses of immortalised murine wild-type, *Nlrc4*$^{-/-}$, *caspase1*$^{-/-}$*caspase11*$^{-/-}$ with canine DH82 cells infected with wild-type SL1344 *S.* Typhimurium at MOI 1, 10 and 50. Percentage of cytotoxicity (Figure 4.2.2) and cytokine release (Figure 4.2.3) were determined at 1, 2, 6 and 24 hours post infection by LDH release and ELISA, respectively. Importantly, the cytotoxicity responses in DH82 cells at all MOIs were similar to that of murine *Nlrc4*$^{-/-}$ and *caspase1*$^{-/-}$*caspase11*$^{-/-}$ cells (Figure 4.2.2) and was in agreement with my initial hypothesis. The NLRC4 inflammasome is rapidly activated upon *S.* Typhimurium infection and murine *Nlrc4*$^{-/-}$ macrophages fail to activate pro-caspase-1 and cell death in response to *S.*

Typhimurium infection [123], results that I also confirmed in my experiments. Regardless of the MOI used, DH82 cells in contrast to wild-type iBMDMs did not release detectable amount of LDH in the first 6 hours post infection (Figure 4.2.2) and resembled responses observed in *Nlrc4*$^{-/-}$ or *caspase1*$^{-/-}$*caspase11*$^{-/-}$ iBMDMs (Figure 4.2.2). DH82 cells infected with *S.* Typhimurium SL1344 MOI of 1 (Figure 4.2.2A) induced a maximum of about 20% cell lysis by 24 hours post infection in comparison to wild-type iBMDMs which induced higher responses (40% cell lysis). A lytic response was observed in all murine cell genotypes and DH82 cells at higher MOI's at later time-points (Figure 4.2.2). The kinetics of DH82 cell lysis at MOI of 1 was similar to what I observed in *Nlrc4*$^{-/-}$ and *caspase-1*$^{-/-}$*caspase-11*$^{-/-}$ murine cells but was reduced at the MOI of 10 and 50 used (Figure 4.2.2C). Based upon my data in the previous chapter, it could indicate that the hybrid caspase-1/4/11 gene is not activated in response to *S.* Typhimurium.

*S.* Typhimurium can activate different NLRs and caspases, which can be recruited to the same inflammasome complex [352]. Both, NLRP3 and caspase-8 have been shown to be recruited to the NLRC4 inflammasome in response to *S.* Typhimurium infection [62], [292]. Further investigation would be required to determine if the delayed lytic responses observed in DH82 cells during *S.* Typhimurium infection are primarily NLRP3 and/or caspase-8 driven.

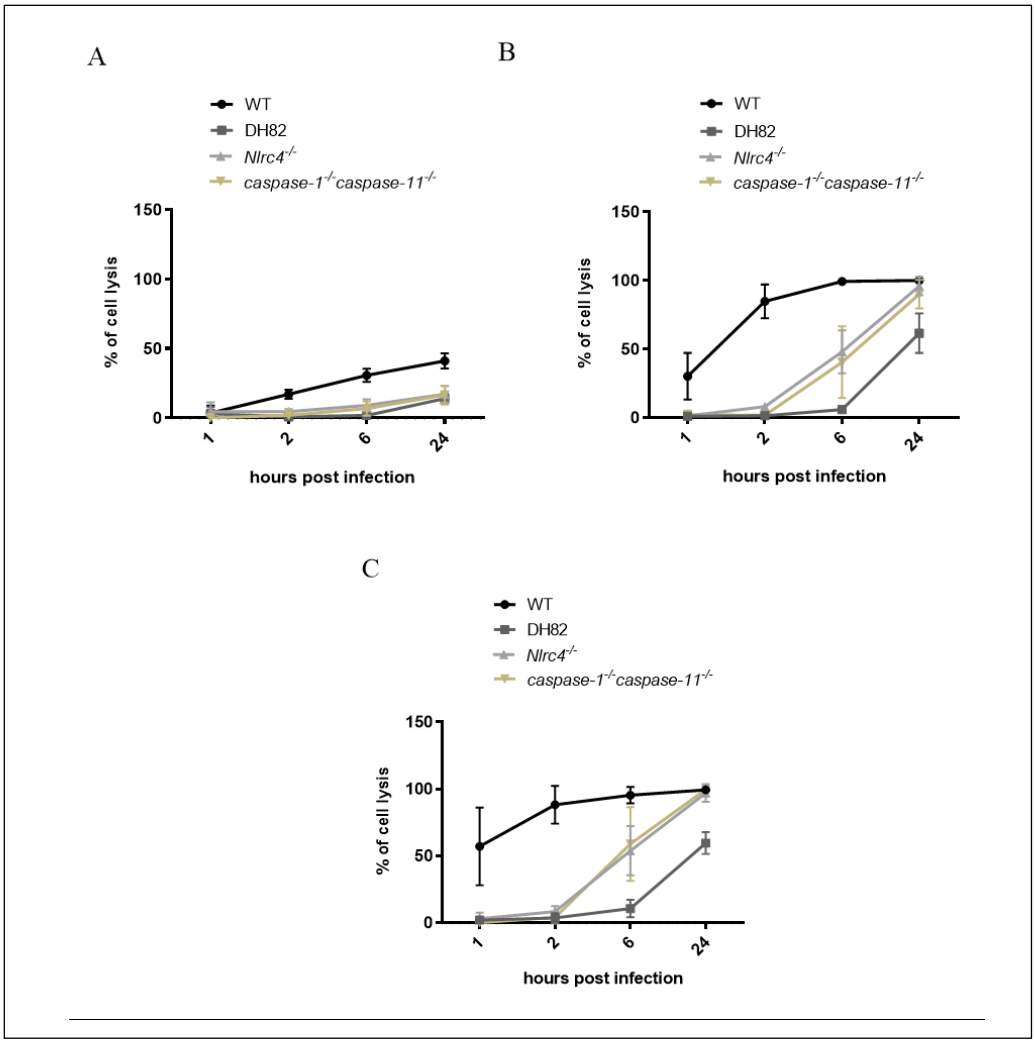


**Figure 4.2.2 DH82 cells show delayed cell lysis responses when infected with wild-type *S.* Typhimurium.** Murine wild-type, *Nlrc4*$^{-/-}$, *caspase1*$^{-/-}$*caspase11*$^{-/-}$ and DH82 cells were infected with *S.* Typhimurium with three different MOIs; (A) 1, (B) 10 and (C) 50. Percentage of cell lysis at 1, 2, 6 and 24 hour post infections was determined via the measurement of relative LDH release. Data shown is pooled from three independent experiments. Error bars represent the standard error of means (SEM) of triplicate wells.

IL-1β release into the supernatant was also measured in DH82 cells infected with *S.* Typhimurium with MOI of 1 (Figure 4.2.3A), 10 (Figure 4.2.3B) and 50 (Figure 4.2.3C) at 1, 2, 6 and 24 hour time-points. Murine wild-type cells released lower amounts of IL-1β than DH82 cells at later time points. This could be attributed to the high levels of pyroptotic cell death (Figure 4.2.3) in the wild-

type cells presumably through GSDMD terminating the infected cells capacity to express and release the cytokine. In contrast, DH82 cells, which underwent a slower cytotoxic response released very small amounts of IL-1β at earlier time-points (1, 2 and 6 hours post infection) irrespective of the MOI used (Figure 4.2.3) but significantly increased amounts by 24 hours post infection at all MOIs investigated (Figure 4.2.3). There is an inverse relationship between the amount of IL-1β released and the increasing MOI used. This could be a result of the reduced cell lysis effect at lower MOIs permitting inflammatory cytokines expression (Figure 4.2.2), but other published studies indicate that the amount of IL-1β released correlates with the amount of cell lysis induced, as IL-1β release requires membrane pore formation or cell lysis [353], [354]. My analysis of canine cells during infection therefore raises some important questions about the processing and release of IL-1β in these cells. I have demonstrated that DH82 cells have significantly reduced early cell lysis responses compared to murine cells but significantly increased inflammatory cytokine production at later time-points. Given the apparent lack of functional inflammasome components in canines, it would be important to understand which PRR's are responding to *S.* Typhimurium infection.

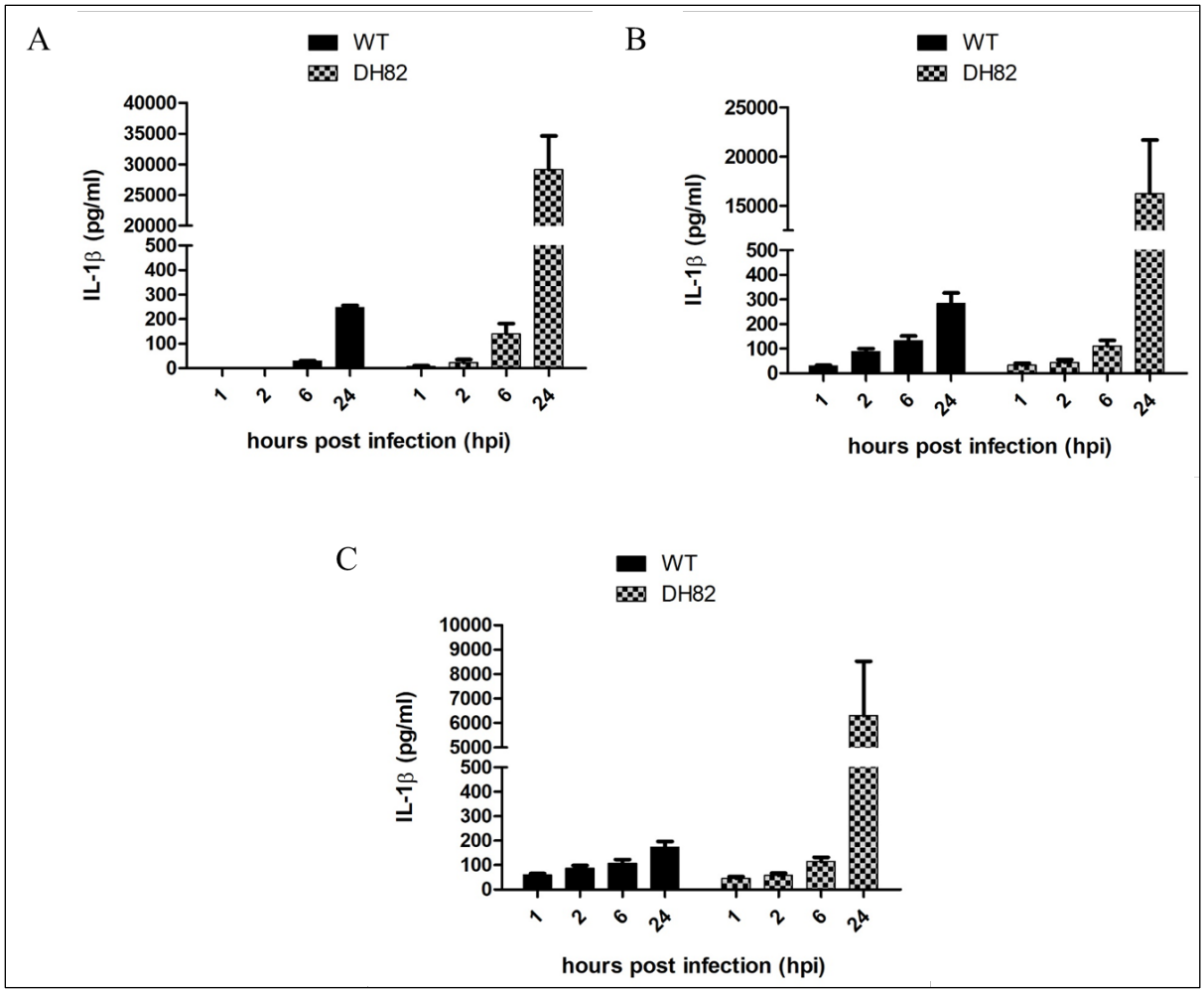


**Figure 4.2.3 DH82 cells release large amount of IL-1β into the supernatant in response to *S.* Typhimurium infection.** Murine wild-type and canine DH82 cells were infected with *S.* Typhimurium with three different MOIs; (A) 1, (B) 10 and (C) 50. IL-1β release in the supernatant was measured by ELISA method at 1, 2, 6 and 24 hour post infections. Data shown is pooled from three independent experiments. Error bars represent the standard error of means (SEM) of triplicate wells.

My previous chapter indicated that canine cells released unprocessed pro-IL-1β into the supernatant only with high amounts nigericin stimulation (Figure 3.5.3). In order to investigate whether the IL-1β in the supernatant following *S.* Typhimurium infection was in a pro or proteolytically activated form, protein precipitates of supernatants from DH82 cells infected with *S.* Typhimurium (MOI 1 for 24 hours) was performed as described in Materials and Methods

section 2.10. Infection with MOI of 1 only resulted in a small percentage of cell lysis (Figure 4.2.2), but the greatest amount of IL-1β release when measured by ELISA (Figure 4.2.3). Immunoblotting against canine IL-1β showed evidence of IL-1β processing (Figure 4.2.4). Importantly and in contrast to infection of murine cells with *S.* Typhimurium, the apparent cleaved form of IL-1β appeared smaller than the P17 form associated with caspase-1 cleavage [355]. I have demonstrated that the canine caspase hybrid has reduced activity during inflammasome activation, so the presence of a smaller molecular weight form of IL-1β could indicate processing by an alternative proteolytic system. Elastase, cathepsin G and collagenase have been shown to process recombinant IL-1β in activated human monocytes, however these proteases produced bioactive IL-1β at around 17 kDa [356], [357]. Chymotrypsin-like serine proteinase chymase in human mast cells was shown to process IL-1β into its bioactive form resulting in a slightly larger 18 kDa product [358]. While proteinase-3 (PR-3) has also been suggested to cleave IL-1β *in vitro* in human monocytes [359]. Further investigation is required to identify which protease(s) is/are contributing to IL-1β processing in canine macrophages.

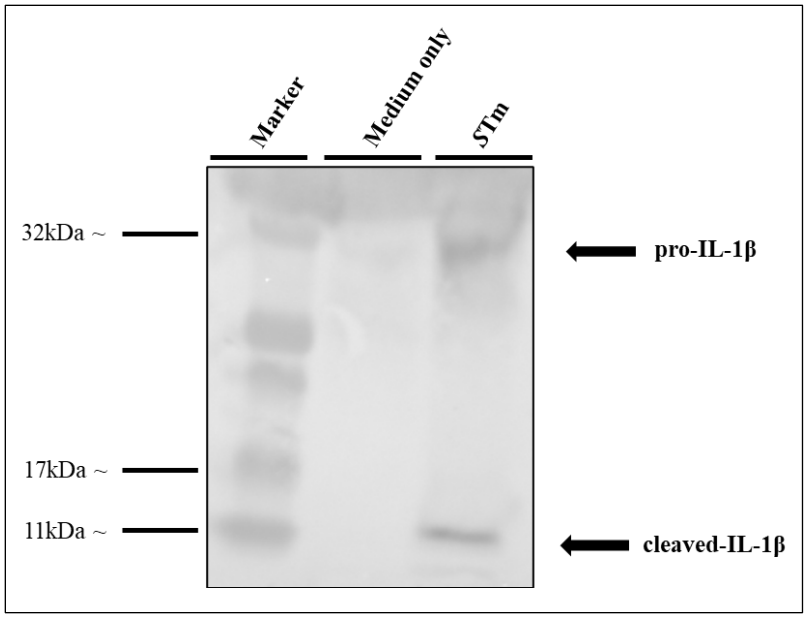


**Figure 4.2.4 *S.* Typhimurium infection of DH82 cells results in the maturation of pro-IL-1β.** DH82 cells were infected with *S.* Typhimurium MOI of 1 for 24 hours. Full protein precipitation and immune blotting against dog IL-1β showed the presence of both, pre- and cleaved form of the cytokine. Representative immunoblot is from two independent experiments.

During pyroptosis caspase cleaved GSDMD induces pore formation in the cell membrane resulting in a rapid osmotic shock causing cell swelling and eventually rupture of the cell membrane [72], [75], [234]. These characteristics can be visualised by bright field microscopy. DH82 cells were infected with *S.* Typhimurium MOI of 50 for 24 hours and bright field images using confocal microscope were taken every 5 minutes of the same focal point during the entire time of the infection (Figure 4.2.5). Representative images can be found in Figure 4.2.5, which shows DH82 cell swelling and later rupturing. Cells undergoing other types of lytic cell death than pyroptosis, for example necroptosis, can also display similar morphology [253]. One interesting observation was that cells appeared to be locked in the swollen phase with rupture only happening at a much later time-point. Given that cell swelling during pyroptosis is a direct result of GSDMD pore forming activity [75], this could perhaps be a result of suboptimal inflammasome activation and therefore reduced GSDMD processing and pore formation. Inefficient GSDMD cleavage could mean that it takes cells much longer time to reach a certain 'threshold' in the number of pores being formed in the membrane [238]. Alternatively, it may be that DH82 cells can actively repair

pores in the membrane [360], [361], delaying the reach of the 'threshold' for the number of pores. It is also possible that cell death is occurring independently of GSDMD.

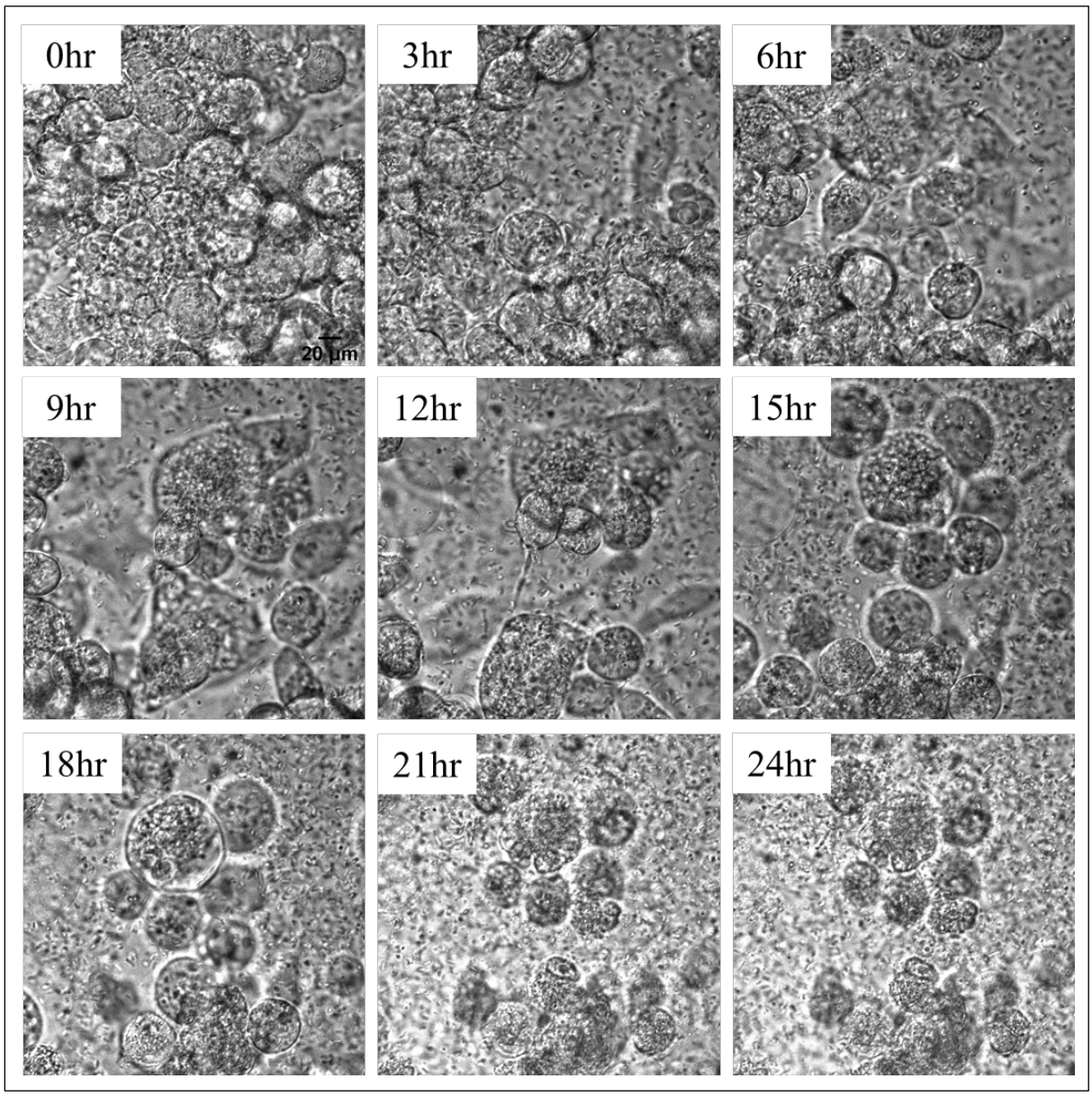


**Figure 4.2.5 DH82 cells display characteristics of lytic form of cell death in response to *S.* Typhimurium infection.** DH82 cells were infected with wild-type *S.* Typhimurium MOI of 50 for 24 hours. Bright field images were taken every 5 minutes during the 24 hours infection on a confocal microscope. Representative bright field images are from a single experiment.

Despite DH82 cells resistance to cell lysis with infection at early time points, the cells succumbed to a lytic cell death at later time-points post infection. I therefore investigated which bacterial components may trigger this delayed death response in canine cells. Using DH82 cells infected with wild-type, *ΔPrgJ*, *ΔFliC/ΔFliB* or *ΔPrgJ/ΔFliC/ΔFliB S.* Typhimurium strains (Figure 4.2.6) at two different MOIs, 10 (Figure 4.2.6A) and 50 (Figure 4.2.6B) I examined cell lysis by LDH release (Figure 4.2.6). DH82 cells died when infected with wild-type *S.* Typhimurium at MOI of 10 by 24 hour post infection (Figure 4.2.6A). Interestingly, *S.* Typhimurium strain lacking flagellin proteins FliC and FliB but expressing type III secretion system protein PrgJ showed similar responses to that of SL1344 wild-type strain (Figure 4.2.6A). *S.* Typhimurium strain lacking PrgJ but expressing FliC and FliB proteins induced significantly reduced lytic responses, most similar to the one observed with *S.* Typhimurium strain *ΔPrgJ/ΔFliC/ΔFliB* (Figure 4.2.6A). These results suggested that the late response is primarily mediated via mechanism dependant on the type III secretion proteins. This is an important observation as it may indicate which PRR(s) are detecting infection in canines in the apparent absence of NAIP and NLRC4. The phenotype observed with MOI of 10 failed to hold when cells were infected with MOI of 50 (Figure 4.2.6B). *S.* Typhimurium strain lacking PrgJ induced the same amount of cell lysis as the strain deficient for FliC and FliB proteins (Figure 4.2.6B). This loss of specificity in the cell death mechanism could be the result of an overwhelming bacterial infection response, with multiple types of recognition, metabolic and signalling pathways being activated at the same time.

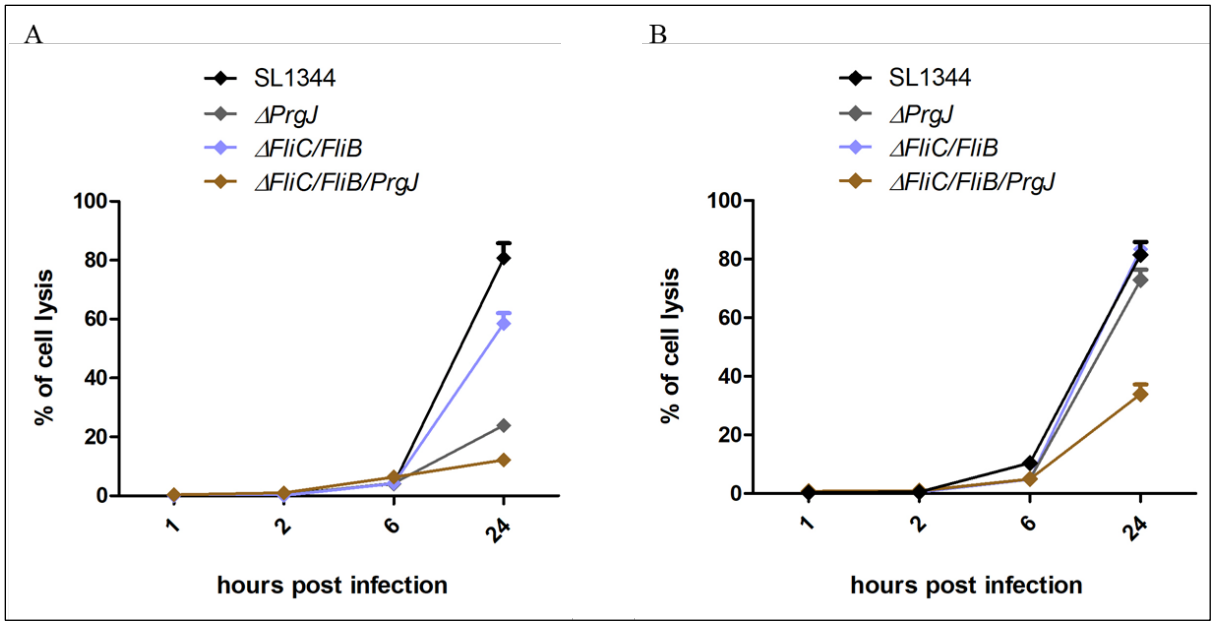


**Figure 4.2.6 *S.* Typhimurium induced delayed cell lysis is reduced in the absence of the type III secretion protein PrgJ.** DH82 cells were infected with *S.* Typhimurium wild-type, *ΔPrgJ*, *ΔFliC/ΔFliB* and *ΔPrgJ/ΔFliC/ΔFliB* strains with MOI (A) 1, (B) 10 and (C) 50. LDH release into the supernatant was measured at 1, 2, 6 and 24 hour post infection. Data shown is pooled from three independent experiments. Error bars represent the standard error of means (SEM) of triplicate wells.

As seen in previous experiments, there was no detectable IL-1β in the supernatant of *S.* Typhimurium infected DH82 cells at early time-points and only a small amount could be detected at 6 hours post infection (Figure 4.2.3). By 24 hours, DH82 cells infected with MOI of 10 (Figure 4.2.7) with either wild-type or FliC/FliB-deficient *S.* Typhimurium strains induced large amount of IL-1β release into the supernatant (Figure 4.2.7A). By contrast, cells infected with either PrgJ or FliC/FliB/PrgJ-deficient strains induced 3-fold less IL-1β release into the supernatant (Figure 4.2.7A) and was a reflection of the cell lysis observations with these mutant bacteria. These results provided further evidence that the cell lysis response observed is primarily mediated by type III secretion proteins. In concert with the cell lysis data (Figure 4.2.6C), DH82 cells infected with wild-type *S.* Typhimurium (MOI 50) produced four times less IL-1β compared to the cells infected with any of the deficient strains (Figure 4.2.7B). This could be explained by the fact that cells

infected with wild-type *S.* Typhimurium underwent cell lysis with faster kinetics and therefore had less time to express and process IL-1β.

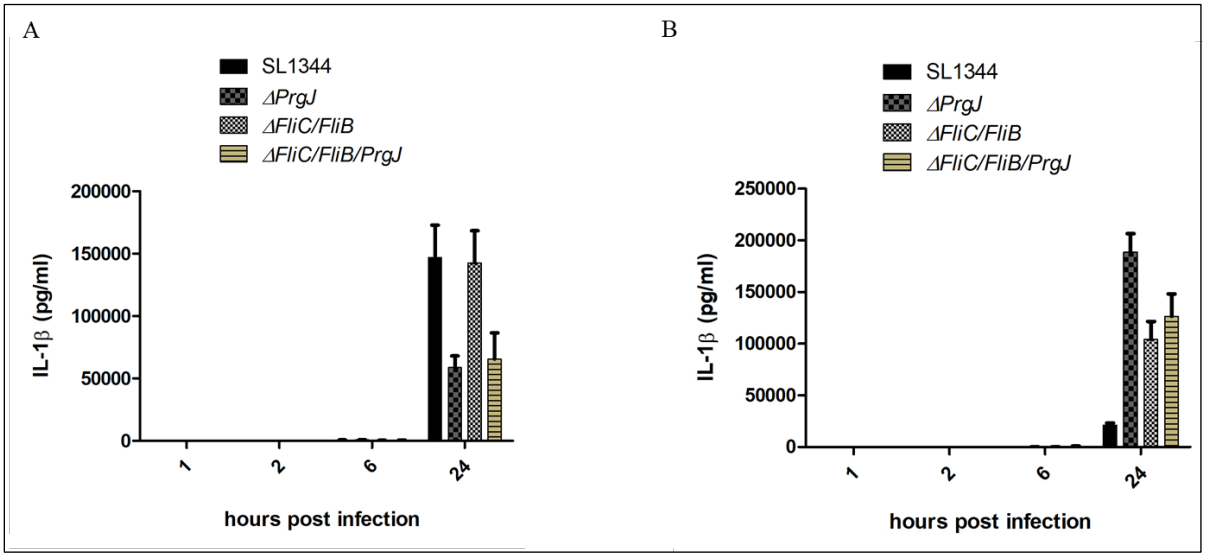


**Figure 4.2.7 Type III secretion system protein PrgJ drives IL-1β release in DH82 cells in response to *S.* Typhimurium infection.** DH82 cells were infected with *S.* Typhimurium wild-type, *ΔPrgJ*, *ΔFliC/ΔFliB* and *ΔPrgJ/ΔFliC/ΔFliB* strains with MOI (A) 10 and (B) 50. IL-1β release was measured at 1, 2, 6 and 24 hours post infection. Data shown is pooled from three independent experiments. Error bars represent the standard error of means (SEM) of triplicate wells.

To confirm my data obtained with an immortalised cell line was representative of primary canine cells, cell lysis and cytokine responses to canonical inflammasome activator *S.* Typhimurium were also investigated in canine primary PBMCs. In these *in vitro* experiments PBMCs were isolated from patients attending the phlebotomy clinic at the Clinical Pathology Laboratory, Department of Veterinary Medicine, University of Cambridge (Table 2.2.1) as described in Materials and Methods sections 2.3 and 2.6. Canine primary and DH82 cells were infected with wild-type *S.* Typhimurium at three different MOIs; MOI 1 (Figure 4.2.8A), MOI 10 (Figure 4.2.8B) and MOI 50 (Figure 4.2.8C). Canine primary cells infected with lower MOI of *S.* Typhimurium showed delayed cell lysis responses, similar to that of seen with DH82 cells (Figure 4.2.8A and B). Infection with MOI of 1 induced negligible amount of cell lysis even at 24 hour time-point (Figure

4.2.8A). While infection with MOI of 10 induced slightly higher percentage of cell lysis, lysing around 70% of the cells by 24 hours (Figure 4.2.8B). Greater differences were observed when cells were infected with MOI of 50 (Figure 4.2.8C). Dog primary cells infected with lower MOIs did not release LDH until 6 hour post infection but high MOIs resulted in nearly all of the cells to lyse by 6 hour post infection with significant lysis being observed as early as 2 hour time-point (Figure 4.2.8C). These results suggested that PBMCs and DH82 cells respond to *S.* Typhimurium infection in a similar manner with PBMCs somewhat more responsive than DH82 cells which would not be unexpected given the immortalised status of the DH82 cells. Nevertheless, this suggested, that conclusions drawn from DH82 cell line responses are a good indication of primary cell behaviour and that canines display refractory responses in terms of cell death to other species when challenged with pathogenic *S.* Typhimurium.

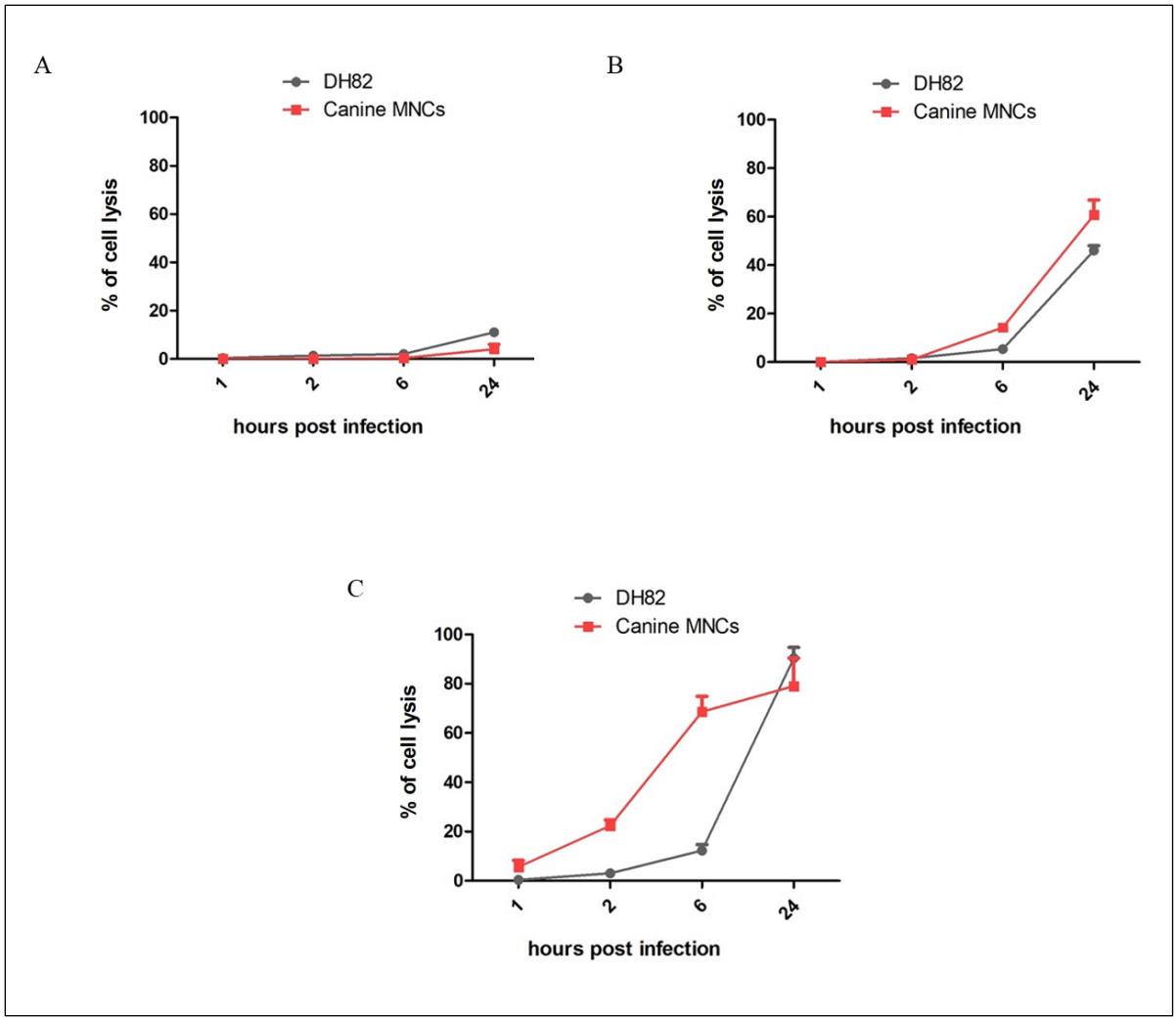


**Figure 4.2.8 Canine PBMC cell lysis responses are similar to that of DH82 cells in response to *S.* Typhimurium infection.** Canine PBMCs and DH82 cells were infected with wild-type *S.* Typhimurium strain at MOI of (A) 1, (B) 10 and (C) 50. Cell lysis was quantified by the relative amount of LDH released at 1, 2, 6 and 24 hour time-points. Data shown is from a single experiment. Error bars represent the standard error of means (SEM) of triplicate wells.

I also investigated the inflammatory capacity of primary canine PBMCs compared to DH82 cells during infection using IL-1β as a read-out. Cells were infected with wild-type *S.* Typhimurium at MOI 1 (Figure 4.2.9A), 10 (Figure 4.2.9B) and 50 (Figure 4.2.9C) at 1, 2, 6 and 24 hour post infection. Although IL-1β was detected in the supernatant of canine primary cells, it was much reduced compared to that of detected of DH82 cells (Figure 4.2.9). This could potentially be

attributed to the presence of a heterogenic population in the isolated PBMCs with some cells such as B and T-cells producing none or very little inflammasome dependent cytokine. Also, some of the samples were from patients who had undergone chemotherapy or suffer from autoimmune disease (Table 2.2.1). It can be assumed that these conditions can create heterogeneity in cell responses and even in their genetic background. Experiments need to be repeated in primary cells to refine this data set.

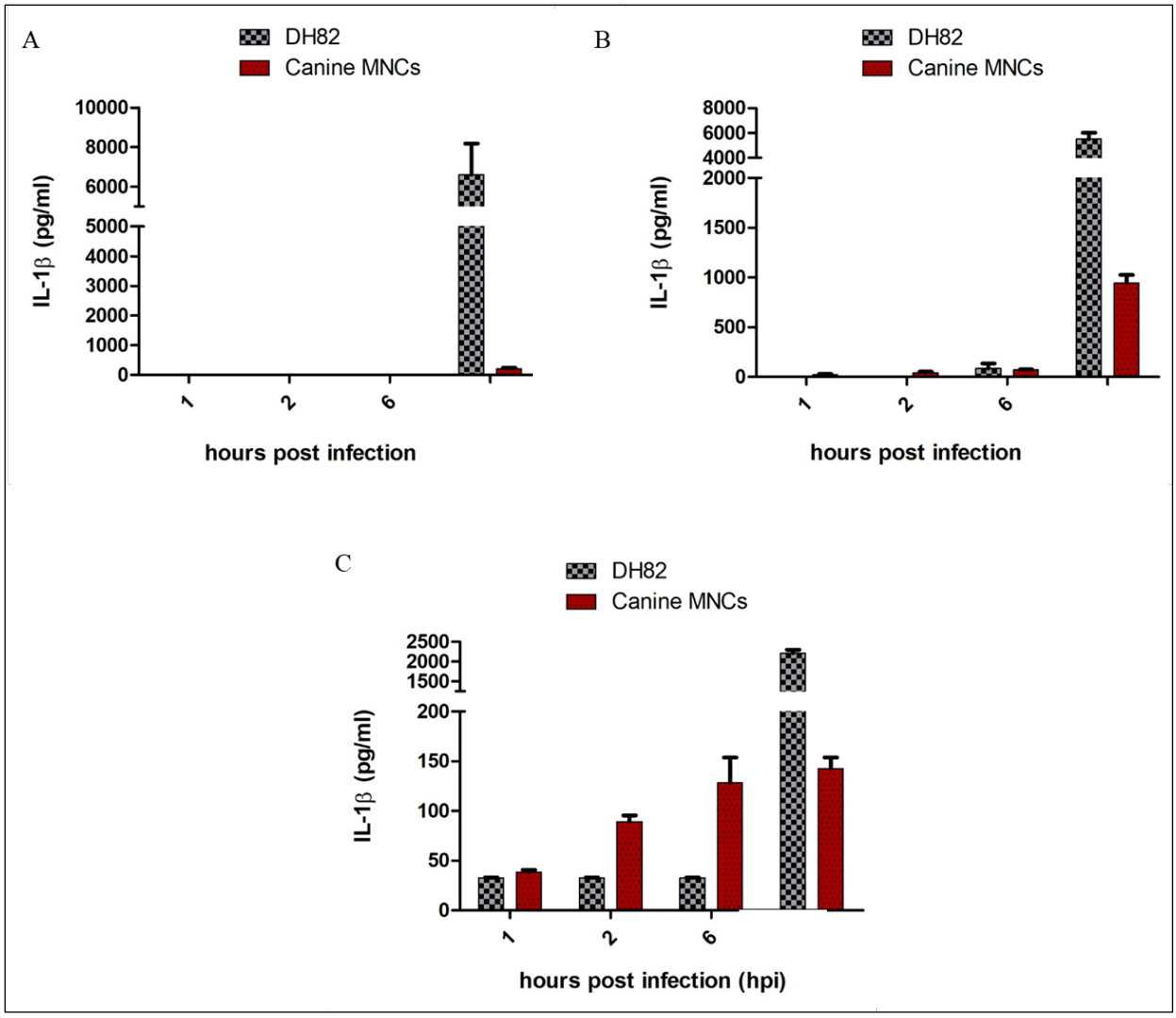


**Figure 4.2.9 Canine PBMCs release IL-1β in response to *S.* Typhimurium infection.** Canine PBMCs and DH82 cells were infected with wild-type *S.* Typhimurium strain at MOI of (A) 1, (B) 10 and (C) 50. IL-1β released into the supernatant was quantified at 1, 2, 6 and 24 hour time-points using ELISA method. Data shown is from a single experiment. Error bars represent the standard error of means (SEM) of triplicate wells.

## 4.3 Discussion

In this chapter I have investigated the inflammatory responses of the canine DH82 macrophage-like cell line and primary canine PBMCs. As I had previously demonstrated that canine cells were refractory to NLRP3 inflammasome agonists (Chapter 3), genomic sequence analysis has shown

additional major differences in canines when compared to the human and mouse genomes. The NLRC4 receptor predominantly responsible for the recognition of conserved components of the type III secretion system and [46] flagellin contains multiple premature stop codons [41]. These mutations result in the presence of a non-functional *NLRC4* pseudogene [41]. Sequence analysis has also demonstrated a total absence of *NAIP* genes [41]. NAIPs can directly sense these bacterial components and are crucial for the activation of the NLRC4 receptors [133], [135]. I have investigated the fate of canine cells when challenged with a canonical NLRC4 infectious agent *S.* Typhimurium. Cells infected with wild-type *S.* Typhimurium showed delayed cell lysis responses, similar to that observed in murine *Nrlc4*$^{-/-}$ and *caspase-1*$^{-/-}$*caspase11*$^{-/-}$ cells (Figure 4.2.2). Processed IL-1β in the supernatant of DH82 cells was also detected which occurred in conjunction with cell lysis but was significantly increased in comparison to murine cells (Figure 4.2.3). This was of a smaller molecular weight than caspase-1 mediated processing would produce and suggested alternate protease maturation of IL-1β in canines (Figure 4.2.4). Further work is required to identify this protease and whether its activation is dependent on inflammasome components. Live cell imaging of *S.* Typhimurium infected DH82 cells showed morphological features characteristic to lytic form of cell death, but with delayed kinetics compared to infected mouse cells (Figure 4.2.5). In this chapter I also examined cell lysis (Figure 4.2.8) and IL-1β (Figure 4.2.9) responses in canine PBMCs. These responses were largely similar to DH82 cells, thus further validating observations in DH82 cells, although there were slight differences in the degree of death seen.

Bacterial components driving the observed late cell lysis was also investigated using different *S.* Typhimurium mutant strains. To my surprise, the cell lysis (Figure 4.2.6) and IL-1β (Figure 4.2.7) responses were largely dependent on the type III secretion proteins. The type III secretory system protein PrgJ in mouse and PrgI in humans has been shown to be directly recognised by NAIPs [133]. No NAIPs are present in dogs yet *S.* Typhimurium lacking PrgJ still drove cell lysis in DH82 cells (Figure 4.2.6). This suggests the presence of another, perhaps not yet identified, receptor present in the dog, is responsible for recognising *S.* Typhimurium PrgJ or other type III secretory component. NLRP3 may be able to sense the homeostatic changes (e.g. potassium efflux) induced by the bacterial encoded effector proteins delivered via the type III secretion system. To test this DH82 cell responses following *S.* Typhimurium infection could be investigated in the

presence of raised extracellular potassium level which has been shown to inhibit NLRP3 inflammasome formation [83]. I have also shown in Chapter 3 that DH82 cells did not undergo lysis in response to transfected LPS (Figure 3.6.2A), therefore LPS-mediated non-canonical activation of NLRP3 through the activation of caspase-11/4/5 activation will not drive *S.* Typhimurium induced DH82 macrophage lysis.

# Chapter 5

# The role of caspase-1/4/11, caspase-8 and RIPK1 in *S.* Typhimurium-induced cell death and IL-1β processing in canine macrophages

## 5.1 Introduction

Over the past 30 years extensive research has resulted in the development of genome engineering techniques that allow direct editing of target gene sequences at specific locations. The discovery and further development of the prokaryotic adaptive immune system CRISPR-Cas9 [362]–[365] has revolutionised genome editing. This approach makes use of the bacterial endonuclease Cas9 that introduces double-stranded DNA breaks (DSB) which, in turn, will activate host-derived endogenous DNA repair mechanisms.

The bacterial CRISPR locus consists of 4 protein-coding genes and CRISPR arrays. CRISPR arrays consist of spacer regions containing foreign, pathogenic (e.g. bacteriophage) DNA fragments integrated in between short palindromic repeats [365]–[370]. CRISPR-associated endonuclease 1 (*cas1*), -*2* and conserved non-coding DNA sequences 2 (*cns2*) are required for the acquisition of new DNA fragments from invading pathogens into the spacer regions [362], [371]. These spacer regions are transcribed into CRISPR RNA (crRNA) that recognise and anneal to spacers matching sequences from invading pathogens [372]. While a small scaffold RNA called trans-activating CRISPR RNA (tracrRNA) is responsible for guiding the Cas9 protein to the complementary sequence recognised by the crRNA [373], [374]. Cas9 protein activity results in blunt-end cleavage of target DNA sequences, that match the already existing spacers, 3 nucleotides upstream of a so called protospacer adjacent motif (Pam) [372], [375]–[377]. Cas9 nuclease recognises a so-called NGG sequence, where the first base can be any of the four known nucleotides followed by two guanine nucleobases.

This system allows accurate and highly efficient gene engineering [378], [379]. In comparison to other available techniques, CRISPR-Cas9 allows genome editing in a high-throughput, multiplexed manner [380], minimising off-target effects while reducing the length and cost of the process. Different CRISPR adaptive immune systems can be found in different bacterial species.

All of them, however, serve the same purpose that is acquiring, storing and recognising invading pathogenic DNA sequences.

As shown in Chapter 4 (Figure 4.1.5), canine DH82 macrophages infected with *S.* Typhimurium underwent a lytic form of cell death (Figure 4.1.5). In this chapter I aimed to identify the mechanism via which DH82 cells lyse in response to *S.* Typhimurium infection.

Previous *in vitro* studies have investigated the recruitment of different NLRs and caspases to the inflammasome in macrophages. Super resolution imaging of differentiated THP1 cells infected with *S.* Typhimurium, for example, has shown that NLRC4, ASC and caspase-1 are recruited into the same inflammasome complex [62]. NLRP3 and caspase-8 recruitment to the same inflammasome complex was also shown in primary murine macrophages [62], [140]. Activated caspase-1 drives pyroptotic cell death by the cleavage of an executioner protein GSDMD [44], while caspase-8 has been shown to modulate IL-1β processing [140], but can also process GSDMD under certain conditions [223]–[225]. My previous results showed that active caspase-1 and caspase-8 were recruited to the ASC speck in DH82 cells in response to canonical NLRP3 activation following stimulation with nigericin (Figure 3.5.4). Necroptosis, another form of lytic cell death, can display morphological features similar to those displayed by pyroptosis [253]. To investigate whether DH82 cells undergo necroptosis in response to *S.* Typhimurium infection, I disrupted the canine *RIPK1* gene whose kinase activity has been shown to be an essential component of necroptotic cell death initiation [208].

In this chapter, I used CRISPR-Cas9 technology to disrupt the canine hybrid caspase-1/4/11, caspase-8 and RIPK1 in DH82 cells in an attempt to investigate their role in driving cell death and IL-1β processing in response to *S.* Typhimurium. I have interrupted gene function by introducing INDELS (insertions and deletions) at the identified catalytic site for each gene as described in Materials and Methods section 2.12. This work was divided into two parts, both of which are covered in this chapter. In the first part, I described the process of cell electroporation with RNP complexes (including target sequence specific crRNA, tracrRNA and Cas9 protein) to introduce genetic mutations followed by identification of these mutations via Illumina MiSeq sequencing.

In the second part, I have investigated cell death mechanisms that could drive cell death responses in DH82 cells following *S.* Typhimurium infection.

### 5.2 Results - Optimisation of nucleofection for DH82 cells

I assessed the tolerance and efficiency of DH82 cells to physical transfection. In this work, I used a Nucleofector 2b device to perform electroporations. Nucleofection allows the introduction of DNA, RNA and proteins directly into the cell cytoplasm and nucleus. Madin-Darby Canine Kidney (MDCK) cells have been shown to successfully uptake cDNA [381], [382] and siRNAs [383], but successful electroporation of DH82 cells using this device has not yet been reported. I therefore first optimised the parameters for electroporation of the DH82 cell line by transfecting a Green Fluorescence Protein (GFP) vector into the cytoplasm.

I performed all transfections as described in Materials and Methods section 2.12.1. In short, DH82 cells were resuspended in either L or V nucleofection solutions containing supplements to promote cell survival. Samples for each type of solution were transfected with pmaxGFP® vector using 7 different, pre-defined electrical parameters (Table 2.6). The electrical pulse permeabilizes the cell membrane and moves molecules into the cytosol and nuclei via an electrical field. Cells that were electroporated without the presence of the GFP vector and cells that were not electroporated in the presence of GFP vector were also included for each electroporation solution as controls in the analysis (Table 2.6).

Following electroporation, cells were left to recover overnight and analysed the next day. I assessed the transfection efficiency of several programmes by measuring GFP expression in single cells by flow cytometry 24 hours post-electroporation (Table 2.6). A forward (FSC) versus side scatter (SSC) scatter plot of the data was generated and a gate was drawn to include intact/viable cells and exclude debris (Figure 5.2.1 A and C). GFP expression and the percentage of $GFP^+$ cells in the gated population was then calculated by plotting GFP intensity versus cell count (Figure 5.2.1 B and D).

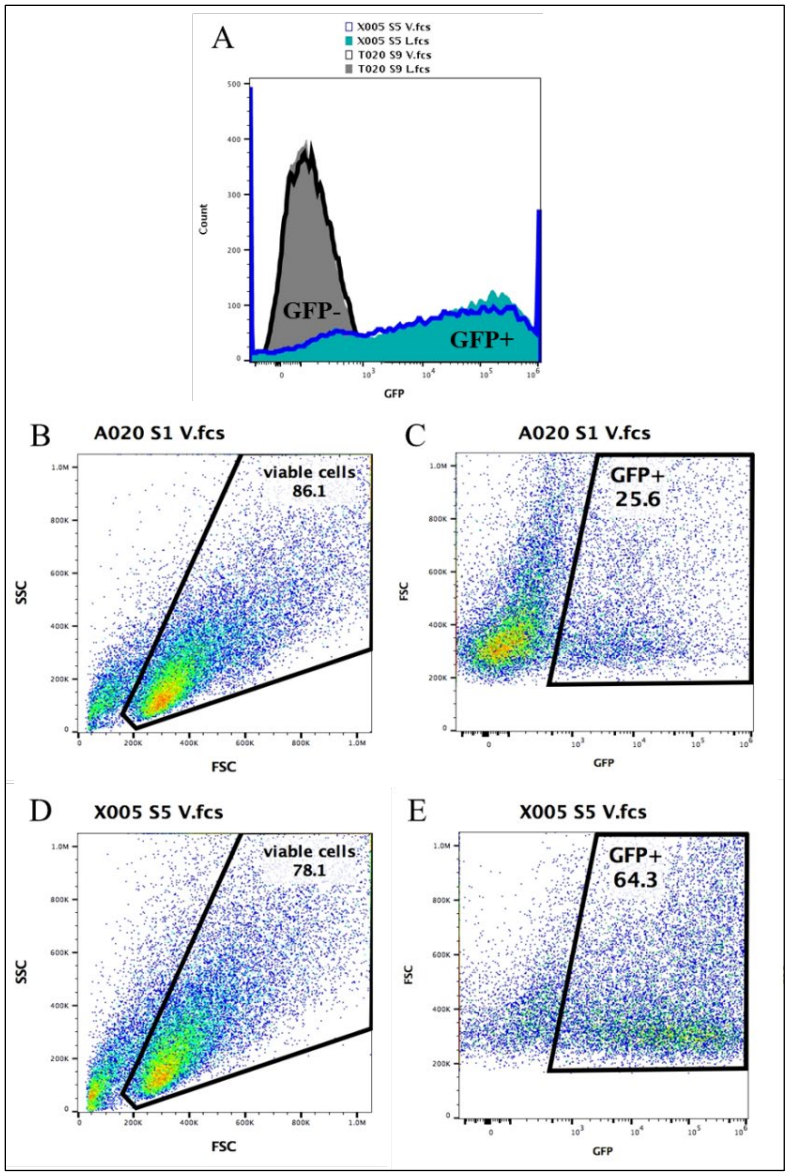


**Figure 5.2.1 Gating strategy used to assess GFP expression in DH82 cells following electroporation.** DH82 cells were resuspended in either nucleofection solution L or V and were electroporated using (A) X005 and T020 settings in the presence of and without GFP vector for both solutions. DH82 cells were also electroporated using 7 different, pre-defined electrical programs in the presence of pmaxGFP® vector for each solution. For reasons of simplicity, data shown in this graph was acquired by cells resuspended in nucleofector solution V and electroporated using programs A020 and X005 (B and D). Debris and dead cells were excluded by gating cells on a forward scatter (FSC) versus side scatter (SSC) plot. (C, E) GFP expression was then assessed on the gated population by plotting GFP intensity versus cell count.

The use of different solutions (L or V) did not have an effect on the transfection efficiency (Figure 5.2.2). The decisive factor in determining transfection efficiency was the specific nucleofector program used to transfect the plasmid into the cells. In particular, the lowest percentage of cells expressing GFP (less than 30%) was obtained following electroporation using program A020 (Figure 5.2.2C and G), while the highest percentage (over 60%) of cells expressing GFP was observed in cells electroporated with program X005 (Figure 5.2.2D and H). Subsequent experiments therefore were carried out using nucleofector program X005.

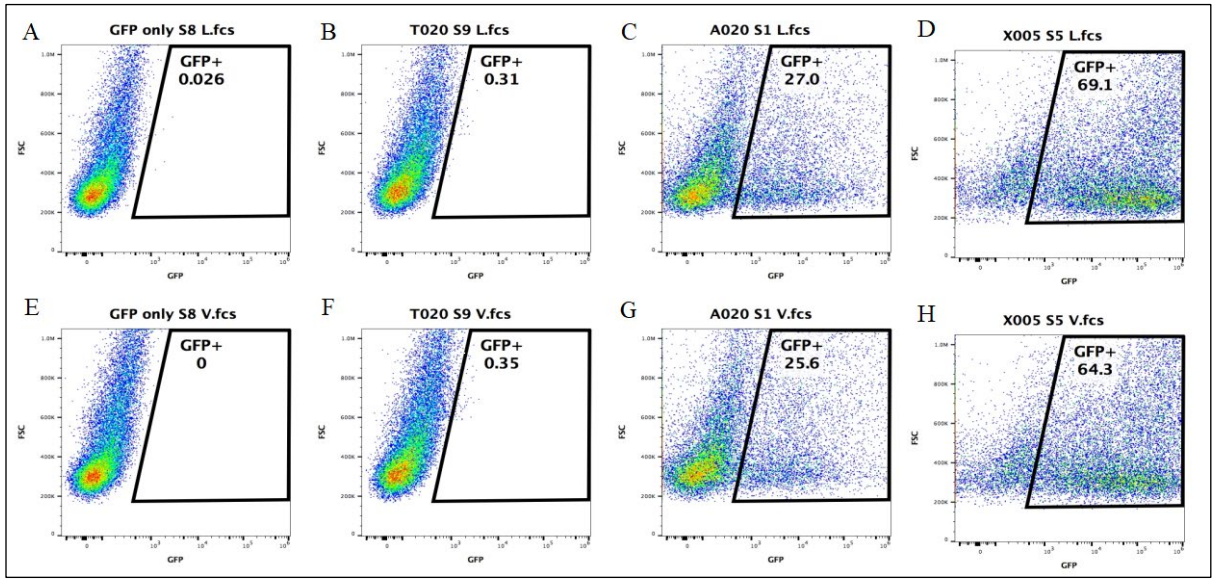


**Figure 5.2.2 Transfection efficiency is determined by the nucleofector program rather than the nucleofection solution.** DH82 cells were resuspended in either nucleofection solution L or V and were (C, D, G, H) electroporated using 7 different, pre-defined electrical programs in the presence of pmaxGFP® vector. Cells electroporated (B, F) without the presence of the GFP vector and (A, E) non-electroporated cells in the presence of the GFP were also included for each solution. GFP expression was assessed on FSC versus SSC gated population using the GFP signal versus cell count. The graph includes representative data for programs resulted in the (C, G) lowest and (D, H) highest GFP expression rate.

## 5.3 Generation of DH82 knock-out cell line for the hybrid caspase-1/4/11 gene

Genomic sequence analysis has previously revealed the presence of the hybrid caspase-1/4/11 gene in the canine genome [154]. The presence of two alternative transcripts has also been reported in canine PBMCs [154]. My previous results using mass spectrometry analysis of DH82 cell lysates showed the presence and constitutive expression of the canine hybrid gene (Figure 3.2.2). Using the MUSLCE analysis software, I additionally identified an evolutionarily conserved catalytic cleavage site (Figure 3.2.3) shared between the canine hybrid, human caspase-4 and mouse caspase-11 transcripts [322]. This suggested the presence of a functional hybrid protein in the dog, its role in driving cell death and cytokine maturation in response to intracellular pathogens has not yet been investigated. I therefore used CRISPR-Cas9 technology to induce out-of-frame mutations near this catalytic residue (Figure 3.2.3) located on exon 6 (Figure 5.3.1) to disrupt protein function.

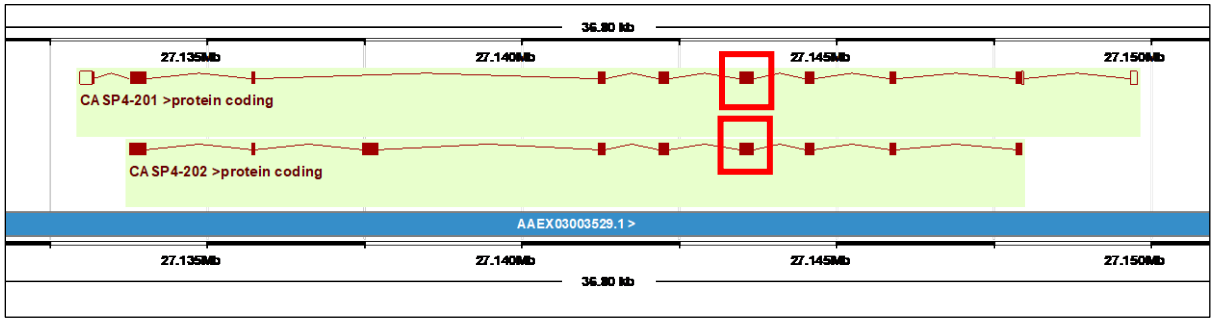


**Figure 5.3.1 Ensembl gene organisation of the hybrid caspase-1/4/11 gene.** Ensembl gene build annotation of the hybrid gene (ENSCAFG00000014860) shows the predicted protein coding exons. The identified catalytic residue is present in both transcripts in exon 6, highlighted by red rectangles.

Target sequence specific crRNAs were designed as described in Materials and Methods section 2.12.2. In short, crRNAs 20-nucleotide in length were designed immediately upstream of the Cas9 recognition Pam sequence (NGG) using Benchling online platform. To maximise efficiency and specificity, I chose the guide RNAs with the highest combined on- and off-target scores as calculated by the software. Their value can range from 0 to 100 and the higher it is the more effective the crRNA will be [384], [385]. I therefore selected two guide RNAs targeting sequences in exon 6 upstream of the catalytic reside (285-Cys). crRNA AACCTCAAGGACAAACCGA

targeted the coding strand of exon 6 and had an on-target score of 81.5 and off-target score of 70.3. The second crRNA GCATCCTGAATGGAATCTGT also targeted the coding strand of exon 6 but had lower on-target and off-target scores (62.4 and 67.2, respectively). To maximise the number of editing events, I performed three rounds of electroporation using three different concentrations of RNP complex (100-, 200 and 400nmol) for each crRNA as described in Materials and Methods section 2.12.3. Genomic DNA extraction and first level locus-specific PCR were performed as described in Materials and Methods sections 2.12.4 and 2.12.5, respectively. I then confirmed amplicon sizes on an agarose gel (Figure 5.3.2). The predicted amplicon size for the hybrid gene containing the sequences targeted by both crRNAs was 368 base pairs (Figure 5.3.2).

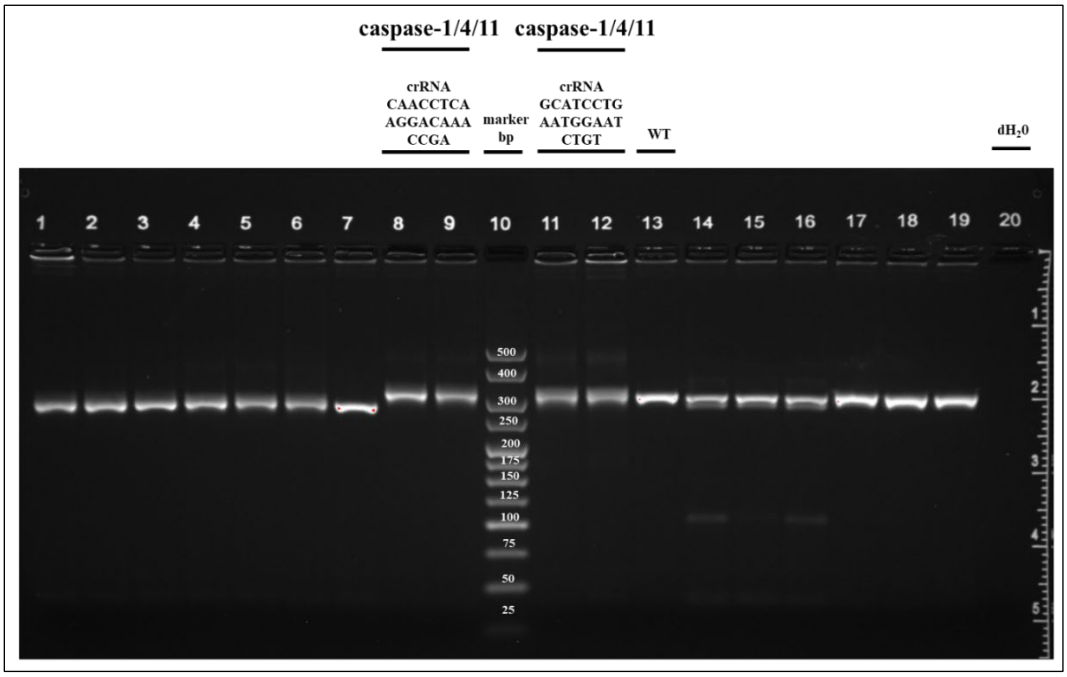


**Figure 5.3.2 Amplicon sizes following first level PCR for the caspase-1/4/11 gene were confirmed on an agarose gel.** After locus-specific PCR, two samples (10µl each) for each guide RNA were run in an agarose gel to confirm that the amplification resulted in the predicted amplicon size of 368bp. Samples 8 and 9 correspond to guide CAACCTCAAGGACAAACCGA, while samples 11 and 12 to guide GCATCCTGAATGGAATCTGT. Sample 20 contains negative ($dH_2O$ only) PCR control. Samples 1-7 and 13-19 corresponds to canine caspase-8 and *RIPK1* genes, respectively, and are discussed later in this chapter.

After confirming the correct amplicon sizes, second level PCR and MiSeq library preparations were performed as described in Materials and Methods sections 2.15 and 2.16, respectively. To determine gene editing efficiency and the type of indels induced, I genotyped bulk-edited cell populations via Illumina sequencing followed by sequence analysis using the OutKnocker online analysis tool. Sequence analysis showed highly efficient editing for both crRNAs independent of the RNP complex concentration (Appendices 1 and 2). Over 50% of the reads aligned contained indels regardless of the concentration used (Appendices 1 and 2). These results showed that DH82 cells tolerated electroporation well, allowing efficient genome editing.

Insertions and deletions of one or more nucleotides by non-homologous end-joining can induce in-frame or out-of-frame mutations. Generally, in-frame mutations occur when the addition or loss of nucleotides happen in multiples of three. This can result in addition or loss of amino acids without affecting the translation of downstream sequences. When the addition or loss of nucleotides does not happen in multiples of three, out-of-frame mutations occur that disrupt the reading frame of the genetic code and can result in the installation of pre-mature termination codons (PTC). A process known as nonsense-mediated decay, is an evolutionarily conserved mRNA surveillance pathway [386] and its role is to suppress aberrant transcription expression of mRNA sequences that acquired PTCs [387]–[389].

I therefore compared the proportion of in-frame and out-of-frame indels induced by each crRNA used. While the gene editing efficiencies of the two crRNAs were comparable (Appendices 1 and 2), GCATCCTGAATGGAATCTGT crRNA induced larger proportion of out-of-frame mutations (Appendix 2). Based on these results, bulk-edited cell populations obtained after using this particular crRNA were then diluted to obtain single cell colonies. I set up limiting dilutions as described in Materials and Methods section 2.12.7 for the chosen bulk population (crRNA GCATCCTGAATGGAATCTGT, 100nmol). I aimed to obtain colonies originating from a single cell to ensure identical genetic composition. I collected up to 96 single cell colonies and used Illumina MiSeq to genotype each colony for indels in the region of the crRNA target sequence. OutKnocker identified colonies A1 and C6 to harbour out-of-frame mutations (Appendix 3) which were then used for subsequent analysis (Figure 5.3.3).

Clone A1 contained only a single type of deletion (11 nucleotides), while clone C6 harboured 8 and 5 nucleotide deletions in each allele, respectively (Figure 5.3.3). Next, I used these clones to investigate the role of the caspase-1/4/11 in cell death and IL-1β processing in response to *S.* Typhimurium infection. In addition to the chosen knock-out clones, wild-type non-electroporated and electroporated only DH82 cells were also included in these experiments. I carried out gentamicin protection assay with wild-type *S.* Typhimurium at three different MOIs (1, 10 and 50) as described in Materials and Methods section 2.5. Percentage of cell lysis induced and the amount of IL-1β released were measured at 1, 2, 6 and 24 hours post infection (Figures 5.3.4 and 5.3.5).


**Figure 5.3.3 Illumina MiSeq sequencing of caspase-1/4/11 identified out-of-frame indel mutations for colonies A1 and C6 near the catalytic site in exon 6.** DH82 cells were electroporated with CRISPR crRNA GCATCCTGAATGGAATCTGT to target the canine hybrid caspase-1/4/11 gene near the catalytic site. Following limiting dilution, up to 96 single cell colonies were selected and genotyped using Illumina MiSeq sequencing. Information displayed by the analysis software includes the file name, number of amplicon reads and indel frequency. The underscored nucleotide sequence represents the wild-type reference sequence, while nucleotides highlighted in yellow show CRISPR crRNA target sites. Information including total percentage and total number of reads corresponding to each identified indel are shown underneath the reference sequence. Nucleotides shown in smaller font sizes are less confident calls based on the sequencing data, while deleted nucleotides have been replaced by hyphens. The software also provides information on the percentage and total number of reads that could not be aligned to the reference sequence and the number of reads that were excluded from analysis (Phred score dropouts). Two colonies, A1 and C6 were chosen for subsequent phenotypic characterisation.

The amount of LDH released in response to infection did not differ between the knock-out clones and wild-type (electroporated or not) DH82 cells (Figure 5.3.4). The lack of catalytically active hybrid caspase-1/4/11 protein did not prevent the cell death observed between 6 and 24 hours (Figure 5.3.4). There is still a possibility that, despite the large deletion near the catalytic site, the protein function was not totally abolished. Perhaps exons encoding the CARD domain of the protein were still translated into a partially functional protein that could be potentially recruited or even drive the recruitment of other proteins to the inflammasome. Cas9 targeted gene editing should, therefore, be repeated using crRNAs targeting the first few N-terminal exons of the hybrid caspase-1/4/11 gene. Further experiments are required to eliminate conclusively the involvement of caspase-1/4/11 in *S.* Typhimurium-induced cell death.

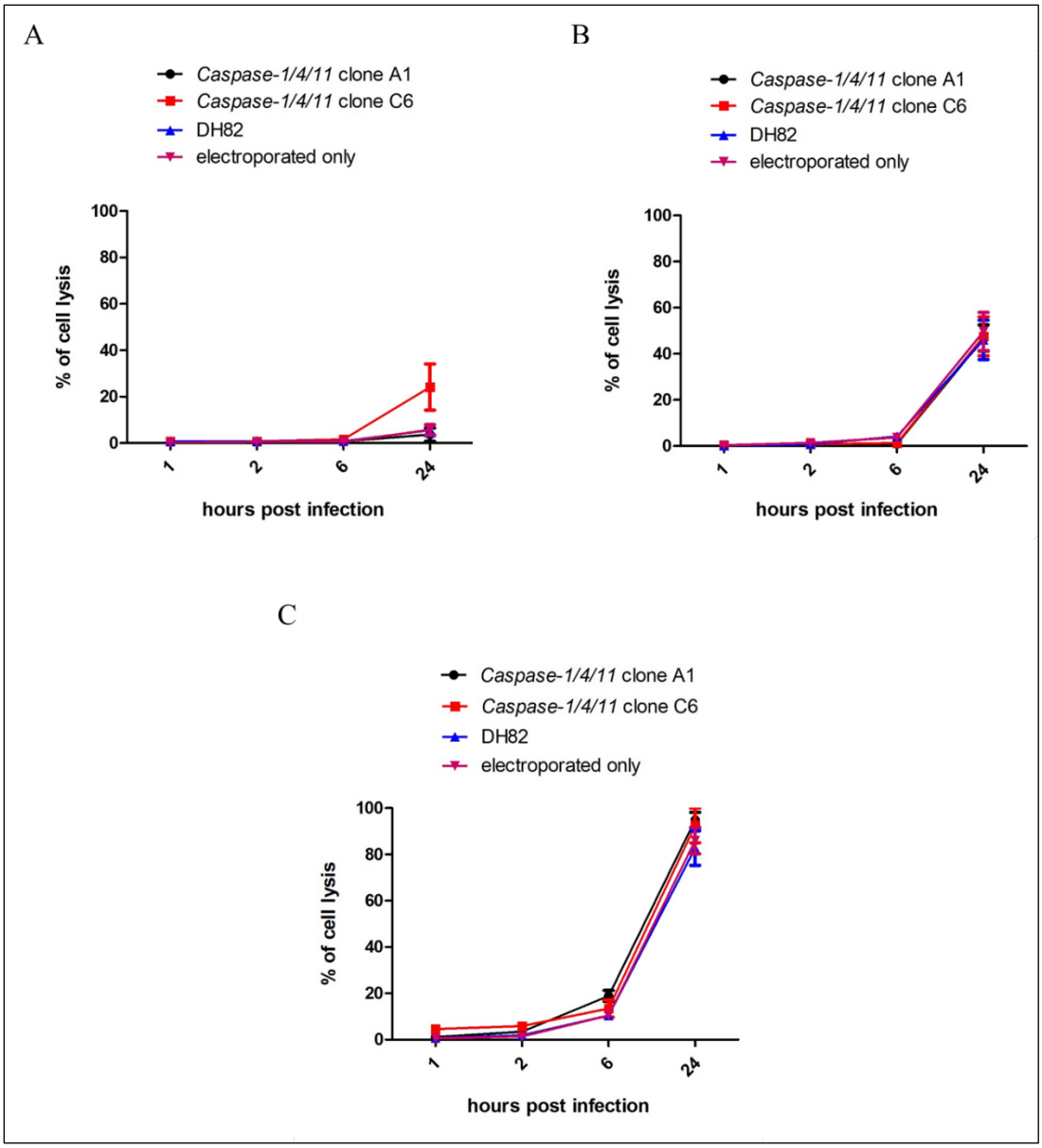


**5.3.4 Genetic deletion of the catalytic site of the canine hybrid caspase-1/4/11 did not affect cell death in response to *S.* Typhimurium infection.** Caspase-1/4/11 knock-out clones A1, C6, non-electroporated and electroporated only wild-type DH82 cells were infected with *S.* Typhimurium at three different MOIs; (A) 1, (B) 10 and (C) 50. Percentage of cell lysis at 1, 2, 6 and 24 hours post infection was determined via measuring the amount of LDH released in the cell culture supernatant as described in Materials and Methods section 2.5. Data shown is pooled from three independent experiments. Error bars represent the standard error of means (SEM) of triplicate wells.

I also measured the amount of IL-1β released in response to infection with *S.* Typhimurium (Figure 5.3.5) and found that cells did not release any IL-1β at 1, 2 and 6 hours. It was only at 24 hours after infection that substantial levels of IL-1β were detected in the cell supernatant (Figure 5.3.5). These results agreed with my previous observations (Figure 4.2.3) where *S.* Typhimurium-infected wild-type DH82 macrophages released negligible amounts of IL-1β in the first 6 hours post infection while large amounts were detected in the supernatant 24 hours post infection (Figure 4.2.3). Similarly to the cell lysis data, both clones were not impaired in secreting IL-1β in response to *S.* Typhimurium infection. On the contrary, cells from clone C6 released significantly higher amounts of IL-1β than that from wild-type cells (Figure 5.3.5). Further experiments are, however, required to confirm the amount, source and form of the IL-1β in the supernatant.

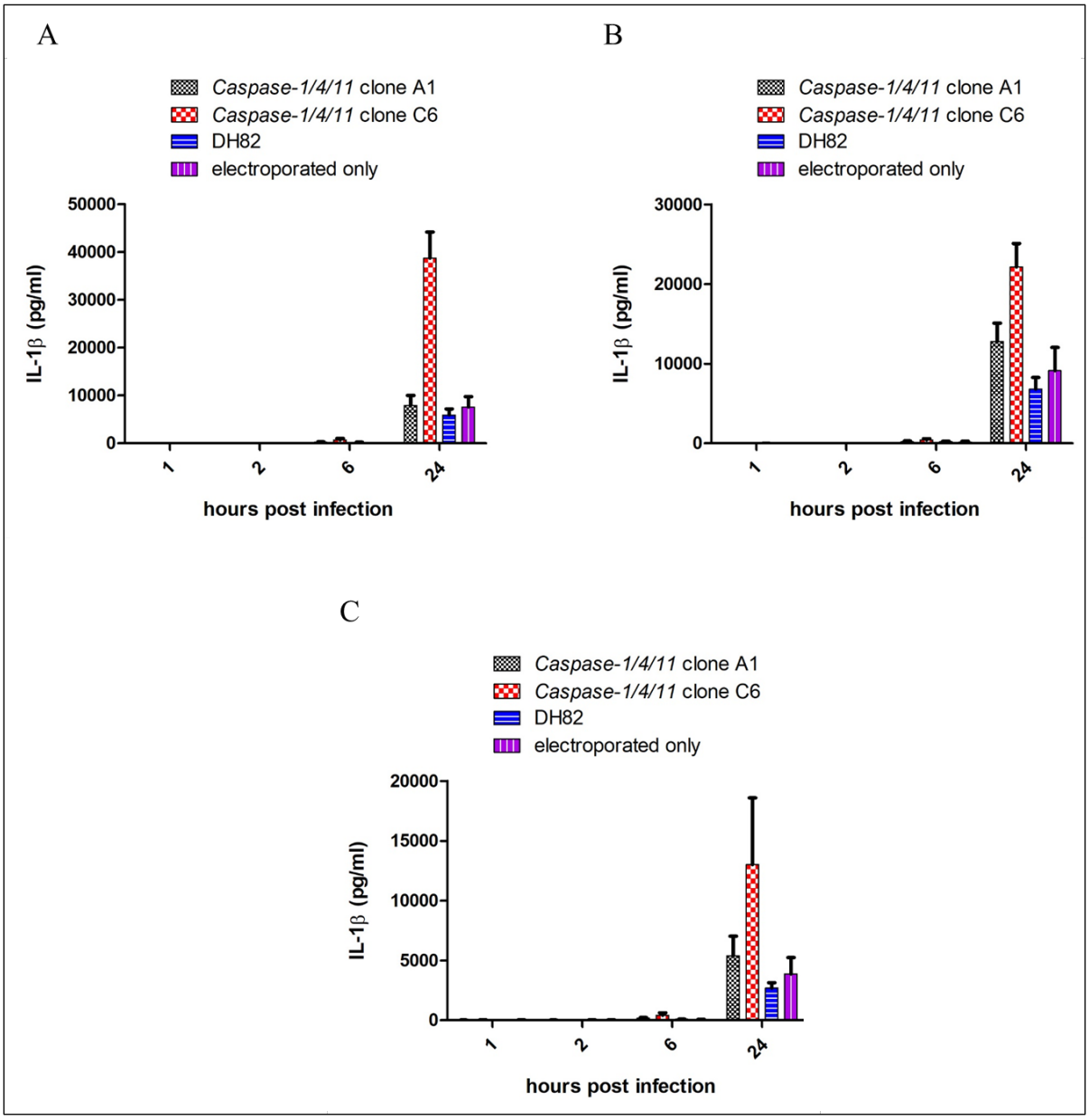


**5.3.5 Genetic deletion of the catalytic site of the canine hybrid caspase-1/4/11 did not impair IL-1β release in response to *S.* Typhimurium infection.** Caspase-1/4/11 knock-out clones A1, C6, non-electroporated and electroporated only wild-type DH82 cells were infected with *S.* Typhimurium at three different MOIs; (A) 1, (B) 10 and (C) 50. The amount of IL-1β released into the supernatant was determined at 1, 2, 6 and 24 hours post infection as described in Materials and Methods section 2.8. Data shown is pooled from three independent experiments. Error bars represent the standard error of means (SEM) of triplicate wells.

To confirm genotypes, I repeated Illumina sequencing on caspase-1/4/11 clones A1 and C6. OutKnocker analysis of sequencing results confirmed the same genotypes as previously described (Appendix 4).

### 5.4 MUSLCE analysis of caspase-8 and RIPK1 transcript sequences

I performed MUSCLE analysis of human, mouse and canine caspase-8 and RIPK1 transcripts to identify similarities in catalytic residues essential for function (Figures 5.4.1 and 5.4.2). I found the key catalytic residue identified in human caspase-8 (377-Cys) [322] essential for function to be also conserved in the dog (367-Cys) (Figure 5.4.1). I also identified key catalytic residues shown to be essential for kinase activity of the human RIPKl at positions 45-Lys [265], [390] and 138-Asp [391] to be conserved in dogs (41-Lys, 134-Asp, respectively) (Figure 5.4.2). Additional residues for caspase-8 cleavage 324-Asp [392] and RIP-mediated NF-κβ activation 377-Lys [272] were also found to be conserved in canine RIPK1 transcript at positions 322-Asp and 375-Lys, respectively (Figure 5.4.2). These results suggested the presence of enzymatically functional, active caspase-8 and RIPK1 proteins in the dog. I therefore proceeded to design target sequence specific crRNAs against these catalytic residues.


**Figure 5.4.1 Multiple sequence alignment comparison between canine, human and mouse caspase-8 transcripts indicate the presence of catalytically active caspase-8 protein in the dog.** Protein sequences of the caspase domain p20 subunit showed high degree of similarity between human, mouse and dog caspase-8. The catalytic residue found in human caspase-8 at 377-Cys position (highlighted in red rectangles) appeared to be conserved in the dog (367-Cys). This suggests that the dog caspase-8 protein possesses enzymatic activity.


**Figure 5.4.2 Multiple sequence alignment comparison between canine, human and mouse RIPK1 transcripts indicate the presence of catalytically active RIPK1 protein in the dog.** Protein sequences in the kinase domain showed high degrees of similarity between human, mouse and dog RIPK1 transcripts. Catalytic residues (highlighted in red rectangles) found in human RIPK1 at position 45-Lys and 138-Asp responsible for kinase activity, the caspase-8 cleavage site at 325-Asp and 377-Lys important for RIPK1-mediated NF-κβ activation are conserved in the dog. This supports the likely presence of enzymatically active RIPK1 protein in the dog.

### 5.5 Disruption of the canine caspase-8 and *RIPK1* genes using CRISPR-Cas9 technology

Both the canine caspase-8 (ENSCAFG00000025192) and *RIPK1* (ENSCAFG00000009321) genes have only one single transcript (ENSCAFT00000019300.2, ENSCAFT00000014829.3, respectively) annotated in Ensembl genome browser [393]. I have identified the catalytic residue (367-Cys) of canine caspase-8 (Figure 5.4.1) to be positioned in exon 7 and for RIPK1 kinase activity (134-Asp) (Figure 5.4.2) in exon 3. I therefore designed crRNAs specific for the exon 7 of the canine caspase-8 and the exon 3 of the canine RIPK1 DNA sequences.

For caspase-8, I chose two crRNAs targeting the coding DNA strand of the caspase domain. crRNA (TTTTATTCAGGCTTGTCAAG) directly overlapped, while crRNA (CCTACCGAAACCCCAATGGAG) targeted downstream of the identified catalytic residue. For RIPK1, I chose two crRNAs (TAATTATGGAGACCATTGAA, TGGAGAAGGCGTAATACACA) targeting the coding DNA strand of the proteinase domain immediately upstream of the residue suspected to be essential for kinase activity.

I performed three rounds of electroporation using three different concentrations of RNP complex (100, 200 and 400nmol) for both crRNAs for each gene as described in Materials and Methods section 2.12.3. After the third electroporation, bulk-edited cells were left to recover, and genomic DNA was extracted from a subset of cells for genotyping purposes as described in Materials and Methods section 2.12.4. Genotyping of the bulk-edited cell population was carried out using Illumina MiSeq sequencing method. In short, the first step was to perform a locus-specific PCR reaction, where the DNA sequence including the crRNA target site was amplified as described in Materials and Methods section 2.12.5. I also confirmed amplicon sizes from the locus-specific PCR via agarose gel electrophoresis (Figure 5.5.1). The predicted amplicon size for caspase-8 for crRNA sequence TTTTATTCAGGCTTGTCAAG was 296 base pairs while for crRNA sequence CCTACCGAAACCCCAATGGAG was 306 base pairs (Figure 5.5.1). A single pair of primers was designed to amplify both crRNAs (TAATTATGGAGACCATTGAA, TGGAGAAGGCGTAATACACA) for RIPK1 with a predicted amplicon size of 266 base pairs (Figure 5.5.1). I also included wild-type and negative ($dH_2O$) controls for PCR amplification (Figure 5.5.1).

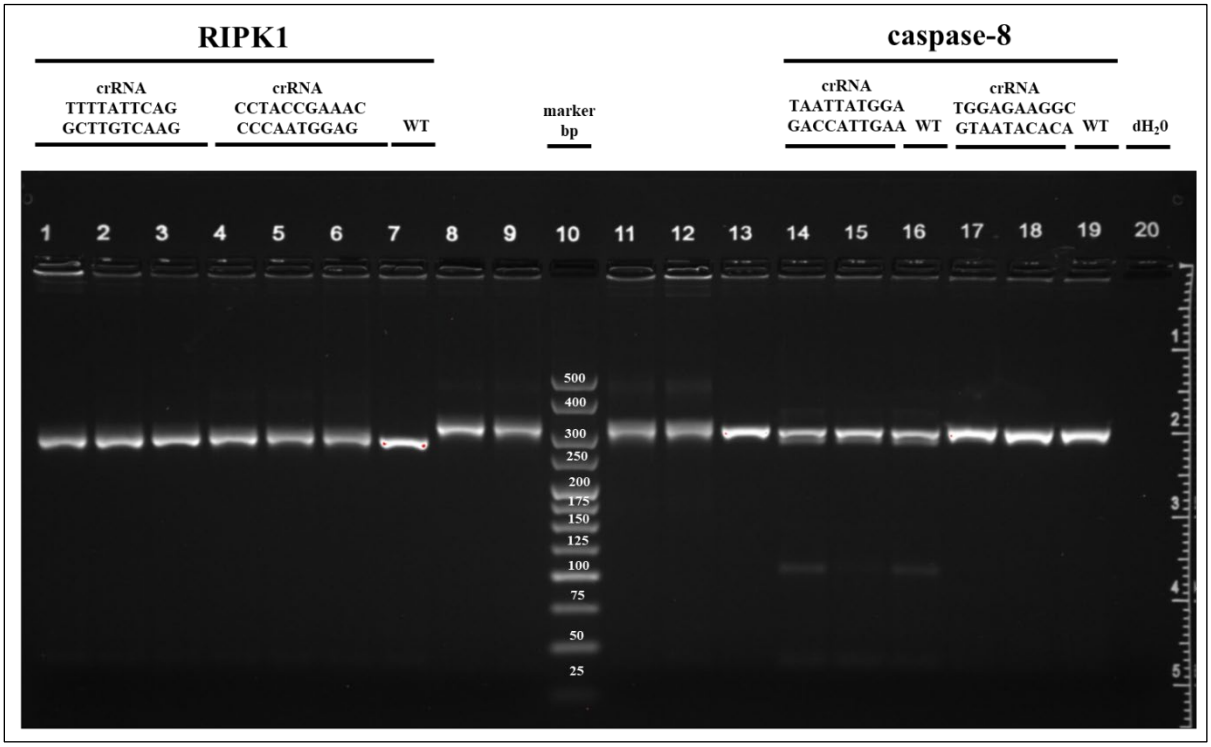


**Figure 5.5.1 Amplicon sizes following first level PCR for *RIPK1* and caspase-8 were confirmed on an agarose gel.** After the locus-specific PCR, a minimum of two samples for each crRNA were run in an agarose gel to confirm amplicon sizes. Wells 1-7 contained amplicons for RIPK1. Of these, wells 1-3 contained amplicons for crRNA TAATTATGGAGACCATTGAA, wells 4-6 for crRNA TGGAGAAGGCGTAATACACA and well 7 for wild-type DNA. Wells 14-19 contained amplicons for caspase-8. Of these, wells 14-15 contained amplicons for crRNA TTTTATTCAGGCTTGTCAAG, wells 16 and 19 for wild-type DNA, wells 17-18 for crRNA CCTACCGAAACCCCAATGGAG and well 20 contained the negative PCR amplification control. Samples 8, 9, 11 and 12 correspond to canine caspase-1/4/11 and were discussed earlier in this chapter (Figure 5.3.2)

## 5.6 Illumina sequence analysis of CRISPR-Cas9 edited bulk populations for the canine caspase-8 gene

Upon confirmation of the correct amplicon size for each set of PCR primers (Figure 5.5.1), second level PCR and MiSeq library preparations were performed as described in Materials and Methods sections 2.15 and 2.16, respectively. Using Illumina sequencing, I genotyped the bulk-edited populations for the canine caspase-8 gene. I used OutKnocker online analysis tool to determine gene editing efficiency (Appendices 5 and 6) and identify the insertions and deletions (indels) induced in the bulk populations for both crRNAs (Appendices 7 and 8).

Sequence analysis of CRISPR-Cas9 edited DH82 cells for the caspase-8 gene showed varying gene editing efficiency for crRNA TTTTATTCAGGCTTGTCAAG (Appendix 5). Repeated electroporation using 400nmol of the RNP complex resulted in the highest, over 60% indel frequency (Appendix 5). Regardless of the RNP concentration, the same type of mutations were observed (Appendix 7). Repeated electroporation of RNP complex using crRNA CCTACCGAAACCCCAATGGAG induced highly efficient gene editing (Appendices 6 and 8). While 100nmol RNP complex induced around 30% indel frequency, both, 200 and 400 nmol RNP complexes resulted in over 70% gene editing events (Figure 5.6.1). crRNA CCTACCGAAACCCCAATGGAG generally showed better gene editing properties compared to crRNA TTTTATTCAGGCTTGTCAAG. Benchling online crRNA designing tool generates on- and off-target scores for each crRNA. Higher on-target scores indicate higher efficiency, while higher off-target scores indicate higher specificity. CrRNA CCTACCGAAACCCCAATGGAG had a higher combined on- and off-target scores (76.27 and 64.51, respectively) compared to crRNA TTTTATTCAGGCTTGTCAAG (62.04 and 53.15, respectively). This could explain the differences observed between the two crRNAs. I therefore used bulk cell populations edited using crRNA CCTACCGAAACCCCAATGGAG in subsequent experiments. It is important to mention that the number of reads identified for the Illumina unique adapter pair was suboptimal in this experiment (Figures 5.6.1). This could be the result of an inefficient locus-specific amplification step.


**Figure 5.6.1 List of indels identified by sequence analysis in CRISPR-Cas9 edited DH82 cells for caspase-8 gene using crRNA CCTACCGAAACCCCAATGGAG.** DH82 cells were electroporated with RNP complexes at three different concentrations (100, 200 and 400 nmol). crRNA was designed to be near the catalytic site of the canine caspase-8 gene. Electroporated only wild-type DH82 cells yielded amplicon reads that matched exclusively the wild-type sequence, while Cas9 edited cells yielded amplicon reads that contained a mixture of in-frame and out-of-frame mutations. The underscored nucleotide sequence represents the wild-type reference sequence, while nucleotides highlighted in yellow show CRISPR crRNA target site. Information including total percentage and total number of reads corresponding to each identified indel are shown underneath the reference sequence. Nucleotides shown in smaller font sizes are less confident calls based on the sequencing data, while nucleotides replaced with hyphens represents the position of nucleotides deleted by CRISPR Cas9. The software also provides information on the percentage and total number of reads that could not be aligned to the reference sequence and the number of reads that were excluded from analysis (Phred score dropouts).

## 5.7 Functional characterisation of bulk-edited DH82 cell populations for caspase-8 gene

Caspase-8 is a functionally diverse protein. It has been shown to have essential roles during embryonic development and in host defence against invading pathogens. I have investigated the role of caspase-8 in promoting cell lysis and IL-1β production in response to *S.* Typhimurium infection. Preliminary screening was performed on bulk edited populations using crRNA CCTACCGAAACCCCAATGGAG (Figures 5.7.1 and 5.7.2). Based on the results obtained using OutKnocker analysis, over 70% of the amplicons screened contained genomic alterations. A large proportion of the observed indels were also identified as out-of-frame mutations (Figure 5.6.1).

In these experiments, I infected caspase-8 bulk-edited, wild-type and electroporated only DH82 cells with wild-type *S*. Typhimurium at three different MOIs (1, 10 and 50) (Figures 5.7.1 and 5.7.2). I measured the percentage of cell lysis and the amount of IL-1β released at 1, 2, 6 and 24 hours post infection (Figures 5.7.1 and 5.7.2). I observed no difference in cell lysis in response to *S.* Typhimurium infection in caspase-8 bulk edited compared to wild type cell populations (Figure 5.7.1).

Caspase-8 was also shown to be recruited to the NLRC4 inflammasome in *S.* Tyhpimurium infected mouse BMDMs where it was shown to primarily mediate pro-IL-1β expression without affecting cell lysis [140]. In line with this, I also observed lower amounts of IL-1β in the supernatant of infected caspase-8 bulk edited cells than that of wild-type cells (Figure 5.7.2).

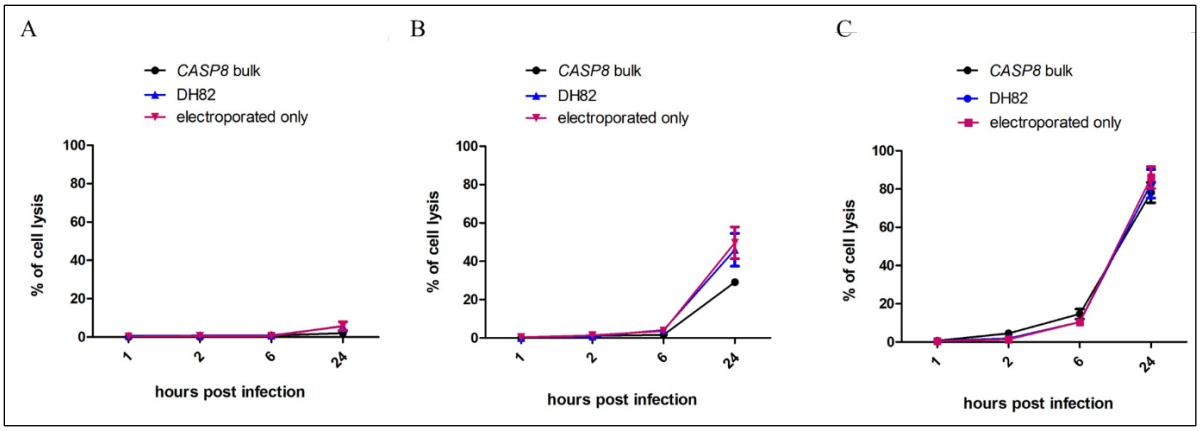


**Figure 5.7.1 Genetic abolition of caspase-8 gene in DH82 cells did not alter lytic cell death processes in response to *S.* Typhimurium infection.** Bulk-edited caspase-8-deficient cells, wild-type and electroporated only wild-type cells were infected with *S.* Typhimurium at three different MOIs; (A) 1, (B) 10 and (C) 50. Percentage of cell lysis at 1, 2, 6 and 24 hours post infection was determined via the measurement of relative LDH release. Data shown is pooled from three independent experiments. Error bars represent the standard error of mean (SEM) of triplicate wells.

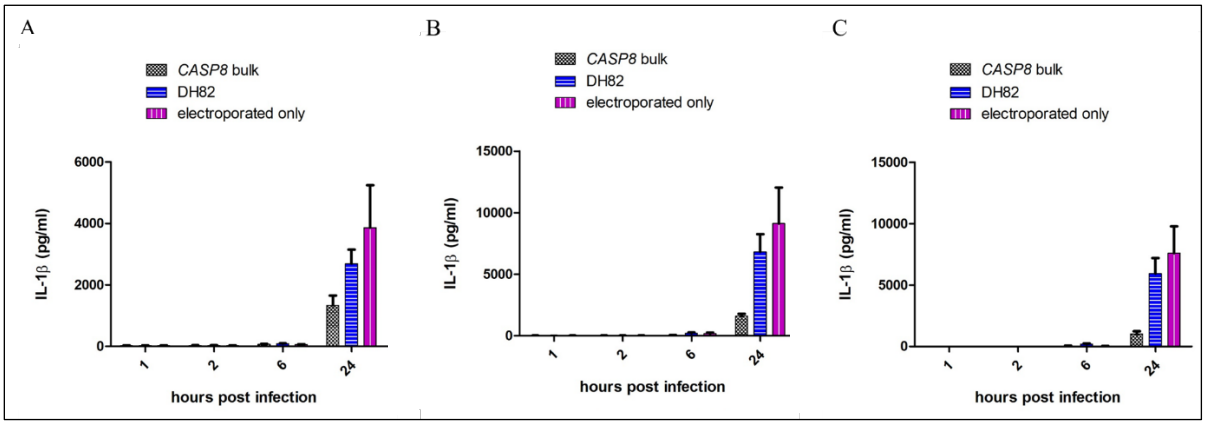


**Figure 5.7.2 Genetic abolition of caspase-8 gene resulted in reduced IL-1β release in response to wild-type *S.* Typhimurium infection.** Bulk-edited caspase-8-deficient DH82 cells, wild-type and electroporated only DH82 cells were infected with *S.* Typhimurium at three different MOIs; 1 (A), 10 (B) and 50 (C). IL-1β release in the supernatant was measured by ELISA at 1, 2, 6 and 24 hours post infections. Data shown is pooled from three independent experiments. Error bars represent the standard error of mean (SEM) of triplicate wells.

## 5.8 Illumina sequence analysis of CRISPR-Cas9 edited bulk populations for the canine *RIPK1* gene

Illumina sequence analysis showed highly efficient gene editing of the *RIPK1* gene using crRNA TAATTATGGAGACCATTGAA (Appendix 9). Regardless of the RNP concentration, over 90% indel frequency was detected (Appendix 10).

I have also identified high indel frequency in the bulk edited cell populations using crRNA TGGAGAAGGCGTAATACACA for the canine *RIPK1* gene (Appendix 11). Sequence analysis showed that the RNP complex as low as 100nmol resulted in gene editing events in over 70% of the cells (Appendix 12) with repeated electroporation using 400nmol of the RNP complex inducing over 90% indel frequency (Appendix 12). Overall, my results showed that both crRNA induced large amount of editing events in the canine *RIPK1* gene. This high efficiency genome editing could be explained by the high on- and off-target scores calculated for crRNA TAATTATGGAGACCATTGAA and TGGAGAAGGCGTAATACACA (64.7, 64.1 and 76.8, 69.1, respectively).

These results suggested that the gene editing efficiency of crRNAs with low on- and off-target scores can be augmented by increasing the concentration of the RNP complex. CrRNA sequences with higher on- and off-target scores can induce a large number of editing events even at low RNP complex concentrations.

## 5.9 Functional characterisation of RIPK1 mutant clones

In this section I aimed to investigate the role of canine RIPK1 in cell lysis and IL-1β processing in response to *S.* Typhimurium infection. I chose bulk-edited cells generated using crRNA TGGAGAAGGCGTAATACACA for subsequent analysis. Using this guide RNA, I have identified deletions up to 14 nucleotides in length in the *RIPK1* gene. I therefore set up limiting dilutions and carried out subsequent Illumina sequencing of 96 clones each originating from a single cell as described in Materials and Methods section 2.12 (Appendix 13).

I chose single cell colonies C9 and D7 (Figure 5.9.1) to perform a series of *in vitro S.* Typhimurium infection assays. *RIPK1* colony C9 contained biallelic deletions, consisting of a 1- and 2-nucleotide deletions, while *RIPK1* D7 colony also contained biallelic mutations, consisting of a 16-nucleotide deletion and 1-nucleotide insertion (Figure 5.9.1). Based on the sequencing results, the canine *RIPK1* gene was successfully disrupted in both of these colonies.


**Figure 5.9.1 Illumina MiSeq sequencing of *RIPK1* knock-out clones C9 and D7 show large deletions in the targeted exon 3.** Following limiting dilution, up to 96 colonies each originating from a single cell were selected and genotyped using Illumina MiSeq sequencing. Based on the Illumina sequencing results using OutKnocker online analysis tool two colonies, C9 and D7 were chosen for subsequent characterisation. Colony C9 contained biallelic, 1- and 2-nucleotide deletions. Colony D7 also contained biallelic mutations, 16-nucleotide deletion and 1-nucleotide insertion in length. Information displayed by the analysis software includes the file name, number of amplicon reads and indel frequency. The underscored nucleotide sequence represents the wild-type reference sequence, while nucleotides highlighted in yellow show CRISPR crRNA target sites. Information including total percentage and total number of reads corresponding to each identified indel are shown underneath the reference sequence. Nucleotides shown in smaller font sizes are less confident calls based on the sequencing data, while nucleotides replaced with hyphens represents the position of nucleotides deleted by CRISPR Cas9. The software also provides information on the percentage and total number of reads that could not be aligned to the reference sequence and the number of reads that were excluded from analysis (Phred score dropouts).

To assess the functional consequences of the loss of *RIPK1* gene, I performed gentamicin protection assay as described in Materials and Methods section 2.5. In these experiments, *RIPK1* clones C9 and D7 together with wild-type and electroporated only DH82 cells were infected with wild-type *S.* Typhimurium using three different MOIs (MOI 1, 10 and 50). I calculated the percentage of cell lysis (Figure 5.9.2) and the amount of IL-1β released (Figure 5.9.3) into the supernatant at 1, 2, 6 and 24 hours post infection.

As I have previously shown, wild-type DH82 cells responded to *S.* Typhimurium infection at later time points, with the strongest response observed at 24 hours post infection (Figures 4.1.1 and 4.1.2). Neither of the selected clones (C9 and D7) lacking functional *RIPK1* gene showed altered cell lysis responses (Figure 5.9.2), since the relative amount of LDH released was comparable between knock-out, wild-type and electroporated only DH82 cells (Figure 5.9.2). In contrast, I failed to detect any IL-1β present in the supernatant in either of the *RIPK1* clones (Figure 5.9.3).

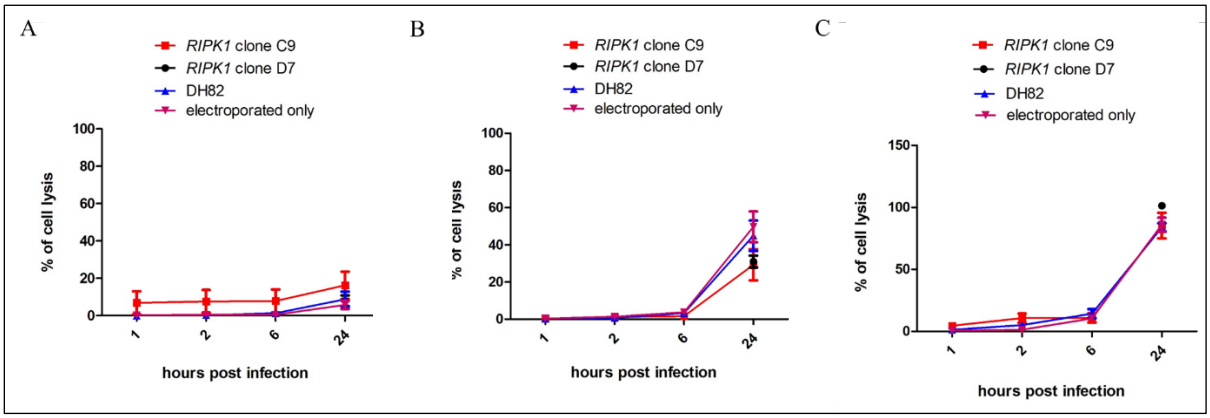


**Figure 5.9.2 Genetic abolition of *RIPK1* gene did not alter cell death responses following infection with wild-type *S.* Typhimurium.** *RIPK1* clones C9, D7, wild-type and electroporated only DH82 cells were infected with *S.* Typhimurium at three different MOIs; (A) 1, (B) 10 and (C) 50. Percentage of cell lysis at 1, 2, 6 and 24 hours post infection for clone C9 and 24 hours post infection for clone D7 was determined via measuring relative LDH release. Data shown for clone C9 is pooled from three independent experiments, while for clone D7 is from a single experiment. Error bars represent the standard error of mean (SEM) of triplicate wells.

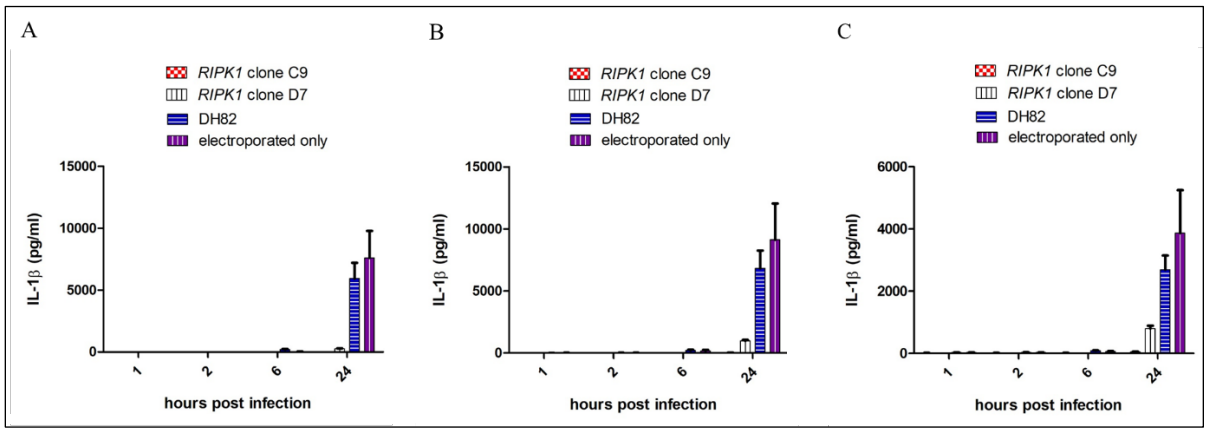


**Figure 5.9.3 Genetic abolition of *RIPK1* gene prevented IL-1β production by cells of the *RIPK1* clones C9 and D7 when infected with wild-type *S.* Typhimurium.** *RIPK1* clones C9, D7, wild-type and electroporated only DH82 cells were infected with *S.* Typhimurium with three different MOIs; (A) 1, (B) 10 and (C) 50. IL-1β release in the supernatant was measured by ELISA at 1, 2, 6 and 24 hours post infection for clone C9 and 24 hours post infection for clone D7. Data shown for clone C9 is pooled from three independent experiments, while for clone D7 is from a single experiment. Error bars represent the standard error of mean (SEM) of triplicate wells.

These experiments confirmed the RIPK1-dependent effect on pro-inflammatory cytokine pro-IL-1β production in response *S.* Typhimurium infection (Figures 5.9.3).

I further investigated the effect of RIPK1 in the induction of pro-IL-1β expression. Following gentamicin protection assay (MOI 1) of *RIPK1* clone C9 and wild-type DH82 cells, I have blotted their full protein extracts (24-hour post infection) against canine IL-1β (Figure 5.9.4). My results showed the presence of pro- and mature IL-1β in DH82 cell extracts, while *RIPK1* clone C9 was severely impaired in pro-IL-1β expression (Figure 5.9.4).

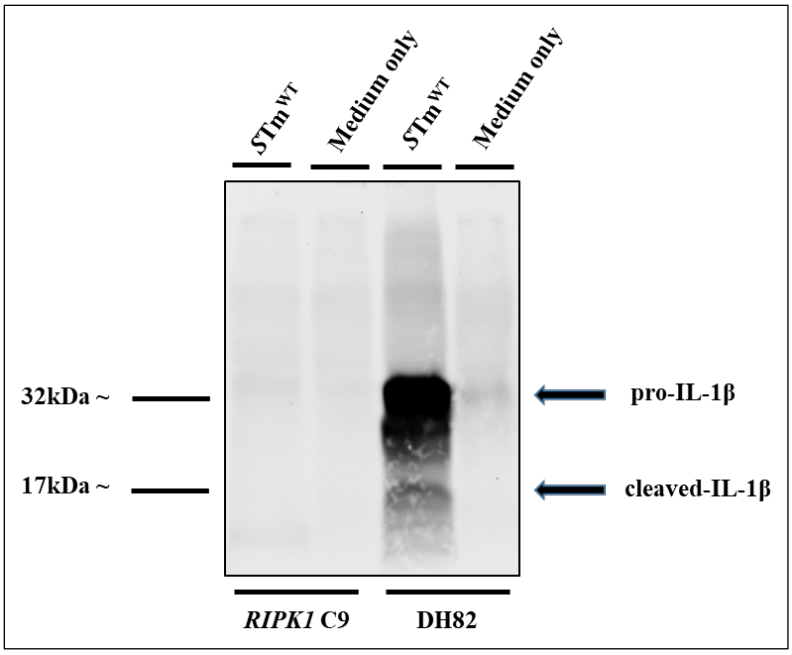


**Figure 5.9.4 RIPK1 is essential for inflammatory cytokine pro-IL-1β expression in response to *S.* Typhimurium infection in the dog.** Wild-type DH82 and *RIPK1* clone C9 cells were infected with wild-type *S.* Typhimurium at MOI of 1 for 24 hours. Full protein extraction of cell lysates was performed, and samples were blotted against canine specific IL-1β. Non-infected controls (shown as medium only) were also included for each cell line. Representative immunoblot is from a single experiment.

My results therefore indicated an essential role for RIPK1 in pro-inflammatory cytokine IL-1β expression in response to *S.* Typhimurium infection.

## 5.10 Discussion

To the best of my knowledge, DH82 cells have not yet been genetically altered using the CRISPR Cas9 technology. To this end, in the first part of this chapter I optimised the electroporation conditions by electroporating DH82 cells with pmaxGFP vectors using two solutions and 7 different pre-defined electrical parameters for each solution. I assessed electroporation efficiency by measuring GFP protein expression via flow cytometry and found that it was the electrical parameters, rather than the type of solution, that determined the level of GFP expression. My

results showed that the use of program X-005 resulted in the highest percentage of intact cells expressing GFP protein.

In the second part of this chapter I have investigated different cell death mechanisms that could drive the late cell lysis seen in canine DH82 cells in response to *S.* Typhimurium infection. I have targeted three major programmed cell death pathways, namely pyroptosis, necroptosis and apoptosis (Figure 3.1). First, I compared the amino acid sequences of canine hybrid caspase-1/4/11, caspase-8 and RIPK1 transcripts against the human and mouse sequences to identify catalytic residues essential for function (Figures 3.2.3, 5.4.1 and 5.4.2, respectively). Sequence analysis showed high amino acid sequence conservation across human, mouse and dog species. Residues suggested to play a role in the catalytic activity of caspase-1/4/11 and caspase-8 and the kinase activity of RIPK1 appeared to be conserved in the dog, indicating the presence of functional proteins (Figures 3.2.3, 5.4.1 and 5.4.2, respectively).

Following the identification of the catalytic residues, I described the generation of knock-out DH82 macrophages lacking functional caspase-1/4/11, caspase-8 and *RIPK1* genes using CRISPR-Cas9 genome editing system. For each gene I chose two crRNAs and used each crRNA at three different concentrations to perform CRISPR-Cas9 gene editing. Guide RNA positions, as well as on- and off-target values, were taken into consideration when choosing guides. My results showed that gene editing efficiency can be increased using higher concentration of the RNP complex for guide RNAs with lower on- and off-target scores. My results also suggested that the size of indels induced by guide RNAs cannot be predicted based on their on- and off-target values.

I then proceeded to investigate the effect of these genetic disruptions on cell lysis (via the measurement of LDH release) and IL-1β release in DH82 cells infected with wild type *S.* Typhimurium. In line with my previous observations (Chapter 4, Figure 4.2.2 and 4.2.3), cell lysis and IL-1β release was only seen at 24 hours after infection (Figure 5.3.4 and 5.3.5). The amount of cell lysis however was comparable between knock-out, wild-type and electroporated only control cells (Figure 5.3.4). This suggested that *S.* Typhimurium-induced cell lysis occurs independently of the catalytic activity of the canine hybrid protein. Interestingly, cells of one of the clones secreted significantly larger amount of IL-1β than that secreted by wild-type cells

(Figure 5.3.5). Perhaps the lack of caspase-1/4/11 fusion protein allows the recruitment of other caspases, for example caspase-8 to drive IL-1β production in response to *S.* Typhimurium infection [140]. While the transcriptional priming of pro-IL-1β was unaltered (Figure 5.3.5), further experiments examining the presence of mature IL-1β should be carried out.

In the last part of this chapter, I investigated the functional consequences of the loss of caspase-8 and *RIPK1* genes in response to *S.* Typhimurium infection. I have obtained single cell colonies for *RIPK1*-deficient cells, due to time limitations, experiments were only performed on canine caspase-8-deficient bulk edited cell populations. Caspase-8 and *RIPK1* knock-out cells infected with wild-type *S.* Typhimurium showed cell lysis responses comparable to those of DH82 wild-type and electroporated only control cells (Figures 5.7.1 and 5.9.2, respectively). My results suggested that the absence of functional caspase-8 or RIPK1 proteins alone did not prevent late cell lysis observed in response to *S.* Typhimurium infection. Secretion of IL-1β was completely abolished in *RIPK1*-deficient cells (Figure 5.9.3), while western blotting analysis of *S.* Typhimurium infected DH82 wild-type and *RIPK1*-deficient cell lysates confirmed the total absence of pro-IL-1β expression (Figure 5.9.4). My results therefore identified canine RIPK1 to be essential in the induction of pro-inflammatory cytokine expression in response to *S.* Typhimurium infection in DH82 cells. Several other studies suggest TLR-mediated RIPK1 activation to be essential for cytokine expression. Murine macrophages deficient for either RIPK1, RIPK3 or caspase-8 showed impaired NF-κβ activation and reduced IL-1β production in response to *Yersinia* Pestis [394]. Human monocytes in the presence of extracellular LPS can form an "alternative" inflammasome which drives IL-1β secretion without apparent ASC speck formation or pyroptotic cell death. This is a TLR4/TRIF-mediated pathway engaging RIPK1, FADD and caspase-8 upstream of the NLRP3 inflammasome [185]. Bulk edited caspase-8 deficient cells also showed a reduction in the amount of IL-1β detected in the supernatant when compared to DH82 wild-type and electroporated only control cells (Figure 5.7.2). Caspase-8 mediated atypical IL-1β processing in murine BMDCs in response to LPS stimulation relies on the presence of intact RIPK1, RIPK3 and FADD proteins [217]. While caspase-8 has been shown to promote IL-1β production in murine BMDMs following *S.* Typhimurium infection, it is dispensable for cell death [140]. Other studies also suggested an essential role for caspase-8 in expression and processing of inflammatory pro-IL-1β [220], [222]. Murine BMDMs deficient for either GSDMD or

proteolytically active caspase-1 has been shown to recruit and activate caspase-8 within the ASC speck to induce a so called secondary pyroptosis and delayed Il-1β release [213]. Caspase-8/FADD complex has been shown to play a necroptosis inhibitory role, while cells lacking caspase-8 or FADD undergo necroptotic cell death in response to death receptor ligand binding [187]. Both, RIPK1 and RIPK3 contain cleavage sites which have been shown to act as caspase-8 substrates [392], [395], [396]. It has also been shown that RIPK3 can mediate necroptosis following TLR activation only [397]. Further experiments however are required to investigate the true effect of caspase-8 in DH82 cells. I therefore aim to perform limiting dilution and genotyping of single cell colonies to identify clones with the caspase-8 gene disrupted.

# Chapter 6

# Characterisation of Dog-Mouse primary bone marrow derived macrophages containing the hybrid caspase-1/4/11 fusion gene

## 6.1 Introduction

Comparative genome analysis has identified differences in a number of key genes involved in inflammasome formation and regulation between humans and dogs [41], [154]. Members of the order Carnivora, which includes both cats and dogs, lack *NAIP* genes [41] which have evolved for the recognition of flagellin [46] and type III secretion system components of bacteria [124], [348]. Furthermore, NLRC4, which is principally involved in flagellin detection, exists as a pseudogene, containing multiple stop codons [41]. Marked differences are also evident in their caspase repertoire, namely fusion of caspase-1, -4 and -11 to generate a novel hybrid gene in dogs and cats, consisting of the CARD domain and the CASP domain of caspase-1 and caspase-11, respectively [154].

In chapter 3 of this thesis the cellular responses of the canine DH82 cell line to well established inflammatory activators were investigated. Cell lysis and IL-1β responses following challenge with whole organisms using wild-type and mutant *S.* Typhimurium strains were also investigated (Chapter 4). Collectively the results obtained from these series of experiments questioned the functionality of the canine caspase-1/4/11 hybrid protein and its role in driving cell death and cytokine processing (Chapter 3).

The genes encoding caspase-1 and caspase-11 are located within close proximity on chromosome 9 of the mouse genome. Using CRISPR-Cas9 technology a large deletion was introduced into wild type mouse embryos which encompassed the CASP domain of caspase-1 and the CARD domain of caspase-11 (unpublished data Vishva Dixit's research group, Genentech Research Facility, South San Francisco, California). Consequently, this deletion resulted in the generation of progeny (designated DogMo) with the same genomic arrangement of mouse caspase-1 and caspase-11 genes that exists in dogs (Figure 3.1.1).

The work in this chapter describes a series of *in vitro* cell culture assays carried out using primary DogMo bone marrow derived macrophages. I characterised the responses of the hybrid caspase-1/4/11 gene to the canonical NLRP3 inflammasome ligand, nigericin [82], [85] and the non-canonical inflammasome caspase-11 activator, intracellular LPS [163], [168]. The role of this gene fusion was also characterised in response to *in vitro S.* Typhimurium infection assays [123]. Inflammasome activation was assessed by the measurement of LDH and pro-inflammatory cytokine IL-1β released into the culture supernatant following stimulation of macrophage cell lines. Hybrid caspase protein expression and the processing of the pyroptotic cell death executioner GSDMD were also assessed by western blotting.

## 6.2 Genotyping of DogMo cells for the caspase-1/4/11 fusion gene

Whole genome sequencing of the DogMo CRISPR-Cas9 edited mice revealed a large deleted region of 20,524 bp in length (Appendix 14) in multiple mouse pups (unpublished data from Dixit group). The deletion encompassed regions of both caspase-1 and caspase-11 genes (Figure 6.2.1). Consequently the CASP domain of caspase-1, the CARD domain of caspase-11 together with the intermediate sequences were deleted (Figure 6.2.1). The genotype of the DogMo primary BMDM cells was confirmed by PCR using the primer set designed by the Dixit group (Table 2.14 and 2.15). PCR was performed using the conditions as outlined in Materials and Methods section 2.13. Briefly, genomic DNA was extracted from differentiated primary mouse wild-type and DogMo primary BMDM cells. Following PCR, amplicon products were analysed by agarose gel electrophoresis (Figure 6.2.2). The predicted amplicon sizes for wild-type and hybrid sequences were 431 bp and 378 bp in length, respectively (Figure 6.2.2).

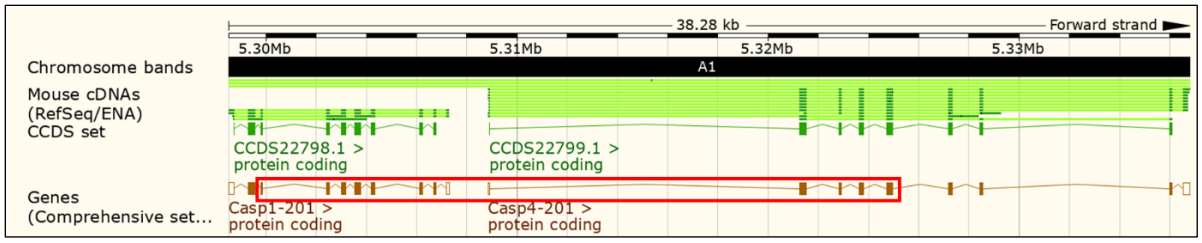


**Figure 6.2.1 Mouse caspase-1 and caspase-11 chromosomal regions targeted by CRISPR-Cas9.** Caspase-1 and caspase-11 genes are located next to each other on chromosome 9 of the mouse genome. Two guide RNAs (AATTTAGATCAACACTAGGA, GGAACTTTGACTAGGTACTA) were designed to target the third exon of mouse caspase-1 and the fourth exon of mouse caspase-11 (regions highlighted in red rectangles).

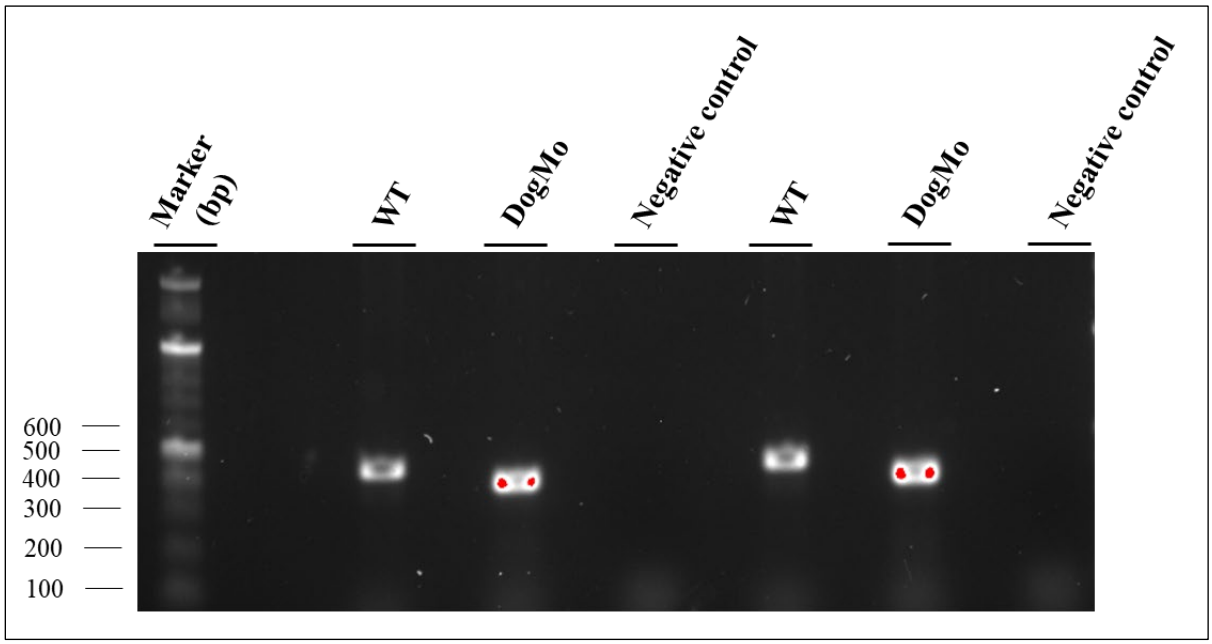


**Figure 6.2.2 Genotyping of differentiated primary wild-type and DogMo macrophages by PCR.** Genomic DNA was extracted from a subset of primary murine wild-type and DogMo macrophages. Genotyping was performed by PCR using the primer set described in Materials and Methods section 2.13. PCR products were resolved by PAGE using 1% agarose gel. Expected amplicon sizes were 431 and 378 bp for wild-type and DogMo sequences, respectively.

### 6.3 Canonical NLRP3 inflammasome activation in DogMo cells containing the hybrid caspase-1/4/11 gene

It has been shown at the cellular level that exposure to nigericin induces potassium efflux which triggers the activation of the canonical NLRP3 inflammasome [82]. Moreover, the subsequent activation of caspase-1 leads to inflammatory cytokine IL-1β maturation [42] and to the cleavage and liberation of the active N-terminal domain of GSDMD protein responsible for inducing pyroptotic cell death. In brief, murine wild-type and DogMo cells were differentiated for 5 days as described in Materials and Methods section 2.3. Murine wild-type, DogMo and DH82 cells were subsequently primed with LPS and stimulated with 20 μM nigericin for a period of 1 hour.

Results previously described in this thesis revealed that murine macrophages lacking caspase-1 and caspase-11 genes failed to undergo pyroptotic cell death in response to standard nigericin stimulation (Figure 3.5.1). DH82 cells stimulated with nigericin at standard concentration (20 μM) however displayed ASC speck formation and activated caspase recruitment to the ASC speck suggesting NLRP3 activation (Figure 3.5.4). Cell lysis in DH82 macrophages was only seen at high concentrations of nigericin (200 μM) (Figure 3.5.1), suggesting that the hybrid caspase is inactive and that the cell lysis occurred through an NLRP3 independent cell death mechanism (Figure 3.5.1). In this experiment I investigated whether the mouse hybrid caspase-1/4/11 protein could be activated within the context of the NLRP3 inflammasome leading to pyroptotic cell death via GSDMD cleavage. DogMo cells responded to standard concentrations of nigericin (20 μM final concentration) producing LDH (Figure 6.3.1). The relative level of response however was marginally lower than that observed in similarly stimulated wild-type murine cells (Figure 6.3.1). These data suggested that the CARD domain of the DogMo caspase-1/4/11 fusion was sufficient to facilitate its' recruitment to the NLRP3 inflammasome and capable of initiating pyroptotic cell death via the CARD domain of caspase-11. IL-1β processing however was significantly reduced, supporting the literature that IL-1β is not a substrate of caspase-11.

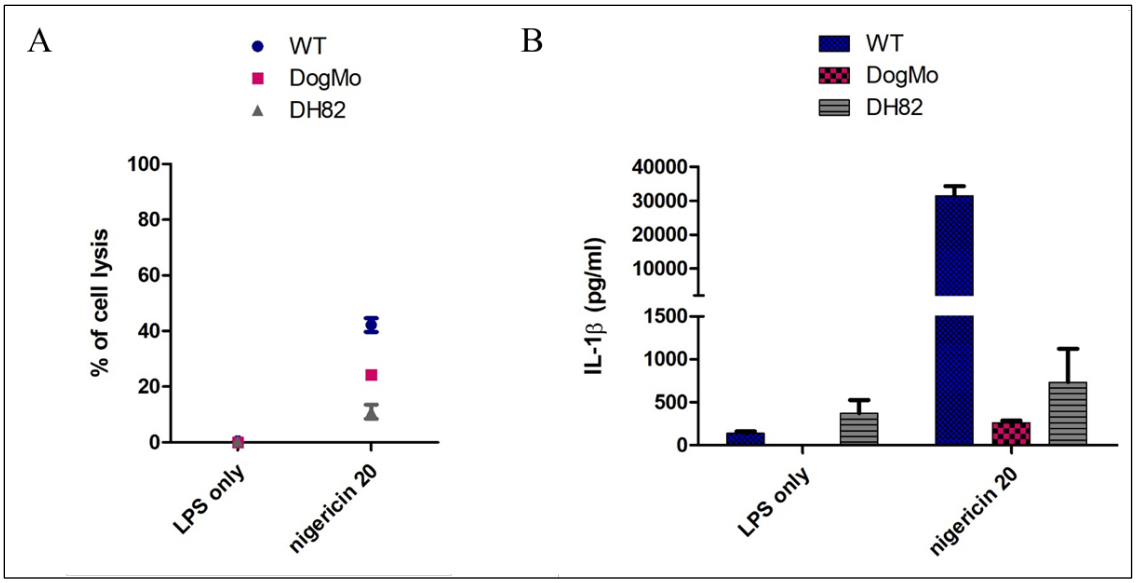


**Figure 6.3.1 Activation of canonical inflammasome in DogMo cells by nigericin causes cell lysis but not IL-1β release.** Murine wild-type, DogMo and canine DH82 cells were primed with LPS (200 ng/ml for 3 hours) prior to incubation with nigericin (20 μM final concentration). Nigericin induced cell lysis was assessed by direct measurement of LDH release into the supernatant. IL-1β release was quantified using canine and murine specific ELISAs, respectively. Data shown is pooled from two independent experiments. Error bars represent the standard error of means (SEM) of triplicate wells.

In 2016, two independent studies identified the GSDMD protein as a substrate of activated inflammatory caspases [70], [72] and underpinned it's key role as the executioner of pyroptotic cell death in response to pathogenic infections [70], [72]. In resting cells, the catalytically active N-terminal domain of GSDMD is locked in an autoinhibited form by its C-terminal anchor [44]. Following cleavage by activated caspases, the N-terminal domain of GSDMD (GSDMD-N) is liberated and upon its oligomerisation induces pore formation in the plasma membrane. I therefore investigated whether GSDMD cleavage in DogMo macrophages occurs in response to canonical NLRP3 inflammasome activation (Figure 6.3.2). Lysates derived from LPS primed cells stimulated with nigericin (Figure 6.3.1) were immunoblotted for evidence of GSDMD cleavage using a murine specific anti-GSDMD antibody (Figures 6.3.2 and 6.3.3) as described in Materials and Methods sections 2.9 and 2.11. Western blot of cell lysates prepared from both medium only

and LPS primed murine wild-type and DogMo primary BMDMs detected a single band of approximately 53 kDa which corresponds to full length GSDMD protein (Figures 6.3.2 and 6.3.3). In contrast, immunoblotting of lysate prepared from LPS primed/nigericin stimulated cells revealed a protein band migrating at approximately 30 kDa which corresponds to GSDMD-N (Figures 6.3.2 and 6.3.3). These results suggested the hybrid protein consisting of caspase-1 CARD domain and caspase-11 CASP domain drives GSDMD cleavage in response to NLRP3 activation. The cell death process triggered by nigericin stimulation of the DogMo macrophages could, therefore, be driven by pyroptosis via the caspase 1/4/11 fusion protein.

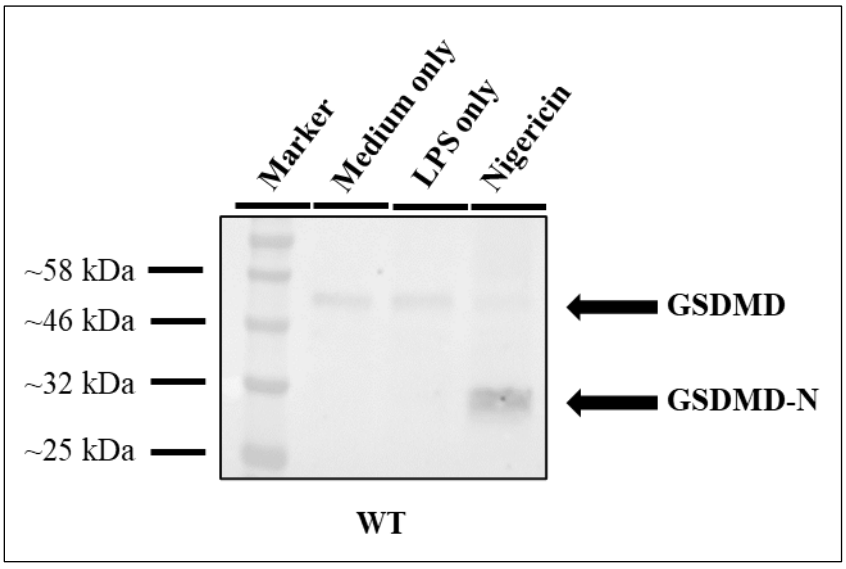


**Figure 6.3.2 NLRP3 activation drives GSDMD cleavage in wild-type macrophages.** Murine primary wild-type macrophages were primed with LPS (200 ng/ml for 3 hours) followed by stimulation with nigericin (20 μM for 1 hour). GSDMD cleavage was determined by western blotting of cell lysates using anti-mouse GSDMD antibody. Representative immunoblot is from a single experiment.

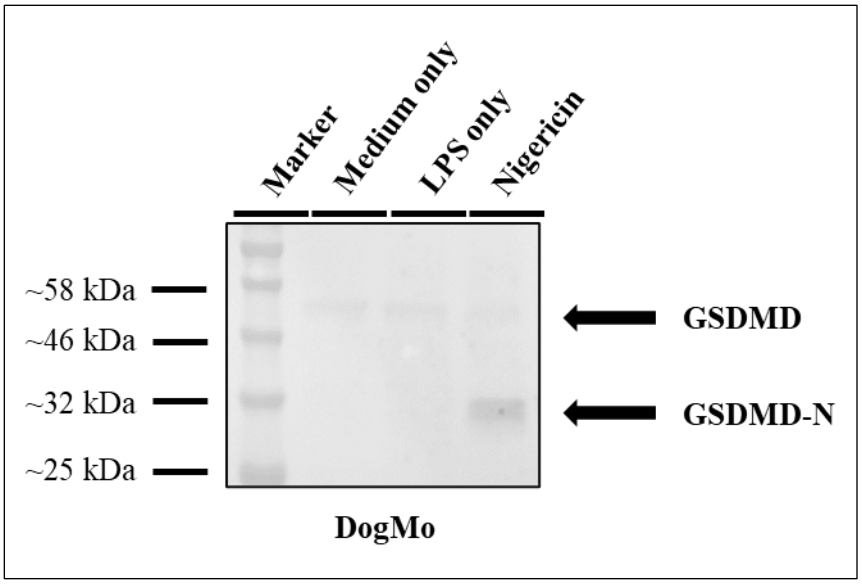


**Figure 6.3.3 Murine hybrid caspase-1/4/11 protein is capable of initiating pyroptosis via GSDMD cleavage.** Murine DogMo cells were primed with LPS (200 ng/ml for 3 hours) followed by stimulation with nigericin bacterial toxin (20 μM for 1 hour). GSDMD cleavage was investigated by western blotting of cell lysates using murine specific GSDMD antibody following protein extraction. Representative immunoblot is from a single experiment.

The expression pattern of the murine hybrid caspase protein following inflammasome activation was also investigated (Figures 6.3.4 and 6.3.5). While murine caspase-11 expression requires priming via TLR/NF-κβ pathways, murine caspase-1 has been shown to be constitutively expressed in murine bone marrow derived macrophages [160]. Consequently, expression of the caspase fusion protein was investigated by a combination of mass spectrometry and western blotting. Mass spectrometry analysis of non-stimulated DH82 cells revealed that the canine hybrid caspase-1/4/11 protein was constitutively expressed in macrophages (Figure 3.2.2). I therefore carried out western blot analysis of protein extracts prepared from cell lysates of non-stimulated (medium only), LPS primed (200 ng/ml for 3 hours) and LPS primed and nigericin (20 μM for 1 hour) stimulated DogMo cells. In accordance with my previous results, western blotting analysis confirmed the constitutive expression of the murine hybrid protein in the DogMo cells (Figure 6.3.5).

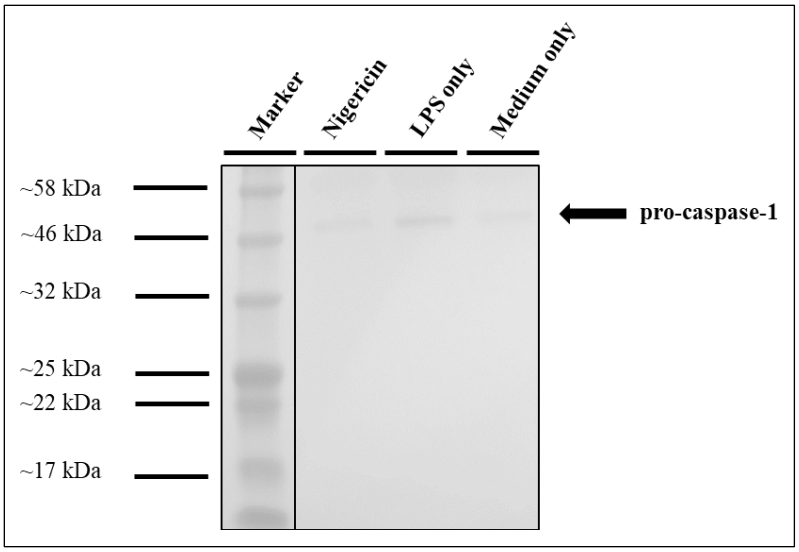


**Figure 6.3.4 Caspase-1 is constitutively expressed in wild-type macrophages.** Murine primary wild-type cells were primed with LPS (200 ng/ml for 3 hours) followed by incubation with nigericin (20 μM for 1 hour). The presence of constitutively expressed caspase-1 protein was confirmed by western blotting of cell lysates using murine specific caspase-1 antibody. Representative immunoblot is from a single experiment.

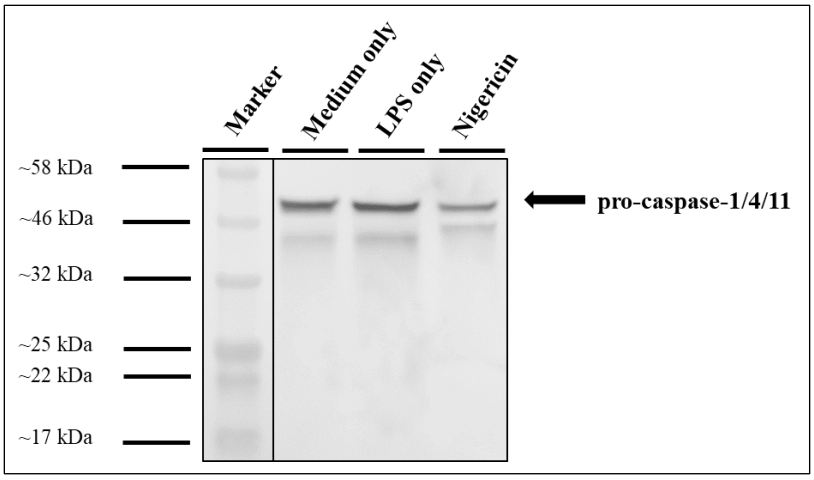


**Figure 6.3.5 Western blotting analysis of DogMo hybrid caspase-1/4/11 protein shows constitutive expression reminiscent of wild-type caspase-1 protein.** Murine primary DogMo cells were primed with LPS (200 ng/ml for 3 hours) followed by stimulation with nigericin bacterial toxin (20 µM for 1 hour). The presence of the hybrid caspase-1/4/11 protein was confirmed by western blotting of cell lysates using murine specific caspase-11 antibody. Representative immunoblot is from a single experiment.

## 6.4 Non-canonical inflammasome formation in DogMo cells containing hybrid caspase-1/4/11 gene

The CARD domain of caspase-11 has been shown to directly bind the lipid A moiety of bacterial LPS [61], [163], [168]. In the following experiments I investigated cell death responses of murine wild-type, DogMo and DH82 cells following transfection of LPS into the cytosol. Briefly, the respective cells were primed using TLR1/2 ligand Pam3CSK4 to initiate cytokine expression [343]. Cells were subsequently transfected with 5 µg or 10 µg LPS using FuGene HD transfection reagent as described in Materials and Methods section 2.6.

My results confirmed the essential role of the CARD domain of caspase-11 in driving pyroptotic cell lysis in response to cytosolic LPS delivery (Figure 6.4.1A). Wild-type murine primary BMDM cells exhibited 20% cell lysis (based on LDH release) in response to cytosolic LPS (Figure 6.4.1A). In accordance with previously described results in this thesis (Figure 3.6.2), canine DH82 cells did

not undergo cell lysis following cytosolic LPS treatment (Figure 6.4.1A). As expected, DogMo cells containing the hybrid protein (lacking the CARD domain of caspase-11), similarly to DH82 cells, did not undergo cell lysis in response to cytosolic LPS (Figure 6.4.1A).

Despite the absence of the caspase-11 CARD domain in DogMo macrophages, a small amount of IL-1β was detected in the culture supernatant post LPS transfection (Figure 6.4.1B). In contrast, wild-type murine and DH82 cells released large amounts of IL-1β into the supernatant (Figure 6.4.1B). These results suggested that despite the lack of caspase-11 CARD domain, either the murine hybrid protein was able to recognise cytosolic LPS, albeit less efficiently compared to wild-type caspase-11 or an alternative mechanism exists to recognise cytosolic LPS.

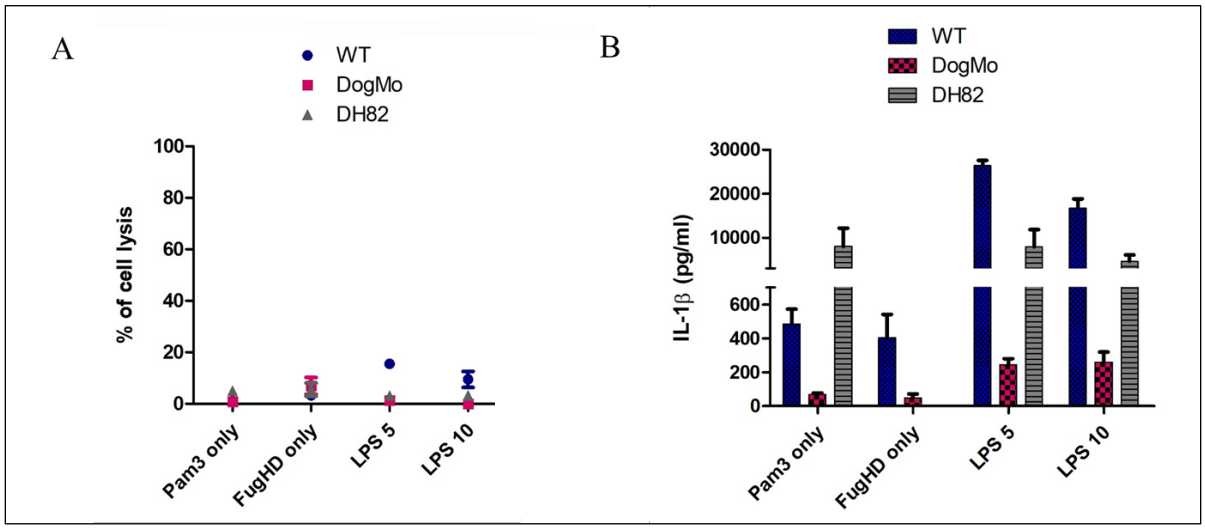


**Figure 6.4.1 Diminished IL-1β release occurs from DogMo cells in response to non-canonical inflammasome activation.** Murine wild-type, DogMo and canine DH82 cells were primed with Pam3CSK4 (10 µg/ml for 4 hours) then transfected with LPS at 5- and 10 µg/ml final concentrations using Fugene HD. (A) Percentage of cell lysis was determined by the measurement of LDH release into the culture supernatant. (B) IL-1β release was measured using murine specific ELISA. Results are representative of two independent experiments. Error bars represent the standard error of means (SEM) of triplicate wells.

I also investigated whether GSDMD cleavage occurs in cell lysates prepared from non-stimulated (medium only), Pam3 primed only (10 µg/ml for 4 hours) and LPS transfected murine wild-type and DogMo primary macrophages (Figure 6.4.1). Previous attempts at western blot to detect canine GSDMD using murine specific anti-GSDMD antibody proved inconclusive (3.3.4). As expected, full length GSDMD (~53 kDa) was detected in both wild-type and DogMo macrophages however, faint protein bands corresponding to the expected size of GSDMD N-terminal domain were also observed (Figure 6.4.2) in all conditions of both cell types.

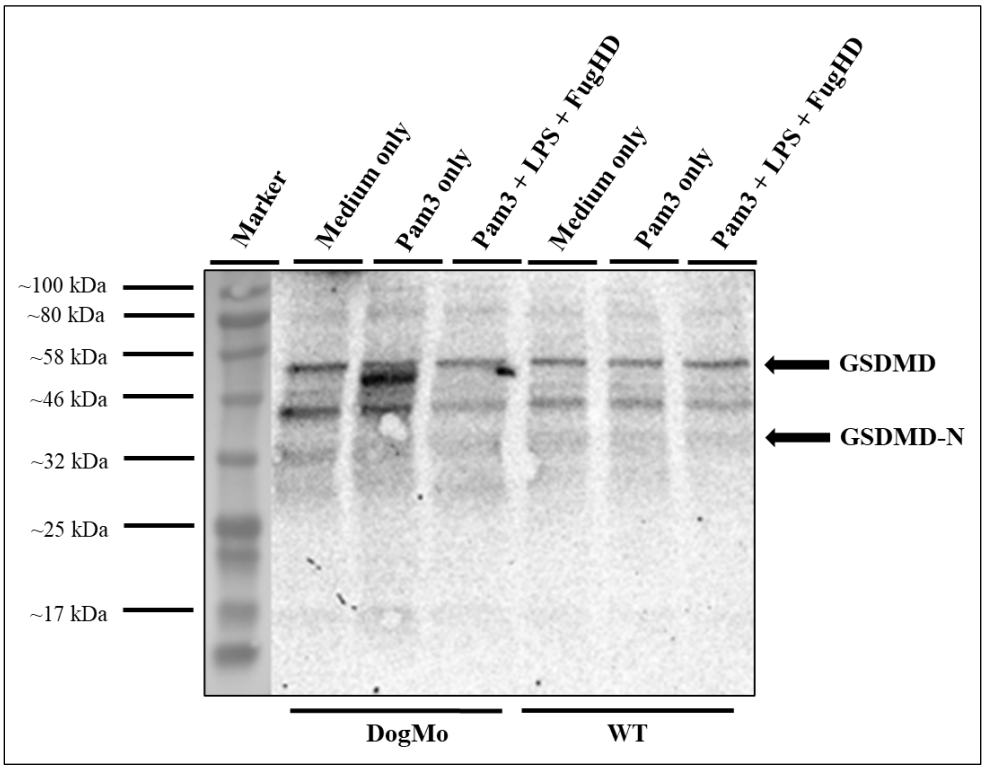


**Figure 6.4.2 Constitutive expression of GSDMD in murine wild-type and DogMo cells.** Murine primary wild-type and DogMo cells were primed with Pam3 (10 µg/ml for 4 hours) followed by LPS transfection (5 µg/ml for 16 hours). The presence of constitutively expressed GSDMD protein was confirmed by western blotting of cell lysates using murine specific GSDMD antibody. Representative immunoblot is from a single experiment.

To investigate whether the relatively small amount of IL-1β released by DogMo cells occurs as a consequence of caspase-1/4/11 hybrid protein activation, cell lysates from non-stimulated

(medium only), Pam3 primed and LPS transfected murine primary wild-type and DogMo cells were prepared for western blot analysis (Figure 6.4.2). Immunoblotting for murine caspase-11 identified the full-length hybrid and wild-type caspase-11 protein, but not the cleaved forms in DogMo cells, but full length and cleaved caspase-11 was seen in wild-type cell lysates (Figure 6.4.3).

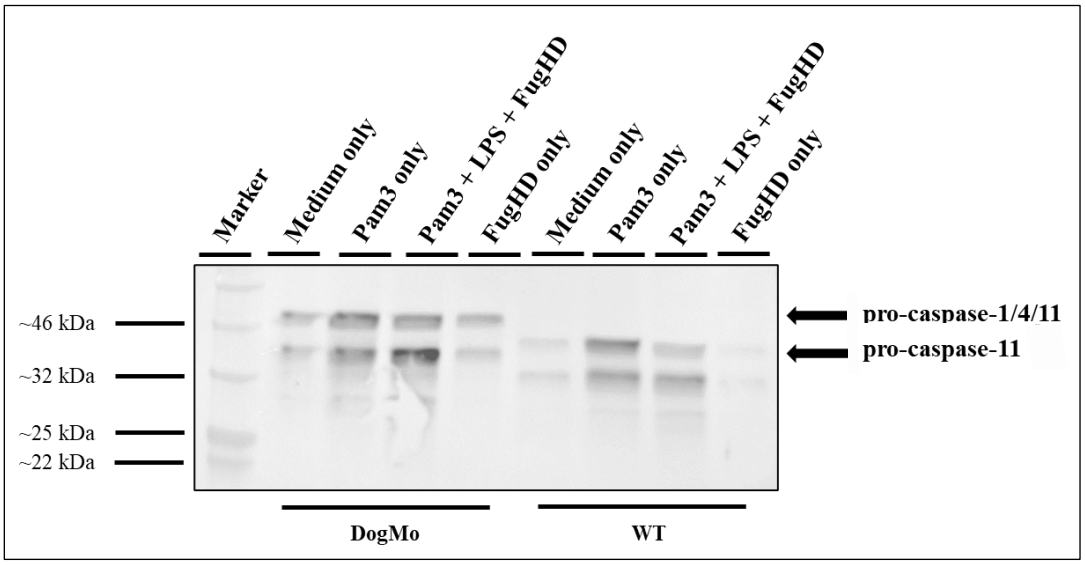


**Figure 6.4.3 Western blotting analysis reveals the presence of full length wild-type caspase-11 and hybrid caspase-1/4/11 proteins following LPS transfection of DogMo cells.** Murine primary wild-type and DogMo cells were primed with Pam3 (10 µg/ml for 4 hours) followed by LPS transfection (5 µg/ml for 16 hours). The presence of caspase-11 expression was confirmed by western blotting of cell lysates using murine specific caspase-11 antibody. Representative immunoblot is from a single experiment.

## 6.5 Functional characterisation of DogMo macrophages in response to *S.* Typhimurium infection

Mouse primary wild-type and DogMo macrophages were differentiated for 5 days and subsequently infected with wild-type *S.* Typhimurium (SL1344) using increasing MOIs (1-, 10-, and 50) as described in Materials and Methods section 2.5. Inflammasome activation was determined by measuring the percentage of cell lysis induced and the amount of IL-1β released

into the supernatant of *S.* Typhimurium infected cells at different time-points post infection (1, 2, 6 and 24 hours). Cell lysis was determined by measuring the relative amount of LDH released into the supernatant. While the presence of IL-1β was determined using canine and murine specific ELISA kits, respectively.

Using these *in vitro* infection assays I investigated the function of the mouse caspase-1/4/11 fusion protein in response to whole organism challenge using *S.* Typhimurium. Surprisingly, my results showed that DogMo cells, similarly to wild-type murine cells, readily recognised intracellular *S.* Typhimurium (Figure 6.5.1A). While DogMo cells lysis was reduced compared to wild-type cells, their cell death responses exhibited similar kinetics (Figure 6.5.1A). These results suggested the hybrid caspase-1/4/11 in murine cells was functional and was capable of driving pyroptotic cell death in response to *S.* Typhimurium infection.

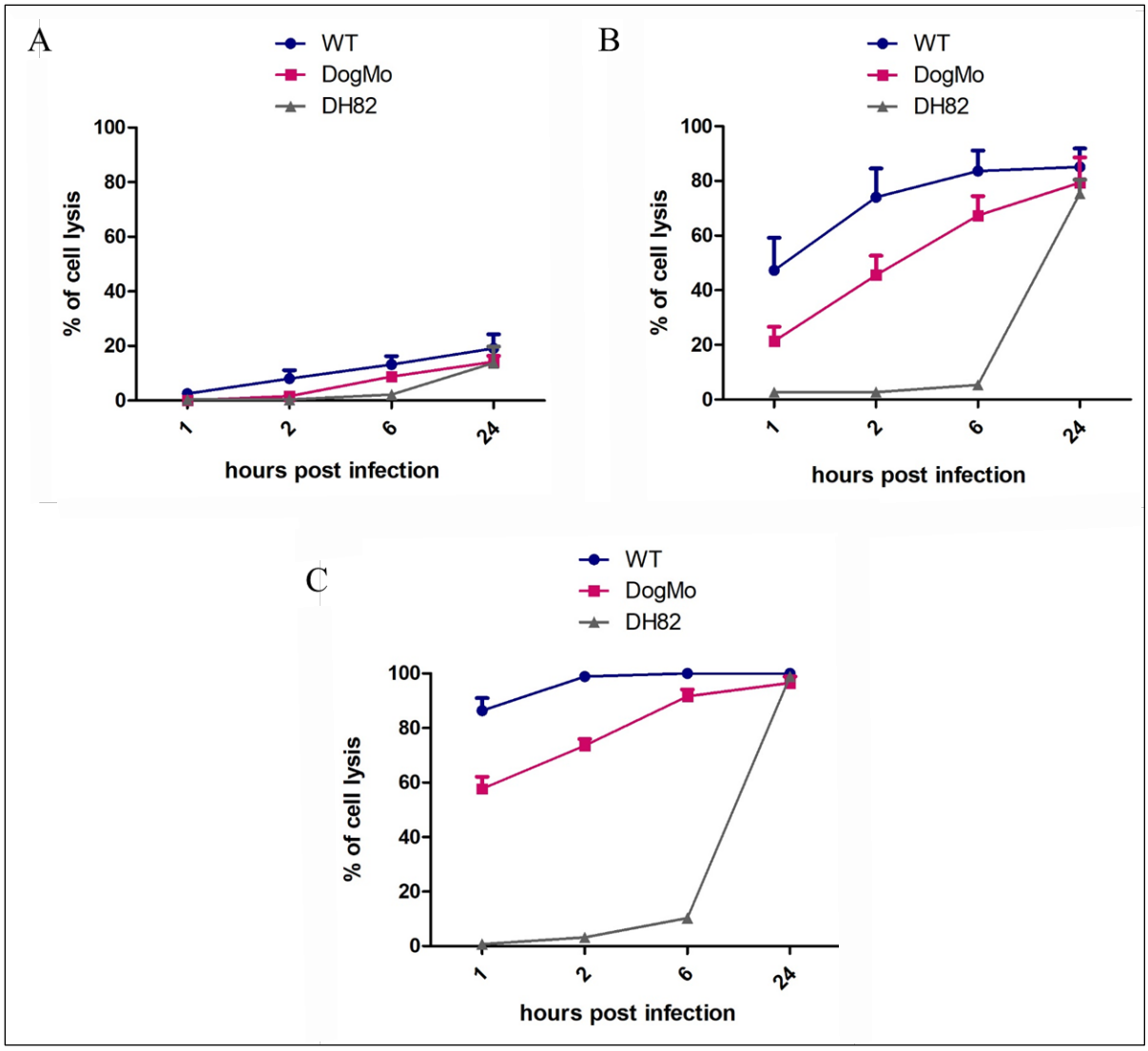


**Figure 6.5.1 Murine caspase-1/4/11 hybrid protein drives cell lysis in response to *S.* Typhimurium infection.** Murine primary wild-type, DogMo and canine immortalised DH82 cells were infected with *S.* Typhimurium with three different MOIs; (A) 1, (B) 10 and (C) 50. Percentage of cell lysis at 1, 2, 6 and 24 hours post infection was determined via the measurement of relative LDH release. Results are representative of two independent experiments. Error bars represent the standard error of means (SEM) of triplicate wells.

Following infection, cell lysates were analysed for GSDMD cleavage by western blotting using murine specific GSDMD antibody (Figures 6.5.2 and 6.5.3). GSDMD-N was observed in both wild-type and DogMo macrophages infected with *S.* Typhimurium (Figures 6.5.2 and 6.5.3). These

results confirmed that the murine caspase-1/4/11 hybrid protein was able to cleave GSDMD in the DogMo macrophages, a role undertaken by caspase-1 in the wild-type counterpart (Figures 6.5.2 and 6.5.3). In summary, the hybrid caspase protein expressed in the DogMo macrophages is capable of initiating pyroptosis by cleaving GSDMD in response to *S.* Typhimurium infection.

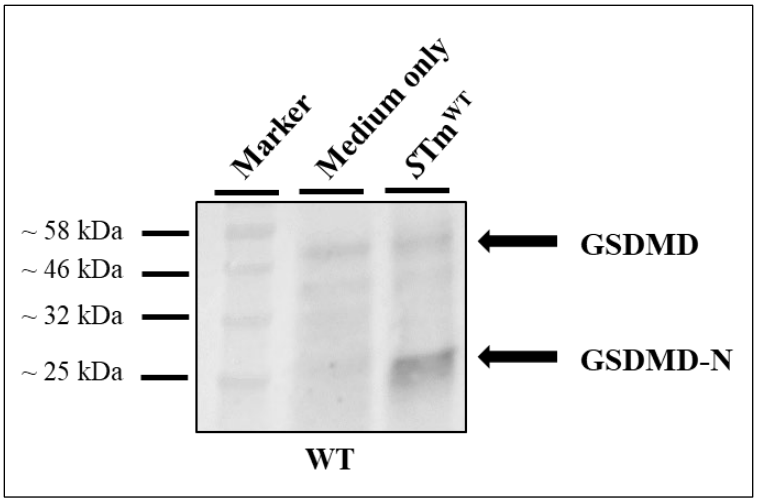


**Figure 6.5.2 GSDMD is cleaved in wild-type murine macrophages in response to *S.* Typhimurium infection.** Murine primary wild-type cells were infected with *S.* Typhimurium using MOI of 10 for 6 hours. GSDMD cleavage was determined by western blotting of cell lysates using anti-mouse GSDMD antibody. Representative immunoblot is from a single experiment.

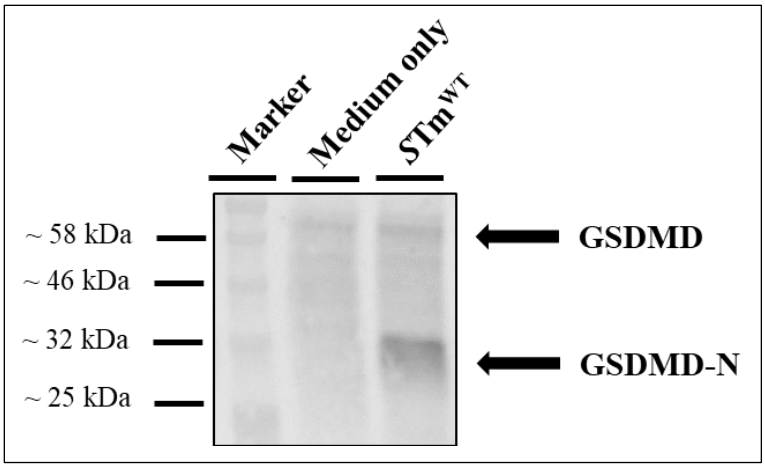


**Figure 6.5.3 DogMo macrophages containing the hybrid caspase-1/4/11 protein can cleave GSDMD following *S.* Typhimurium infection.** Murine primary DogMo cells were infected with *S.* Typhimurium using MOI of 10 for 6 hours. GSDMD cleavage was investigated by western blotting of cell lysates using murine specific GSDMD antibody following full protein extraction. Representative immunoblot is from a single experiment.

Wild-type murine primary and canine DH82 cells underwent cell lysis (Figure 6.5.1) and released large amounts of IL-1β into the supernatant (Figure 6.5.4) following *S.* Typhimurium infection. While IL-1β release from DogMo cells was diminished (Figure 6.5.4), a small amount of IL-1β was detected in the cell culture supernatant. These results suggested that, similarly to what I observed following stimulation with nigericin and cytosolic LPS, the CARD domain of the DogMo fusion protein was capable of driving cell lysis.

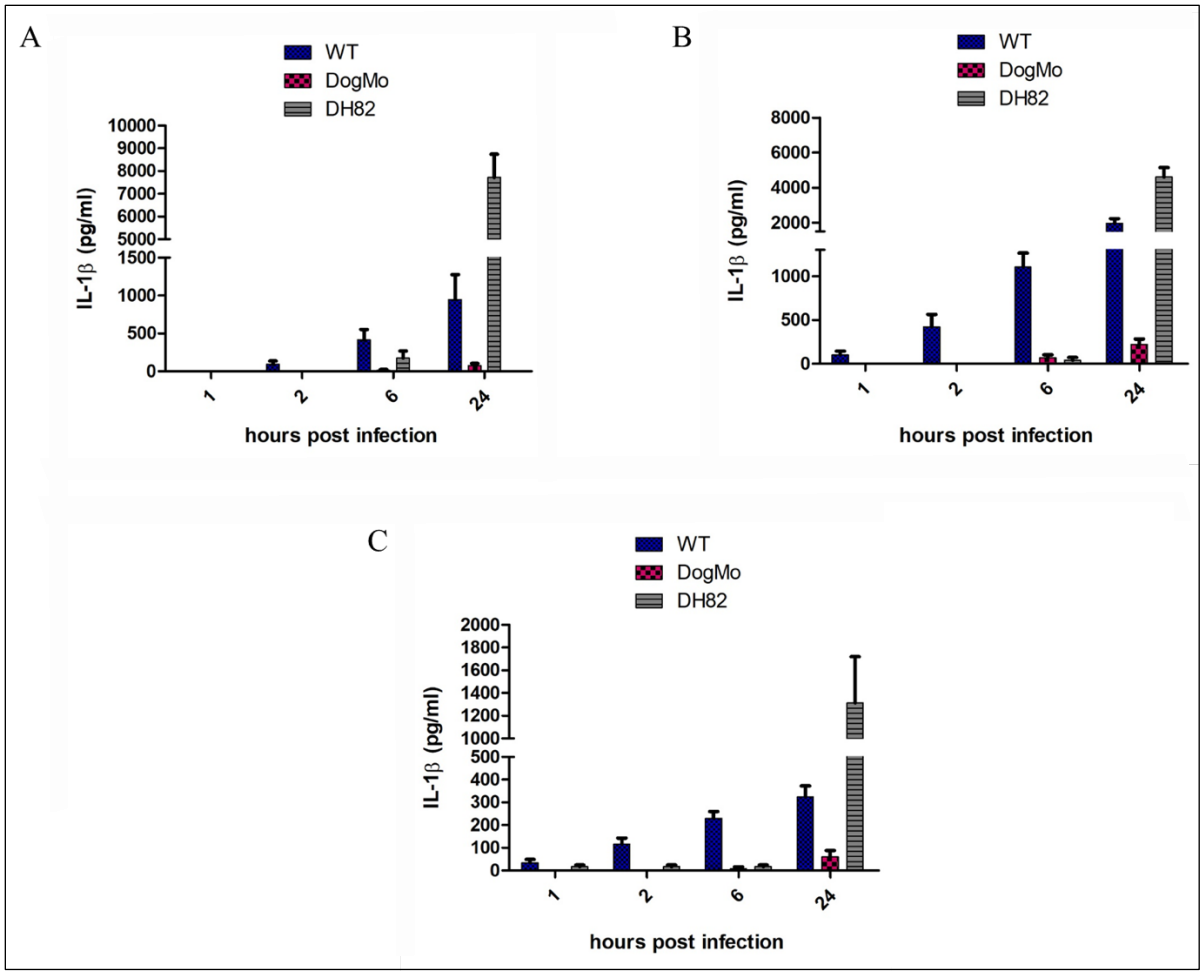


**Figure 6.5.4 Diminished IL-1β release occurs from DogMo cells in response to *S.* Typhimurium infection.** Murine wild-type, DogMo and canine DH82 cells were infected with S. Typhimurium with three different MOIs; (A) 1, (B) 10 and (C) 50. IL-1β release in the supernatant was measured by ELISA at 1, 2, 6 and 24 hours post infection. Results are representative of two independent experiments. Error bars represent the standard error of means (SEM) of triplicate wells.

### 6.6 Pharmacological inhibition of caspase-8 activity within the inflammasome

It has been shown that in addition to caspase-1, caspase-8 can also be recruited to the inflammasome in *S.* Typhimurium infected murine BMDMs [140]. Its activation has been proposed to play an important role in regulating IL-1β expression and maturation [140]. I therefore

investigated whether caspase-8 activity was driving the lytic cell response seen in DogMo macrophages in response to canonical and non-canonical inflammasome activators. Caspase-8 was pharmacologically inhibited using Z-IETD-FMK at a final concentration of 10μM and inflammasome activation was assessed by measuring the relative amount of LDH and IL-1β released into the culture supernatant.

Stimulation of DogMo macrophages with nigericin in the presence of the caspase-8 inhibitor resulted in approximately 50% reduction in cell lysis when compared to cells in the absence of the inhibitor (Figure 6.6.1A). Only a small reduction in cell lysis was observed with wild-type mouse macrophages is response to nigericin stimulation in the presence of the caspase-8 inhibitor (Figure 6.6.1A). This suggested that in the DogMo cells, caspase-8 played a key role in driving cell lysis in response to nigericin. A marked reduction in IL-1β release was also evident in wild-type murine macrophages stimulated with nigericin and caspase-8 inhibitor (Figure 6.6.1B). Taken together these data suggested that in the absence of bonifide caspase-1, as is the case for the DogMo cells, caspase-8 played a key role in driving cell lysis in response to nigericin induced NLRP3 activation. These conclusions however were made with the caveat that interpreting results involving the majority of inhibitors caution must be taken with regards specificity and off-target pharmacological effects.

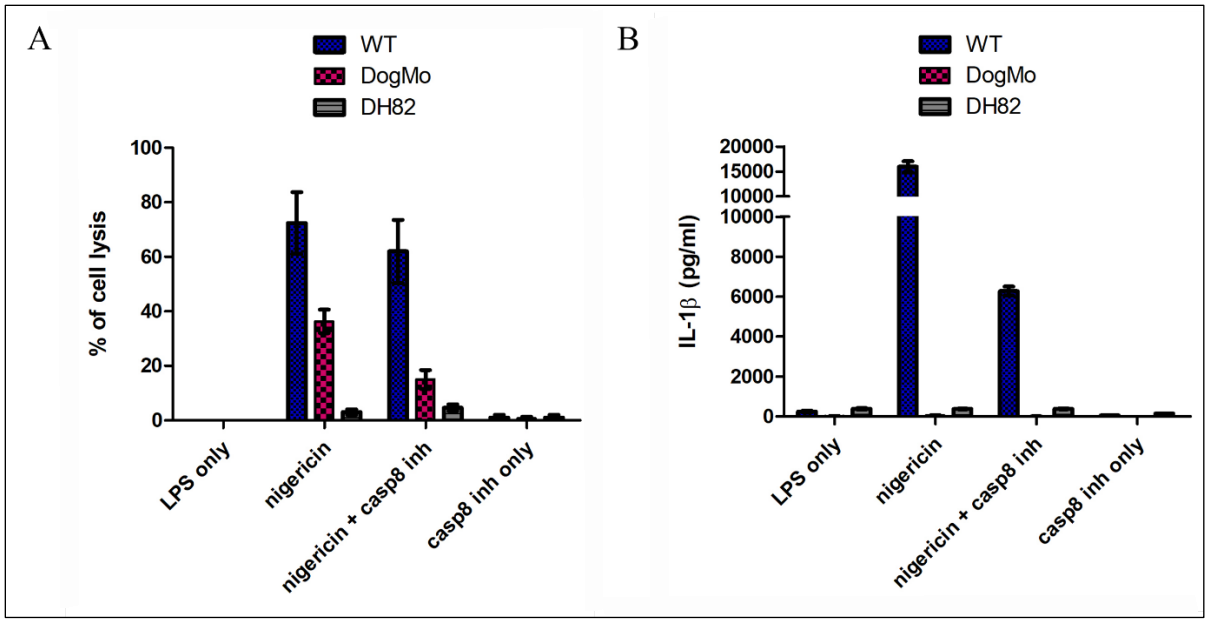


**Figure 6.6.1 Pharmacological inhibition of caspase-8 reduces cell lysis in response to nigericin.** Murine wild-type, DogMo and canine DH82 cells were primed with LPS (200 ng/ml for 3 hours) then stimulated with nigericin bacterial toxin (20 µM) and caspase-8 inhibitor (Z-IETD-FMK) at 10µM final concentration. Nigericin induced cell lysis was assessed by directly measuring LDH released into the supernatant. IL-1β release was quantified using canine and murine specific ELISAs, respectively. Results are representative of a single experiment. Error bars represent the standard error of means (SEM) of triplicate wells.

Pharmacological inhibition of caspase-8 in LPS transfected wild-type murine macrophages resulted in reduced cell lysis compared to those cells transfected with LPS alone (Figure 6.6.2). Independent studies have shown that pyroptotic cell death following cytosolic LPS recognition is driven by inflammatory caspase-11 [61], [163], [168], [342]. The reduced cell lysis observed in wild-type murine macrophages suggested that either caspase-8 was also recruited to the non-canonical inflammasome or the caspase-8 inhibitor could also inhibit caspase-11. Lack of specificity in the caspase-8 inhibitor has been suggested [398], [399]. An alternative approach to investigate the role of caspase-8 in the context of cell lytic response would be to repeat these experiments in caspase-8/RIPK3 double knock-out mice. Unfortunately in this experiment LPS transfection did not result in either LDH or IL-1β release into the supernatant of DogMo cells therefore, the effect of pharmacological inhibition of caspase-8 could not be investigated.

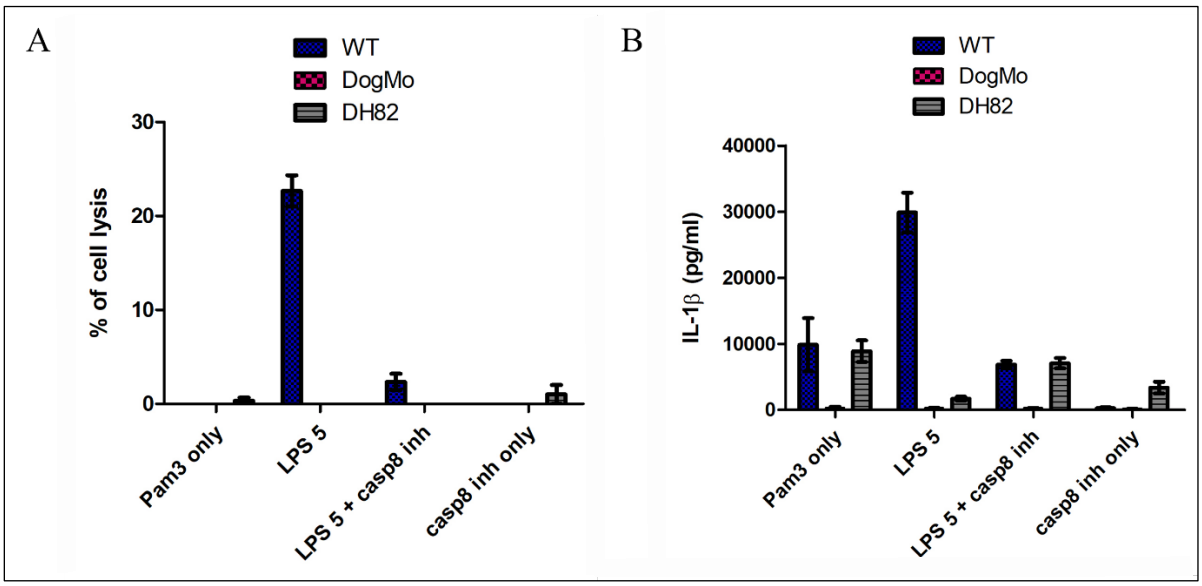


**Figure 6.6.2 The effect of pharmacological inhibition of caspase-8 activity on cell lysis and IL-1β production in LPS transfected DogMo cells could not be investigated.** Murine wild-type, DogMo and canine DH82 cells were primed with Pam3CSK4 (10 µg/ml for 4 hours) then transfected with LPS at 5 µg/ml final concentration and stimulated with caspase-8 inhibitor (Z-IETD-FMK) at 10 µM final concentration. (A) Percentage of cell lysis induced was determined by measuring LDH released into the supernatant, while (B) IL-1β release was measured using murine and canine specific ELISA kits. Results are representative of a single experiment. Error bars represent the standard error of means (SEM) of triplicate wells.

Inhibition of caspase-8 using Z-IETD-FMK in *S.* Typhimurium (MOI of 10) infected wild-type murine BMDMs had little, if any, effect on cell lysis at any of the time-points post infection (Figure 6.6.3). In contrast to wild-type cells, inhibition of caspase-8 significantly reduced the percentage of cell lysis induced at early time-points, 1 and 2 hours post infection (Figure 6.6.3A and B) in DogMo cells containing the hybrid caspase-1/4/11 protein. Marginal inhibition was observed at later time-points (6 and 24 hours post infection). I therefore aim to confirm these results in a cell line containing the hybrid caspase-1/4/11 gene in a caspase-8-deficient background.

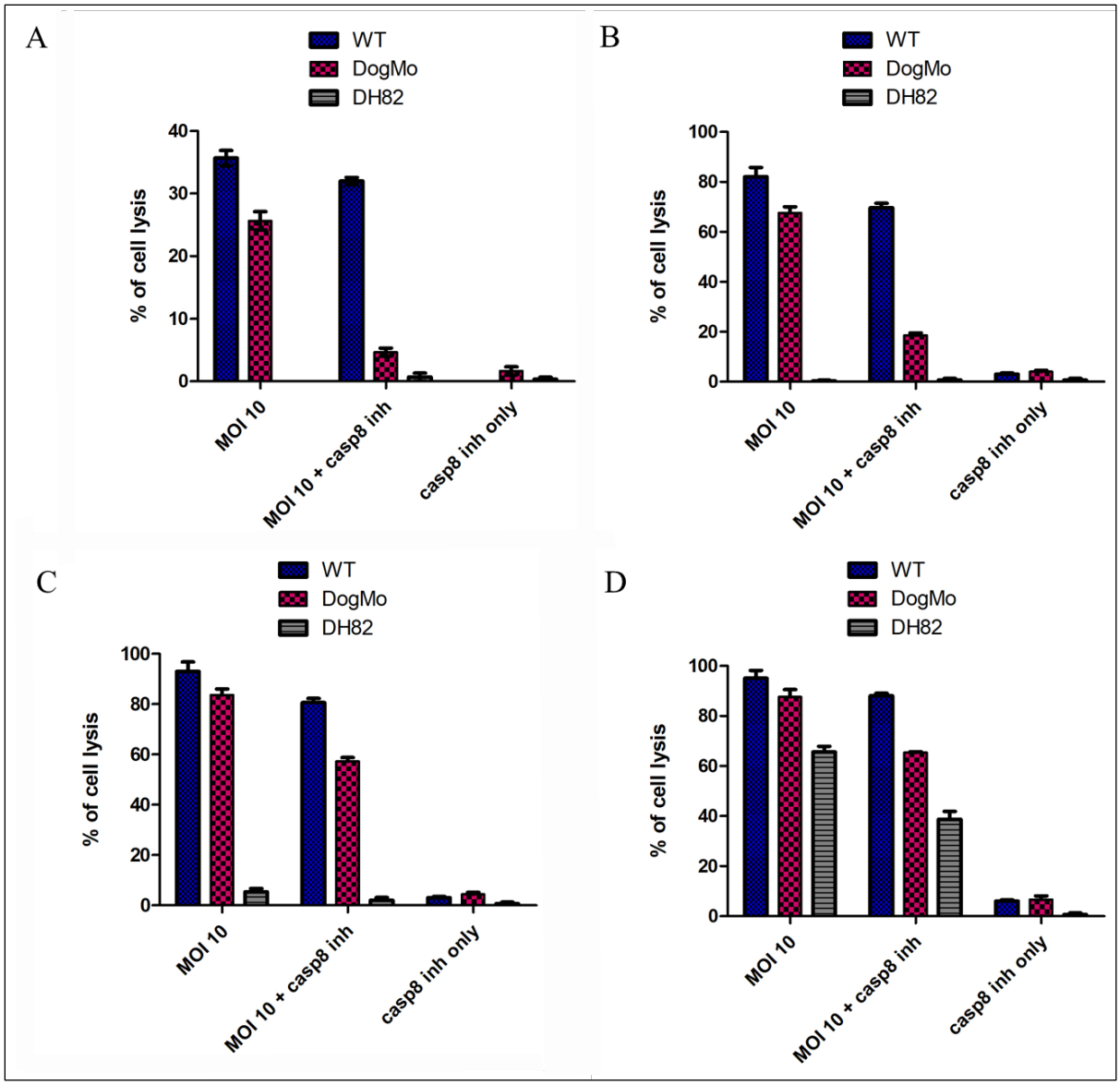


**Figure 6.6.3 Pharmacological inhibition of caspase-8 reduced cell lysis induced at early time-points following *S.* Typhimurium infection in DogMo cells.** Murine primary wild-type, DogMo and canine DH82 cells were infected with *S.* Typhimurium with MOI of 10 and stimulated with caspase-8 inhibitor (Z-IETD-FMK) at 10 µM final concentration. Percentage of cell lysis at (A) 1, (B) 2, (C) 6 and (D) 24 hours post infection was determined by measurement of LDH release into the culture supernatant. Results are representative of a single experiment. Error bars represent the standard error of means (SEM) of triplicate wells.

Pharmacological inhibition of caspase-8 in wild-type murine BMDMs reduced the amount of IL-1β detected in the supernatant at all time-points investigated while it showed no effect on canine DH82 cells (Figure 6.6.3). In contrast to wild-type cells, no IL-1β was detected in the supernatant of DogMo cells at early time-points, therefore the effect of caspase-8 inhibition could not be investigated (Figure 6.6.4A and B). At later time-points (6 and 24 hour post infection) however the inhibition of caspase-8 reduced the amount of IL-1β detected in the supernatant of DogMo cells (Figure 6.6.4C and D). These results suggested that the small amount of IL-1β in the supernatant could be processed by caspase-8 activity.

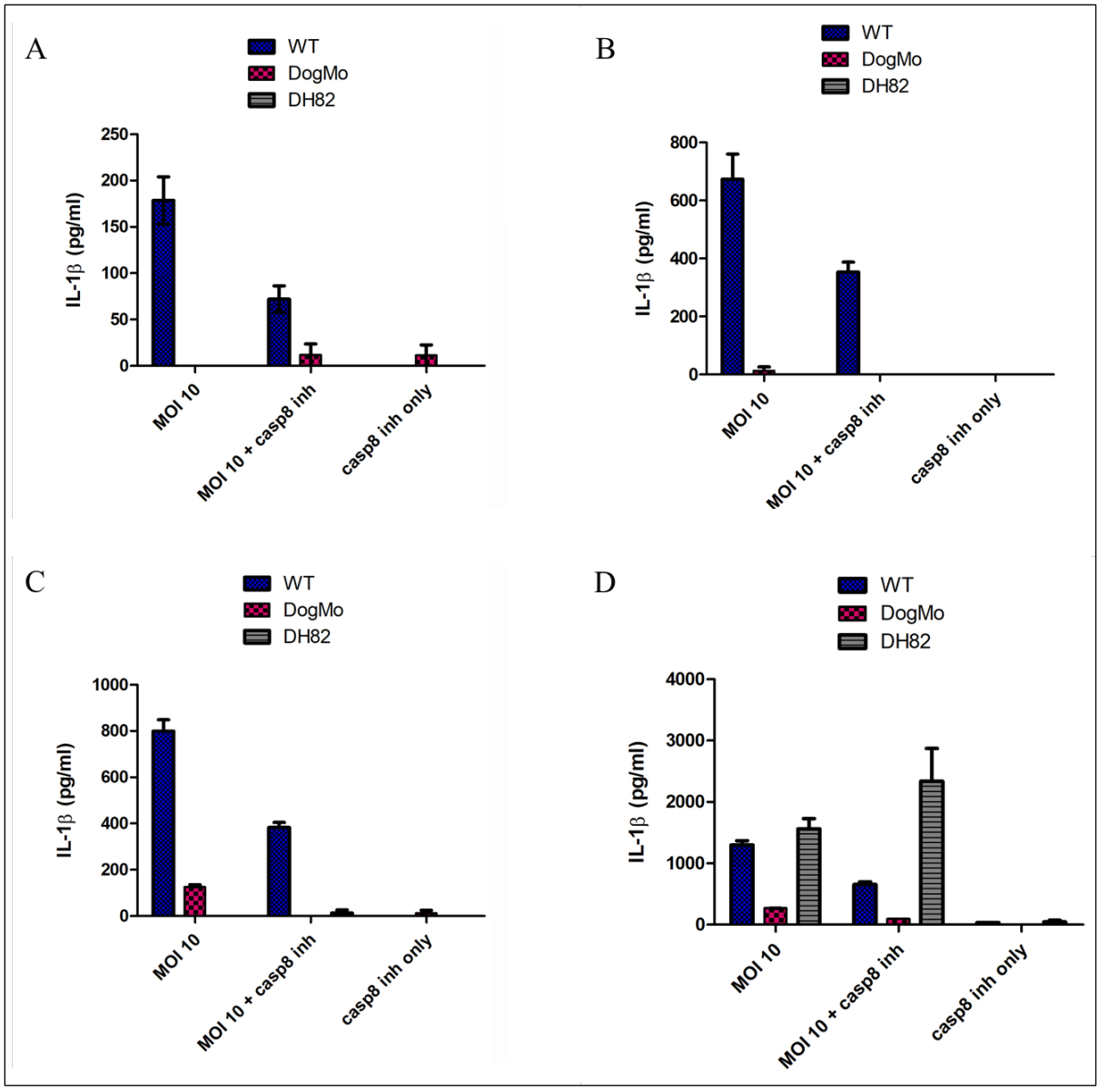


**Figure 6.6.4 The effect of pharmacological inhibition of caspase-8 activity on IL-1β release could not be investigated in DogMo cells.** Murine wild-type, DogMo and canine DH82 cells were infected with *S.* Typhimurium using MOI of 10 and stimulated with caspase-8 inhibitor (Z-IETD-FMK) at 10 μM final concentration. IL-1β release in the supernatant was measured by ELISA method at (A) 1, (B) 2, (C) 6 and (D) 24 hours post infection. Results are representative of a single experiment. Error bars represent the standard error of means (SEM) of triplicate wells.

## 6.7 Discussion

MUSCLE analysis of the canine caspase-1/4/11 transcript suggested the presence of a functional caspase protein (Figure 3.2.3) and mass spectrometry provided confirmation of its constitutive expression in DH82 cells (Figure 3.2.2). Genetic deletion of the catalytic residue of the caspase domain of the canine hybrid protein failed to rescue the late cell death phenotype observed during infection of DH82 macrophages with *S.* Typhimurium. In this chapter I have therefore carried out a series of functional assays on murine primary BMDM cells which have been genetically engineered to contain the hybrid caspase-1/4/11gene (DogMo cells) in order to determine whether the caspase1/11 fusion is not functional or whether there is something unique about its functional activity in dogs. Wild-type mice were genetically modified by the Dixit lab using CRISPR-Cas9 gene editing technology to induce a large deletion extending to the caspase domain of caspase-1 and the CARD domain of caspase-11. This 20,524 bp deletion (Figure 6.2.2) generated a similar gene organisation to that of the shorter transcript of the canine hybrid caspase-1/4/11 gene (Figure 3.1.1).

The results obtained from a series of *in vitro* experiments to characterise inflammasomes revealed that wild-type and DogMo cells exhibited similar lytic responses to canonical NLRP3 (nigericin) and NLRC4 (*S.* Typhimurium infection) (Figures 6.3.1 and 6.5.1) activators albeit with marginally lower responses in DogMo cells compared to wild-type murine macrophages (Figures 6.3.1 and 6.5.1). These results were in contrast to what I observed and have previously shown in canine DH82 cells (Figure 3.7.2). Mouse hybrid caspase-1/4/11 harbours the normal NAIP/NLRC4 receptor repertoire whereas DH82 cells lack *NAIP* genes and their *NLRC4* gene is a pseudogene due to two stop codons [41] The intact NAIP/NLRC4 inflammasome must, therefore, either activate the hybrid caspase-1/4/11 to drive cell death albeit at a lower efficiency than that driven by full length caspase-1 or other caspases e.g. caspase-8 could drive cell death [224]. The hybrid protein could function as a scaffold protein rather than an effector molecule, to recruit additional effector proteins to the inflammasome. These data showing pyroptosis in response to *S.* Typhimurium infection in the DogMo cells are in contrast to the results seen in DH82 macrophages where inflammasome activation downstream of ASC is almost absent. My data shows the NLRP3/ASC/active FLICA-caspase 1 speck is formed, but this complex cannot process IL-1β or

drive cell death. It is possible that the canine caspase-1/4/11 protein is, in some way, switched off although mechanisms by which this may occur are unclear.

I have shown that GSDMD was processed in DogMo cells in response to both nigericin stimulation and *S.* Typhimurium infection (Figures 6.3.3 and 6.5.3). The expression of caspase-1, caspase-11 and the hybrid caspase-1/4/11 proteins was confirmed by western blotting. To date caspase-11 is thought to only detect intracellular LPS, cleave GSDMD and activate a non-canonical inflammasome [168]. Wild-type murine macrophages, as expected, processed IL-1β in response to nigericin stimulation and *S.* Typhimurium infection, whilst DogMo cells were not able to process IL-1β (Figures 6.3.1, 6.5.1 and 6.5.4). Taken together, these data suggested that the hybrid caspase-1/4/11 protein expressed in murine cells was functional for GSDMD driven cell death, but not for IL-1β processing.

The CARD domain of caspase-11 has been shown to directly recognise and bind the outer membrane component lipid A moiety of LPS [61]. Wild-type murine cells released LDH and IL-1β in response to LPS transfection (Figure 6.4.1). Despite the apparent lack of DogMo cell responsiveness to transfected LPS (no LDH or IL-1β release) (Figure 6.4.1) protein bands corresponding to full length and cleaved GSDMD were detected by western blotting (Figure 6.4.2) Both protein bands however were also present in medium only (non-stimulated) samples (Figure 6.4.2). These results, therefore require further investigation. These observations provided supportive evidence for the importance of the CARD domain of caspase-11 in the recognition of cytosolic LPS. As discussed in Chapter 3 of this thesis, murine GSDMD antibodies were unsuitable for the detection of canine GSDMD (Figure 3.3.4). Preliminary results suggested that the mouse hybrid caspase-1/4/11 protein was able to cleave GSDMD to yield GSDMD-N. To investigate the processing of canine GSDMD, I have subsequently utilized CRISPR-Cas9 gene editing approaches to introduce a FLAG-tag onto the endogenous canine GSDMD gene immediately upstream of the STOP codon as described in Materials and Methods section 2.12. Sequencing confirmed the insertion of the FLAG-tag motif for one of the guide RNAs (CTGAGCGAGGACCCCTGTTA**)** used and subsequent single cell cloning and further experiments are required to determine FLAG-tag expression and protein functionality (Appendix 28).

Surprisingly, pharmacological inhibition of caspase-8 reduced the extent of cell lysis in DogMo cells following both nigericin stimulation (Figure 6.6.1) and at early time-points post *S.* Typhimurium infection (Figure 6.6.3). Caspase-8 has been shown to play an important role in the priming and modulation of IL-1β production, but not cell death, in response to *S.* Typhimurium infection [140]. Results obtained here suggest a crucial role of caspase-8 in driving cell lysis in response to canonical NLPR3 and NLRC4 inflammasome activation in DogMo cells.

# Chapter 7
# Discussion and Future Work

Inflammasomes are macromolecular multiprotein complexes that assemble in response to a wide range of inflammatory stimuli. Inflammasomes are composed of a receptor (e.g. NLRP3, NLRC4), an adaptor (ASC) and effector proteins (e.g. caspase-1). Inflammasome activation leads to the processing of inflammatory cytokines IL-1β and IL-18 into their bioactive forms and cleavage of GSDMD to execute pyroptotic cell death. Their assembly and activation is thought to be essential to mount effective host defence responses against invading pathogens. Their putative importance established in human and mouse systems suggest that their components should be conserved across different animal species. There are however major differences in inflammatory receptors and particularly in caspase repertoire found in different species, raising questions about their function and importance in host defence.

The primary aim of my research was, originally, to investigate the role of the inflammatory caspase-1/4/11 isoform found in the dog (*Canis lupus familiaris*). Little is known about how this unique gene organization affects inflammasome formation and ultimately innate immune responses in the dog. In this work I have characterized inflammasome functions using a canine immortalized DH82 macrophage-like cell line. For that, I investigated DH82 cell responses to well established inflammatory activator ligands and in response to infectious whole organism, *Salmonella enterica serovar* Typhimurium. I have also validated some of the major responses observed in DH82 cells using canine PBMCs. Inflammasome activation was measured by immunofluorescent detection of ASC and active caspase speck formation, IL-1β production and maturation and the morphological analysis of cell lysis using live cell imaging. I have also generated DH82 cell lines deficient for pivotal genes involved in inflammasome formation, while also attempting to endogenously tag target genes using recombinant CRISPR-Cas9 technology.

Results that were obtained using primary canine blood MNCs suggested responses observed in the immortalised DH82 cell line to be a true representation of how primary dog cells behave in response to canonical/non-canonical activators. However, due to the low number of blood samples available from the clinic, only a single replicate could be performed for each inflammatory stimuli

used (Figures 3.5.6, 3.6.6 and 4.2.8). The nature of the samples (Figure 2.2.1 ) could possibly affect cell responses, it is therefore essential that additional experiments are performed on blood MNCs derived from healthy volunteers. In order to gain access to fresh blood samples from healthy volunteers, I have set up an informal collaboration with a charity called Pet Blood Bank UK (https://www.petbloodbankuk.org/) that provides a canine blood bank service for all veterinary practitioners throughout the UK. There are known breed-specific predispositions to diseases, therefore it would be of interest to investigate the responses of different dog breeds to various inflammasome activators.

In this thesis, the initial responses of caspase-1/4/11- (Figures 5.3.4 and 5.3.5) and RIPK1-deficient (Figures 5.9.2, 5.9.3) DH82 CRISPR generated DH82 macrophages to *S*. Typhimurium challenge were investigated. For completeness, further characterisation of responses to sterile inflammatory ligands should also be addressed through cell lysis quantification (LDH release and live cell imaging), ASC speck formation, fluorescent caspase localisation (FLICA staining) and the production and maturation of IL-1β.

*In vitro* cleavage of the canine hybrid protein in an overexpression system provided evidence that the protein was fully functional and was able to cleave classic caspase-1 substrates; IL-1β and GSDMD (Guy Salvesen's lab, unpublished data). As expected, cytosolic LPS transfection of primary murine BMDMs harvested from the genetically engineered DogMo mice harbouring the hybrid gene fusion (that is a functional equivalent of the canine caspase1/4/11 gene) failed to activate non-canonical inflammasome formation (Figure 7.4.1). For completeness, it would be of interest to apply microscopy to rule out ASC speck formation and active caspase recruitment in DogMo cells following LPS transfection.

Due to the limited resource of frozen DogMo primary BMDMs, only a small number of experiments could be performed. To fully characterise DogMo cells I aimed to generate the equivalent caspase-1/4/11 hybrid gene organisation in both wild-type and NLRC4-deficient mouse iBMDMs. For this, I have successfully performed electroporation for CRISPR-Cas9 gene editing using the guide RNA sequences kindly provided by Vishva Dixit (Genentech).

Bulk-edited DH82 cells for the caspase-8 gene exhibited a reduction in the amount of IL-1β released into the supernatant following *S.* Typhimurium infection (Figure 5.7.2) despite no change in cell lytic responses (Figure 5.7.1). Caspase-8 has been shown to regulate transcriptional priming of pro-IL-1β and has also been implicated in pro-IL-1β cleavage, and therefore maturation. In order to investigate the role of caspase-8, single cell dilution of bulk CRISPR-Cas9 edited DH82 cells for the caspase-8 gene should be performed. Thereafter, infection with *S.* Typhimurium can then be repeated on selected clones harbouring out-of-frame indels in the caspase-8 gene. IL-1β release and cleavage should be assessed using ELISA and western-blot, respectively.

Results described in Chapter 4 of this thesis suggested that cell lysis (Figure 4.2.6) and IL-1β (Figure 4.2.7) responses following *S.* Typhimurium infection were largely dependent on the type III secretion system. PrgJ, a component of the type III secretory system has been shown to be directly recognised by NAIPs [133]. However, NAIPs are absent in the dog genome, yet *S.* Typhimurium lacking PrgJ still drove cell lysis in DH82 cells (Figure 4.2.6). A possible explanation for this result is that NLRP3 is able to sense the homeostatic changes (e.g. potassium efflux) induced by the delivery of bacterial effector proteins into the dog macrophage via the type III secretion system. It would be of interest to investigate DH82 cell responses following *S.* Typhimurium infection in the presence of elevated levels of extracellular potassium which has been reported to inhibit NLRP3 inflammasome formation [83, 126]

Based on previous genomic sequence analysis, the NLRC4 inflammasome should not be functional in the dog [41]. DH82 cells infected with wild-type *S.* Typhimurium did not show ASC speck formation or activated caspase recruitment. Interestingly, DH82 cells showed delayed cell lysis responses, similarly to what I observed with their *Nlrc4*$^{-/-}$ and *caspase-1*$^{-/-}$*caspase-11*$^{-/-}$ mouse counterparts (Figure 4.2.2). The presence of cleaved IL-1β in the supernatant of *S.* Typhimurium infected DH82 cells, which coincided with cell lysis at 24 hour post infection suggested inflammasome activation (Figures 4.2.3 and 4.2.4). The processed IL-1β in response to *S.* Typhimurium infection appeared to be smaller than the p17 fragment normally observed following caspase-1 mediated cleavage (Figure 4.4.4). Other proteins including elastase, cathepsin G and collagenase have been shown to process recombinant IL-1β. These proteases however produced cleaved IL-1β at around or larger than 17 kDa [356], [357]. This suggested the presence of a

perhaps not yet discovered protease driving pro-IL-1β maturation in the dog. For that, genome-scale loss-of-function screens could be utilized to identify the protease responsible for the generation of mature IL-1β [400], [401]. In an effort to narrow down the search, it would also be useful to determine the different cleavage sites of the canine pro-IL-1β. For that, mass spectrometry analysis of *S.* Typhimurium infected and nigericin stimulated DH82 cells containing endogenously tagged IL-1β could be utilised to identify potential cleavage sites.

Genomic sequence analysis suggested the total absence of the *NAIP* gene and the presence of multiple stop codons in the gene encoding the canine NLRC4 receptor. Analysis showed the genes flanking human *NAIP* to be direct neighbours in the dog genome, the genome sequence however was not contiguous in that region [41]. The lack of *NAIP* gene was further confirmed by blasting the human NAIP transcript against the canine Expressed Sequence Tag (EST) database. The assembly level of the canine reference genome on Ensembl is still incomplete, potentially containing gaps in the genome sequence (https://www.ncbi.nlm.nih.gov/assembly/GCF_000002285.3/). It would therefore be interesting to complete the reference genome of this region and confirm the total absence of *NAIP* genes. NAIP/NLRC4 receptors have been shown to be essential in controlling *S.* Typhimurium infections at early stages [402], [403]. The presence of the *NLRC4* pseudogene suggests that the protein used to be functional. It would be intriguing to investigate whether the correction of the early stop codons present in the dog *NLRC4* gene (equivalent of the human NLRC4 at positions Trp 30 and Arg 35) could restore early *S.* Typhimurium detection in DH82 macrophages. This could be carried out by introducing double-stranded DNA breaks (DSB) followed by either homology-directed repair (HDR) or base-editing system utilizing CRISPR-Cas9 gene editing systems [404].

Sequence analysis of the known NLRP3 inflammasome constituents suggested the presence of functional NLRP3 inflammasome in the dog (Figures 3.2.3, 3.3.1, 3.4.3 and 3.4.1). DH82 macrophages however appeared to be refractory to the NLRP3 inflammasome activator, nigericin bacterial toxin. The rate of inflammasome formation measured by ASC speck formation and active caspase recruitment was reduced compared to wild-type murine macrophages (Figure 3.5.4). My results suggested that canine DH82 macrophages are not responsive to NLRP3 inflammasome activation by nigericin at concentrations generally reported to be potent activators of human and

mouse NLRP3. NLRP3 is a promiscuous receptor, without a clear direct ligand, but research so far has identified $K^+$ efflux as a common trigger for its activation [82]. It would therefore be interesting to investigate cell lysis and IL-1β maturation in cells incubated in low-$K^+$ media [82]. To fully characterize NLRP3 inflammasome activation of canine macrophages, other well established NLRP3 inflammasome activators such as extracellular ATP [78], [85], uric acid crystals [116], silica crystals and aluminum salts [91] should also be explored in a range of concentrations. The adapter protein ASC facilitates pro-caspase-1 recruitment to the inflammasome, therefore, it is required for NLRP3 inflammasome formation which only has a pyrin domain and requires ASC to recruit CARD domain containing proteins [405]. Cells deficient for ASC fail to activate the NLRP3 inflammasome [123]. I observed only very limited NLRP3 activation in response to high concentration of nigericin bacterial toxin (Figure 3.5.3). NEK7 promotes NLRP3 oligomerisation and it is an essential regulator of the NLRP3 inflammasome [108]. NEK7 is present in canine macrophages, but whether it is an important regulatory of NLRP3 activation in dog cells is unknown. Its' role in NLRP3 inflammasome regulation could be investigated by the generation of NEK7-deficient canine macrophages. [406].

Eckhart *et al* has predicted the presence of two alternative transcripts for the dog hybrid gene [154]. The larger transcript contains the CARD domain of the caspase-1 gene and the entirety of the caspase-4/-11 equivalent genes. While the shorter transcript of the dog hybrid gene lacks the CARD domain of the caspase-4 gene [154] which has been shown to directly recognize and bind the lipid A moiety of Gram-negative bacterial LPS [168], [170]. Non-canonical inflammasome formation did not induce ASC speck formation or activated caspase recruitment in dog cells, which suggested the expression of the shorter transcript of the canine hybrid gene. TLR priming alone induced large amount of mature IL-1β release without concomitant cell lysis (Figure 3.6.2). This phenomenon has been reported in primary human monocytes following incubation with extracellular LPS [185]. The authors claimed this pathway to be dependent on TLR4, RIPK1, FADD and caspase-8 upstream of the NLRP3 inflammasome. It would therefore be interesting to investigate IL-1β maturation following priming with TLR4 ligands in the presence of TAK-242, a TLR4 specific small molecule inhibitor [407] or caspase-8 specific inhibitors (e.g. Z-IETD-FMK). Alternatively, non-canonical inflammasome activation could be re-examined using DH82 cells lacking functional RIPK1 or caspase-8. RIPK1-deficient DH82 cells failed to express pro-

IL-1β (Figure 5.9.5), while caspase-8-deficient bulk population showed it's a large reduction following *S.* Typhimurium infection supporting the possible formation of this alternative inflammasome (Figure 5.7.2).

Different inflammatory caspases could also be activated in the DH82 cells where the caspase 1/4/11 fusion is poorly active. I therefore looked to identify additional caspases present in the dog genome, which may have functional roles that are distinct to those imparted to the hybrid caspase-1/4/11 protein as described in Materials and Methods section 2.13. I have generated a phylogenetic tree for the analysis of putative and confirmed caspases for different species investigated (Appendix 29). Phylogenetic tree analysis showed the presence of different clusters within the caspase-1-like and caspase-14-like clusters. Caspases within these clusters showed pronounced species-based differences (Appendix 30). The caspase-1 like cluster contained the unique hybrid caspase-1/4/11 gene whereas the caspase-14 like cluster contained caspase-15 which is present in the dog, but absent in mouse and humans (Appendix 30) [408]. Analysis showed the presence of a putative PYRIN domain, which could potentially facilitate recruitment of caspase-15 to the inflammasome [409] and the presence of a caspase domain containing both large and small caspase catalytic subunits including amino acid residues in caspase 15 essential for its activity [408]. Using CRISPR-Cas9 technology I aimed to generate a caspase-15 knock-out DH82 cell line as described in Materials and Methods section 2.12.2 (Appendix 31). It will therefore be interesting to investigate the possible role of caspase-15 in DH82 cell lytic responses to *S.* Typhimurium infection.

Overall, functional characterisation of the canine hybrid caspase-1/4/11 hybrid protein in DH82 cells in response to well established canonical NLRP3, NLRC4 and non-canonical inflammasome activators could suggest that the hybrid protein has significantly reduced activity or perhaps is actively downregulated. This was also validated in DH82 cells deficient for the hybrid gene generated by CRISPR-Cas9 gene editing technology. The lack of catalytically active hybrid protein did not alter cell lytic responses or IL-1β production (Figures 5.3.4 and 5.3.5) however further experiments should be performed to validate the total disruption of the hybrid gene. Nigericin stimulated wild-type DH82 cells showed low level of ASC speck formation and active caspase recruitment (Figure 3.5.4). To confirm gene disruption, nigericin experiment could be

performed on canine caspase-1/4/11 deficient clones followed by immunofluorescent labelling for active caspases.

DogMo cells retained their ability to induce cell death in response to NLRP3 inflammasome activation using nigericin (Figure 7.3.1). The amount of cell lysis induced was slightly less than that of wild-type murine macrophages (Figure 7.3.1). This data provided *in vitro* evidence that the protein encoded by the hybrid caspase-1/4/11 gene is indeed functional and is capable of driving pyroptotic cell death by cleaving GSDMD (Figure 7.3.3) [43], [44]. The lack of IL-1β however observed in the supernatant suggested that the hybrid protein, as expected, showed functional characteristics more similar to caspase-11 rather than caspase-1 (Figure 7.3.1B). It would be very interesting to generate additional hybrid caspases containing different CARD and caspase domains. For example; the CARD domain of caspase-11 and the caspase domain of caspase-1, or including CARD and caspase domains of apoptotic caspases. It would be fascinating to characterise their specificity, function and the type of stimuli they are activated by along with their potential substrates. We could then perhaps reprogram the type of cell death pathway that is induced in response to well established inflammatory stimuli. Furthermore, it would be an interesting tool to compare caspase specificity between different species and to investigate whether caspases present in different species have alternative cleavage sites.

One of the major differences between canine and DogMo cells is that DogMo cells express NAIP/NLRC4 receptors. NLRC4 inflammasome activation was also reconstituted in DogMo cells (Figures 7.5.1 and 7.5.4). These responses were slightly lower to that of their wild-type counterpart, but not ablated as seen in either murine *Nlrc4*$^{-/-}$ or *caspase-1*$^{-/-}$*caspase-11*$^{-/-}$ macrophages (Figure 4.2.2). There was no detectable IL-1β present, as expected, in the supernatant of wild-type *S.* Typhimurium infected DogMo cells (Figure 7.5.2). Further experiments confirming the lytic form of cell death of DogMo macrophages using bright field live cell imaging would be useful. Other carnivore species for example the cat (*Felis Catus*) contains this unique caspase-1/4/11 hybrid gene organisation [154]. Genomic sequence analysis suggested the presence of functional NLRC4 receptor in the cat, but NAIP is absent [41]. It would be rather interesting to investigate the kinetics of *S.* Typhimurium induced cell lysis in an immortalised feline

macrophage-like cell line (Fcwf-4) and also in primary PBMCs and compare their responses to what I observed in the canine DH82 cells [410], [411].

DogMo cells containing the hybrid caspase-1/4/11 gene completely lost their ability to process pro-IL-1β, but retained their functionality to induce pyroptotic cell lysis in response to NLRP3 and NLRC4 inflammasome activators (Chapter 6). The functional differences between the canine DH82 and murine DogMo cells are intriguing. While DH82 cells failed to induce rapid cell lysis but produced large amount of bioactive IL-1β, DogMo cells retained their capability to induce rapid cell lysis without the ability to process pro-Il-1β (Chapters 3, 4 and 6). This really raises questions about the functionality and perhaps the cellular regulation of the canine hybrid protein. Caspase-8 can compensate for the absence of caspase-1 and the percentage of cell lysis induced in DogMo cells following NLRP3 and NLRC4 inflammasome stimulation was reduced when cells were pre-incubated with Z-VAD-IEDT caspase-8 inhibitor (Figures 6.6.1A, 6.6.2A and 6.6.3). In caspase-8-deficient DH82 cells lytic responses were intact, but IL-1β processing was affected (Figures 5.7.1 and 5.7.2). Previous studies documented in *S.* Typhimurium infected murine macrophages lacking caspase-1 and -11 [352] showed that caspase-8 modulates pro-IL-1β maturation but failed to identify a role in cell lysis [352]. DogMo cells showed rapid cell lytic responses following *S.* Typhimurium infection, while *Nlrc4*$^{-/-}$ and *caspase-1*$^{-/-}$*caspase-11*$^{-/-}$ murine macrophages remained intact up until 6 hour post infection (Figure 4.2.2). This observation raises fundamental questions about how inflammasomes function in dogs. Ideally, NLRC4 inflammasome activation should be repeated in DogMo cells also deficient in their NLRC4 and/or NAIP receptors. To this end, I am in the process of generating the equivalent of the DogMo primary cells in immortalised murine BMDMs in both, wild-type and *Nlrc4*$^{-/-}$ background.

There are marked differences in the functionality of the hybrid caspase-1/4/11 protein in DH82 and mouse macrophages, it is interesting to highlight that DH82 cell lytic responses were similar to that of *Nlrc4*$^{-/-}$ and *caspase-1*$^{-/-}$*caspase-11*$^{-/-}$ murine immortalised macrophages. My results however suggested the existence of two separate pathways; one controlling cytokine maturation while the other driving cell lysis. There is a possibility that the same cell death pathway is responsible for driving cell death responses in murine *Nlrc4*$^{-/-}$ and *caspase-1*$^{-/-}$*caspase-11*$^{-/-}$ cells as well as DH82 macrophages.

More importantly, results obtained using DogMo cells could point towards inflammasome downregulation in DH82 cells. It is convenient to speculate the presence of an inhibitory protein driving dampening of inflammasome responses in the dog. For that, it would be interesting to investigate differential transcription patterns in non-stimulated and stimulated primary canine, murine, DogMo and human macrophages. There is a possibility that the(se) inhibitory protein(s) are constitutively upregulated or perhaps they require transcriptional priming following ligand recognition. Firstly, it would be interesting to examine whether one splice variant of the canine hybrid is preferentially expressed over the other depending on the activating ligand. It would also allow me to investigate whether both transcripts are expressed but with different abundancy. RNA-seq could potentially provide the identification of potential known regulatory proteins or novel transcripts that are differentially expressed in the dog compared to human, mouse and DogMo macrophages.

It also raises questions about the importance and true functions of inflammasomes. Could it be that the inflammasome deficit is actually an evolutionary adaptation mechanism to tolerate microorganisms associated with their mode of life? Research shows that dogs can shed live *S.* Typhimurium in their stool without displaying any clinical symptoms [412]. Some dogs however do develop salmonellosis which mainly coincides with other pathogens or clinical conditions [311]. It would be interesting to conduct a study investigating inflammasome activation in canine gut epithelial cells alongside with enumerating their intracellular burden and bacterial replication using GFP-tagged wild-type *S.* Typhimurium strain. Dogs are carnivores and an alternative explanation is that the high protein diet may alter how bacteria behave in the gut and thus host immune genes may have been lost because they are no longer required. Based on our current knowledge and my thesis work, it is convenient to speculate that the presence of dysfunctional inflammasomes may prevent *Salmonellae* passage through gut epithelial cells and therefore gastroenteritis.

## Bibliography


[1] S. Saeed *et al.*, "Epigenetic programming of monocyte-to-macrophage differentiation and trained innate immunity," *Science (80-. ).*, vol. 345, no. 6204, pp. 1–26, 2015.

[2] J. Kleinnijenhuis *et al.*, "Bacille Calmette-Guérin induces NOD2-dependent nonspeci fi c protection from reinfection via epigenetic reprogramming of monocytes," *PNAS*, vol. 109, no. 43, pp. 17537–17542, 2012.

[3] B. Lemaitre, E. Nicolas, L. Michaut, J. Reichhart, and J. A. Hoffmann, "The Dorsoventral Regulatory Gene Cassette spätzle/Toll/cactus Controls the Potent Antifungal Response in Drosophila Adults Bruno," *Cell*, vol. 86, no. 6, pp. 973–983, 1996.

[4] C. A. Janeway, "Approaching the Asymptote? Evolution and revolution in immunology.," *J. Immunol.*, vol. 191, no. 9, pp. 4475–4487, 1989.

[5] O. Takeuchi and S. Akira, "Pattern Recognition Receptors and Inflammation," *Cell*, vol. 140, no. 6, pp. 805–820, 2010.

[6] K. Schroder and J. Tschopp, "The Inflammasomes," *Cell*, vol. 140, pp. 821–832, 2010.

[7] C. A. Janeway and R. Medzhitov, "INNATE IMMUNE RECOGNITION," *Annu. Rev. Immunol.*, vol. 20, no. 1, pp. 197–216, 2002.

[8] M. Lamkanfi and V. M. Dixit, "Mechanisms and functions of inflammasomes," *Cell*, vol. 157, no. 5, pp. 1013–1022, 2014.

[9] J. C. Roach *et al.*, "The evolution of vertebrate Toll-like receptors," *PNAS*, vol. 102, no. 27, pp. 9577–9582, 2005.

[10] T. M. Burch-Smith, M. Schiff, J. L. Caplan, J. Tsao, K. Czymmek, and S. P. Dinesh-Kumar, "A novel role for the TIR domain in association with pathogen-derived elicitors," *PLoS Biol.*, vol. 5, no. 3, pp. 501–514, 2007.

[11] S. Hosein, A. Rodríguez-Cortés, D. P. Blake, K. Allenspach, J. Alberola, and L. Solano-Gallego, "Transcription of toll-like receptors 2, 3, 4 and 9, FoxP3 and Th17 cytokines in a susceptible experimental model of canine Leishmania infantum infection," *PLoS One*, vol. 10, no. 10, pp. 1–19, 2015.

[12] A. Cuscó, A. Sánchez, L. Altet, L. Ferrer, and O. Francino, "Non-synonymous genetic

variation in exonic regions of canine Toll-like receptors," *Canine Genet. Epidemiol.*, vol. 1, no. 1, pp. 1–12, 2014.

[13] J. K. Bell, G. E. D. Mullen, C. A. Leifer, A. Mazzoni, D. R. Davies, and D. M. Segal, "Leucine-rich repeats and pathogen recognition in Toll-like receptors," *Trends Immunol.*, vol. 24, no. 10, pp. 528–533, 2003.

[14] M. S. Jin *et al.*, "Crystal Structure of the TLR1-TLR2 Heterodimer Induced by Binding of a Tri-Acylated Lipopeptide," *Cell*, vol. 130, no. 6, pp. 1071–1082, 2007.

[15] J. Y. Kang *et al.*, "Recognition of Lipopeptide Patterns by Toll-like Receptor 2-Toll-like Receptor 6 Heterodimer," *Immunity*, vol. 31, no. 6, pp. 873–884, 2009.

[16] T. Kawai and S. Akira, "The role of pattern-recognition receptors in innate immunity: Update on toll-like receptors," *Nat. Immunol.*, vol. 11, no. 5, pp. 373–384, 2010.

[17] T. Kawai and S. Akira, "Toll-like Receptors and Their Crosstalk with Other Innate Receptors in Infection and Immunity," *Immunity*, vol. 34, no. 5, pp. 637–650, 2011.

[18] O. Takeuchi *et al.*, "Cutting Edge: Role of Toll-Like Receptor 1 in Mediating Immune Response to Microbial Lipoproteins," *J. Immunol.*, vol. 169, no. 1, pp. 10–14, 2002.

[19] O. Takeuchi *et al.*, "Discrimination of bacterial lipoproteins by Toll-like recepttor 6," *Int. Immunol.*, vol. 13, no. 7, pp. 933–940, 2001.

[20] A. Poltorak *et al.*, "Defective LPS signaling in C3H/HeJ and C57BL/10ScCr mice: Mutations in Tlr4 gene," *Science (80-. ).*, vol. 282, no. 5396, pp. 2085–2088, 1998.

[21] M. Saruta, S. R. Targan, L. Mei, A. F. Ippoliti, K. D. Taylor, and J. I. Rotter, "High-frequency haplotypes in the X chromosome locus TLR8 are associated with both CD and UC in females," *Inflamm. Bowel Dis.*, vol. 15, no. 3, pp. 321–327, 2009.

[22] L. A. Mcmahon *et al.*, "Expression of Toll-like receptor 2 in duodenal biopsies from dogs with inflammatory bowel disease is associated with severity of disease," *Vet. Immunol. Immunopathol.*, vol. 135, no. 1–2, pp. 158–163, 2010.

[23] I. A. Burgener *et al.*, "Upregulation of Toll-Like Receptors in Chronic Enteropathies in Dogs," *J. Vet. Intern. Med.*, vol. 22, no. 3, pp. 553–560, 2008.

[24] B. C. Meyers, A. Kozik, A. Griego, H. Kuang, and R. W. Michelmore, "Genome-wide

analysis of NBS-LRR-encoding genes in Arabidopsis," *Plant Cell*, vol. 15, no. 4, pp. 809–834, 2003.

[25] D. Marone, M. A. Russo, G. Laidò, A. M. De Leonardis, and A. M. Mastrangelo, "Plant nucleotide binding site-leucine-rich repeat (NBS-LRR) genes: Active guardians in host defense responses," *Int. J. Mol. Sci.*, vol. 14, no. 4, pp. 7302–7326, 2013.

[26] J. Bertin *et al.*, "Human CARD4 protein is a novel CED-4/Apaf-1 cell death family member that activates NF-κB," *J. Biol. Chem.*, vol. 274, no. 19, pp. 12955–12958, 1999.

[27] J. A. Duncan *et al.*, "Cryopyrin/NALP3 binds ATP/dATP, is an ATPase, and requires ATP binding to mediate inflammatory signaling," *PNAS*, vol. 104, no. 19, pp. 8041–8046, 2007.

[28] P. Broz and D. M. Monack, "Newly described pattern recognition receptors team up against intracellular pathogens," *Nat. Rev. Immunol.*, vol. 13, no. 8, pp. 551–565, 2013.

[29] P. Broz and V. M. Dixit, "Inflammasomes: mechanism of assembly, regulation and signalling," *Nat. Rev. Immunol.*, vol. 16, no. 7, pp. 407–420, 2016.

[30] M. Lamkanfi and V. M. Dixit, "Inflammasomes and Their Roles in Health and Disease," *Annu. Rev. Cell Dev. Biol.*, vol. 28, no. 1, pp. 137–161, 2012.

[31] Y. Ogura, N. Inohara, A. Benito, F. F. Chen, S. Yamaoka, and G. Núñez, "Nod2, a Nod1/Apaf-1 Family Member That Is Restricted to Monocytes and Activates NF-KB," *J. Biol. Chem.*, vol. 276, no. 7, pp. 4812–4818, 2001.

[32] J. P. Y. Ting *et al.*, "The NLR gene family: An official nomenclature," *Immunity*, vol. 28, no. 3, pp. 285–287, 2008.

[33] B. Yuen, J. M. Bayes, and S. M. Degnan, "The characterization of sponge nlrs provides insight into the origin and evolution of this innate immune gene family in animals," *Mol. Biol. Evol.*, vol. 31, no. 1, pp. 106–120, 2014.

[34] T. Hibino *et al.*, "The immune gene repertoire encoded in the purple sea urchin genome," *Dev. Biol.*, vol. 300, no. 1, pp. 349–365, 2006.

[35] E. V. Koonin and L. Aravind, "The NACHT family - A new group of predicted NTPases implicated in apoptosis and MHC transcription activation," *Trends Biochem. Sci.*, vol. 25, no. 5, pp. 223–224, 2000.

[36] F. Martinon, A. Mayor, and J. Tschopp, “The Inflammasomes: Guardians of the Body,” *Annu. Rev. Immunol.*, vol. 27, no. 1, pp. 229–265, 2009.

[37] X. Tian, G. Pascal, and P. Monget, “Evolution and functional divergence of NLRP genes in mammalian reproductive systems,” *BMC Evol. Biol.*, vol. 9, no. 202, pp. 1–13, 2009.

[38] M. G. Endrizzi, V. Hadinoto, J. D. Growney, W. Miller, and W. F. Dietrich, “Genomic sequence analysis of the mouse Naip gene array,” *Genome Res.*, vol. 10, no. 8, pp. 1095–1102, 2000.

[39] K. Howe *et al.*, “Structure and evolutionary history of a large family of NLR proteins in the zebrafish,” *Open Biol.*, vol. 6, no. 4, pp. 1–15, 2016.

[40] K. J. Laing, M. K. Purcell, J. R. Winton, and J. D. Hansen, “A genomic view of the NOD-like receptor family in teleost fish: Identification of a novel NLR subfamily in zebrafish,” *BMC Evol. Biol.*, vol. 8, no. 42, pp. 1–15, 2008.

[41] L. Eckhart *et al.*, “Duplication of the caspase-12 prodomain and inactivation of NLRC4/IPAF in the dog,” *Biochem. Biophys. Res. Commun.*, vol. 384, no. 2, pp. 226–230, 2009.

[42] F. Martinon, K. Burns, and J. Tschopp, “The Inflammasome: A molecular platform triggering activation of inflammatory caspases and processing of proIL-β,” *Mol. Cell*, vol. 10, no. 2, pp. 417–426, 2002.

[43] N. Kayagaki *et al.*, “Caspase-11 cleaves gasdermin D for non-canonical inflammasome signalling,” *Nature*, vol. 526, no. 7575, pp. 666–671, 2015.

[44] J. Shi *et al.*, “Cleavage of GSDMD by inflammatory caspases determines pyroptotic cell death,” *Nature*, vol. 526, no. 7575, pp. 660–665, 2015.

[45] L. Agostini, F. Martinon, K. Burns, M. F. Mcdermott, P. N. Hawkins, and J. Rg Tschopp, “NALP3 Forms an IL-1-Processing Inflammasome with Increased Activity in Muckle-Wells Autoinflammatory Disorder,” *Immunity*, vol. 20, no. 322, pp. 319–325, 2004.

[46] Y. Zhao *et al.*, “The NLRC4 inflammasome receptors for bacterial flagellin and type III secretion apparatus,” *Nature*, vol. 477, no. 7366, pp. 596–600, Sep. 2011.

[47] T. Fernandes-Alnemri *et al.*, “The AIM2 inflammasome is critical for innate immunity to

Francisella tularensis," *Nat. Immunol.*, vol. 11, no. 5, pp. 385–393, 2010.

[48] M. A. Gavrilin *et al.*, " Activation of the Pyrin Inflammasome by Intracellular Burkholderia cenocepacia ," *J. Immunol.*, vol. 188, no. 7, pp. 3469–3477, 2012.

[49] N. Kerur *et al.*, "IFI16 acts as a nuclear pathogen sensor to induce the inflammasome in response to Kaposi Sarcoma-associated herpesvirus infection," *Cell Host Microbe*, vol. 9, no. 5, pp. 363–375, 2011.

[50] J. Minkiewicz, J. P. de Rivero Vaccari, and R. W. Keane, "Human astrocytes express a novel NLRP2 inflammasome," *Glia*, vol. 61, no. 7, pp. 1113–1121, 2013.

[51] S. Khare *et al.*, "An NLRP7-Containing Inflammasome Mediates Recognition of Microbial Lipopeptides in Human Macrophages," *Immunity*, vol. 36, no. 3, pp. 464–476, 2012.

[52] P. K. Anand *et al.*, "NLRP6 negatively regulates innate immunity and host defence against bacterial pathogens," *Nature*, vol. 488, no. 7411, pp. 389–393, 2012.

[53] S. Zhu *et al.*, "Nlrp9b inflammasome restricts rotavirus infection in intestinal epithelial cells," *Nature*, vol. 546, no. 7660, pp. 667–670, 2017.

[54] I. C. Allen *et al.*, "NLRP12 Suppresses Colon Inflammation and Tumorigenesis through the Negative Regulation of Noncanonical NF-κB Signaling," *Immunity*, vol. 36, no. 5, pp. 742–754, 2012.

[55] E. A. Miao *et al.*, "Cytoplasmic flagellin activates caspase-1 and secretion of interleukin-1β via Ipaf," *Nat. Immunol.*, vol. 7, no. 6, pp. 569–575, 2006.

[56] X. Cai *et al.*, "Prion-like polymerization underlies signal transduction in antiviral immune defense and inflammasome activation," *Cell*, vol. 156, no. 6, pp. 1207–1222, 2014.

[57] M. S. Dick, L. Sborgi, S. Rühl, S. Hiller, and P. Broz, "Corrigendum: ASC filament formation serves as a signal amplification mechanism for inflammasomes," *Nat. Commun.*, vol. 7, no. 11929, pp. 1–12, 2016.

[58] A. Lu *et al.*, "Unified Polymerization Mechanism for the Assembly of ASC- dependent Inflammasomes," *Cell*, vol. 156, no. 6, pp. 1193–1206, 2014.

[59] P. Broz, J. Von Moltke, J. W. Jones, R. E. Vance, and D. M. Monack, "Differential requirement for caspase-1 autoproteolysis in pathogen-induced cell death and cytokine

processing," *Cell Host Microbe*, vol. 8, no. 6, pp. 471–483, 2010.

[60] N. Kayagaki *et al.*, "Non-canonical inflammasome activation targets caspase-11," *Nature*, vol. 479, no. 7371, pp. 117–121, 2011.

[61] J. Shi *et al.*, "Inflammatory caspases are innate immune receptors for intracellular LPS.," *Nature*, vol. 514, no. 7521, pp. 187–192, 2014.

[62] S. Ming *et al.*, "Inflammasome activation causes dual recruitment of NLRC4 and NLRP3 to the same macromolecular complex," *PNAS*, vol. 111, no. 20, pp. 7403–7408, 2014.

[63] L. Sborgi *et al.*, "Structure and assembly of the mouse ASC inflammasome by combined NMR spectroscopy and cryo-electron microscopy," *PNAS*, vol. 112, no. 43, pp. 13237–13242, 2015.

[64] E. F. Halff, C. A. Diebolder, M. Versteeg, A. Schouten, T. H. C. Brondijk, and E. G. Huizinga, "Formation and structure of a NAIP5-NLRC4 inflammasome induced by direct interactions with conserved N- and C-terminal regions of flagellin," *J. Biol. Chem.*, vol. 287, no. 46, pp. 38460–38472, 2012.

[65] N. Haloupek, P. Grob, J. Tenthorey, R. E. Vance, and E. Nogales, *Cryo-EM studies of NAIP–NLRC4 inflammasomes*, 1st ed., vol. 625. Elsevier Inc., 2019.

[66] J. Masumoto, S. Taniguchi, and J. Sagara, "Pyrin N-terminal homology domain- and caspase recruitment domain-dependent oligomerization of ASC.," *Biochem. Biophys. Res. Commun.*, vol. 280, no. 3, pp. 652–655, 2001.

[67] J. Masumoto *et al.*, "ASC, a novel 22-kDa protein, aggregates during apoptosis of human promyelocytic leukemia HL-60 cells.," *J. Biol. Chem.*, vol. 274, no. 48, pp. 33835–33838, 1999.

[68] T. Fernandes-Alnemri *et al.*, "The pyroptosome: A supramolecular assembly of ASC dimers mediating inflammatory cell death via caspase-1 activation," *Cell Death Differ.*, vol. 14, no. 9, pp. 1590–1604, 2007.

[69] T. Fujii *et al.*, "Gasdermin D (Gsdmd) is dispensable for mouse intestinal epithelium development," *Genesis*, vol. 46, no. 8, pp. 418–423, 2008.

[70] X. Liu *et al.*, "Inflammasome-activated gasdermin D causes pyroptosis by forming

membrane pores," *Nature*, vol. 535, no. 7610, pp. 153–158, 2016.

[71] W. He *et al.*, "Gasdermin D is an executor of pyroptosis and required for interleukin-1β secretion.," *Cell Res.*, vol. 25, no. 12, pp. 1285–1298, 2015.

[72] S. Rühl, P. Broz, and E. Al, "GSDMD membrane pore formation constitutes the mechanism of pyroptotic cell death," *EMBO J.*, vol. 35, no. 16, pp. 1766–1778, 2016.

[73] J. A. Wright and C. E. Bryant, "The killer protein Gasdermin D," *Cell Death Differ.*, vol. 23, no. 12, pp. 1897–1898, 2016.

[74] R. A. Aglietti *et al.*, "GsdmD p30 elicited by caspase-11 during pyroptosis forms pores in membranes.," *PNAS*, vol. 113, no. 28, pp. 7858–7863, 2016.

[75] J. Ding *et al.*, "Pore-forming activity and structural autoinhibition of the gasdermin family," *Nature*, vol. 535, no. 7610, pp. 111–116, 2016.

[76] H. M. Hoffman, J. L. Mueller, D. H. Broide, A. A. Wanderer, and R. D. Kolodner, "Mutation of a new gene encoding a putative pyrin-like protein causes familial cold autoinflammatory syndrome and Muckle-Wells syndrome," *Nat. Genet.*, vol. 29, no. 3, pp. 301–305, 2001.

[77] C. Miceli-Richard *et al.*, "CARD15 mutations in Blau syndrome," *Nat. Genet.*, vol. 29, no. 1, pp. 19–20, 2001.

[78] S. Mariathasan *et al.*, "Cryopyrin activates the inflammasome in response to toxins and ATP," *Nature*, vol. 440, no. 7081, pp. 228–232, 2006.

[79] J. A. Hayward, A. Mathur, C. Ngo, and S. M. Man, "Cytosolic Recognition of Microbes and Pathogens: Inflammasomes in Action," *Microbiol. Mol. Biol. Rev.*, vol. 82, no. 4, pp. 1–40, 2018.

[80] E. Latz, T. S. Xiao, and A. Stutz, "Activation and regulation of the inflammasomes," *Nat. Rev. Immunol.*, vol. 13, no. 6, pp. 397–411, 2013.

[81] G.-S. Lee *et al.*, "The calcium-sensing receptor regulates the NLRP3 inflammasome through Ca2+ and cAMP," *Nature*, vol. 492, no. 7427, pp. 123–127, 2012.

[82] R. Muñoz-Planillo, P. Kuffa, G. Martínez-Colón, B. Smith, T. Rajendiran, and G. Núñez, "K+ Efflux Is the Common Trigger of NLRP3 Inflammasome Activation by Bacterial

Toxins and Particulate Matter," *Immunity*, vol. 38, no. 6, pp. 1142–1153, 2013.

[83] L. Franchi, T. D. Kanneganti, G. R. Dubyak, and G. Núñez, "Differential requirement of P2X7 receptor and intracellular K+ for caspase-1 activation induced by intracellular and extracellular bacteria," *J. Biol. Chem.*, vol. 282, no. 26, pp. 18810–18818, 2007.

[84] A. Piccini, S. Carta, S. Tassi, D. Lasiglié, G. Fossati, and A. Rubartelli, "ATP is released by monocytes stimulated with pathogen-sensing receptor ligands and induces IL-1β and IL-18 secretion in an autocrine way," *PNAS*, vol. 105, no. 23, pp. 8067–8072, 2008.

[85] D. Perregaux and C. A. Gabel, "Interleukin-1β Maturation and Release in Response to ATP and Nigericin.," *J. Biol. Chem.*, vol. 269, no. 21, pp. 15195–15203, 1994.

[86] R. R. Craven *et al.*, "Staphylococcus aureus a-Hemolysin Activates the NLRP3-Inflammasome in Human and Mouse Monocytic Cells," *PLoS One*, vol. 4, no. 10, 2009.

[87] C. E. Diamond, K. W. K. Leong, M. Vacca, J. Rivers-Auty, D. Brough, and A. Mortellaro, "*Salmonella* typhimurium-induced IL-1 release from primary human monocytes requires NLRP3 and can occur in the absence of pyroptosis," *Sci. Rep.*, vol. 7, no. 6861, pp. 1–9, 2017.

[88] I. C. Allen *et al.*, "The NLRP3 Inflammasome Mediates In Vivo Innate Immunity to Influenza A Virus through Recognition of Viral RNA," *Immunity*, vol. 30, no. 4, pp. 556–565, 2009.

[89] O. Rogiers *et al.*, "Candidalysin crucially contributes to nlrp3 inflammasome activation by Candida albicans hyphae," *MBio*, vol. 10, no. 1, pp. 1–7, 2019.

[90] D. S. Lima-Junior *et al.*, "Inflammasome-derived IL-1β production induces nitric oxide-mediated resistance to Leishmania," *Nat. Med.*, vol. 19, no. 7, pp. 909–915, 2013.

[91] V. Hornung *et al.*, "Silica crystals and aluminum salts activate the NALP3 inflammasome through phagosomal destabilization," *Nat. Immunol.*, vol. 9, no. 8, pp. 847–856, 2008.

[92] J. Chu, L. M. Thomas, S. C. Watkins, L. Franchi, G. Núñez, and R. D. Salter, "Cholesterol-dependent cytolysins induce rapid release of mature IL-1β from murine macrophages in a NLRP3 inflammasome and cathepsin B-dependent manner," *J. Leukoc. Biol.*, vol. 86, no. 5, pp. 1227–1238, 2009.

[93] R. Zhou, A. S. Yazdi, P. Menu, and J. Tschopp, "A role for mitochondria in NLRP3 inflammasome activation.," *Nature*, vol. 469, no. 7329, pp. 221–225, 2011.

[94] S. S. Iyer *et al.*, "Mitochondrial cardiolipin is required for Nlrp3 inflammasome activation," *Immunity*, vol. 39, no. 2, pp. 311–323, 2013.

[95] K. Shimada *et al.*, "Oxidized Mitochondrial DNA Activates the NLRP3 Inflammasome during Apoptosis," *Immunity*, vol. 36, no. 3, pp. 401–414, 2012.

[96] S. Fan *et al.*, "Activation of interleukin-1β release by the classical swine fever virus is dependent on the NLRP3 inflammasome, which affects virus growth in monocytes," *Front. Cell. Infect. Microbiol.*, vol. 8, no. 225, pp. 1–13, 2018.

[97] R. Li *et al.*, "Characterization and roles of cherry valley duck nlrp3 in innate immunity during avian pathogenic escherichia coliinfection," *Front. Immunol.*, vol. 9, no. 2300, pp. 1–10, 2018.

[98] F. Bauernfeind *et al.*, "NF-kB activating pattern recognition and cytokine receptors license NLRP3 inflammasome activation by regulating NLRP3 expression," *J. Immunol.*, vol. 183, no. 2, pp. 787–791, 2009.

[99] J. G. Kim, S. J. Lee, and M. F. Kagnoff, "Nod1 Is an Essential Signal Transducer in Intestinal Epithelial Cells Infected with Bacteria That Avoid Recognition by Toll-Like Receptors Nod1 Is an Essential Signal Transducer in Intestinal Epithelial Cells Infected with Bacteria That Avoid Recognition," *Infect. Immun.*, vol. 72, no. 3, pp. 1487–1495, 2004.

[100] L. Franchi, T. Eigenbrod, and G. Núñez, "TNF-α Mediate Sensitization to ATP and Silica via the NLRP3 Inflammasome in the Absence of Microbial Stimulation1," *J. Immunol.*, vol. 183, no. 2, pp. 792–796, 2009.

[101] M. G. Ghonime *et al.*, "Inflammasome priming by LPS is dependent upon ERK signaling and proteasome function," *J. Immunol.*, vol. 192, no. 8, pp. 3881–3888, 2014.

[102] K. Schroder *et al.*, "Acute lipopolysaccharide priming boosts inflammasome activation independently of inflammasome sensor induction," *Immunobiology*, vol. 217, no. 12, pp. 1325–1329, 2012.

[103] B. F. Py, M. S. Kim, H. Vakifahmetoglu-Norberg, and J. Yuan, "Deubiquitination of NLRP3 by BRCC3 Critically Regulates Inflammasome Activity," *Mol. Cell*, vol. 49, no. 2,

pp. 331–338, 2013.

[104] P. Gurung *et al.*, “FADD and Caspase-8 Mediate Priming and Activation of the Canonical and Noncanonical Nlrp3 Inflammasomes,” *J. Immunol.*, vol. 192, no. 4, pp. 1835–1846, 2014.

[105] K.-M. Lin *et al.*, “IRAK-1 bypasses priming and directly links TLRs to rapid NLRP3 inflammasome activation,” *PNAS*, vol. 111, no. 2, pp. 775–780, 2014.

[106] T. Fernandes-Alnemri, S. Kang, C. Anderson, S. Junji, K. A. Fitzgerald, and E. S. Alnemri, “Toll-Like Receptor Signaling Licenses IRAK1 For Rapid Activation Of The NLRP3 Inflammasome,” *J. Immunol.*, vol. 191, no. 8, pp. 3995–3999, 2013.

[107] H. Shi *et al.*, “NLRP3 activation and mitosis are mutually exclusive events coordinated by NEK7, a new inflammasome component,” *Nat. Immunol.*, vol. 17, no. 3, pp. 250–258, 2016.

[108] Y. He, M. Y. Zeng, D. Yang, Benny Motro, and G. Núñez, “Nek7 is an essential mediator of NLRP3 activation downstream of potassium efflux,” *Nature*, vol. 530, no. 7590, pp. 354–357, 2016.

[109] J. L. Schmid-Burgk *et al.*, “A genome-wide CRISPR (clustered regularly interspaced short palindromic repeats) screen identifies NEK7 as an essential component of NLRP3 inflammasome activation,” *J. Biol. Chem.*, vol. 291, no. 1, pp. 103–109, 2016.

[110] Y.-C. Lin *et al.*, “Syk is involved in NLRP3 inflammasome-mediated caspase-1 activation through adaptor ASC phosphorylation and enhanced oligomerization,” *J. Leukoc. Biol.*, vol. 97, no. 5, pp. 825–835, 2015.

[111] I. C. Chung *et al.*, “Pyk2 activates the NLRP3 inflammasome by directly phosphorylating ASC and contributes to inflammasome-dependent peritonitis,” *Sci. Rep.*, vol. 6, no. 36214, pp. 1–13, 2016.

[112] M. Ito *et al.*, “Bruton’s tyrosine kinase is essential for NLRP3 inflammasome activation and contributes to ischaemic brain injury,” *Nat. Commun.*, vol. 6, no. 7360, pp. 1–11, 2015.

[113] L. Mortimer, F. Moreau, J. A. MacDonald, and K. Chadee, “NLRP3 inflammasome inhibition is disrupted in a group of auto-inflammatory disease CAPS mutations,” *Nat. Immunol.*, vol. 17, no. 10, pp. 1176–1186, 2016.

[114] D. T. Hess and J. S. Stamler, "Regulation by S-nitrosylation of protein post-translational modification," *J. Biol. Chem.*, vol. 287, no. 7, pp. 4411–4418, 2012.

[115] C. S. Shi *et al.*, "Activation of autophagy by inflammatory signals limits IL-1β production by targeting ubiquitinated inflammasomes for destruction," *Nat. Immunol.*, vol. 13, no. 3, pp. 255–263, 2012.

[116] F. Martinon, V. Pétrilli, A. Mayor, A. Tardivel, and J. Tschopp, "Gout-associated uric acid crystals activate the NALP3 inflammasome," *Nature*, vol. 440, no. 7081, pp. 237–241, 2006.

[117] H. M. Lee, J. J. Kim, H. J. Kim, M. Shong, B. J. Ku, and E. K. Jo, "Upregulated NLRP3 inflammasome activation in patients with type 2 diabetes," *Diabetes*, vol. 62, no. 1, pp. 194–204, 2013.

[118] B. Weichand *et al.*, "S1PR1 on tumor-associated macrophages promotes lymphangiogenesis and metastasis via NLRP3/IL-1ß," *J. Exp. Med.*, vol. 214, no. 9, pp. 2695–2713, 2017.

[119] P. Duewell *et al.*, "NLRP3 inflammasomes are required for atherogenesis and activated by cholesterol crystals," *Nature*, vol. 464, no. 7293, pp. 1357–1361, 2010.

[120] L. Vande Walle *et al.*, "Negative regulation of the NLRP3 inflammasome by A20 protects against arthritis," *Nature*, vol. 512, no. 7512, pp. 69–73, 2014.

[121] J. L. Poyet, S. M. Srinivasula, M. Tnani, M. Razmara, T. Fernandes-Alnemri, and E. S. Alnemri, "Identification of Ipaf, a Human Caspase-1-activating Protein Related to Apaf-1," *J. Biol. Chem.*, vol. 276, no. 30, pp. 28309–28313, 2001.

[122] L. Franchi *et al.*, "Cytosolic flagellin requires Ipaf for activation of caspase-1 and interleukin 1β in *Salmonella*-infected macrophages," *Nat. Immunol.*, vol. 7, no. 6, pp. 576–582, 2006.

[123] S. Mariathasan *et al.*, "Differential activation of the inflammasome by caspase-1 adaptors ASC and Ipaf," *Nature*, vol. 430, no. 6996, pp. 213–218, 2004.

[124] E. A. Miao *et al.*, "Innate immune detection of the type III secretion apparatus through the NLRC4 inflammasome," *PNAS*, vol. 107, no. 7, pp. 3076–3080, 2010.

[125] J. Masumoto *et al.*, "ASC is an activating adaptor for NF-κB and caspase-8-dependent apoptosis," *Biochem. Biophys. Res. Commun.*, vol. 303, no. 1, pp. 69–73, 2003.

[126] Z. Hu *et al.*, "Crystal Structure of NLRC4 Reveals Its Autoinhibition Mechanism," *Science (80-. ).*, vol. 341, no. 6142, pp. 172–175, 2013.

[127] W. Liu *et al.*, "LRRK2 promotes the activation of NLRC4 inflammasome during *Salmonella* Typhimurium infection," *J. Exp. Med.*, vol. 214, no. 10, pp. 3051–3066, 2017.

[128] Y. Qu *et al.*, "Phosphorylation of NLRC4 is critical for inflammasome activation," *Nature*, vol. 490, no. 7421, pp. 539–542, 2012.

[129] M. Matusiak, N. Van Opdenbosch, L. Vande Walle, J.-C. Sirard, T.-D. Kanneganti, and M. Lamkanfi, "Flagellin-induced NLRC4 phosphorylation primes the inflammasome for activation by NAIP5," *PNAS*, vol. 112, no. 5, pp. 1541–1546, 2015.

[130] E. Israeli, "Phosphorylation of NLRC4 is critical for inflammasome activation," *Isr. Med. Assoc. J.*, vol. 490, no. 12, pp. 539–543, 2012.

[131] J. L. Tenthorey, E. M. Kofoed, M. D. Daugherty, H. S. Malik, and R. E. Vance, "Molecular basis for specific recognition of bacterial ligands by NAIP/NLRC4 inflammasomes," *Mol. Cell*, vol. 54, no. 1, pp. 17–29, 2014.

[132] Y. Zhao, J. Shi, X. Shi, Y. Wang, F. Wang, and F. Shao, "Genetic functions of the NAIP family of inflammasome receptors for bacterial ligands in mice," *J. Exp. Med.*, vol. 213, no. 5, pp. 647–656, 2016.

[133] J. Yang, Y. Zhao, J. Shi, and F. Shao, "Human NAIP and mouse NAIP1 recognize bacterial type III secretion needle protein for inflammasome activation," *PNAS*, vol. 110, no. 35, pp. 14408–14413, 2013.

[134] L. Zhang *et al.*, "Cryo-EM structure of the activated NAIP2-NLRC4 inflammasome reveals nucleated polymerization," *Science (80-. ).*, vol. 350, no. 6259, pp. 404–409, 2015.

[135] J. Kortmann, S. W. Brubaker, and D. M. Monack, "Cutting Edge: Inflammasome Activation in Primary Human Macrophages Is Dependent on Flagellin," *J. Immunol.*, vol. 195, no. 3, pp. 815–819, 2015.

[136] S. D. Tyrkalska *et al.*, "Neutrophils mediate *Salmonella* Typhimurium clearance through

the GBP4 inflammasome-dependent production of prostaglandins," *Nat. Commun.*, vol. 7, no. 12077, pp. 1–17, 2016.

[137] J. F. A. Varga, M. P. Bui-Marinos, and B. A. Katzenback, "Frog skin innate immune defences: Sensing and surviving pathogens," *Front. Immunol.*, vol. 9, no. 3128, pp. 1–21, 2019.

[138] C. Sakuma *et al.*, "Pig lacks functional NLRC4 and NAIP genes," *Immunogenetics*, vol. 69, no. 2, pp. 125–130, 2017.

[139] Z. Hu *et al.*, "Structural and biochemical basis for induced self-propagation of NLRC4," *Science (80-. ).*, vol. 350, no. 6259, pp. 399–404, 2015.

[140] S. M. Man, P. Tourlomousis, L. Hopkins, T. P. Monie, K. A. Fitzgerald, and C. E. Bryant, "Salmonella Infection Induces Recruitment of Caspase-8 to the Inflammasome To Modulate IL-1β Production," *J. Immunol.*, vol. 191, no. 10, pp. 5239–5246, 2013.

[141] P. Broz, K. Newton, M. Lamkanfi, S. Mariathasan, V. M. Dixit, and D. M. Monack, "Redundant roles for inflammasome receptors NLRP3 and NLRC4 in host defense against *Salmonella*.," *J. Exp. Med.*, vol. 207, no. 8, pp. 1745–55, 2010.

[142] C. Pop and G. S. Salvesen, "Human caspases: Activation, Specificity, and Regulation," *J. Biol. Chem.*, vol. 284, no. 33, pp. 21777–21781, 2009.

[143] M. Lamkanfi, W. Declercq, M. Kalai, X. Saelens, and P. Vandenabeele, "Alice in caspase land. A phylogenetic analysis of caspases from worm to man," *Cell Death Differ.*, vol. 9, no. 4, pp. 358–361, 2002.

[144] D. P. Cerretti *et al.*, "Molecular cloning of the interleukin-1 beta converting enzyme," *Science (80-. ).*, vol. 256, no. 5053, pp. 97–100, 1992.

[145] N. A. Thornberry *et al.*, "A novel heterodimeric cysteine protease is required for interleukin-1β processing in monocytes," *Nature*, vol. 355, no. 6372, pp. 768–774, 1992.

[146] O. Julien and J. A. Wells, "Caspases and their substrates," *Cell Death Differ.*, vol. 24, no. 8, pp. 1380–1389, 2017.

[147] G. S. Salvesen and V. M. Dixit, "Caspase activation: The induced-proximity model," *PNAS*, vol. 96, no. 20, pp. 10964–10967, 1999.

[148] D. W. Nicholson, “Caspase structure, proteolytic substrates, and function during apoptotic cell death.,” *Cell Death Differ.*, vol. 6, no. 11, pp. 1028–1042, 1999.

[149] S. Shalini, L. Dorstyn, S. Dawar, and S. Kumar, “Old, new and emerging functions of caspases,” *Cell Death Differ.*, vol. 22, no. 4, pp. 526–539, 2015.

[150] L. Eckhart *et al.*, “Terminal differentiation of human keratinocytes and stratum corneum formation is associated with caspase-14 activation,” *J. Invest. Dermatol.*, vol. 115, no. 6, pp. 1148–1151, 2000.

[151] J. L. Schmid-Burgk, M. M. Gaidt, T. Schmidt, T. S. Ebert, E. Bartok, and V. Hornung, “Caspase-4 mediates non-canonical activation of the NLRP3 inflammasome in human myeloid cells,” *Eur. J. Immunol.*, vol. 45, no. 10, pp. 2911–2917, 2015.

[152] M. Saleh *et al.*, “Enhanced bacterial clearance and sepsis resistance in caspase-12-deficient mice,” *Nature*, vol. 440, no. 7087, pp. 1064–1068, 2006.

[153] H. Fischer, U. Koenig, L. Eckhart, and E. Tschachler, “Human caspase 12 has acquired deleterious mutations,” *Biochem. Biophys. Res. Commun.*, vol. 293, no. 2, pp. 722–726, 2002.

[154] L. Eckhart *et al.*, “Identification of Novel Mammalian Caspases Reveals an Important Role of Gene Loss in Shaping the Human Caspase Repertoire,” *Mol. Biol. Evol.*, vol. 25, no. 5, pp. 831–841, 2008.

[155] H. M. Ellis and H. R. Horvitz, “Genetic control of programmed cell death in the nematode C. elegans.,” *Cell*, vol. 44, no. 6, pp. 817–829, 1986.

[156] J. Yuan, S. Shaham, S. Ledoux, H. M. Ellis, and H. R. Horvitz, “The C. elegans cell death gene ced-3 encodes a protein similar to mammalian interleukin-1β-converting enzyme,” *Cell*, vol. 75, no. 4, pp. 641–652, 1993.

[157] S. M. Srinivasula, J. L. Poyet, M. Razmara, P. Datta, Z. Zhang, and E. S. Alnemri, “The PYRIN-CARD protein ASC is an activating adaptor for caspase-1,” *J. Biol. Chem.*, vol. 277, no. 24, pp. 21119–21122, 2002.

[158] S. Rühl and P. Broz, “Caspase-11 activates a canonical NLRP3 inflammasome by promoting K+ efflux,” *Eur. J. Immunol.*, vol. 45, no. 10, pp. 2927–2936, 2015.

[159] P. J. Baker *et al.*, "NLRP3 inflammasome activation downstream of cytoplasmic LPS recognition by both caspase-4 and caspase-5," *Eur. J. Immunol.*, vol. 45, no. 10, pp. 2918–2926, 2015.

[160] S. Wang *et al.*, "Identification and characterization of ich-3, a member of the interleukin-1β converting enzyme (ICE)/Ced-3 family and an upstream regulator of ICE," *J. Biol. Chem.*, vol. 271, no. 34, pp. 20580–20587, 1996.

[161] S. Wang, M. Miura, Y. K. Jung, H. Zhu, E. Li, and J. Yuan, "Murine caspase-11, an ICE-interacting protease, is essential for the activation of ICE," *Cell*, vol. 92, no. 4, pp. 501–509, 1998.

[162] P. Li *et al.*, "Mice Deficient in IL-lβ-Converting Enzyme Are Defective in Production of Mature IL-lβ and Resistant to Endotoxic Shock," *Cell*, vol. 80, no. 3, pp. 401–411, 1995.

[163] N. Kayagaki *et al.*, "Noncanonical Inflammasome Activation by Intracellular LPS Independent of TLR4," *Science (80-. ).*, vol. 341, no. September, pp. 1246–1249, 2013.

[164] V. A. K. Rathinam *et al.*, "TRIF licenses caspase-11-dependent NLRP3 inflammasome activation by gram-negative bacteria," *Cell*, vol. 150, no. 3, pp. 606–619, 2012.

[165] V. M. Dixit and D. M. Monack, "Caspase-11 increases susceptibility to *Salmonella* infection in the absence of caspase-1," *Nature*, vol. 490, no. 7419, pp. 288–291, 2013.

[166] Y. Aachoui *et al.*, "Caspase-11 protects against bacteria that escape the vacuole," *Science (80-. ).*, vol. 339, no. 6122, pp. 975–978, 2013.

[167] L. A. Knodler *et al.*, "Noncanonical inflammasome activation of caspase-4/caspase-11 mediates epithelial defenses against enteric bacterial pathogens," *Cell Host Microbe*, vol. 16, no. 2, pp. 249–256, 2014.

[168] J. A. Hagar, D. A. Powell, Y. Aachoui, A. Robert K. Ernst, and E. A. Miao, "Cytoplasmic LPS activates caspase-11: implications in TLR4- independent endotoxic shock," *Computer (Long. Beach. Calif).*, vol. 144, no. 5, pp. 724–732, 2013.

[169] R. Schauvliege, J. Vanrobaeys, P. Schotte, and R. Beyaert, "Caspase-11 gene expression in response to lipopolysaccharide and interferon-γ requires nuclear factor-κB and signal transducer and activator of transcription (STAT) 1," *J. Biol. Chem.*, vol. 277, no. 44, pp. 41624–41630, 2002.

[170] Nobuhiko Kayagaki *et al.*, "Noncanonical Inflammasome Activation by Intracellular LPS Independent of TLR4," *Science (80-. ).*, vol. 341, no. 6151, pp. 1246–1249, 2012.

[171] C. Ross, A. H. Chan, J. Von Pein, D. Boucher, and K. Schroder, "Dimerization and auto-processing induce caspase-11 protease activation within the non-canonical inflammasome," *Life Sci. Alliance*, vol. 1, no. 6, pp. 1–10, 2018.

[172] T. J. Beveridge, "Structures of Gram-Negative Cell Walls and Their Derived Membrane Vesicles," *J. Bacteriol.*, vol. 181, no. 16, pp. 4725–4733, 1999.

[173] M. Kaparakis-Liaskos and R. L. Ferrero, "Immune modulation by bacterial outer membrane vesicles," *Nat. Rev. Immunol.*, vol. 15, no. 6, pp. 375–387, 2015.

[174] S. K. Vanaja *et al.*, "Bacterial outer membrane vesicles mediate cytosolic localization of LPS and caspase-11 activation," *Cell*, vol. 165, no. 5, pp. 1106–1119, 2016.

[175] J. C. Santos *et al.*, "LPS targets host guanylate-binding proteins to the bacterial outer membrane for non-canonical inflammasome activation," *EMBO J.*, vol. 37, no. 6, pp. 1–19, 2018.

[176] L. Gu *et al.*, "Toll-Like Receptor 4 Signaling Licenses the Cytosolic Transport of Lipopolysaccharide From Bacterial Outer Membrane Vesicles," *Shock*, vol. 51, no. 2, 2019.

[177] D. M. Pilla *et al.*, "Guanylate binding proteins promote caspase-11-dependent pyroptosis in response to cytoplasmic LPS," *PNAS*, vol. 111, no. 16, pp. 6046–6051, 2014.

[178] E. Meunier *et al.*, "Caspase-11 activation requires lysis of pathogen-containing vacuoles by IFN-induced GTPases," *Nature*, vol. 509, no. 7500, pp. 366–370, 2014.

[179] S. M. Man *et al.*, "IRGB10 Liberates Bacterial Ligands for Sensing by the AIM2 and Caspase-11-NLRP3 Inflammasomes," *Cell*, vol. 167, no. 2, pp. 382-396.e17, 2016.

[180] A. K. Haldar *et al.*, "IRG and GBP Host Resistance Factors Target Aberrant, 'Non-self' Vacuoles Characterized by the Missing of 'Self' IRGM Proteins," *PLoS Pathog.*, vol. 9, no. 6, pp. 1–16, 2013.

[181] R. Finethy *et al.*, "Inflammasome activation by bacterial outer membrane vesicles requires guanylate binding proteins," *MBio*, vol. 8, no. 5, pp. 1–11, 2017.

[182] X. Y. Lin, M. S. K. Choi, and A. G. Porter, "Expression analysis of the human caspase-1

subfamily reveals specific regulation of the CASP5 gene by lipopolysaccharide and interferon-γ," *J. Biol. Chem.*, vol. 275, no. 51, pp. 39920–39926, 2000.

[183] E. Vigano, C. E. Diamond, R. Spreafico, A. Balachander, R. M. Sobota, and A. Mortellaro, "Human caspase-4 and caspase-5 regulate the one-step non-canonical inflammasome activation in monocytes," *Nat. Commun.*, vol. 6, no. 8761, pp. 1–13, 2015.

[184] N. J. Bitto *et al.*, "Membrane vesicles from Pseudomonas aeruginosa activate the noncanonical inflammasome through caspase-5 in human monocytes," *Immunol. Cell Biol.*, vol. 96, no. 10, pp. 1120–1130, 2018.

[185] M. M. Gaidt *et al.*, "Human Monocytes Engage an Alternative Inflammasome Pathway," *Immunity*, vol. 44, no. 4, pp. 833–846, 2016.

[186] W. J. Kaiser *et al.*, "Toll-like receptor 3-mediated necrosis via TRIF, RIP3, and MLKL," *J. Biol. Chem.*, vol. 288, no. 43, pp. 31268–31279, 2013.

[187] A. Oberst *et al.*, "Catalytic activity of the caspase-8-FLIP L complex inhibits RIPK3-dependent necrosis," *Nature*, vol. 471, no. 7338, pp. 363–368, 2011.

[188] E. E. Varfolomeev *et al.*, "Targeted disruption of the mouse Caspase 8 gene ablates cell death induction by the TNF receptors, Fas/Apo1, and DR3 and is lethal prenatally," *Immunity*, vol. 9, no. 2, pp. 267–276, 1998.

[189] K. Huang *et al.*, "Cleavage by caspase 8 and mitochondrial membrane association activate the BH3-only protein bid during TRAIL-induced apoptosis," *J. Biol. Chem.*, vol. 291, no. 22, pp. 11843–11851, 2016.

[190] W. J. Kaiser *et al.*, "RIP3 mediates the embryonic lethality of caspase-8-deficient mice," *Nature*, vol. 471, no. 7338, pp. 368–373, 2011.

[191] F. L. Scott *et al.*, "The Fas-FADD death domain complex structure unravels signalling by receptor clustering," *Nature*, vol. 457, no. 7232, pp. 1019–1022, 2009.

[192] L. Wang *et al.*, "The Fas-FADD death domain complex structure reveals the basis of DISC assembly and disease mutations," *Nat. Struct. Mol. Biol.*, vol. 17, no. 11, pp. 1324–1329, 2010.

[193] A. M. Chinnaiyan, K. O'Rourke, M. Tewari, and V. M. Dixit, "FADD, a novel death

domain-containing protein, interacts with the death domain of fas and initiates apoptosis," *Cell*, vol. 81, no. 4, pp. 505–512, 1995.

[194] M. A. Ermolaeva *et al.*, "Function of TRADD in tumor necrosis factor receptor 1 signaling and in TRIF-dependent inflammatory responses," *Nat. Immunol.*, vol. 9, no. 9, pp. 1037–1046, 2008.

[195] Y. L. Pobezinskaya *et al.*, "The function of TRADD in signaling through tumor necrosis factor receptor 1 and TRIF-dependent Toll-like receptors," *Nat. Immunol.*, vol. 9, no. 9, pp. 1047–1054, 2008.

[196] B. Gerlach *et al.*, "Linear ubiquitination prevents inflammation and regulates immune signalling," *Nature*, vol. 471, no. 7340, pp. 591–596, 2011.

[197] G. Takaesu, R. M. Surabhi, K. J. Park, J. Ninomiya-Tsuji, K. Matsumoto, and R. B. Gaynor, "TAK1 is critical for IκB kinase-mediated activation of the NF-κB pathway," *J. Mol. Biol.*, vol. 326, no. 1, pp. 105–115, 2003.

[198] A. Oeckinghaus and S. Ghosh, "The NF-kB Family of Transcription Factors and Its Regulation," *Cold Spring Harb. Perspect. Biol.*, vol. 1, no. 4, pp. 1–15, 2019.

[199] I. Jaco *et al.*, "MK2 Phosphorylates RIPK1 to Prevent TNF-Induced Cell Death," *Mol. Cell*, vol. 66, no. 5, pp. 698-710.e5, 2017.

[200] L. Wang, F. Du, and X. Wang, "TNF-α Induces Two Distinct Caspase-8 Activation Pathways," *Cell*, vol. 133, no. 4, pp. 693–703, 2008.

[201] O. Micheau and J. Tschopp, "Induction of TNF receptor I-mediated apoptosis via two sequential signaling complexes," *Cell*, vol. 114, no. 2, pp. 181–190, 2003.

[202] M. Muzio, B. R. Stockwell, H. R. Stennicke, G. S. Salvesen, and V. M. Dixit, "An Induced Proximity Model for Caspase-8 Activation," *J. Biol. Chem.*, vol. 273, no. 5, pp. 2926–2930, 1998.

[203] L. S. Dickens *et al.*, "A Death Effector Domain Chain DISC Model Reveals a Crucial Role for Caspase-8 Chain Assembly in Mediating Apoptotic Cell Death," *Mol. Cell*, vol. 47, no. 2, pp. 291–305, 2012.

[204] M. Enari, R. V. Talanian, W. W. Wong, and S. Nagata, "Sequential activation of ICE-like

and CPP32-like proteases during Fas-mediated apoptosis," *Nature*, vol. 380, no. 6576, pp. 723–726, 1996.

[205] H. Li, H. Zhu, C. J. Xu, and J. Yuan, "Cleavage of BID by caspase 8 mediates the mitochondrial damage in the Fas pathway of apoptosis," *Cell*, vol. 94, no. 4, pp. 491–501, 1998.

[206] A. Degterev *et al.*, "Chemical inhibitor of nonapoptotic cell death with therapeutic potential for ischemic brain injury," *Nat. Chem. Biol.*, vol. 1, no. 2, pp. 112–119, 2005.

[207] N. Holler *et al.*, "Fas triggers an alternative, caspase-8-independent cell death pathway using the kinase RIP as effector molecule.," *Nat. Immunol.*, vol. 1, no. 6, pp. 489–495, 2000.

[208] Y. S. Cho *et al.*, "Phosphorylation-Driven Assembly of the RIP1-RIP3 Complex Regulates Programmed Necrosis and Virus-Induced Inflammation," *Cell*, vol. 137, no. 6, pp. 1112–1123, 2009.

[209] S. He *et al.*, "Receptor Interacting Protein Kinase-3 Determines Cellular Necrotic Response to TNF-α," *Cell*, vol. 137, no. 6, pp. 1100–1111, 2009.

[210] L. Sun *et al.*, "Mixed lineage kinase domain-like protein mediates necrosis signaling downstream of RIP3 kinase," *Cell*, vol. 148, no. 1–2, pp. 213–227, 2012.

[211] M. Chen *et al.*, "Internalized Cryptococcus neoformans Activates the Canonical Caspase-1 and the Noncanonical Caspase-8 Inflammasomes," *J. Immunol.*, vol. 195, no. 10, pp. 4962–4972, 2015.

[212] S. I. Gringhuis *et al.*, "Dectin-1 is an extracellular pathogen sensor for the induction and processing of IL-1β via a noncanonical caspase-8 inflammasome," *Nat. Immunol.*, vol. 13, no. 3, pp. 246–254, 2012.

[213] K. S. Schneider *et al.*, "The Inflammasome Drives GSDMD-Independent Secondary Pyroptosis and IL-1 Release in the Absence of Caspase-1 Protease Activity," *Cell Rep.*, vol. 21, no. 13, pp. 3846–3859, 2017.

[214] B. L. Lee *et al.*, "ASC- and caspase-8-dependent apoptotic pathway diverges from the NLRC4 inflammasome in macrophages," *Sci. Rep.*, vol. 8, no. 3788, pp. 1–12, 2018.

[215] D. P. A. Mascarenhas *et al.*, "Inhibition of caspase-1 or gasdermin-D enable caspase-8

activation in the Naip5/NLRC4/ASC inflammasome," *PLoS Pathog.*, vol. 13, no. 8, pp. 1–28, 2017.

[216] J. Maelfait *et al.*, "Stimulation of Toll-like receptor 3 and 4 induces interleukin-1β maturation by caspase-8," *J. Exp. Med.*, vol. 205, no. 9, pp. 1967–1973, 2008.

[217] K. Moriwaki, J. Bertin, P. J. Gough, and F. K.-M. Chan, "A RIPK3–Caspase 8 Complex Mediates Atypical Pro–IL-1β Processing," *J. Immunol.*, vol. 194, no. 4, pp. 1938–1944, 2015.

[218] K. Shenderov *et al.*, "Cutting Edge: Endoplasmic Reticulum Stress Licenses Macrophages To Produce Mature IL-1β in Response to TLR4 Stimulation through a Caspase-8– and TRIF-Dependent Pathway," *J. Immunol.*, vol. 192, no. 5, pp. 2029–2033, 2014.

[219] P. R. Vajjhala *et al.*, "The inflammasome adaptor ASC induces procaspase-8 death effector domain filaments," *J. Biol. Chem.*, vol. 290, no. 49, pp. 29217–29230, 2015.

[220] R. Allam *et al.*, "Mitochondrial apoptosis is dispensable for NLRP3 inflammasome activation but non-apoptotic caspase-8 is required for inflammasome priming," *EMBO Rep.*, vol. 15, no. 9, pp. 982–990, 2014.

[221] J. E. Vince *et al.*, "Inhibitor of Apoptosis Proteins Limit RIP3 Kinase-Dependent Interleukin-1 Activation," *Immunity*, vol. 36, no. 2, pp. 215–227, 2012.

[222] D. Chauhan *et al.*, "BAX/BAK-Induced Apoptosis Results in Caspase-8-Dependent IL-1β Maturation in Macrophages," *Cell Rep.*, vol. 25, no. 9, pp. 2354–2368, 2018.

[223] P. Orning *et al.*, "Pathogen blockade of TAK1 triggers caspase-8–dependent cleavage of gasdermin D and cell death," *Science (80-. ).*, vol. 362, no. 6418, pp. 1064–1069, 2018.

[224] J. Sarhan *et al.*, "Caspase-8 induces cleavage of gasdermin D to elicit pyroptosis during Yersinia infection," *PNAS*, vol. 115, no. 46, pp. E10888–E10897, 2018.

[225] K. W. Chen *et al.*, "Extrinsic and intrinsic apoptosis activate pannexin-1 to drive NLRP3 inflammasome assembly," *EMBO J.*, vol. 38, no. 10, p. e101638, 2019.

[226] J. Shi, W. Gao, and F. Shao, "Pyroptosis: Gasdermin-Mediated Programmed Necrotic Cell Death," *Trends Biochem. Sci.*, vol. 42, no. 4, pp. 245–254, 2017.

[227] N. Saeki, Y. Kuwahara, H. Sasaki, H. Satoh, and T. Shiroishi, "Gasdermin (Gsdm)

localizing to mouse chromosome 11 is predominantly expressed in upper gastroiatestinal tract but significantly suppressed in human gastric cancer cells," *Mamm. Genome*, vol. 11, no. 9, pp. 718–724, 2000.

[228] M. Tamura *et al.*, "Members of a novel gene family, Gsdm, are expressed exclusively in the epithelium of the skin and gastrointestinal tract in a highly tissue-specific manner," *Genomics*, vol. 89, no. 5, pp. 618–629, 2007.

[229] Z. Liu *et al.*, "Structures of the Gasdermin D C-Terminal Domains Reveal Mechanisms of Autoinhibition," *Structure*, vol. 26, no. 5, pp. 778–784, 2018.

[230] S. Kuang *et al.*, "Structure insight of GSDMD reveals the basis of GSDMD autoinhibition in cell pyroptosis," *PNAS*, vol. 114, no. 40, pp. 10642–10647, 2017.

[231] X. Chen *et al.*, "Pyroptosis is driven by non-selective gasdermin-D pore and its morphology is different from MLKL channel-mediated necroptosis," *Cell Res.*, vol. 26, no. 9, pp. 1007–1020, 2016.

[232] Y. Wang *et al.*, "Chemotherapy drugs induce pyroptosis through caspase-3 cleavage of a gasdermin," *Nature*, vol. 547, no. 7661, pp. 99–103, 2017.

[233] C. Rogers, D. A. Erkes, A. Nardone, A. E. Aplin, T. Fernandes-Alnemri, and E. S. Alnemri, "Gasdermin pores permeabilize mitochondria to augment caspase-3 activation during apoptosis and inflammasome activation," *Nat. Commun.*, vol. 10, no. 1, pp. 1–17, 2019.

[234] E. Mulvihill, L. Sborgi, S. A. Mari, M. Pfreundschuh, S. Hiller, and D. J. Müller, "Mechanism of membrane pore formation by human gasdermin-D," *EMBO J.*, vol. 37, no. 14, pp. 1–11, 2018.

[235] N. M. de Vasconcelos, N. Van Opdenbosch, H. Van Gorp, E. Parthoens, and M. Lamkanfi, "Single-cell analysis of pyroptosis dynamics reveals conserved GSDMD-mediated subcellular events that precede plasma membrane rupture," *Cell Death Differ.*, vol. 26, no. 1, pp. 146–161, 2018.

[236] R. Heilig, M. S. Dick, L. Sborgi, E. Meunier, S. Hiller, and P. Broz, "The Gasdermin-D pore acts as a conduit for IL-1β secretion in mice," *Eur. J. Immunol.*, vol. 48, no. 4, pp. 584–592, 2018.

[237] K. W. Chen *et al.*, "The Neutrophil NLRC4 Inflammasome Selectively Promotes IL-1β

Maturation without Pyroptosis during Acute *Salmonella* Challenge," *Cell Rep.*, vol. 8, no. 2, pp. 570–582, 2014.

[238] C. L. Evavold, J. Ruan, Y. Tan, S. Xia, H. Wu, and J. C. Kagan, "The Pore-Forming Protein Gasdermin D Regulates Interleukin-1 Secretion from Living Macrophages," *Immunity*, vol. 48, no. 1, pp. 35-44.e6, 2018.

[239] M. Varela, M. van der Vaart, A. Groenewoud, and A. H. Meijer, "Extracellular mycobacterial DNA triggers Caspase-11-dependent pyroptosis of infected macrophages and drives disease progression," *bioRxiv*, pp. 1–27, 2019.

[240] F. T. Bosman, B. C. Visser, and J. Van Oeveren, "Apoptosis: Pathophysiology of programmed cell death," *Pathol. Res. Pract.*, vol. 192, no. 7, pp. 676–683, 1996.

[241] J. F. Kerr, A. H. Wyllie, and A. R. Currie, "Apoptosis: a Basic Biological Phenomenon With Wide- Ranging Implications in Tissue Kinetics," *J. Intern. Med.*, vol. 26, no. 4, pp. 239–257, 1972.

[242] A. Samali, B. Zhivotovsky, D. Jones, S. Nagata, and S. Orrenius, "Apoptosis: Cell death defined by caspase activation.," *Cell Death Differ.*, vol. 6, no. 6, pp. 495–496, 1999.

[243] N. Itoh *et al.*, "The polypeptide encoded by the cDNA for human cell surface antigen Fas can mediate apoptosis," *Cell*, vol. 66, no. 2, pp. 233–243, 1991.

[244] M. A. Fernández-Terán, J. R. Hinchliffe, and M. A. Ros, "Birth and death of cells in limb development: A mapping study," *Dev. Dyn.*, vol. 235, no. 9, pp. 2521–2537, 2006.

[245] H. W. Rogers, B. Deck, E. R. Unanue, and M. P. Callery, "Listeria monocytogenes induces apoptosis of infected hepatocytes," *J. Immunol.*, vol. 156, no. 2, pp. 679–684, 1996.

[246] S. L. Fink and B. T. Cookson, "Caspase-1-dependent pore formation during pyroptosis leads to osmotic lysis of infected host macrophages," *Cell. Microbiol.*, vol. 8, no. 11, pp. 1812–1825, 2006.

[247] H. Hilbi, Y. Chen, K. Thirumalai, and A. Zychlinsky, "The Interleukin 1β-Converting Enzyme, Caspase 1, Is Activated during Shigella flexneri-Induced Apoptosis in Human Monocyte-Derived Macrophages," *Infect. Immun.*, vol. 65, no. 12, pp. 5165–5170, 1997.

[248] J. A. Collins, C. A. Schandl, K. K. Young, J. Vesely, and M. C. Willingham, "Major DNA

fragmentation is a late event in apoptosis," *J. Histochem. Cytochem.*, vol. 45, no. 7, pp. 923–934, 1997.

[249] W. Wood *et al.*, "Mesenchymal cells engulf and clear apoptotic footplate cells in macrophageless PU.1 null mouse embryos," *Development*, vol. 127, no. 24, pp. 5245–5252, 2000.

[250] K. S. Ravichandran, "Beginnings of a Good Apoptotic Meal: The Find-Me and Eat-Me Signaling Pathways," *Immunity*, vol. 35, no. 4, pp. 445–455, 2011.

[251] R. E. Voll, M. Herrmann, E. A. Roth, C. Stach, and J. R. Kalden, "Immunosuppressive effects of apoptotic cells," *Nature*, vol. 390, no. 6658, pp. 350–351, 1997.

[252] S. Rello *et al.*, "Morphological criteria to distinguish cell death induced by apoptotic and necrotic treatments," *Apoptosis*, vol. 10, no. 1, pp. 201–208, 2005.

[253] P. Scaffidi, T. Misteli, and M. E. Bianchi, "Release of chromatin protein HMGB1 by necrotic cells triggers inflammation.," *Nature*, vol. 418, no. 6894, pp. 191–195, 2002.

[254] P. R. Watson, A. V. Gautier, S. M. Paulin, A. P. Bland, P. W. Jones, and T. S. Wallis, "*Salmonella enterica* Serovars Typhimurium and Dublin Can Lyse Macrophages by a Mechanism Distinct from Apoptosis," *Infect. Immun.*, vol. 68, no. 6, pp. 3744–3747, 2000.

[255] G. W. Sun, J. Lu, S. Pervaiz, W. P. Cao, and Y. H. Gan, "Caspase-1 dependent macrophage death induced by Burkholderia pseudomallei," *Cell. Microbiol.*, vol. 7, no. 10, pp. 1447–1458, 2005.

[256] D. M. Monack, B. Raupach, A. E. Hromockyj, and S. Falkow, "*Salmonella* typhimurium invasion induces apoptosis in infected macrophages.," *PNAS*, vol. 93, no. 18, pp. 9833–9838, 1996.

[257] R. Karki *et al.*, "Concerted activation of the AIM2 and NLRP3 inflammasomes orchestrates host protection against aspergillus infection," *Cell Host Microbe*, vol. 17, no. 3, pp. 357–368, 2015.

[258] A. Cauwels, B. Janssen, A. Waeytens, C. Cuvelier, and P. Brouckaert, "Caspase inhibition causes hyperacute tumor necrosis factor-induced shock via oxidative stress and phospholipase A2.," *Nat. Immunol.*, vol. 4, no. 4, pp. 387–393, 2003.

[259] N. Dupont, S. Jiang, M. Pilli, W. Ornatowski, D. Bhattacharya, and V. Deretic, "Autophagy-based unconventional secretory pathway for extracellular delivery of IL-1beta," *Embo J.*, vol. 30, no. 23, pp. 4701–4711, 2011.

[260] R. Shindo, H. Kakehashi, K. Okumura, Y. Kumagai, and H. Nakano, "Critical contribution of oxidative stress to TNFα-induced necroptosis downstream of RIPK1 activation," *Biochem. Biophys. Res. Commun.*, vol. 436, no. 2, pp. 212–216, 2013.

[261] J. W. Upton, W. J. Kaiser, and E. S. Mocarski, "Cytomegalovirus M45 cell death suppression requires receptor-interacting protein (RIP) homotypic interaction motif (RHIM)-dependent interaction with RIP1," *J. Biol. Chem.*, vol. 283, no. 25, pp. 16966–16970, 2008.

[262] W. J. Kaiser *et al.*, "RIP1 suppresses innate immune necrotic as well as apoptotic cell death during mammalian parturition," *PNAS*, vol. 111, no. 21, pp. 7753–7758, 2014.

[263] C. P. Dillon *et al.*, "RIPK1 blocks early postnatal lethality mediated by caspase-8 and RIPK3," *Cell*, vol. 157, no. 5, pp. 1189–1202, 2014.

[264] B. Z. Stanger, P. Leder, T.-H. Lee, E. Kim, and B. Seed, "RIP A Novel Protein Containing a Death Domain That Interacts with FadAPO-1 (CD95) in Yeast and Causes Cell Death," *Cell*, vol. 81, no. 4, pp. 513–523, 1995.

[265] H. Hsu, J. Huang, H. B. Shu, V. Baichwal, and D. V. Goeddel, "TNF-dependent recruitment of the protein kinase RIP to the TNF receptor-1 signaling complex," *Immunity*, vol. 4, no. 4, pp. 387–396, 1996.

[266] S. M. Laster, J. G. Wood, and L. R. Gooding, "Tumor necrosis factor can induce both apoptic and necrotic forms of cell lysis.," *J. Immunol.*, vol. 141, no. 8, pp. 2629–2634, 1988.

[267] X. Zhang, J. P. Dowling, and J. Zhang, "RIPK1 can mediate apoptosis in addition to necroptosis during embryonic development," *Cell Death Dis.*, vol. 10, no. 3, pp. 1–11, 2019.

[268] J. Li *et al.*, "The RIP1/RIP3 necrosome forms a functional amyloid signaling complex required for programmed necrosis," *Cell*, vol. 150, no. 2, pp. 339–350, 2012.

[269] T. Tenev *et al.*, "The Ripoptosome, a Signaling Platform that Assembles in Response to Genotoxic Stress and Loss of IAPs," *Mol. Cell*, vol. 43, no. 3, pp. 432–448, 2011.

[270] A. T. Ting, F. X. Pimentel-Muiños, and B. Seed, "RIP mediates tumor necrosis factor receptor 1 activation of NF-κB but not Fas/APO-1-initiated apoptosis.," *EMBO J.*, vol. 15, no. 22, pp. 6189–6196, 1996.

[271] H. Li, M. Kobayashi, M. Blonska, Y. You, and X. Lin, "Ubiquitination of RIP is required for tumor necrosis factor α-induced NF-κB activation," *J. Biol. Chem.*, vol. 281, no. 19, pp. 13636–13643, 2006.

[272] C. K. Ea, L. Deng, Z. P. Xia, G. Pineda, and Z. J. Chen, "Activation of IKK by TNFα Requires Site-Specific Ubiquitination of RIP1 and Polyubiquitin Binding by NEMO," *Mol. Cell*, vol. 22, no. 2, pp. 245–257, 2006.

[273] H. AH *et al.*, "World Health Organization Global Estimates and Regional Comparisons of the Burden of Foodborne Disease in 2010," *PLoS Med.*, vol. 12, no. 12, p. e1001923, 2015.

[274] J. A. Crump, S. P. Luby, and E. D. Mintz, "The global burden of typhoid fever," *Bull. World Health Organ.*, vol. 82, no. 5, pp. 346–353, 2004.

[275] E. A. Groisman and H. Ochman, "How *Salmonella* became a pathogen," *Trends Microbiol.*, vol. 5, no. 9, pp. 343–349, 1997.

[276] X. Chen *et al.*, "Biophysical characterization of the type III secretion system translocator proteins and the translocator proteins attached to bacterium-like particles," *J. Pharm. Sci.*, vol. 104, no. 12, pp. 4065–4073, 2015.

[277] I. Hautefort *et al.*, "During infection of epithelial cells *Salmonella enterica* serovar Typhimurium undergoes a time-dependent transcriptional adaptation that results in simultaneous expression of three type 3 secretion systems," *Cell. Microbiol.*, vol. 10, no. 4, pp. 958–984, 2008.

[278] M. Lara-Tejero and J. E. Galán, "*Salmonella enterica* serovar Typhimurium pathogenicity island 1-encoded type III secretion system translocases mediate intimate attachment to nonphagocytic cells," *Infect. Immun.*, vol. 77, no. 7, pp. 2635–2642, 2009.

[279] J. E. Galan and D. Zhou, "Striking a balance: modulation of the actin cytoskeleton by *Salmonella*.," *PNAS*, vol. 97, no. 16, pp. 8754–8761, 2000.

[280] O. Steele-Mortimer, S. Meresse, J. P. Gorvel, B. H. Toh, and B. B. Finlay, "Biogenesis of *Salmonella* typhimurium-containing vacuoles in epithelial cells involves interactions with

the early endocytic pathway," *Cell. Microbiol.*, vol. 1, no. 1, pp. 33-49., 1999.

[281] D. M. Cirillo, R. H. Valdivia, D. M. Monack, and S. Falkow, "Macrophage-dependent induction of the *Salmonella* pathogenicity island 2 type III secretion system and its role in intracellular survival.," *Mol. Microbiol.*, vol. 30, no. 1, pp. 175–188, 1998.

[282] A. Gallois, J. R. Klein, L.-A. H. Allen, B. D. Jones, and W. M. Nauseef, "*Salmonella* Pathogenicity Island 2-Encoded Type III Secretion System Mediates Exclusion of NADPH Oxidase Assembly from the Phagosomal Membrane," *J. Immunol.*, vol. 166, no. 9, pp. 5741–5748, 2001.

[283] M.-L. Crouch, L. A. Becker, I.-S. Bang, H. Tanabe, A. J. Ouellette, and F. C. Fang, "The alternative sigma factor σE is required for resistance of *Salmonella enterica* serovar Typhimurium to anti-microbial peptides," *Mol. Microbiol.*, vol. 56, no. 3, pp. 789–799, 2005.

[284] A. Haraga, M. B. Ohlson, and S. I. Miller, "*Salmonellae* interplay with host cells," *Nat. Rev. Microbiol.*, vol. 6, no. 1, pp. 53–66, 2008.

[285] S. Talbot *et al.*, "Toll-like receptor 4 signalling through MyD88 is essential to control *Salmonella enterica* serovar Typhimurium infection, but not for the initiation of bacterial clearance," *Immunology*, vol. 128, no. 4, pp. 472–483, 2009.

[286] D. S. Weiss, B. Raupach, K. Takeda, S. Akira, and A. Zychlinsky, "Toll-Like Receptors Are Temporally Involved in Host Defense," *J. Immunol.*, vol. 172, no. 7, pp. 4463–4469, 2004.

[287] A. T. Gewirtz, T. A. Navas, S. Lyons, P. J. Godowski, and J. L. Madara, "Cutting Edge: Bacterial Flagellin Activates Basolaterally Expressed TLR5 to Induce Epithelial Proinflammatory Gene Expression," *J. Immunol.*, vol. 167, no. 4, pp. 1882–1885, 2001.

[288] C. A. Kasper *et al.*, "Cell-cell propagation of NF-κB transcription factor and MAP kinase activation amplifies innate immunity against bacterial infection," *Immunity*, vol. 33, no. 5, pp. 804–816, 2010.

[289] I. Rauch *et al.*, "NAIP-NLRC4 Inflammasomes Coordinate Intestinal Epithelial Cell Expulsion with Eicosanoid and IL-18 Release via Activation of Caspase-1 and -8," *Immunity*, vol. 46, no. 4, pp. 649–659, 2017.

[290] B. Raupach, S. K. Peuschel, D. M. Monack, and A. Zychlinsky, “Caspase-1-mediated activation of interleukin-1β (IL-1β) and IL-18 contributes to innate immune defenses against *Salmonella enterica* serovar typhimurium infection,” *Infect. Immun.*, vol. 74, no. 8, pp. 4922–4926, 2006.

[291] M. Lara-Tejero *et al.*, “Role of the caspase-1 inflammasome in *Salmonella* typhimurium pathogenesis,” *J. Exp. Med.*, vol. 203, no. 6, pp. 1407–1412, 2006.

[292] Y. Qu *et al.*, “ NLRP3 recruitment by NLRC4 during *Salmonella* infection ,” *J. Exp. Med.*, vol. 213, no. 6, pp. 877–885, 2016.

[293] E. A. Miao *et al.*, “Caspase-1-induced pyroptosis is an innate immune effector mechanism against intracellular bacteria,” *Nat. Immunol.*, vol. 11, no. 12, pp. 1136–1142, 2010.

[294] T. L. M. Thurston *et al.*, “Growth inhibition of cytosolic *Salmonella* by caspase-1 and caspase-11 precedes host cell death,” *Nat. Commun.*, vol. 7, no. 13292, pp. 1–15, 2016.

[295] C. N. Casson *et al.*, “Human caspase-4 mediates noncanonical inflammasome activation against gram-negative bacterial pathogens,” *PNAS*, vol. 112, no. 21, pp. 6688–6693, 2015.

[296] H. L. Bruce, P. A. Barrow, and A. N. Rycroft, “Zoonotic potential of *Salmonella enterica* carried by pet tortoises,” *Vet. Rec.*, vol. 182, no. 5, pp. 141–144, 2017.

[297] M. T. Jay-Russell, A. F. Hake, Y. Bengson, A. Thiptara, and T. Nguyen, “Prevalence and characterization of Escherichia coli and *Salmonella* strains isolated from stray dog and coyote feces in a major leafy greens production region at the United States-Mexico border,” *PLoS One*, vol. 9, no. 11, 2014.

[298] X. Kuang *et al.*, “Serotypes and antimicrobial susceptibility of *Salmonella* spp. isolated from farm animals in China,” *Front. Microbiol.*, vol. 6, no. 602, pp. 1–11, 2015.

[299] H. L. Shivaprasad, “Fowl typhoid and pullorum disease,” *OIE Rev. Sci. Tech.*, vol. 19, no. 2, pp. 405–424, 2000.

[300] N. Paudyal *et al.*, “Characterization of *Salmonella* Dublin isolated from bovine and human hosts,” *BMC Microbiol.*, vol. 19, no. 226, pp. 1–8, 2019.

[301] L. E. Hughes, E. A. Gibson, H. E. Roberts, E. T. Davies, G. Davies, and W. J. Sojka, “Bovine salmonellosis in England and Wales.,” *Br. Vet. J.*, vol. 127, no. 5, pp. 225–238,

1971.

[302] E. Klein, “The Bacteria of Swine Plague,” *J. Physiol.*, vol. 5, no. 1, pp. 1–13, 1884.

[303] B. P. Smith, F. Habasha, M. Reina-Guerra, and A. J. Hardy, “Bovine salmonellosis: experimental production and characterization of the disease in calves, using oral challenge with *Salmonella* typhimurium.,” *Am. J. Vet. Res.*, vol. 40, no. 11, pp. 1510–1513, 1979.

[304] A. Baskerville and C. Dow, “Pathology of experimental pneumonia in pigs produced by *Salmonella* cholerae-suis,” *J. Comp. Pathol.*, vol. 83, pp. 207–215, 1973.

[305] P. Pardon, R. Sanchis, J. Marly, F. Lantier, M. Pépin, and M. Popoff, “Ovine salmonellosis caused by *Salmonella* abortus ovis,” *Ann. Rech. Vet.*, vol. 19, no. 4, p. 221—235, 1988.

[306] L. Belloy, L. Decrausaz, P. Boujon, H. Hächler, and A. S. Waldvogel, “Diagnosis by culture and PCR of *Salmonella* Abortusovis infection under clinical conditions in aborting sheep in Switzerland,” *Vet. Microbiol.*, vol. 138, no. 3–4, pp. 373–377, 2009.

[307] S. P. Brown *et al.*, “Intracellular demography and the dynamics of *Salmonella enterica* infections,” *PLoS Biol.*, vol. 4, no. 11, pp. 2091–2098, 2006.

[308] A. G. Gow, D. J. Gow, E. J. Hall, D. Langton, C. Clarke, and K. Papasouliotis, “Prevalence of potentially pathogenic enteric organisms in clinically healthy kittens in the UK,” *J. Feline Med. Surg.*, vol. 11, no. 8, pp. 655–662, 2009.

[309] B. Kiflu, H. Alemayehu, M. Abdurahaman, Y. Negash, and T. Eguale, “*Salmonella* serotypes and their antimicrobial susceptibility in apparently healthy dogs in Addis Ababa, Ethiopia,” *BMC Vet. Res.*, vol. 13, no. 134, pp. 1–9, 2017.

[310] E. K. Leonard *et al.*, “Evaluation of Pet-Related Management Factors and the Risk of *Salmonella* spp. Carriage in Pet Dogs from Volunteer Households in Ontario (2005-2006),” *Zoonoses Public Health*, vol. 58, no. 2, pp. 140–149, 2011.

[311] A. W. Philbey, H. A. Mather, J. F. Gibbons, H. Thompson, D. J. Taylor, and J. E. Coia, “Serovars, bacteriophage types and antimicrobial sensitivities associated with salmonellosis in dogs in the UK (1954-2012),” *Vet. Rec.*, vol. 174, no. 4, pp. 94–102, 2014.

[312] J. L. Schmid-Burgk *et al.*, “OutKnocker: A web tool for rapid and simple genotyping of designer nuclease edited cell lines,” *Genome Res.*, vol. 24, no. 10, pp. 1719–1723, 2014.

[313] T. Schmidt, J. L. Schmid-burgk, T. S. Ebert, M. M. Gaidt, and V. Hornung, "Designer Nuclease-Mediated Generation of Knockout THP1 Cells," *Methods Mol. Biol.*, vol. 1338, pp. 261–272, 2016.

[314] D. M. Monack, W. W. Navarre, and S. Falkow, "*Salmonella*-induced macrophage death: The role of caspase-1 in death and inflammation," *Microbes Infect.*, vol. 3, no. 14–15, pp. 1201–1212, 2001.

[315] R. E. Morgan, P. D. Clegg, J. A. Hunt, J. F. Innes, and S. R. Tew, "Interaction with macrophages attenuates equine fibroblast-like synoviocyte ADAMTS5 (aggrecanase-2) gene expression following inflammatory stimulation," *J. Orthop. Res.*, vol. 36, no. 8, pp. 2178–2185, 2018.

[316] J. M. Soto, J. A. Rodrigo, A. Mas, G. Domínguez-Bernal, and T. Alieva, "Label-free bioanalysis of Leishmania infantum using refractive index tomography with partially coherent illumination," *J. Biophotonics*, vol. 9, no. January, pp. 1–10, 2019.

[317] C. J. R. M. do Rosário *et al.*, "Anti-Ehrlichia properties of the essential oil of Ageratum conyzoides L. and its interaction with doxycycline," *AMB Express*, vol. 9, no. 1, pp. 1–9, 2019.

[318] M. Balachandran, D. A. Bemis, and S. A. Kania, "Expression and function of protein A in Staphylococcus pseudintermedius," *Virulence*, vol. 9, no. 1, pp. 390–401, 2018.

[319] P. H. B. Mendonça *et al.*, "canine Macrophage Dh82 cell line as a Model to study susceptibility to Trypanosoma cruzi infection Pedro," *Front. Immunol.*, vol. 8, no. 604, pp. 1–11, 2017.

[320] Q. Feng, P. Li, P. C. K. Leung, and N. Auersperg, "Caspase-1ζ, a new splice variant of the caspase-1 gene," *Genomics*, vol. 84, no. 3, pp. 587–591, 2004.

[321] A. Weigert *et al.*, "Cleavage of sphingosine kinase 2 by caspase-1 provokes its release from apoptotic cells," *Blood*, vol. 115, no. 17, pp. 3531–3540, 2010.

[322] D. Chéreau, L. Kodandapani, K. J. Tomaselli, A. P. Spada, and J. C. Wu, "Structural and Functional Analysis of Caspase Active Sites," *Biochemistry*, vol. 42, no. 14, pp. 4151–4160, 2003.

[323] A. Lu *et al.*, "Unified Polymerization Mechanism for the Assembly of ASC-Dependent

Inflammasome," *Cell*, vol. 156, no. 6, pp. 1193–1206, 2014.

[324] M. Moriya, S. Taniguchi, P. Wu, E. Liepinsh, G. Otting, and J. Sagara, "Role of Charged and Hydrophobic Residues in the Oligomerization of the PYRIN Domain of ASC," *Biochemistry*, vol. 44, no. 2, pp. 575–583, 2005.

[325] P. C. Liao *et al.*, "Lipopolysaccharide/adenosine triphosphate-mediated signal transduction in the regulation of NLRP3 protein expression and caspase-1-mediated interleukin-1β secretion," *Inflamm. Res.*, vol. 62, no. 1, pp. 89–96, 2013.

[326] J. M. Platnich *et al.*, "Shiga Toxin/Lipopolysaccharide Activates Caspase-4 and Gasdermin D to Trigger Mitochondrial Reactive Oxygen Species Upstream of the NLRP3 Inflammasome," *Cell Rep.*, vol. 25, no. 6, pp. 1525-1536.e7, 2018.

[327] A. Baroja-Mazo *et al.*, "The NLRP3 inflammasome is released as a particulate danger signal that amplifies the inflammatory response," *Nat. Immunol.*, vol. 15, no. 8, pp. 738–748, 2014.

[328] L. Wang *et al.*, "PYPAF7, a novel PYRIN-containing Apaf1-like protein that regulates activation of NF-kappa B and caspase-1-dependent cytokine processing.," *J. Biol. Chem.*, vol. 277, no. 33, pp. 29874–29880, 2002.

[329] W. Sha *et al.*, "Human NLRP3 inflammasome senses multiple types of bacterial RNAs," *PNAS*, vol. 111, no. 45, pp. 16059–16064, 2014.

[330] L. Franchi *et al.*, "Cytosolic double-stranded RNA activates the NLRP3 inflammasome via MAVS- induced membrane permeabilization and K+ efflux," *J. Immunol.*, vol. 193, no. 8, pp. 4214–4222, 2014.

[331] C. M. Cruz, A. Rinna, H. J. Forman, A. L. M. Ventura, P. M. Persechini, and D. M. Ojcius, "ATP Activates a Reactive Oxygen Species-dependent Oxidative Stress Response and Secretion of Proinflammatory Cytokines in Macrophages," *J. Biol. Chem.*, vol. 282, no. 5, pp. 2871–2879, 2007.

[332] J. Hewinson, S. F. Moore, C. Glover, A. G. Watts, and A. B. MacKenzie, " A Key Role for Redox Signaling in Rapid P2X 7 Receptor-Induced IL-1β Processing in Human Monocytes ," *J. Immunol.*, vol. 180, no. 12, pp. 8410–8420, 2008.

[333] A. E. P. *et al.*, "Lysosomal cathepsin release is required for NLRP3-inflammasome activation by Mycobacterium tuberculosis in infected macrophages," *Front. Immunol.*, vol.

9, no. 1427, pp. 1–12, 2018.

[334] H. Bai, B. Yang, W. Yu, Y. Xiao, D. Yu, and Q. Zhang, “Cathepsin B links oxidative stress to the activation of NLRP3 inflammasome,” *Exp. Cell Res.*, vol. 362, no. 1, pp. 180–187, 2018.

[335] S. N. Graven, S. Estrada-O., and H. A. Lardy, “Alkali Metal Cation Release and Respiratory Inhibition Induced by Nigericin in Rat Liver Mitochondria,” *PNAS*, vol. 56, no. 2, pp. 654–658, 1966.

[336] J. F. Burd and M. Usategui-Gomez, “A colorimetric assay for serum lactate dehydrogenase,” *Clin. Chim. Acta*, vol. 46, no. 3, pp. 223–227, 1973.

[337] S. Ming Man *et al.*, “Differential roles of caspase-1 and caspase-11 in infection and inflammation,” *Sci. Rep.*, vol. 7, no. 45126, pp. 1–11, 2017.

[338] T. Fernandes-Alnemri, J. W. Yu, P. Datta, J. Wu, and E. S. Alnemri, “AIM2 activates the inflammasome and cell death in response to cytoplasmic DNA,” *Nature*, vol. 458, no. 7237, pp. 509–513, 2009.

[339] A. Stutz, G. L. Horvath, B. G. Monks, and E. Latz, “ASC Speck Formation as a Readout for Inflammasome Activation,” *Methods Mol. Biol.*, vol. 1040, no. 15, pp. 91–101, 2013.

[340] M. L. Wellman, S. Krakowka, R. M. Jacobs, and G. J. Kociba, “A macrophage-monocyte cell line from a dog with malignant histiocytosis,” *Vitr. Cell. Dev. Biol.*, vol. 24, no. 3, pp. 223–229, 1988.

[341] B. S. Park, D. H. Song, H. M. Kim, B. S. Choi, H. Lee, and J. O. Lee, “The structural basis of lipopolysaccharide recognition by the TLR4-MD-2 complex,” *Nature*, vol. 458, no. 7242, pp. 1191–1195, 2009.

[342] B. Lagrange *et al.*, “Human caspase-4 detects tetra-acylated LPS and cytosolic Francisella and functions differently from murine caspase-11,” *Nat. Commun.*, vol. 9, no. 1, pp. 1–14, 2018.

[343] A. Ozinsky *et al.*, “The repertoire for pattern recognition of pathogens by the innate immune system is defined by cooperation between toll-like receptors.,” *PNAS*, vol. 97, no. 25, pp. 13766–13771, 2000.

[344] A. O. Aliprantis *et al.*, “Cell Activation and Apoptosis by Bacterial Lipoproteins Through Toll-like Receptor-2,” *Science (80-. ).*, vol. 285, no. 5428, pp. 736–739, 1999.

[345] R. R. Schumann *et al.*, “Lipopolysaccharide Activates Caspase-1 (Interleukin-1–Converting Enzyme) in Cultured Monocytic and Endothelial Cells,” *Blood*, vol. 91, no. 2, pp. 577–584, 1998.

[346] M. G. Netea *et al.*, “Differential requirement for the activation of the inflammasome for processing and release of IL-1β in monocytes and macrophages,” *Blood*, vol. 113, no. 10, pp. 2324–2335, 2009.

[347] B. Lemmers *et al.*, “Essential Role for Caspase-8 in Toll-like Receptors and NF-κB Signaling,” *J. Biol. Chem.*, vol. 282, no. 10, pp. 7416–7423, 2007.

[348] M. Rayamajhi, D. E. Zak, J. Chavarria-Smith, R. E. Vance, and E. A. Miao, “Cutting Edge: Mouse NAIP1 Detects the Type III Secretion System Needle Protein,” *J. Immunol.*, vol. 191, no. 8, pp. 3986–3989, 2013.

[349] E. M. Kofoed and R. E. Vance, “Innate immune recognition of bacterial ligands by NAIPs determines inflammasome specificity,” *Nature*, vol. 477, no. 7366, pp. 592–597, 2011.

[350] D. P. Cerretti *et al.*, “Molecular cloning of interleukin-1 beta converting enzyme.,” *Science (80-. ).*, vol. 256, no. April, pp. 97–100, 1992.

[351] M. Proell, M. Gerlic, P. D. Mace, J. C. Reed, and S. J. Riedl, “The CARD plays a critical role in ASC foci formation and inflammasome signalling,” *Biochem. J.*, vol. 449, no. 3, pp. 613–621, 2012.

[352] S. M. Man, P. Tourlomousis, L. Hopkins, T. P. Monie, K. A. Fitzgerald, and C. E. Bryant, “*Salmonella* infection induces recruitment of Caspase-8 to the inflammasome to modulate interleukin-1β production,” *J. Immunol.*, vol. 191, no. 10, pp. 1–18, 2014.

[353] F. Martin-Sanchez *et al.*, “Inflammasome-dependent IL-1β release depends upon membrane permeabilisation,” *Cell Death Differ.*, vol. 23, no. 7, pp. 1219–1231, 2016.

[354] V. S. Tapia *et al.*, “The three cytokines IL-1β, IL-18, and IL-1α share related but distinct secretory routes,” *J. Biol. Chem.*, vol. 294, no. 21, pp. 8325–8335, 2019.

[355] J. G. Giri, P. T. Lomedica, S. B. Mizel, and E. Al, “Studies on the synthesis and secretion

of interleukin 1. I. A 33,000 molecular weight precursor for interleukin 1.," *J. Immunol.*, vol. 134, no. 1, pp. 343–349, 1985.

[356] R. A. Black *et al.*, "Generation of Biologically Active Interleukin-1β by Proteolytic Cleavage of the Inactive Precursor," *J. Biol. Chem.*, vol. 263, no. 19, pp. 9437–9442, 1988.

[357] D. J. Hazuda, J. Stricklerll, F. Kueppers, P. L. Simon, and P. R. Young, "Processing of Precursor Interleukin 1β and Inflammatory Disease," *J. Biol. Chem.*, vol. 265, no. 11, pp. 6318–6323, 1990.

[358] H. Mizutani, N. Schechter, G. Lazarus, R. A. Black, and T. S. Kupper, "Rapid and Specific Conversion of Precursor Interleukin 1β (IL-1β) to an Active IL-1 Species by Human Mast Cell Chymase," *J. Exp. Med.*, vol. 174, no. 4, pp. 821–825, 1991.

[359] C. Coeshott *et al.*, "Converting enzyme-independent release of tumor necrosis factor α and IL-1β from a stimulated human monocytic cell line in the presence of activated neutrophils or purified proteinase 3," *PNAS*, vol. 96, no. 11, pp. 6261–6266, 1999.

[360] S. Rühl, K. Shkarina, B. Demarco, R. Heilig, J. C. Santos, and P. Broz, "ESCRT-dependent membrane repair negatively regulates pyroptosis downstream of GSDMD activation," *Science (80-. ).*, vol. 362, no. 6417, pp. 956–960, 2018.

[361] Y. N. Gong *et al.*, "ESCRT-III Acts Downstream of MLKL to Regulate Necroptotic Cell Death and Its Consequences," *Cell*, vol. 169, no. 2, pp. 286–300, 2017.

[362] F. J. M. Mojica, C. Díez-Villaseñor, J. García-Martínez, and E. Soria, "Intervening sequences of regularly spaced prokaryotic repeats derive from foreign genetic elements," *J. Mol. Evol.*, vol. 60, no. 2, pp. 174–182, 2005.

[363] C. Pourcel, G. Salvignol, and G. Vergnaud, "CRISPR elements in Yersinia pestis acquire new repeats by preferential uptake of bacteriophage DNA, and provide additional tools for evolutionary studies," *Microbiology*, vol. 151, no. 3, pp. 653–663, 2005.

[364] A. Bolotin, B. Quinquis, A. Sorokin, and S. Dusko Ehrlich, "Clustered regularly interspaced short palindrome repeats (CRISPRs) have spacers of extrachromosomal origin," *Microbiology*, vol. 151, no. 8, pp. 2551–2561, 2005.

[365] R. Barrangou *et al.*, "CRISPR Provides Acquired Resistance Against Viruses in Prokaryotes," *Science (80-. ).*, vol. 315, no. 5819, pp. 1709–1712, 2007.

[366] F. J. M. Mojica, C. Díez-Villaseñor, E. Soria, and G. Juez, “Biological significance of a family of regularly spaced repeats in the genomes of Archaea, Bacteria and mitochondria,” *Mol. Microbiol.*, vol. 36, no. 1, pp. 244–246, 2000.

[367] R. Jansen, J. D. A. Van Embden, W. Gaastra, and L. M. Schouls, “Identification of genes that are associated with DNA repeats in prokaryotes,” *Mol. Microbiol.*, vol. 43, no. 6, pp. 1565–1575, 2002.

[368] Y. Ishino, “Nucleotide sequence of the iap gene, responsible for alkaline phosphatase isozyme conversion in Escherichia coli, and identification of the gene product.,” *J. Bacteriol.*, vol. 169, no. 12, pp. 5429–5433, 1987.

[369] F. J. M. Mojica, G. Juez, and F. Rodriguez-Valera, “Transcription at different salinities of Haloferax mediterranei sequences adjacent to partially modified PstI sites,” *Mol. Microbiol.*, vol. 9, no. 3, pp. 613–621, 1993.

[370] F. J. M. Mojica, C. Ferrer, and F. Rodriguez-valera, “Long stretches of short tandem repeats are present in the largest replicons of the Archaea Haloforax mediterranei and Haloferax volcanii and could be involved in replicon partitioning,” *Mol. Microbiol.*, vol. 17, no. 1, pp. 85–93, 1995.

[371] K. S. Makarova, N. V Grishin, S. A. Shabalina, Y. I. Wolf, and E. V Koonin, “A putative RNA-interference-based immune system in prokaryotes: computational analysis of the predicted enzymatic machinery, functional analogies with eukaryotic RNAi, and hypothetical mechanisms of action.,” *Biol. Direct*, vol. 16, no. 1, pp. 7–33, 2006.

[372] S. J. J. Brouns *et al.*, “Small CRISPR RNAs Guide Antiviral Defense in Prokaryotes,” *Science (80-. ).*, vol. 321, no. 5891, pp. 960–964, Aug. 2008.

[373] E. Deltcheva *et al.*, “CRISPR RNA maturation by trans-encoded small RNA and host factor RNase III.,” *Nature*, vol. 471, no. 7340, pp. 602–607, 2011.

[374] M. Jinek, K. Chylinski, I. Fonfara, M. Hauer, J. A. Doudna, and E. Charpentier, “A Programmable Dual-RNA–Guided DNA Endonuclease in Adaptive Bacterial Immunity,” *Science (80-. ).*, vol. 337, no. 6096, pp. 816–822, 2012.

[375] J. E. Garneau *et al.*, “The CRISPR/Cas bacterial immune system cleaves bacteriophage and plasmid DNA.,” *Nature*, vol. 468, no. 7320, pp. 67–71, 2010.

[376] R. Sapranauskas, G. Gasiunas, C. Fremaux, R. Barrangou, P. Horvath, and V. Siksnys, "The Streptococcus thermophilus CRISPR/Cas system provides immunity in Escherichia coli," *Nucleic Acids Res.*, vol. 39, no. 21, pp. 9275–9282, 2011.

[377] L. A. Marraffini and E. J. Sontheimer, "CRISPR Interference Limits Horizontal Gene Transfer in Staphylococci by Targeting DNA," *Science (80-. ).*, vol. 322, no. 5909, pp. 1843–1845, 2008.

[378] J. R. Brouwer *et al.*, "RNA-Guided Human Genome Engineering via Cas9," *Science (80-. ).*, vol. 339, no. 6121, pp. 823–826, 2013.

[379] W. Y. Hwang *et al.*, "Efficient genome editing in zebrafish using a CRISPR-Cas system.," *Nat. Biotechnol.*, vol. 31, no. 3, pp. 227–229, 2013.

[380] L. Cong *et al.*, "Multiplex Genome Engineering Using CRISPR/Cas Systems," *Science (80-. ).*, vol. 339, no. 6121, pp. 819–823, 2013.

[381] S. M. Storey, T. F. Gibbons, C. V. Williams, R. D. Parr, F. Schroeder, and J. M. Ball, "Full-Length, Glycosylated NSP4 Is Localized to Plasma Membrane Caveolae by a Novel Raft Isolation Technique," *J. Virol.*, vol. 81, no. 11, pp. 5472–5483, 2007.

[382] D. Chen *et al.*, "Par1b Promotes Hepatic-type Lumen Polarity in Madin Darby Canine Kidney Cells via Myosin II- and E-Cadherin–dependent Signaling," *Mol. Biol. Cell*, vol. 18, no. 6, pp. 2203–2215, 2007.

[383] S. Deborde *et al.*, "Clathrin is a key regulator of basolateral polarity," *Nature*, vol. 452, no. 7188, pp. 719–723, 2008.

[384] P. D. Hsu *et al.*, "DNA targeting specificity of RNA-guided Cas9 nucleases," *Nat. Biotechnol.*, vol. 31, no. 9, pp. 827–832, 2013.

[385] J. G. Doench *et al.*, "Optimized sgRNA design to maximize activity and minimize off-target effects of CRISPR-Cas9.," *Nat. Biotechnol.*, vol. 34, no. 2, pp. 184–191, 2016.

[386] I. Behm-Ansmant, I. Kashima, J. Rehwinkel, J. Saulière, N. Wittkopp, and E. Izaurralde, "mRNA quality control: An ancient machinery recognizes and degrades mRNAs with nonsense codons," *FEBS Lett.*, vol. 581, no. 15, pp. 2845–2853, 2007.

[387] J. T. Mendell and H. C. Dietz, "When the Message Goes Awry: Disease- Producing

Mutations that Influence mRNA Content and Performance," *Cell*, vol. 107, no. 4, pp. 411–414, 2001.

[388] A. Kishor, S. E. Fritz, and J. R. Hogg, "Nonsense-mediated mRNA decay: The challenge of telling right from wrong in a complex transcriptome," *Wiley Interdiscip. Rev. RNA*, vol. 10, no. 6, pp. 1–22, 2019.

[389] T. Kurosaki, M. W. Popp, and L. E. Maquat, "Quality and quantity control of gene expression by nonsense-mediated mRNA decay," *Nat. Rev. Mol. Cell Biol.*, vol. 20, no. 7, pp. 406–420, 2019.

[390] S. B. Berger *et al.*, "Cutting Edge: RIP1 Kinase Activity Is Dispensable for Normal Development but Is a Key Regulator of Inflammation in SHARPIN-Deficient Mice," *J. Immunol.*, vol. 192, no. 12, pp. 5476–5480, 2014.

[391] K. Newton *et al.*, "Activity of Protein Kinase RIPK3 Determines Whether Cells Die by Necroptosis or Apoptosis," *Science (80-. ).*, vol. 343, no. 6177, pp. 1357–1360, 2014.

[392] Y. Lin, A. Devin, Y. Rodriguez, and Z. G. Liu, "Cleavage of the death domain kinase RIP by Caspase-8 prompts TNF-induced apoptosis," *Genes Dev.*, vol. 13, no. 19, pp. 2514–2526, 1999.

[393] D. R. Zerbino *et al.*, "Ensembl 2018," *Nucleic Acids Res.*, vol. 46, no. D1, pp. 754–761, 2018.

[394] D. Weng *et al.*, "Caspase-8 and RIP kinases regulate bacteria-induced innate immune responses and cell death," *PNAS*, vol. 111, no. 20, pp. 7391–7396, 2014.

[395] F. K. M. Chan *et al.*, "A Role for Tumor Necrosis Factor Receptor-2 and Receptor-interacting Protein in Programmed Necrosis and Antiviral Responses," *J. Biol. Chem.*, vol. 278, no. 51, pp. 51613–51621, 2003.

[396] S. Feng *et al.*, "Cleavage of RIP3 inactivates its caspase-independent apoptosis pathway by removal of kinase domain," *Cell. Signal.*, vol. 19, no. 10, pp. 2056–2067, 2007.

[397] S. He, Y. Liang, F. Shao, and X. Wang, "Toll-like receptors activate programmed necrosis in macrophages through a receptor-interacting kinase-3-mediated pathway," *PNAS*, vol. 108, no. 50, pp. 20054–20059, 2011.

[398] M. Poreba, K. Groborz, M. Navarro, S. J. Snipas, M. Drag, and G. S. Salvesen, “Caspase selective reagents for diagnosing apoptotic mechanisms,” *Cell Death Differ.*, vol. 26, no. 2, pp. 229–244, 2019.

[399] K. Groborz, M. L. Gonzalez Ramirez, S. J. Snipas, G. S. Salvesen, M. Drąg, and M. Poręba, “Exploring the prime site in caspases as a novel chemical strategy for understanding the mechanisms of cell death: a proof of concept study on necroptosis in cancer cells,” *Cell Death Differ.*, vol. 27, no. 1, pp. 451–465, 2019.

[400] D. E. Root, N. Hacohen, W. C. Hahn, E. S. Lander, and D. M. Sabatini, “Genome-scale loss-of-function screening with a lentiviral RNAi library,” *Nat. Methods*, vol. 3, no. 9, pp. 715–719, 2006.

[401] S. Sharma and E. Petsalaki, “Application of CRISPR-Cas9 based genome-wide screening approaches to study cellular signalling mechanisms,” *Int. J. Mol. Sci.*, vol. 19, no. 4, pp. 1–14, 2018.

[402] L. Franchi *et al.*, “NLRC4-driven production of IL-1β discriminates between pathogenic and commensal bacteria and promotes host intestinal defense,” *Nat. Immunol.*, vol. 13, no. 5, pp. 449–456, 2012.

[403] F. A. Carvalho *et al.*, “Cytosolic flagellin receptor NLRC4 protects mice against mucosal and systemic challenges,” *Nature*, vol. 5, no. 3, pp. 288–298, 2012.

[404] F. Song and K. Stieger, “Optimizing the DNA Donor Template for Homology-Directed Repair of Double-Strand Breaks,” *Mol. Ther. - Nucleic Acids*, vol. 7, pp. 53–60, 2017.

[405] P. R. Vajjhala, R. E. Mirams, and J. M. Hill, “Multiple Binding Sites on the Pyrin Domain of ASC Protein Allow Self-association and Interaction with NLRP3 Protein,” *J. Biol. Chem.*, vol. 287, no. 50, pp. 41732–41743, 2012.

[406] R. C. Coll *et al.*, “MCC950 directly targets the NLRP3 ATP-hydrolysis motif for inflammasome inhibition,” *Nat. Chem. Biol.*, vol. 15, no. 6, pp. 556–559, 2019.

[407] N. Matsunaga, N. Tsuchimori, T. Matsumoto, and M. Ii, “TAK-242 (Resatorvid), a Small-Molecule Inhibitor of Toll-Like Receptor (TLR) 4 Signaling, Binds Selectively to TLR4 and Interferes with Interactions between TLR4 and Its Adaptor Molecules,” *Mol. Pharmacol.*, vol. 79, no. 1, pp. 34–41, Jan. 2011.

[408] L. Eckhart, A. Uthman, W. Sipos, and E. Tschachler, “Genome Sequence Comparison Reveals Independent Inactivation of the Caspase-15 Gene in Different Evolutionary Lineages of Mammals,” *Mol. Biol. Evol.*, vol. 23, no. 11, pp. 2081–2089, 2006.

[409] L. Eckhart *et al.*, “Identification and characterization of a novel mammalian caspase with proapoptotic activity,” *J. Biol. Chem.*, vol. 280, no. 42, pp. 35077–35080, 2005.

[410] H. E. Jacobse-Geels and M. C. Horzinek, “Expression of feline infectious peritonitis coronavirus antigens on the surface of feline macrophage-like cells.,” *J. Gen. Virol.*, vol. 64, no. 9, pp. 1859–1866, 1983.

[411] A. Balint *et al.*, “Molecular Characterization of Feline Infectious Peritonitis Virus Strain DF-2 and Studies of the Role of ORF3abc in Viral Cell Tropism,” *J. Virol.*, vol. 86, no. 11, pp. 6258–6267, 2012.

[412] R. Finley *et al.*, “The risk of *Salmonellae* shedding by dogs fed *Salmonella*-contaminated commerical raw food diets,” *Can. Vet. J.*, vol. 48, no. 1, pp. 69–75, 2007.

# Appendix

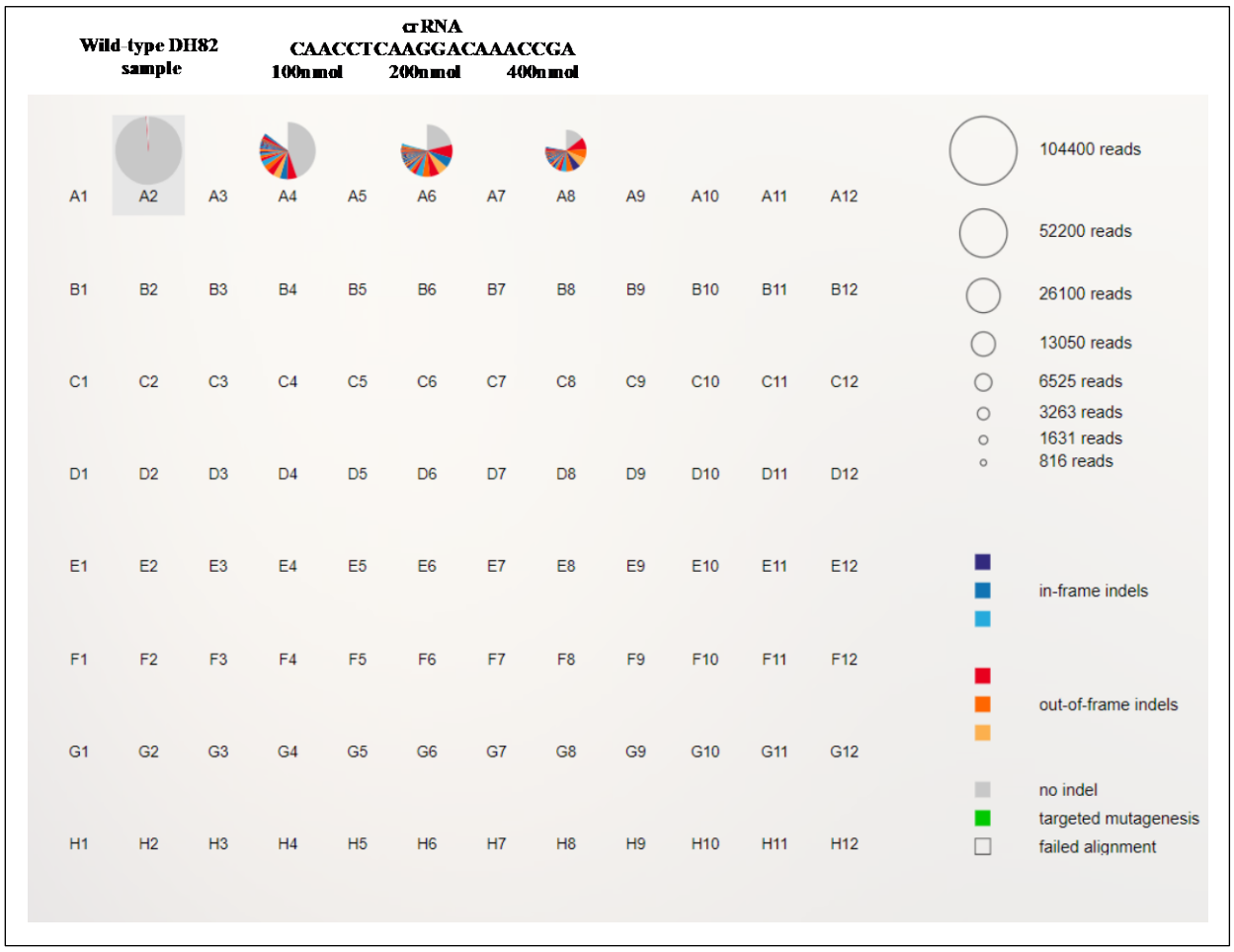


**Appendix 1 Sequencing analysis of bulk-edited DH82 cell populations for indels induced by CAACCTCAAGGACAAACCGA crRNA for the canine caspase-1/4/11 hybrid gene.** DH82 cells were electroporated with RNP complexes at three different concentrations (100, 200 and 400 nmol). CrRNA was designed to be near the catalytic site of the canine hybrid gene. Genotyping using Illumina MiSeq sequencing showed electroporated only wild-type cells did not carry any mutations, while Cas9-edited cells showed a mixture of in-frame and out-of-frame mutations. The size of each pie chart corresponds to the number of reads that were analysed for each sample (see legend in top right corner). Pie areas in the shade of red represents out-of-frame, areas in the shade of blue represents in-frame insertions and deletions, grey areas represent no indel calls (see legend in bottom right corner) while empty wedges show sequences that failed alignment.

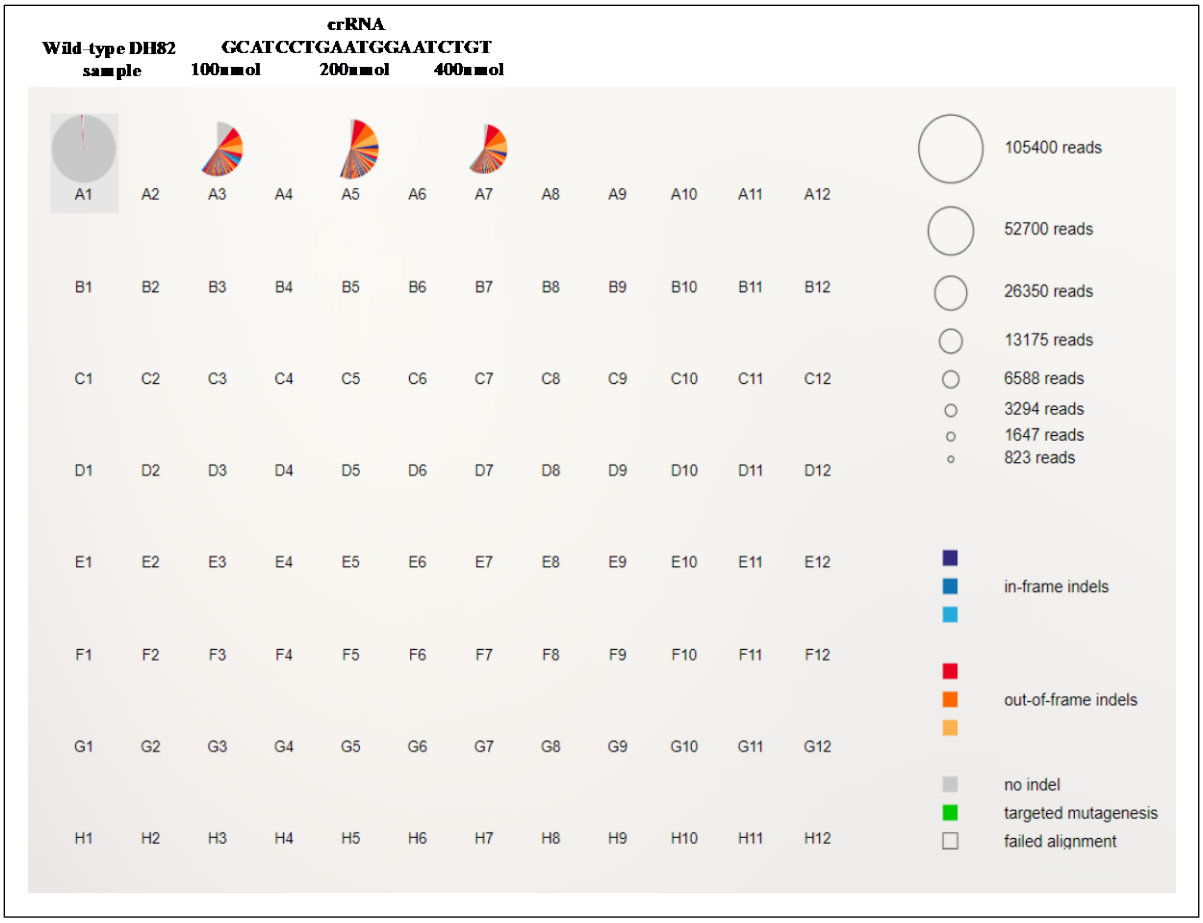


**Appendix 2 Sequencing analysis of bulk-edited DH82 cell populations for indels induced by GCATCCTGAATGGAATCTGT crRNA for the canine caspase-1/4/11 hybrid gene.** DH82 cells were electroporated with RNP complexes at three different concentrations (100, 200 and 400 nmol). CrRNA was designed to be near the catalytic site of the canine hybrid gene. Genotyping using Illumina MiSeq sequencing showed electroporated only wild-type cells did not carry any mutations, while Cas9-edited cells showed a mixture of in-frame and out-of-frame mutations. The size of each pie chart corresponds to the number of reads that were analysed for each sample (see legend in top right corner). Pie areas in the shade of red represents out-of-frame, areas in the shade of blue represents in-frame insertions and deletions, grey areas represent no indel calls (see legend in bottom right corner) while empty wedges show sequences that failed alignment.

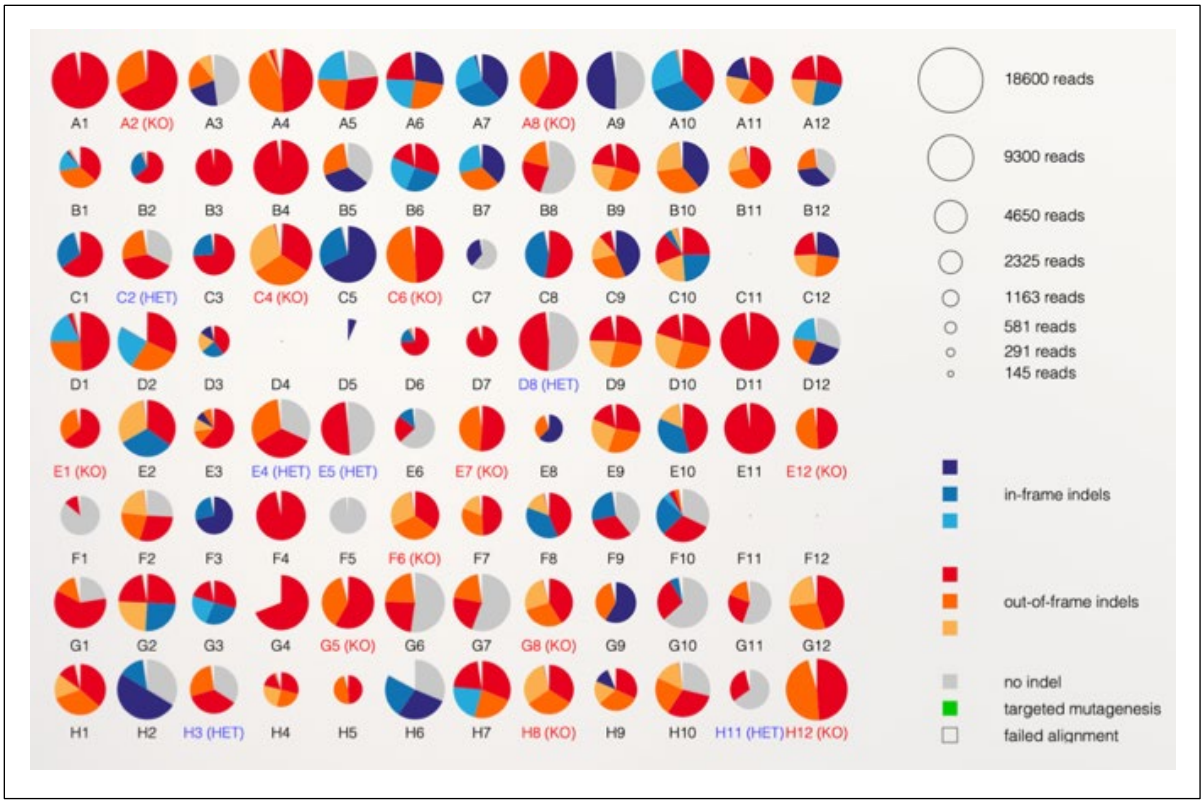


**Appendix 3 OutKnocker analysis of 96 DH82 single cell colonies electroporated with CRISPR crRNA targeting the canine caspase-1/4/11 hybrid gene.** DH82 cells were electroporated with CRISPR crRNA GCATCCTGAATGGAATCTGT to target the canine hybrid caspase-1/4/11 gene. Following limiting dilution, up to 96 single cell colonies were selected and genotyped using Illumina MiSeq sequencing. Sequencing results were analysed using OutKnocker online analysis tool. Each pie chart represents a single colony, whereas the size of each pie chart corresponds to the number of reads that were analysed for each colony (see legend in top right corner). Pie areas in the shade of red represents out-of-frame, areas in the shade of blue represents in-frame insertions and deletions, while grey areas represent no indel calls (see legend in bottom right corner). Colony positions in red letters highlight knock-out colonies, while blue letters highlight heterozygous colonies for the canine caspase-1/4/11 hybrid gene.

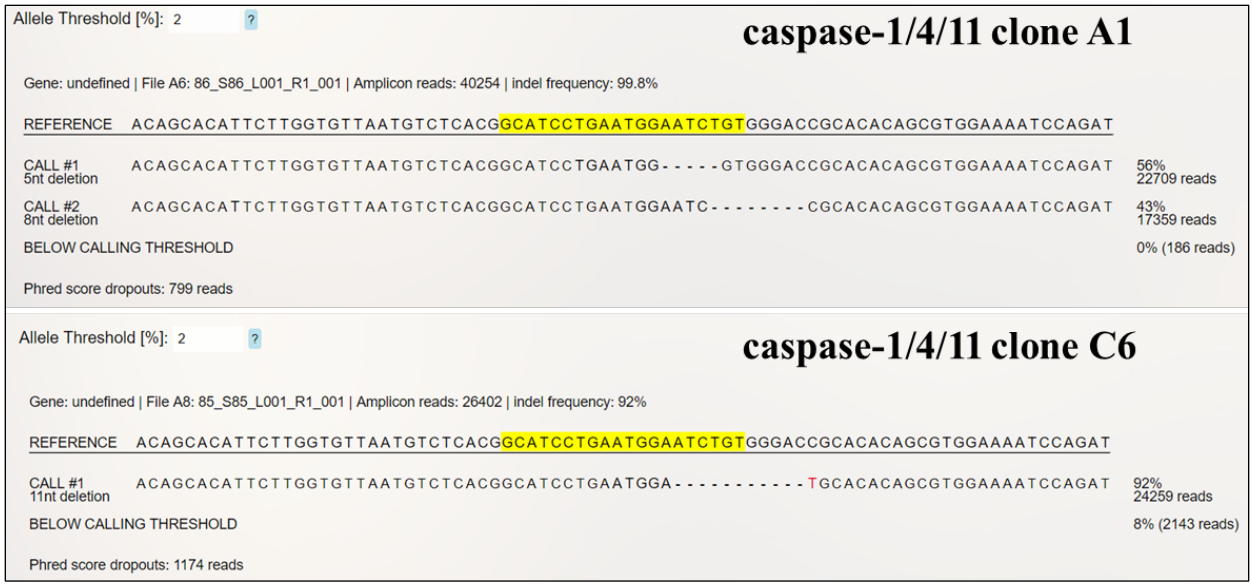


**Appendix 4 Illumina MiSeq sequencing confirmed genotypes of caspase-1/4/11 knock-out clones A1 and C6.** DH82 cells were electroporated with CRISPR crRNA GCATCCTGAATGGAATCTGT to target the canine hybrid caspase-1/4/11 gene near the catalytic site. Following limiting dilution, up to 96 single cell colonies were selected and genotyped using Illumina MiSeq sequencing. Two colonies, A1 and C6 were chosen for subsequent phenotypic characterisation. DNA extraction and genotyping using Illumina MiSeq sequencing were repeated on a subset of cells for each clone. Information displayed by the analysis software includes the file name, number of amplicon reads and indel frequency. The underscored nucleotide sequence represents the wild-type reference sequence, while nucleotides highlighted in yellow show CRISPR crRNA target sites. Information including total percentage and total number of reads corresponding to each identified indel are shown underneath the reference sequence. Nucleotides shown in smaller font sizes are less confident calls based on the sequencing data, while deleted nucleotides have been replaced by hyphens. The software also provides information on the percentage and total number of reads that could not be aligned to the reference sequence and the number of reads that were excluded from analysis (Phred score dropouts).

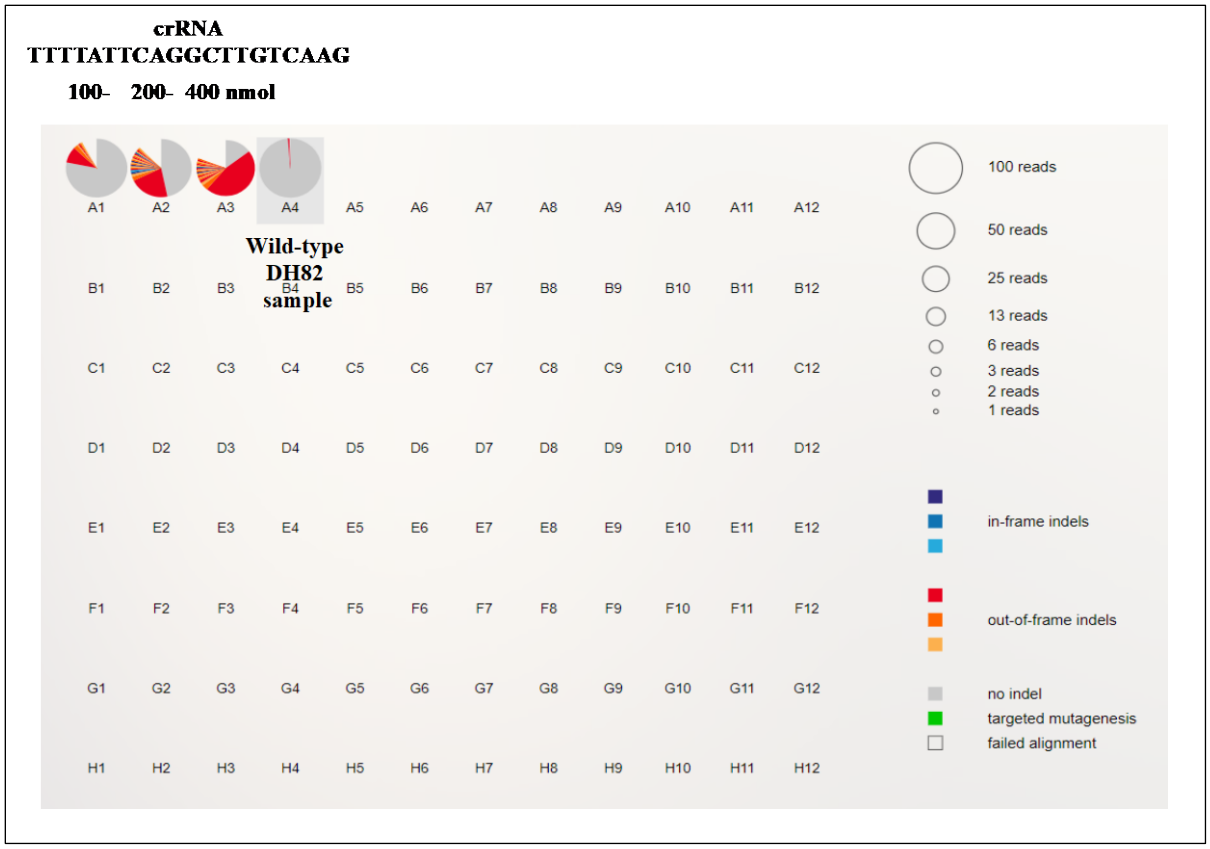


**Appendix 5 Sequencing analysis of indels induced by TTTTATTCAGGCTTGTCAAG crRNA for the canine caspase-8 gene.** DH82 cells were electroporated with RNP complexes at three different concentrations (100, 200 and 400 nmol). CrRNA was designed to be near the catalytic site of the canine caspase-8 gene. Genotyping using Illumina MiSeq sequencing showed electroporated only wild-type cells did not carry any mutations, while Cas9-edited cells showed a mixture of in-frame and out-of-frame mutations. The size of each pie chart corresponds to the number of reads that were analysed for each sample (see legend in top right corner). Pie areas in the shade of red represents out-of-frame, areas in the shade of blue represents in-frame insertions and deletions, grey areas represent no indel calls (see legend in bottom right corner) while empty wedges show sequences that failed alignment.

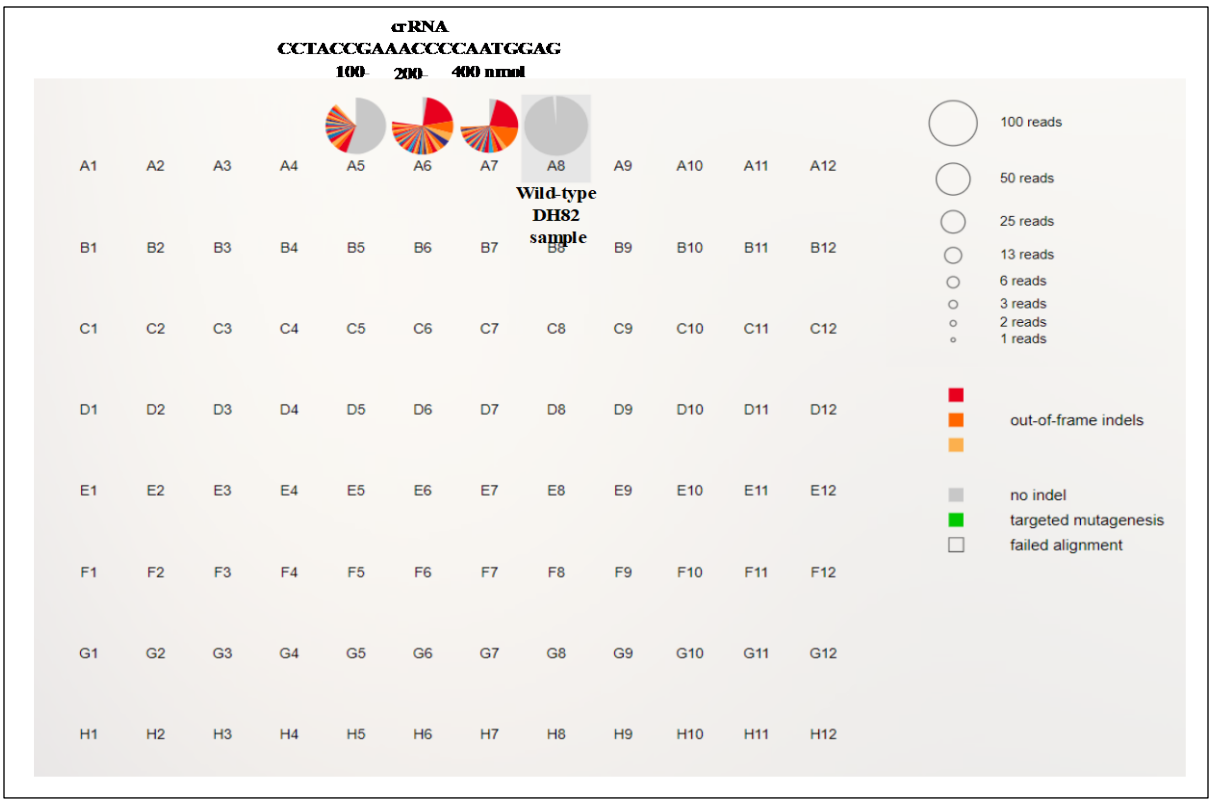


**Appendix 6 Sequencing analysis of indels induced by CCTACCGAAACCCCAATGGAG crRNA for the canine caspase-8 gene.** DH82 cells were electroporated with RNP complexes at three different concentrations (100, 200 and 400 nmol). CrRNA was designed to be near the catalytic site of the canine caspase-8 gene. Genotyping using Illumina MiSeq sequencing showed electroporated only wild-type cells did not carry any mutations, while Cas9-edited cells showed a mixture of in-frame and out-of-frame mutations. The size of each pie chart corresponds to the number of reads that were analysed for each sample (see legend in top right corner). Pie areas in the shade of red represents out-of-frame, areas in the shade of blue represents in-frame insertions and deletions, grey areas represent no indel calls (see legend in bottom right corner) while empty wedges show sequences that failed alignment.


**Appendix 7 List of indels identified by sequence analysis in CRISPR-Cas9 edited DH82 cells for caspase-8 gene using crRNA TTTTATTCAGGCTTGTCAAG.** DH82 cells were electroporated with RNP complexes at three different concentrations (100-, 200- and 400nmol). CrRNA was designed to be near the identified catalytic residue of the canine caspase-8 gene. The analysis detected amplicon reads corresponding to wild-type sequences only in the non-electroporated wild-type control. Cas9 edited cells exhibited a mixture of in-frame and out-of-frame mutations. These results gave an indication on the type, position, percentage and the number of reads identified for the mutations occurred in the bulk edited population.

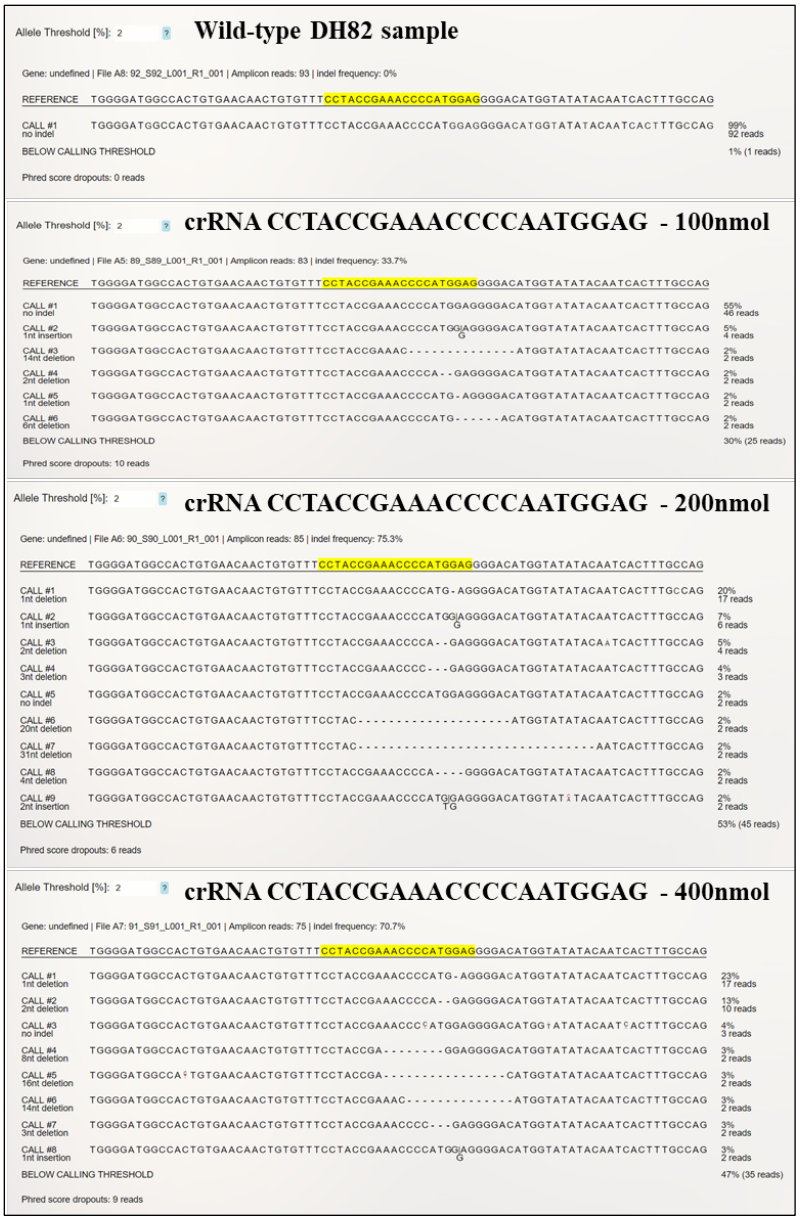


**Appendix 8 List of indels identified by sequence analysis in CRISPR-Cas9 edited DH82 cells for caspase-8 gene using crRNA TTTTATTCAGGCTTGTCAAG.** DH82 cells were electroporated with RNP complexes at three different concentrations (100-, 200- and 400nmol). CrRNA was designed to be near the identified catalytic residue of the canine caspase-8 gene. The analysis detected amplicon reads corresponding to wild-type sequences only in the non-electroporated wild-type control. Cas9 edited cells exhibited a mixture of in-frame and out-of-frame mutations. These results gave an indication on the type, position, percentage and the number of reads identified for the mutations occurred in the bulk edited population.

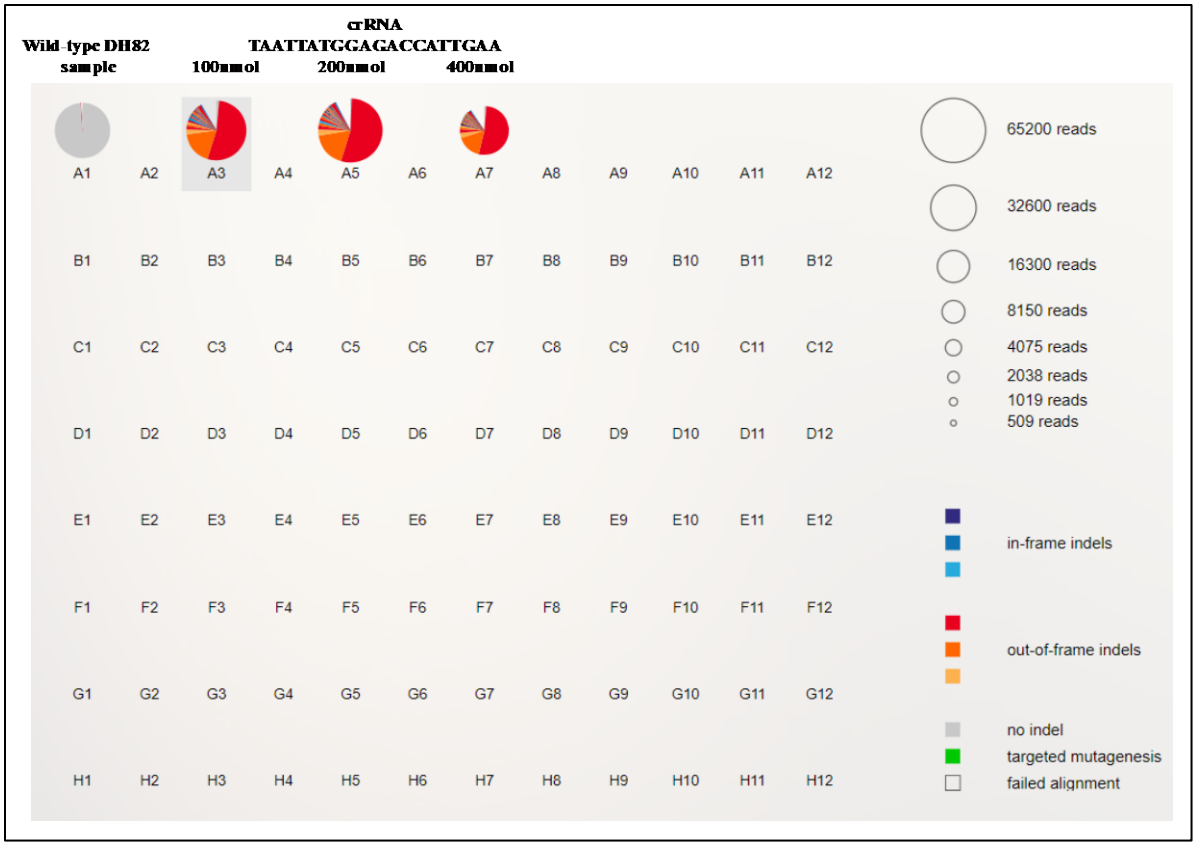


**Appendix 9 Sequencing analysis of indels induced by TAATTATGGAGACCATTGAA crRNA for the canine *RIPK1* gene.** DH82 cells were electroporated with RNP complexes at three different concentrations (100, 200 and 400 nmol). CrRNA was designed to be near the catalytic site of the canine *RIPK1* gene. Genotyping using Illumina MiSeq sequencing showed electroporated only wild-type cells did not carry any mutations, while Cas9-edited cells showed a mixture of in-frame and out-of-frame mutations. The size of each pie chart corresponds to the number of reads that were analysed for each sample (see legend in top right corner). Pie areas in the shade of red represents out-of-frame, areas in the shade of blue represents in-frame insertions and deletions, grey areas represent no indel calls (see legend in bottom right corner) while empty wedges show sequences that failed alignment.

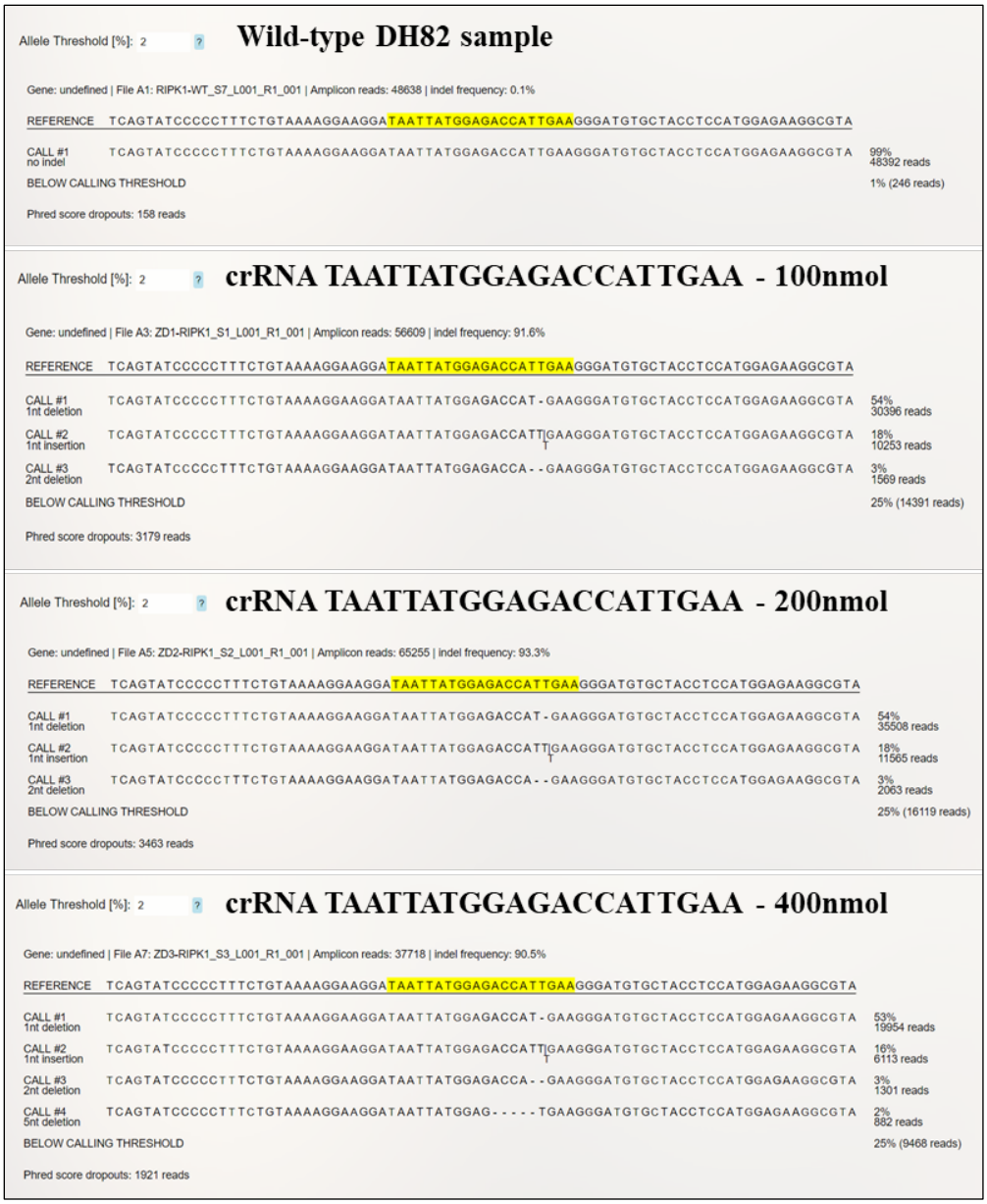


**Appendix 10 List of indels identified by sequence analysis in CRISPR-Cas9 edited DH82 cells for *RIPK1* gene using crRNA TAATTATGGAGACCATTGAA.** DH82 cells were electroporated with RNP complexes at three different concentrations (100, 200 and 400 nmol). CrRNA was designed to be near the catalytic site of the canine *RIPK1* gene. Electroporated only wild-type DH82 cells yielded amplicon reads that matched exclusively the wild-type sequence, while Cas9 edited cells yielded amplicon reads that contained a mixture of in-frame and out-of-frame mutations. These results are indicative of the type, position, percentage and number of reads associated with each mutation present in the bulk edited population. The underscored nucleotide

sequence represents the wild-type reference sequence, while nucleotides highlighted in yellow show CRISPR crRNA target site. Information including total percentage and total number of reads corresponding to each identified indel are shown underneath the reference sequence. Nucleotides shown in smaller font sizes are less confident calls based on the sequencing data, while nucleotides replaced with hyphens represents the position of nucleotides deleted by CRISPR Cas9. The software also provides information on the percentage and total number of reads that could not be aligned to the reference sequence and the number of reads that were excluded from analysis (Phred score dropouts).

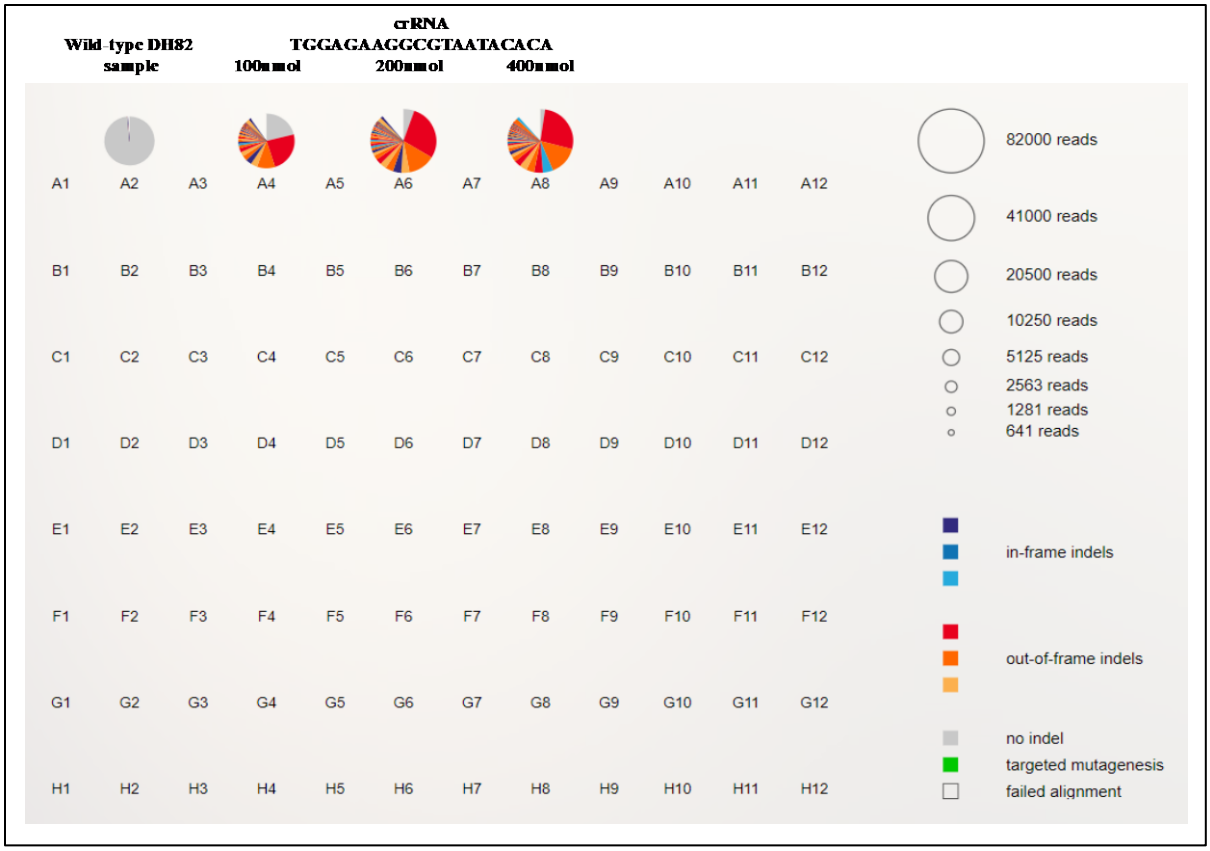


**Appendix 11 Sequencing analysis of indels induced by TGGAGAAGGCGTAATACACA crRNA for the canine *RIPK1* gene.** DH82 cells were electroporated with RNP complexes at three different concentrations (100, 200 and 400 nmol). CrRNA was designed to be near the catalytic site of the canine *RIPK1* gene. Genotyping using Illumina MiSeq sequencing showed electroporated only wild-type cells did not carry any mutations, while Cas9-edited cells showed a mixture of in-frame and out-of-frame mutations. The size of each pie chart corresponds to the number of reads that were analysed for each sample (see legend in top right corner). Pie areas in the shade of red represents out-of-frame, areas in the shade of blue represents in-frame insertions and deletions, grey areas represent no indel calls (see legend in bottom right corner) while empty wedges show sequences that failed alignment.


**Appendix 12 List of indels identified by sequence analysis in CRISPR-Cas9 edited DH82 cells for *RIPK1* gene using crRNA TGGAGAAGGCGTAATACACA.** DH82 cells were electroporated with RNP complexes at three different concentrations (100, 200 and 400 nmol).

CrRNA was designed to be near the catalytic site of the canine *RIPK1* gene. Electroporated only wild-type DH82 cells yielded amplicon reads that matched exclusively the wild-type sequence, while Cas9 edited cells yielded amplicon reads that contained a mixture of in-frame and out-of-frame mutations. These results are indicative of the type, position, percentage and number of reads associated with each mutation present in the bulk edited population. The underscored nucleotide sequence represents the wild-type reference sequence, while nucleotides highlighted in yellow show CRISPR crRNA target site. Information including total percentage and total number of reads corresponding to each identified indel are shown underneath the reference sequence. Nucleotides shown in smaller font sizes are less confident calls based on the sequencing data, while nucleotides replaced with hyphens represents the position of nucleotides deleted by CRISPR Cas9. The software also provides information on the percentage and total number of reads that could not be aligned to the reference sequence and the number of reads that were excluded from analysis (Phred score dropouts).

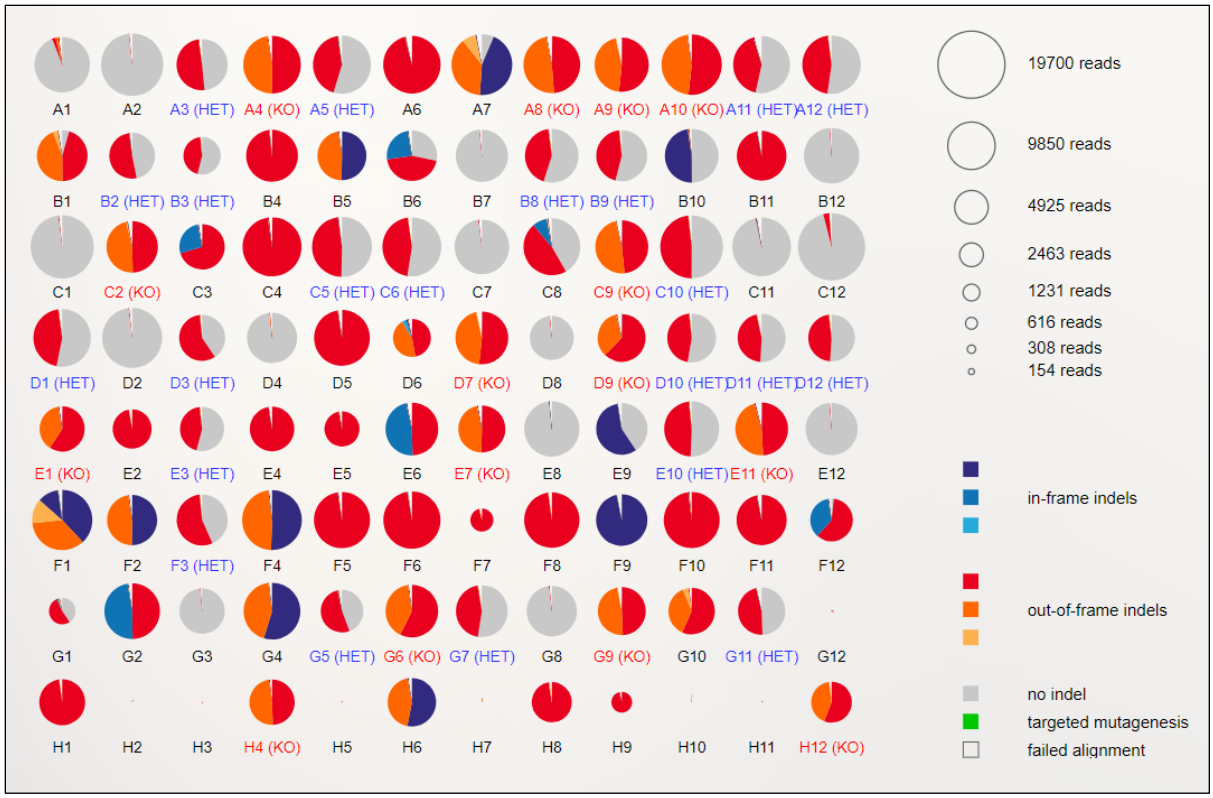


**Appendix 13 Illumina MiSeq sequencing identified knock-out cell clones for the canine *RIPK1* gene.** Limiting dilution of bulk-edited cells generated using crRNA GCATCCTGAATGGAATCTGT were carried out. Following limiting dilution, up to 96 colonies each originating from a single cell were selected and genotyped using Illumina MiSeq sequencing. Sequencing results were analysed using OutKnocker online analysis tool. Each pie chart represents a single colony, whereas the size of each pie chart corresponds to the number of reads that were analysed for each colony (see legend in top right corner). Pie areas in the shade of red represents out-of-frame, areas in the shade of blue represents in-frame insertions and deletions, while grey areas represent no indel calls (see legend in bottom right corner). Colony positions in red letters highlight knock-out colonies, while blue letters highlight heterozygous colonies for the canine *RIPK1* gene.

AGTGTTGATCTAAATTTAACAAGGTTGGTTTCTTGAAAGGACTAAGAAAAGCAATTAGA
AACTGTCATATGTCATACATAAAGTAGATAATGAATTAAGCAAGGCTGTTCATTCAATC
TTTTCATACAGATTTATCCAATAATGAATACAACCACTCGTACACGTCTTGCCCTCATTA
TCTGCAACACAGAGTTTCAACATCTTTCTCCGAGGGTTGGAGCTCAAGTTGACCTCAGA
GAAATGAAGTTGCTGCTGGAGGATCTGGGGTATACCGTGAAAGTGAAAGAAAATCTCA
CAGCTCTGGTAAAACTTCTCAAGATATAGAAAGTGTCCATGTCTTTCTTCCCCTTAGAAA
ATGCTAGAAGAGATGTTACAGAAGCCTTGCTAGTTCTGTACTGGTGATATTCTGTGGTGA
CTAACCGATAATATTAGACATGGCTGTCAAATTCAAACATGGTTTAGCCATGTAACATC
CAATTGCAAAATATTTCTATCAACTCAATAATCTCAGGATGAGATTATAAAGTTTTATAT
AAAAACTTGCTTTATATAAAATTAAAAATTAGAAATTTTCATTTCCATGTCACTGACTTT
TGTGTATTTATTCAAGGACTCCTTTTACTGTCCTTAGAGAAGTCAAAGTGTAAAATCACT
GGTCTTGTCTCTTATAGGAGATGGTGAAAGAGGTGAAAGAATTTGCTGCCTGCCCAGAG
CACAAGACTTCTGACAGTACTTTCCTTGTATTCATGTCTCATGGTATCCAGGAGGGAATA
TGTGGGACCACATACTCTAATGAAGTTTCAGATATTTTAAAGGTTGACACAATCTTTCAG
ATGATGAACACTTTGAAGTGCCCAAGCTTGAAAGACAAGCCCAAGGTGATCATTATTCA
GGCATGCCGTGGAGGTAAGTGCTGATGGTTTAAAATAACAGGGCATTCCCATTGAGACT
TTATCATTTATAGATAGAGAGTACTCTTCAGTGTTTGGGGTTGATTCCTGAATATCAAAC
ATCTATTTTACCACTCATATATCCTGTGGATTTTATTTCAAACTGGTAAATATTTGCTTCA
TTTTCCACTAAAGAATATCACTATTAATAGTCAATACATTGATCTTTTGGTACTATTGGA
AAAATTATTAAGGGAAAAAAATTTTTGAGACATGGCTTATAACAAATATTTTATACACA
TGTGTATTTTCATATTATAAATAAAAGACAGACTAATATGTTTAGAAATAGAGTTTAAG
AGAATTTCAAGACAGCAATAATTCCCTTGGAAATTGTTAGTAATATGAAATCATCTTTGA
ATTTCAAGAGAAACAAGGAGTGGTGTTGTTAAAAGATTCAGTAAGAGACTCTGAAGAG
GATTTCTTAACGGATGCAATTTTTGAAGATGATGGCATTAAGAAGGCCCATATAGAGAA
AGATTTTATTGCTTTCTGCTCTTCAACACCAGGTAAACAGTTTTTATACAGGTCACTTTTC
TCTCTGTTATTGTTAGAAAGAAGGACTCTATACATTGCATTATGCATTACATAAGACTCttt
ttaatttatatttattttgtttatttagaagttattatttttattagatattttctttatttacatttcaaatattatccctttttctggtttcccctcccaaagccccctat
cctctccctccttcccctgcttaccaacccacccactcctgcttattggccctggcatttcccttcactggagcatagagctttcacagtaccaagggc
ctctcctcccactgatgacctactaggccatcctctgctatataagcaactggagccatgagtcccaccatgtgtactttggttggtggtttagtctctg
ggagctctggaggtactggttggttcatattgttgttcctcctatggggcttgaaacccccttcaactccttCAGTCTTCTTTTGTTTCCT
GAACTTTCCATTTTTTGAGGCCTACATTCTTTTACTCAAATATATCCTTAAGGCCTTGCAT
CTAATTAAATAGCTTACAAATTATATTACTGAATATGGTTACACGTTTCAGATATAGCCT
ACACCTATATTGGGTAAACCATGCCTTGATGTATATCTCACTACATTTTTTTCTCCAATG

ATAAAAATCACAATGGCTCTTGATATATTCTCAGACCATAGAGCCTTACTGAACTATTGG
CTACTGATAAATTCTGGCACATGGATAATCATATGAAGAAATATACCAATTAGTAAGCC
CATAAGACTATTGTTACATAGTTTATCCTCGTGGTCACTCTGACATTCTTAATTATACTCA
GTGAATCACTAAAAATACAACAGACATGCATACAGTAAAGAGACATATAAGGGAGAAG
GGTTTGTTAATGAGTGTAAGGATATTAGAGAACAAGTCATAAACATTTTACAAAAGAAA
GAAATTGAAATTTAACTTAAAAATACCACTCCAAAGCACCCACAGGTTTCTAGCTTAAG
AATGCAGCCAGCTTTATTATTAGACTTAACTGTTCCTTTAAATCATTTCCTTTTGTCTTGT
ACCATATATAGATCTCTAGATCTCCAATTCTAGAGTCTTCTGAACTCTTGCAGTCCACCA
TCTGAATTCTGTCACCCTTTCTTTTGCCTTCTTCACTATTCATTATAAGTGAATCAGACTC
TACTCTTCCACTACCAAGCCTGTATAAACTCCAACCATATTAGGACTTTTAAAAAAATAA
CCTGTACTTTCAATGTGCAAAGTGCTTTCAGAAACACCTGCCTCTACTTTTTCCATTTATT
TTCTTTATCTTACTCCGATATCTGTGGTGTGCCATCTCTTCTTCAAGTATCTCTTTTAGTA
GACATAATTATCTTCATCTTATAGTTAAGAACATTGCATTTAAAAATGTACAATGAACTT
CTATCACAGTCATTATATTGAACCCTAGAGTCACACACTCAGATTTTTATTCTCCCAAAC
TTAATAACATTATCTTCTGTAGTCAGCCTAATTTTCTATTAGATTTTTACCTTCTTGAAAT
CAGAAGATACACTGTCTTAATATCTGTATTTTTACAACAACCATCTTTAGTAAGAGGGAA
AATATACTCATTGAATTTTGTATACACTGAAAAAATAGCAGGCAGAATATAGAATAGAG
TATAAGCTCTATAATCTGTCCACCTAGAGTGGAAAGGCTAGATCTGTATCAAGGGTTAG
GTCTATCCTAATATTTGGAATGTAATTTATTCTCAGATAATGTGTCTTGGAGACATCCTG
TCAGGGGCTCACTTTTCATTGAGTCACTCATCAAACACATGAAAGAATATGCCTGGTCTT
GTGACTTGGAGGACATTTTCAGAAAGGTGGGGTTCTATATGCTTTATCAATTCTATTTTA
TTGGTCTTTAGCTCTTCAAACTGCTTCTAATGGTAAAGTTCATATTGTCatttttataaaaagaatattt
atttatttatttatttatttattGGTTAGTCAACAATCCATACATGGTGTCAATGTTTTATAATCAGAAACC
TTAAGAAATAATCATATATATTAATATATATCTTTACCTTGGTAGAATATGGAGCAGATT
CTAATATCCCTGGGCCCATCATATTTGTCAGCTACAGAAAGAAAGTTTAATAATCTGGC
AAATATTCTCATAACTTTTGTTTTTATAAGTGCCATGAGTTATTGTTTCATTGTTTATTGT
CATGCTAGTCAATGCAGTCTTTGTCCATCTTGATTCGAGATCCTACTCTCTGAAAATTAT
GGCTATAAACCTTCCTTTTACTTCTAGGTTCGATTTTCATTTGAACAACCAGAATTTAGG
CTACAGATGCCCACTGCTGATAGGGTGACCCTGACAAAACGTTTCTACCTCTTCCCGGG
ACATTAAACGAAGTATGTCATACCAATGCctttgtacacttgtgtgtgtatacgtgtgtgtgtgtgtgtgtgtgtgtg
cagtAGGGGGAGGTTGGATGAAGACCACTGAAGTATAGTAAACAACTGATCCTGATCCAA
GTTTCTACATTTGGTATATTATATAGAGAAATCAGGAACAGACTGAAGGGACTGCTTGT
TTTCTTAATATTCTCAGATTTTGTGGTTGGTCCTATCTCAGGTTGGCTGCTATGAGACAA

AATTTTAAGAGGCTCTATATGTCTATATTTTATCTTAGTAAGATAAACACTTACACATGC
CTTGGGCTCTTCTCTGTTGTGAGTGTATATACCAGCATTACAGTGTTGTGCACTGATCTC
AGAAGAATGCTTATGTTTTTGTAATTTCTCTTTCTCATAGGAATCCAGTTCATTCTTATGT
ACCTATGCTGAGAATCGTGCCAATAAGAAGCCAATACTTCCTTAGATGATGCAATAAAT
ATTAAAATAAAACAAAACAGAAAGGCTATCCTGTTTGTTGTTTCTGTTGCGACCTTATTT
TCCTTTATTTGACTTGACTTTCAGACAGAACACAAGAAGAGTAACTCATGTCTTTATTAT
TGTATTTATTTGTAAAAATTTTACACATGTGTAAAATGCATTCTGATTACTATAACCTCA
CACACTCTGTAGTACTCTTCTATTCCTACAATTATTCTCCTCTGTACAATTCCTATTCAAA
CACCTATATCttttttgtttgtttgttttGAGACCCACTGAGTTTAACCAGAATTCACAGTGTAACCAT
GGAGTGTCCACTGGAGCCTGGTATACACCAAAGACTGTCTCTCTCCCAGAATCCCTCAG
TAGCCAGAGCATCAGCAGAGTTCTTAGACTTGGTTCTTAAATGCAGAACTGGCTGAGTG
CCATTATTTCTTTTATAATATCATTTGCTTGTCTTTTCCTACAGTCATATAGACACCACAG
GTTTCTGAATTCCAAGAATTTAGTGCTCAGAAGAAGAAACATATAAAATATAACTGGGA
CCATTATAGCCAAAATAATAAATGGAATCTCAAAATGGAGTGTTTACTTATTACTCTGG
AAGCCTGGACCAGAACAAAGCAATTTTTATGTGCTATTATCCttcatggattaaaaaattcatggatcaaag
aatATTGACTTAGCCCATGAACCTTAAAATTTCACATTCTGATTGAGACTATAAAACAGTC
AGTGCCACCAACAACCAGGGAACAATTACCAGATAAGTATGACACTGAGGAGATGGGC
GATAGTGGCATTACTTTATCCATTCTCTCAGCAGTATTTGTTAACTGTAGGAGGAGCTGA
AGAAGGACACTTTCACAAGAGCCTTTCTAATCCTTCCTATTTAATCCAACGTTCCCCAAA
GACTCAAAGTTGAACACACCACAGCATTTGTCTTTTCCCCTTTCTCTAACCATTCCCCTG
ACATACCTCTCTCCTCAGATCATGTGATCATGCATTCATTATATTGCACCGTGCAAGTGC
CCCTATTTGTTCAAGAGGCTACGAACAGGTAGTAGTAATCATCACTCTCAGTAAAAATTT
GTCTTGCACAATTAATGAAATGCACCCAGGGTGGACAAAAGGATTGCTCTGAACTATGT
CTAATAAAAACGAAGTCTGTAGAAATATGTATAGAAAGGCTGTAGTACCTTGAATTAGG
AAACAATTGCTTAATTTTCCAGTAGAAATGAATATGTTAAATTTCATTGACTTAGAACTG
ATGTTTTAGAAAGCAGAGGTTGAGTTACTGAGAAGCCAGACTAGAATATAAGCAGCACT
GTGTCTTACTGGAGCCCTGAAGAATAGAGAAAATGCAAAGGTAAACAACTTCAAttttttttttt
ctatttttGCAGCCGCTTTAGTTGTGTTTGTTTGTTCCCATGACGAAGTGATAAAATTCAGGAA
AAGGGAGGCCAGTTTTATGAGTTACAGGGGATTTCCCCACAGCAGTTGATACTTTCTGA
GCAGCTCTTTCAACATCTCCTGGAAGTCCCCGCCTCCCTATGCTAAGGAAATGCCCAGTA
ACTTTCATTTTACTCTGTCAAGCTGTCTTCACGGTGCGAAAGAACTGAGGCTTTTTCTCA
TGGCTGGTGAGTCTGGGGGCTCTTCCTGAATAGGGGCTTTGACTTGAGTCCTAGAATTTA
GACTTTGCGAAAGCAGAGAATTaaaaaaaaaaaaTAGTGGTGACAGAGCAGAGCAGTGGCATA

AAAGCCTGATTACTGTACTGCCGGAAAGGACTGTTTATTGGGAGTGTGGACATGCTGAG
ATATATGTAGCTTTGAGCCACAAAGAACTTCATCTCTCAGTTTCCTTTTTGGAAATCAAA
GAGGAGGGTAAAGCCAGAATAACACATTAAAACAactctagaagtctgtatgagctctaggactctagaagtctg
taatgagctctagaactctagaagtctgtatgagctctaggactctagaagtctgtaatgagctctaggactctagaagtctgtaatgagctctaggac
tctagaagtctgtaatgagctctagaactctagaagtctgtaatgagctctaggactctagaagtctgtaatgagctctaggactctagaagtctgtaa
tgagctctaggactGTTACATTTTTCTGAGATGCTGATTGGCACATATTTGAAGTCACCACCTATT
TCCCAAGCATAGAGTTACTCTCTTCTTCCATTTTAAATGATTCCATTTTTCTTGCTAGATC
TCTGCGTCTGCTAAAATCACCACTGTTGTAACTCATTCATGGACTCCTGTCACAATGTTT
TGACTCATGTCTTCCTTTCCAGGTCTTAGCCTTCTGTTCTATCCTTAACATTCCTTTCAAA
TCATATACCCTTCTTACACTCAGAAGCTGAAAAGGCACAGGACTGAGAAATCACTTGGT
ATTTTGGTAGCAAGTGTTCAAATGCATCTTATAATATTTTTAGCTTTATTCTTAAAATGTG
TACGTGAGGATGAACAAAAAAGTTGTATTTGTCAGCTTAGGTCCAATGTCCTTTGGGCA
GAGTAAACTTGTTCTCACATGCAAGACACCGACTTTACCTTATCTCTCTGCAAAAGTCTT
TTAAAAACGACAAGCGTCTGATCATTGCCTTTTCTGCTGCTGTTGCCCACATTTGACCAA
AGTAACCTGTTTCTAACACCCAGCCCCTCCACCTTGCTGTCTATACCAGATACTTTCAAG
AAACTTTCAACCTTGCCAGAACAGATACTAGCTCTACACACTATCTTCTCTGGGACACTG
TCTTTTAATGGATGAAAGTTTTAAAACATGATGTTTTCTTGAACATACATCAGTCATTTA
AATGATTATAGTGTCTTGTACTTTGTTTGTTTGAATAACTATTTTTACCTCTGCCCTATAT
ACTTTAGTGTACAGAGATTGATGTTCAAAATGATATTCCCAAAACTAAAAAATTAGAAT
TTAAAATGAGATGTTTAATAAAAATTGCTGACTCAGGGGAAAGATAATCACACCTCAAT
TTGATATCTTCAATGTGCAATATTTCTTGTTTAGTATGCCAAACCTACCTTGTTTATGTtcta
tatacttcatcactaggagtcctcactagggtagtcttaactcatagattccaggaaatttccactacactagatttccacatcacccctgcctaaatacc
ctttaaatccaataatttcttcctgtacccccacccctccgttattctagccctatacctaatcccattgcccattgccatatacccattgccaccctcccct
agtccacttgcaaaatctatatccccttcccaaggagatcaatgcatcctctctagggtcctccttgttacttattctctctgggtttgtgggttgtagctta
attatcttttactagacatgcaatatccacttataagtgaatacataccatgtttgtctttctgggtctgagtagcctcattcaggatgataatttccagttcc
atccatttttatgcaaatttcatgatgttaccatttttttaactgctgagaaatgcttcattgtgtatatacacaatattttctgtatccattctttagttcagggac
atcaaggttgtttccagtttctgactgttatgtataaagctgctatgagcatagttgagcaagtgtccctatgataagatggaaagttctataggtttatcc
tcaagagtcatacagctagatattaggtagatcaattcccaattttctgagaaaccaccatattgattttcatattgactatataaacttATGGCAT
TATAATTATGCTcattctcttagacatcagatgatatcttactgtggctttaatattcatttcctgattattcaaattactgtttttgtgtttctttgta
catatatattggctacctgtgtttttctgtgaatttgtctgttcagttcctgtctctatgttcttactcggttttcttgctattaaggctattaataggttgcctctc
ttacataatcaaggtattagcttctcagattgcaaatctgttcttcaattctacaagctgtgtgttctttcattgtttcctttggttccagctgggttgcttgttg
tgaggaatattcaaaaagaatggcatcctcccatactatacccagctactctctgcccaggtgggctggccatgaactggtgggcagtggccgacc
tgttcttatctcatggagactctgattcatagctccaaaatgtctccacccacctctctaagtttccacttgcaggtcattatcatgccagccccatgcttc

aaaatctccacggccttttatggtgcacatctggcaaacccacactcgttgaaccatgaaggaaaacagcatacaaatttagttcagaaacaatggt
aattcaatcactgggtacagttagaatcctaatcttgtaagccatgttaaatctaagtcctctggtggtgaaccctggcagatctgccatagaaaccgg
gagactttagcagttatatcttgtcctctcctatccctgatctctctcctgcttcctcttttcctccatccacccaggaattccctttttttcattggggaaacat
ttacaagaagtcacatgagtaaatgattcattcctattccataaaaccccttctgggaaagcagaagtaacatcaaaatacaggcagcaccagggcc
atggacaactgttgctttgaatttgctcatttatttgttgtttacattgatttatattaaatattcttacctgctttaaggtcattagggtaaaaatcattacaca
gagtaatgtaaatggaaattctctctgtgtttttctggtgttaaataattactggtctaaactttaattattgaggtacttttttgtttgatctgagatatagaact
aatttcattttctacaaatatatccataatagtatttattaaagaggcaatctttAAAGATGGCAGGTTTACAGTGTTTTGATT
GAAAAGTAATTCCACTCTATCATGTGGGATTTCATGTTTGCTTCTCTGTCGGCCTCACTC
CACTTTGATTATTTTAGCCTTGTAGTTACATAATCTGTTTTGCCTTCATGTTTAAAGGTTG
ATTTGTGATTATAACAAAATTTTGTCATTTTTCAATTTCTTTTTCTCCCTACAATCTAGTA
TATCCATCTTTGCTTCCTTACCCTTCCTCATGATCTAAATCTTCTTGTTTTCTCTCAAACTC
ATAGCCTCTTTTTTATAATAATTTCTGTTATACATATATTTATTTCAAGTTTTACAATGTG
GTATGGAGTGaattttaagttttcttacaacttttattaaaatgaagcttgaatgttgatagagatttcattgaaattatagtttgttttaaatacttct
gttcaacaaacacagggtatcattctatttatacataatatttcatttcttttctaatatggattagttttaatggtatacatctttcactttcttggccaaattca
ttcttgtgcaatttttttgtaggtacttttagtggaatttatttttttagttacttttcagacacttAATACCATAGAACAGGTAGCATTT
CTATGTTGAATATTTTTGTAATTTTATTGAAAAGATTTCATACAATATTTTCTAATCAATG
TTTCCATTGCTTCAATCTCTACTTAACCACCTACTCAACTCCATGCTCAtcttctctcacttttttgtctctc
tctctctgtctctcttttctctctttctcgaactatctctctacctctttctAttttattagatttttttctttatttacatttcaaatgttaccctctttcctagtttccct
ctgaaaatcccctgacccctcatcccccacccctgctcctcaacccacccactcccattccctgtcctggcaatcccctatactggggcatagaatct
tcctaggaccaaggtcctctcctaccattgataatcagctaggctatcctcaggtacatatacagctagagccacaagttccaccatgtgttttctttga
ttggtggtttagttccaaggagctctaggggtacgggttagttattttgatgttcctccaatggggcttcagacccccttcagctcctagacattttctagc
tcactcattggagaccttgcgctctgtccaatggatgattgtgagcatccactgctgtatttaccaggcactggcagagcccctcaggagacagcta
catgaggctcctgtcagcaggctgttgttggtatctgcatagtgtctgggtttggtggttgtttatggagtggatccccaagtggggcagtccctggat
ggtcgttcactcagtctctgctccaaactttgtctctgtgacttcttccatgggtatgttgttcccccttctaagaaggattctgagcttctgggctaatata
cacgtatcagtgagtgtatatgatgtgtgttcttttgtgattgggttgcctcactagagatgatatcctccagttccattaatttgtataagaattttataaatt
cattgtatttaatatctgagtagtactccattgagtaaatgtaccacattttctgtatccattcctctgttgagggacatctgggttcttcccagcttctggct
attataaatagggctgctatgaacgtagtggagcatgtttccttattaccagttggaacatcttctgggtatatgcccaggagaggaattgctagatctt
ctggtaatactatgtccaattttctgaggaactgccattctgatttcaagatggttgtaccagcttgtaggacttttcctctttctccaaaacctccccagc
atatcctttcacctgatttttgatcttagccattttgacaggtgtgaggggggtctcagggttgttttgatttgcatttctctgatgcctaaggatgttga
ataatttttaggtgcttcttagcccattggtattcctcagttgagaattctttgtttagctctgtaccccatttttttaatagagttgttcagttttctggattcga
acatcttgagttctttatatatattggatattagccccaggtatgatttaggatgggtaaagatttttttttctcaatctgttggttgccttctattcttattatcag
aagctttgcaattttatgaggtcccatttgtcaattcttgatcttacagcacaagccattgctgttctgttcaggaatctttcccctgtgcccatatcttcga
ggctcttccatgcttcctcctctataagtttcagtgtctctggttttatgtggagttccttgatccacttagacctgagctttgtacagggagataagaatg

gatcaattcacattttaccccagttaagccagcaccactcgttgaagatgttgtcttctttccactggatggttttagctcctttgtcaaagctcaagtgac
cataggtgtgtgggttcacttctgggtcttcaattctgttccatagatctacctgtctgtcattgtgccagtaacatgcagtttttatcacagttgctctata
gcacaccttgaagtcaggcatggtgattccaccagaggttgtttcattgttgagaaaagttttgctattctaggttttttgttattccagatgaatttaaag
attgccctttttaattcggtgaagaatttagttggaattttgatggggattgcatttaatctatagatgactttcagcgggatagccatttttactatattaatc
ctgctgatccatgagcatgggagatctttccatcttctgagatcttcttcaatttctttcttcagagacttgaagttcttatcatacagatctttcacatcctt
ggttagagtcacaccaaggtattttatattatttgtgactattatgaaggttcttgtttccctaatttctttctcagaccgtttatcctttgtgtagagaaaggc
cattggttcatttgaggtaattttatatccagctacttcactgaagctgtttatcaggtttaggagttctctgttggaatttttgggggtcacttatatctacta
tcatatcacctgcaaatagtgatattttgacttcttcctttccaatttgtatccccttgatgtccttttgttgtcgaattgctctggttagaacttcaagtactat
attggataggtaggaagaaagtgggcatccttgtctagtccctgattttagtgggattacttcgagtttctctccatttaatttgatgttggttactggtttg
ctgtagattgcttttattatgtttagttatgggccttgaattcttgatctttgcaaaacttttatcatgaaggggtgttggattttgtcaaatgccttctcagcat
ctaatgagatgatcatgtgacttttgcctttgagtttgtttacatagtgattacgttgatggatttccgtatattaaaccattcctgcatccctgggatgaag
cctacttggtcatgatggatgattgttttgatgtgttcttggattcggttagtgagaattttattgagtatttttgcatcgatattcataagggaaattggtctg
aagttctctttctttttttggatctttgtgttgtttatgtatcagagtaattgtggcttcatagaatgaattgggtagagtatcttctgtttctattttgtggaatag
cttgaggagtattggaattaggtcttctttgaaggtctgatagaactctgcactaaacccatctggtcctggacttttatgtttgggagactattaatgac
tgcttctatttctttaggggatatgggactgtttagatcgttaacttgatcctgatttaactttggtacctgttatctgactagacaattgtccatttcattcag
gttttccagttttgtacagtatagtttttccagtacgatttgatttttttttcctcagattctgttttctctctccctttcatttctgattttgttaatttggatactg
ttcctgtgccctctagttagtctggctaaggatttatctatcttgttgattttctcaaaaaccagctcctggtttggttgatttttgtatagttcttttggtttcca
cttggttgatttcagtcctaagtttgattatttcctgccatctactcctctttggtgaaattactttcttttgttctagagattttaggtgttctgtcaagctgcta
gtgtatgctctctctagtttctctttggaggcactcagggctatgagttttcctcttaggactgctttcattttgtcccctaagtttggatatgttttgtcttcttt
ttcattaaactctaaaaagtctttaatttattactttatttcttccttgactgagctatccttgagtagtgttgttcagctttaatgtgtatgtgggttttctattac
caatgttgttatagttctcagtgatctgatagggtgcatgggattatttcgatatttttatatctgctgatgcctgtttggcgactgattgtatggtaaattttg
gagaaggtaccatgaggtcctgagtagaaggtatatccttttgttttaggataaaatgttgtgtagatacctgttcaattcatttgtttcataacttctgaa
ggaagttttcttctgtaattttgttgaagatatttactgtccctttaagttgaaaatcttccttcttgtctatgcctattatccttatgcttggtcttttcgttgtgtc
ttgggttttctagatgtttggggttaggatctttttgcatttagcattttcggtgattgtagtgtcaatgctttttatggtatcttctgtacctgaaattcactctt
ctatctcttgtattctgttggttatgcttgcatcaatgtctcctgacttctttcctaggttttcgagagtggtctccctttgtgatttctttattgttttacttccatt
tttagatcctggatggtttttgttaaattctttcacctgattggatgtgttctcctgtatttctttaagggagttatttatttccttcttatagtcatccatcgccatc
atgagaagtgactttagatccatatcttgcttttctggtgtgatggtatatccaggaattgctatggtgggagagtttggttctgatgatacaaagtaacc
ttggtttctgttgcttctgttctgatgcttgcctcctaccatctgattatctcaaatgcttgctgccctcaatatatctgattggagcctgtccttcctataatc
caggttgattccaaacacctcagagtccagctttctctgggatcctgtgattctgggatcctgtgaacctgagattctgggtgtgtcagagttcttagc
agtcaagcttcctctgagaccctgagttcctggtgtgaccaagctcctgggatcctggaatcctaagacccttgtcatattacagtgcctggaagtgtt
aactcctctgggtacaatggggttgtctgctgtgttcaaaacctaggtagaccagcaccaactaaaaggaactctatacgctggtcagtcaggggg
cacctgtgcccttgcttctgctgtcacatgcccctcgtgattgttttgggaccaatgttgagttccactcaccagtgatcctaggatcctggaagttcta
ggtctcctgcagcatggagagttctctggggactgtgggaccatctgctgactttgcacccaaggtggtctggagctggcgctgactagagggaa

cccaaacagcttctttaatgggtttcctgtgtccctgttcctgcttgcacaggcccctcgctatttttttttggaacagatgttgcatttcactcaccaatgat
cctaagaacctgggtgtggagagtcctctggtaactgtgggcctgtccacagagtttgcacacaaggcggtctaggaccggtgcagactggaG
TGAACCTCTCTATCTCTTTCTaaaccaaaaaaaaaaaaaaaccaaaaaaaaaaaaaaaaaaaaaaCCTCCCCCCAAA
ATGTCAAGCGAAATAAATCTAACTagaaaataaaaaactagaaagaagcgcaaaaaaacatatgcacacaagtaaatcta
atataaaaataaaattaaaagctataatataatcaaaatataagtaatattaaaaaaagcaatatggaacaaaatgtcaaaatatatacacttgaatttatt
ttgtattggacactgacagctgggcatgtgatgaaccttaagtgtggtttgtatatccaatgagagtccattggagaaagctatttttgtgtgggggt
taGTTTTATTAATTTTATTTATATATCATAGAATACACGTATACATACACAAACTCATAAG
AAAGATGCAAGCTTTGTAAAAATGAATTGAAAGGGCCTTCTTCCCTTTTTTAAGATAttttta
ttagatattttcttcatttacatttcaaatgctatccctaaagtcccctatactctccccccaccttgttccctacccactcactcccacttcttggccctgg
tgttccactctactggggtatataaagtttgctagaccaaggggcctctcttcccaCTAGGGAGAAAGCTAATTTTTAAGTC
ATATAATCTACTAGTAGAATAAGTAGTTCGttatttattattattattattatGTGGTAAGAATGTTGAAA
CAGGTTCTCCCTATATATCCAAGTCTGCCTCATATCTGTAGCCATCCTTCTGTCTCAGTTT
TCCAAGTTTGAGAATTCTGATGCGAAAATCATTACACCTATTAGTTTCTATAGCTTTTGT
AAAATGCTTGAAGTTCCTGTTTATAAGACCCAATCTGTTTCTCTAGAATCAGCTGCTTCC
ATTTTTTTCTGATTTCTAGAATTCTCAATATTTTATGGAACAAAAGTATAGAGGGTAACT
TTTTTTCTGGTCATAGTAAAATTTAGGTTATTTGTGACCATCGAATATGATGTTAAACAT
GGCGAATTACACGCCACAGACATATATGTAttttttttATAATTTTAATCTCTTTAGTCCCTACT
ATTGATCACCCATTCAGCACTGTTCTTCTTCTTTTGAATATAAAAATTACTATAACAGAG
AACCAAAGCTCAGGCCAAATAGATGCTTCAACACTAACCTGAGTTTTATTTACATTATCA
AAGTGTGAGATGACATTTATAGACTATCATCCAAGACCAACATCTCTTCATCTCTTCTAT
ATAATAGAGACACTTTAAACACAGTTTTTCCTCTTTTCTATGTCCTGAAACATATTACTA
GTATCTTTCCAAGTATCTCTTTACCAAAAGACATGGAACACCATATGCTGTTATAAAAGA
GTGTCTCTAACATGTGAGCTAACATGTTCTGTTTAATTTATAGTATTTTTATGATTTGATC
AATTAATAGCTAAGTTCTCTGTGTATAGGGTGTCTTACTAATATTCTTTTCACAAAGATT
TTTTTGTGTGACATTTTTGGAAAAACATTCATCTAAATTAATTGGTGCAATGGCAAATCA
GCAAATTTTTATTGTTATAGAGCCTATGAAATGGTTGAGTATGTAttatctttttttaaaatatttttttattagg
tattttccttatttacatttccaatgctatcccaaaagtcccACTCCCCTAGAGTATGTATTATCTTAATTTATATACT
TTATAGTAACTTGTTAATGAACTAATATTATATTTATTTGTGAAGATCATAAAATAAGTA
ATATTATTACTGTACAGGCTTACTGTGAAGGTCCGGTATATCAATATGAACAAAAATCTC
AACCTACACATTTTACCTCACAGTGGTTTTGTTGTCTTTTATTGTTTATTTTTTGGGGGGT
GGGTGGGTACTTCCACGTTTAGTCATAAGTGTAGAGTAGTGTTATACCTATTGAGTTAAC
TGATATTAGGTACTTTTTTATGTATTATAATTCCTATGTGTCTTTTTGCAGAATAAATGCC
CAGAAAATGCTGAAAAGAAAATACAAAACAATAAAGAAAATAAGCATTGTGATCTGGG

CCAAAGCCCTTGTTTACTATGTAGTTAAATATTCTTTTACTATGCCATTTTCATGTGAAAG
TTATTTTGACATTTTCACTAAGTAATTAATATGGCAATCTTAAGTGAGAATTACTTAAAT
ATTCTGTCTTTATATATACTTCATGCTCAAATCTTATTTTAAAAATTAAAATTAAAAATG
GTACTTTGATATCTCTGTTTTACTACCCTATAAAAATGTATCCATGCTAAGGAGTAATAT
ATAACTCTTAATTTTGCTATACCAGAATATTAATATTTATAATATATTGATTTCTAATTTC
TGTTTATGAACAAAATGAAATAATTAGAAATTTTGATGCATTTGTTTATAATTAATGTTT
AAAAATAAATCAATTAATGTATTAAGCACAAACAGCTGAGTACAATATAAGTTTAATAT
AATTAGAATAAAAAGCATACTGCTTTAACTGAACTAAATACAAAGGAGTGACTCTACAG
ACTAGTGAGAACAATTTCCTGTCTTGACAAGAGCTTTGCCTTCCCCCAAAAACACACATT
CTCTTCAGAATTGACCAAGACATTGGTAAAAATCAAACCAATGAATGACCAATGCTATA
CAATAAAGAGAAGCAGCTACTGAAAAGCCTGCATAGTGATGCCCTAATAAGCATAGAC
TGCTGCAAACTTGCAAGGTTAACCCATTTCTCCAGGTACAATGAAATAGGCATGTAGCT
TCCTGGTAAATGGGAAAAGAGAGCTTGTTTTTTAGAAAAGTTGTTAGCTCACAAAGACT
AAGTTGATTCCAAGCTCTACCTGTTGTAGTTGAACAAGTCTTTTGTCTCTGACAGAAAAC
AAACACCCTGACAAACCACTTAAGGTGTTGGAACAGCTGGGCAAAGAAGTCCTTACGG
AGTACCTAGAAAAATTAGTACAAAGCAATGTACTGAAATTAAAGGAGGAAGATAAACA
AAAATTTAACAATGCTGAACGCAGTGACAAGCGTTGGGTTTTTGTAGATGCCATGAAAA
AGAAACACAGCAAAGTAGGTGAAATGCTTCTCCAGACATTCTTCAGTGTGGACCCAGGC
AGCCACCATGGTGAAGGTAAGAGCAGAATGTACTGTGAACAACAGCTCAGGGTGCTCA
TGATCTGTTCGATTTTCAGGCCCAACACTTGCTTTGGTCTGCTAATCTTTGTGTCACTATC
ACTTTTCTCCAAAATAGATAATACTTTAGAAAGTGTGTTGACTTTCATAGGTAGGTCTCA
GAATCCAACGTGGTAAAAAAGCTAAGTCCTTTGTTCAAGCTATTTTGAGAAATAGCTAG
TCATCTGACAATTATAAAATGGAACACTAATCCTAAAGTTTATAAATTTTGTGGCTCTCA
TCAGTTTTAGCTTATGGAAAATGGGTGCCTTCTAATACTGTCTCTCATGTTTTTCCAAAGT
TAGAAACATAGTCAAGCCATGAACACAACTTCCCAAATGCTGGCTCTCATCCAAGGTAA
TTTTCTGGACTACATACTCACTGAACACTGCCTCCATAGTTAATATTTCTGAGCACATGT
TCCATTTTTTTAATGAAATGAACACCTGTAAAACTAAACAGTCTTCTTCCATTAAGCCAA
TTAGATGCATTCACACAAACTGAAAGAATCTCAAGCATAAAACTAAACTAAAAAAATAT
TATATCCAATAAGGATCAGAATTGGAGGAAGGTGTTCAAAATACTTTTAGTAATTTCAG
GAATTCCTTACATGTTATATCAATTAATAGGGTTTCTTATCAGTTTATACGAATCAAAAA
TTAAAAATTTATCTACATTCCTATGTTTTCAAATTTCTTCCCCTCCAAGACTGTAGCTAGG
AGCCACTTGAGCATAGTAACGCATGCCAAAATGGCAAAAATCTGTGATGCATTGCACTG
AAGAGTAAGAGTATTACTAAAATTATGCCCTTGTTTTTCCTTTTATTTTATATGATATTAG

AGAAGCTAAACTGGAATATCAATTAAAGTAATTTTTAGTAAATAACACTCTGGTAAGTA
AATTATTTGGTAAAGGTAAAGTTGAAATGAACAAGAATGAGGATTGAAATAAATGAAC
AAGAGTAAAATCATCAGAAATTTAAAGTTGTCGAGAGTGGAAGTCAGGTTTGATTCCAA
ATTACAATGGTGTTCTCCCAAGAATTACCAGAACTCAGGGTCTCATTGTTGGGCTGTTCT
GCTTTTCACCTCAACCATCTCCTTCTGCCATCTTAGTTGTACAATATCCTGTGCTATTGAT
TACCAATAGTAATTGTTATATACCAAAGTGCTATCTTCACTTAGTTTTCTTAAAGACCAT
TCTGCCCAGCCAACAAATGAGGGATCTACATCAGACTGAAACATTTACATCATATGATG
TATTTTACAGCTAATCTGGAAATGGAGGAACCAGAAGAATCATTGAACACTCTCAAGCT
TTGTTCCCCTGAAGAGTTCACAAGGCTTTGCAGAGAAAAGACACAAGAAGTACTCTCCT
TTGTTGTTGAAATAGAGACACCAAACCAATTGTTCATACTAAAGACAATTTCTTAGATCT
CTGAGCCCAAGAGATGGTGATATAACTGCTATAGATTATGATCTTGATTATAAGCAAGA
TCAATTTTTCTTTTAATGCAGTGAAAAAAATCATGGTGTTAATTATTTTATTTATTTTTC
TCTCCTGTTCATGAGTTATGAAAATTTTTTCTGCAGTCATGGTATCAAAATATCTATAAA
ACTACACAGTTGACTAATAGTTATCTGTATACTGGTTTAAAAAACACAAATACTGAAGA
AGGTTTATTGTTACAGTATATAGAATATAATATTGATATATCAAAACTGGTATCACAATA
ATAGTAGTAGATGCAATTTTTTAATAATTTTCTTGACATGAGCTGATATCTTTGGATTTTA
TAGTTAAGCTATCCCTTACATTCTAGGGAACTTTGACTAGGTACT

**Appendix 14 Large deletion (20,524bp deletion in length) was introduced in the CASP domain of caspase-1 and the CARD domain of caspase-11 in wild-type mouse pups.**

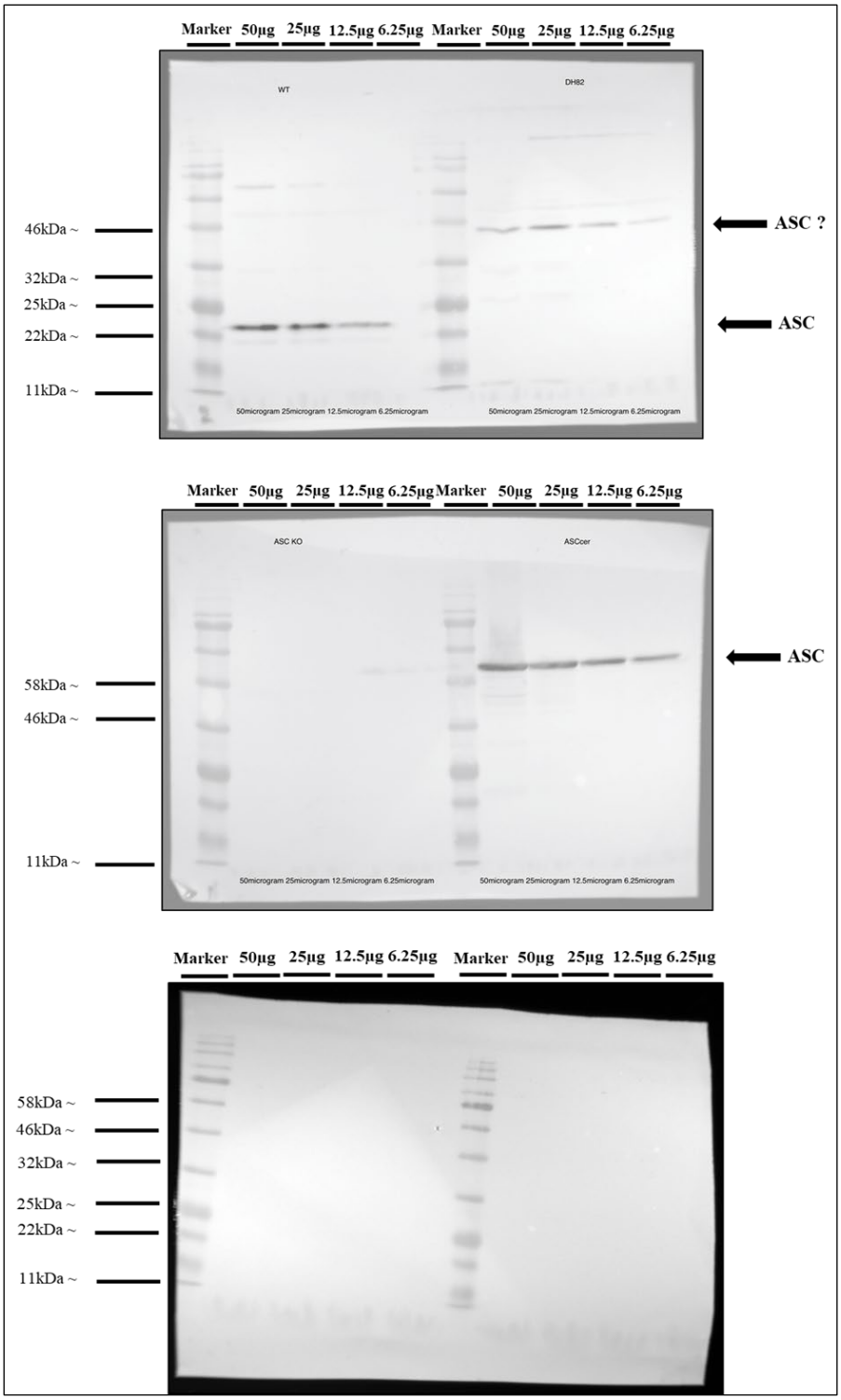


**Appendix 15 Uncropped immunoblots presented in Figure 3.3.2.** Western blotting analysis of full protein extracts of immortalised murine wild-type, *Asc*$^{-/-}$ and DH82 cell lysates using primary anti-ASC and HRP-conjugated secondary antibodies.

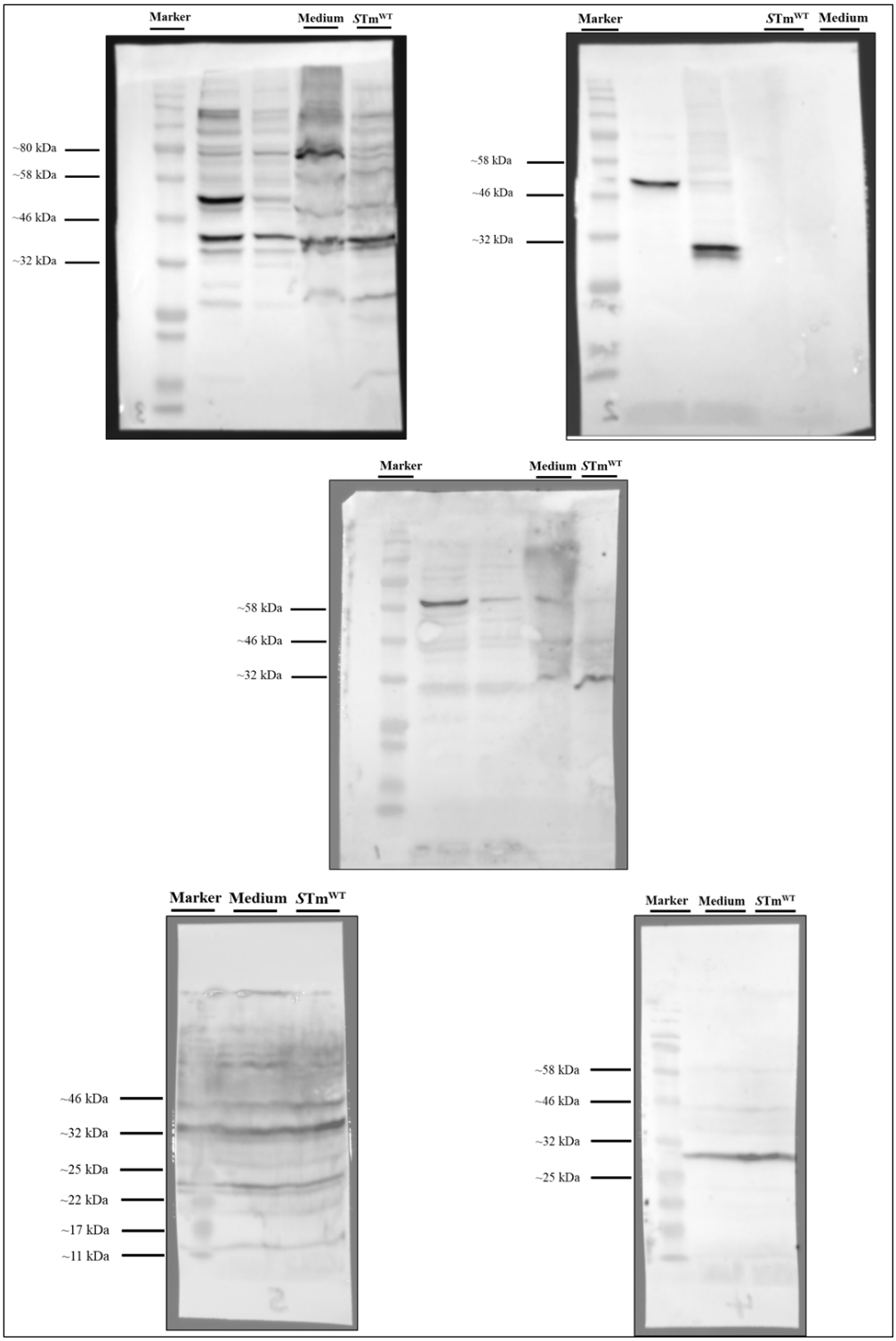


**Appendix 16 Uncropped immunoblots presented in Figure 3.3.4, GSDMD immunoprecipitation.** Immunoblotting of GSDMD protein from DH82 cell lysates infected with *S.* Typhimurium with an MOI of 1 for 24 hours.

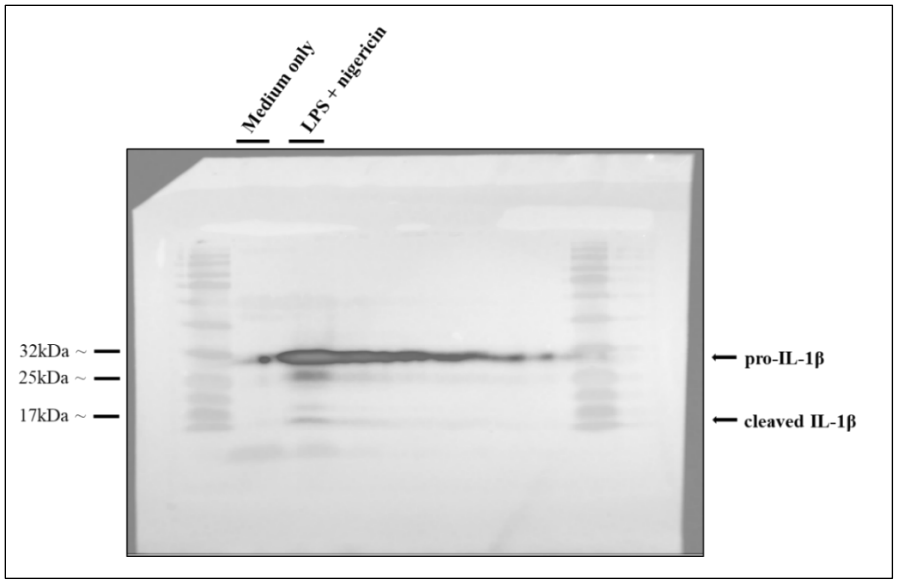


**Appendix 17 Uncropped immunoblots presented in Figure 3.5.3, IL-1β immunoprecipitation.** Western blot analysis of the supernatant reveals small degree of IL-1β cleavage in nigericin stimulated DH82 cells.

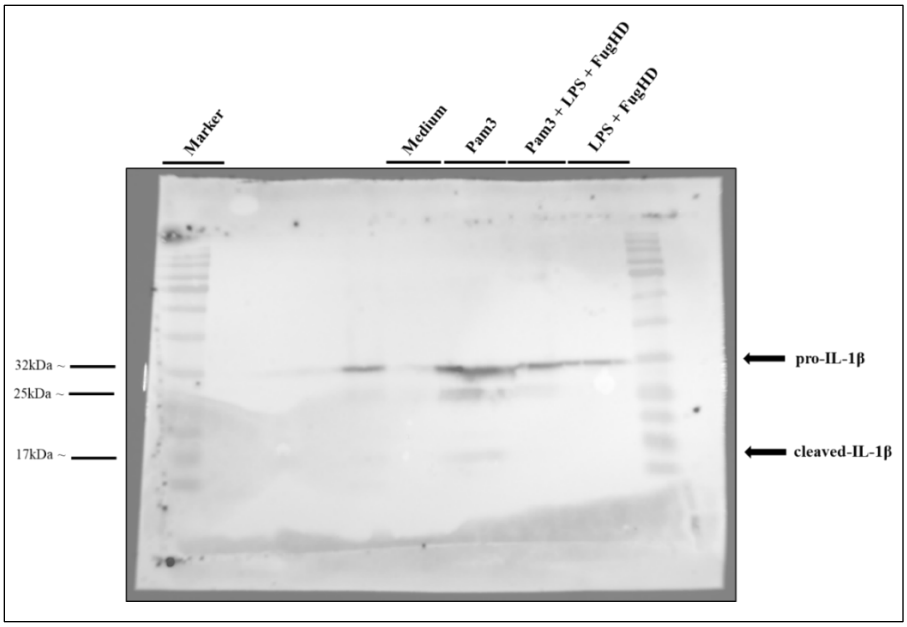


**Appendix 18 Uncropped immunoblots presented in Figure 3.6.3, IL-1β immunoprecipitation.** Priming only is sufficient to drive IL-1β secretion and cleavage in DH82 cells.

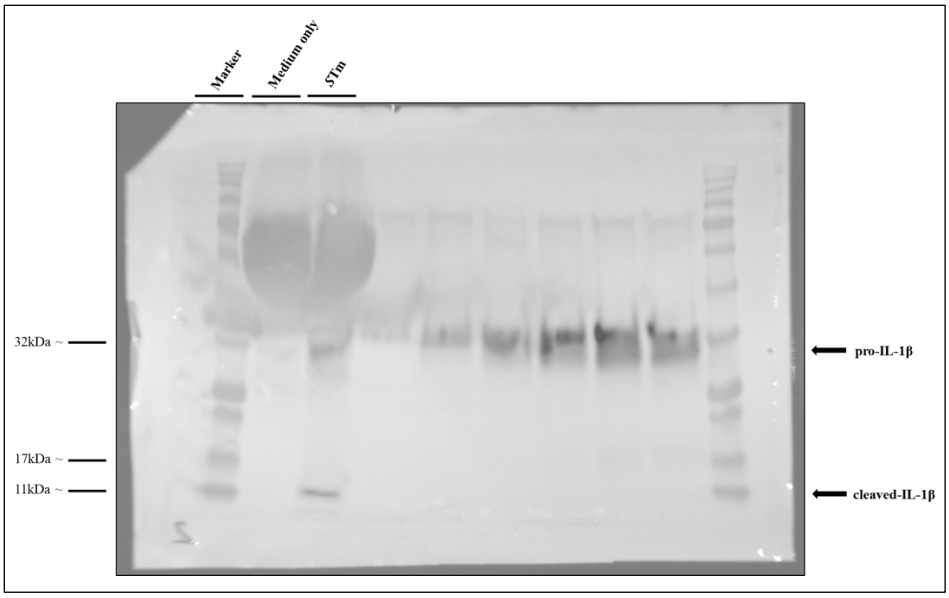


**Appendix 19 Uncropped immunoblots presented in Figure 4.2.4, IL-1β immunoprecipitation.** *S.* Typhimurium infection of DH82 cells results in the maturation of pro-IL-1β.

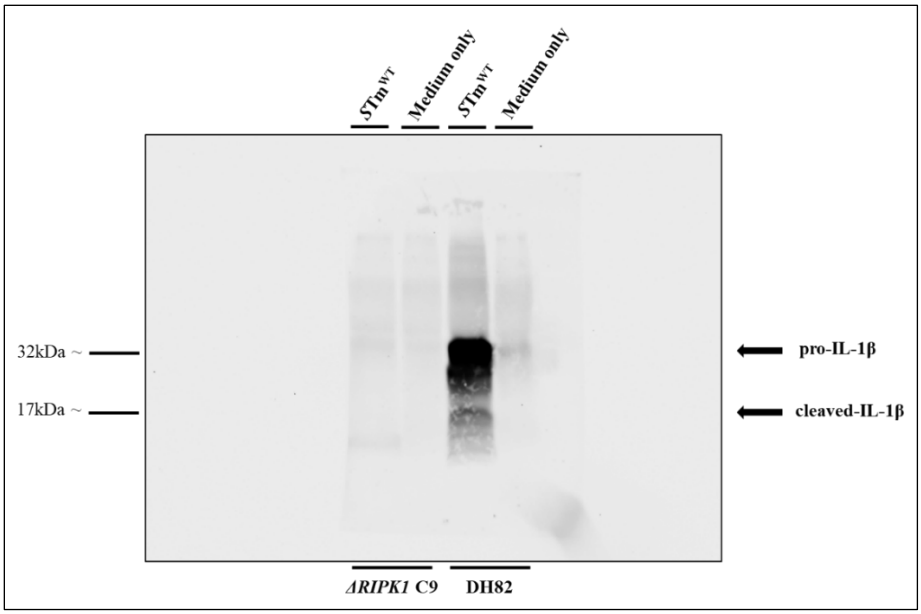


**Appendix 20 Uncropped immunoblots presented in Figure 5.9.4, IL-1β immunoprecipitation.** RIPK1 is essential for inflammatory cytokine pro-IL-1β expression in response to *S.* Typhimurium infection in the dog.

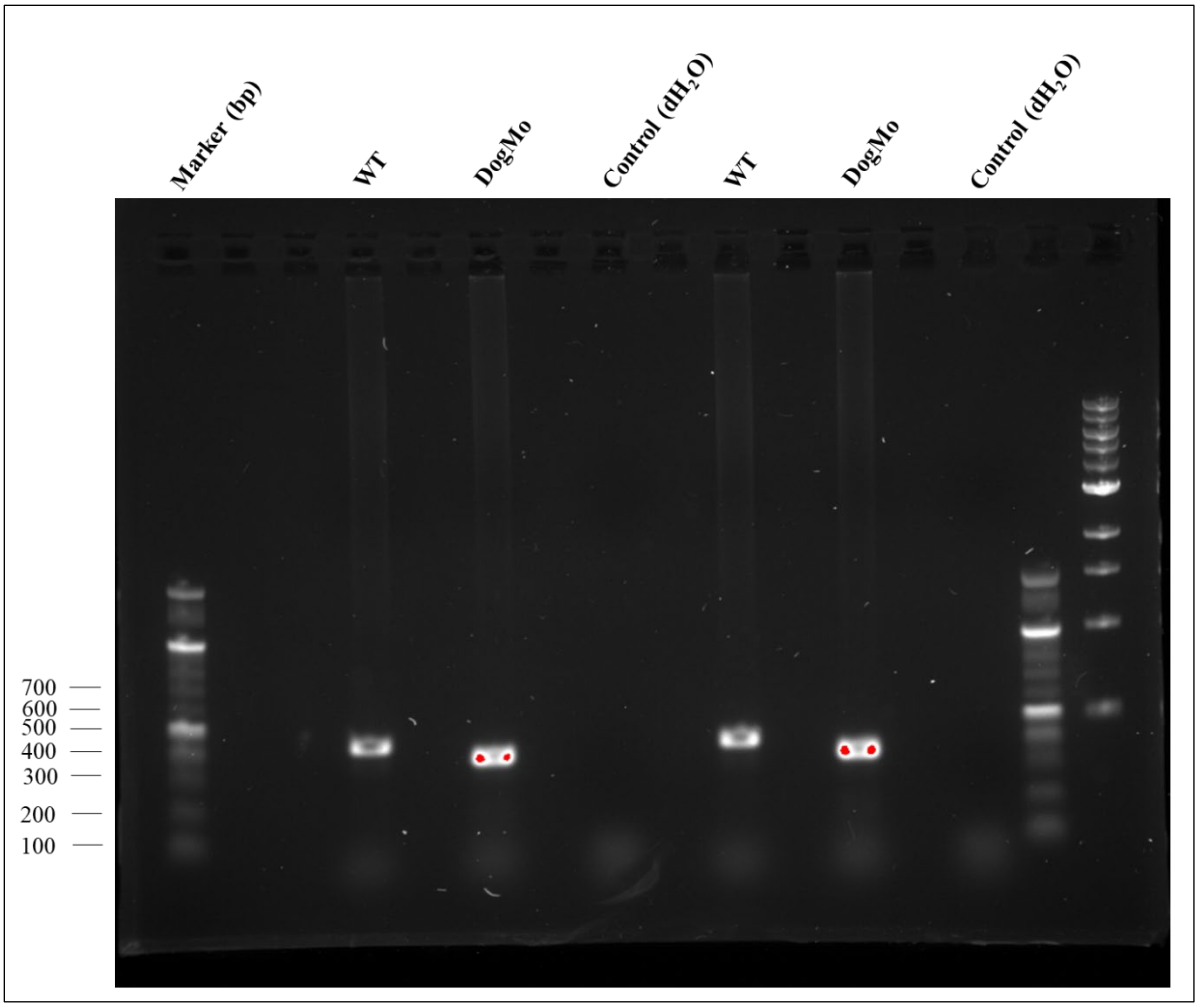


**Appendix 21 Uncropped agarose gel presented in Figure 7.2.2.** Genotypes of differentiated primary wild-type and DogMo macrophages were confirmed by running amplicons on an agarose gel.

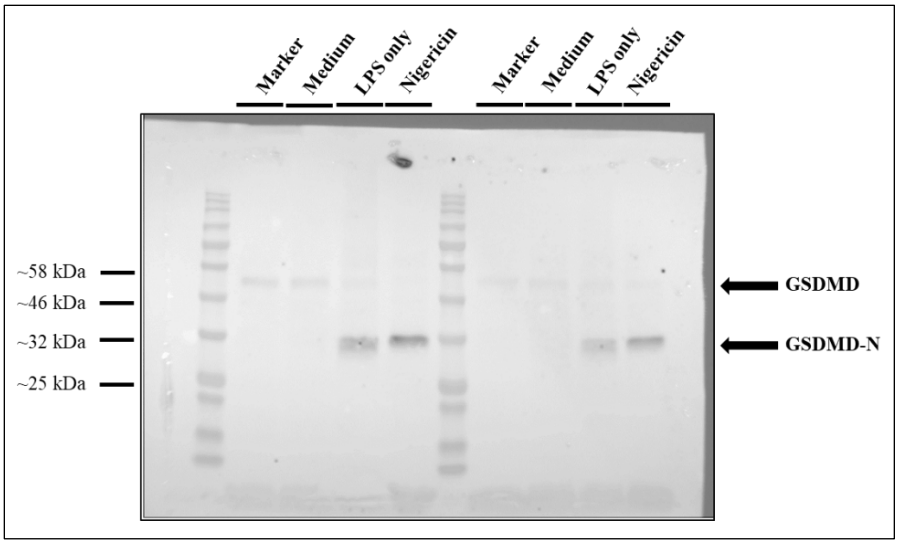


**Appendix 22 Uncropped immunoblot presented in Figures 7.3.2 and 7.3.3, GSDMD immunoprecipitations.** Activated NLPR3 inflammasome cleaves GSDMD protein which induces pyroptotic cell death in response to nigericin treatment while murine hybrid caspase-1/4/11 protein is capable of initiating pyroptosis via GSDMD cleavage.

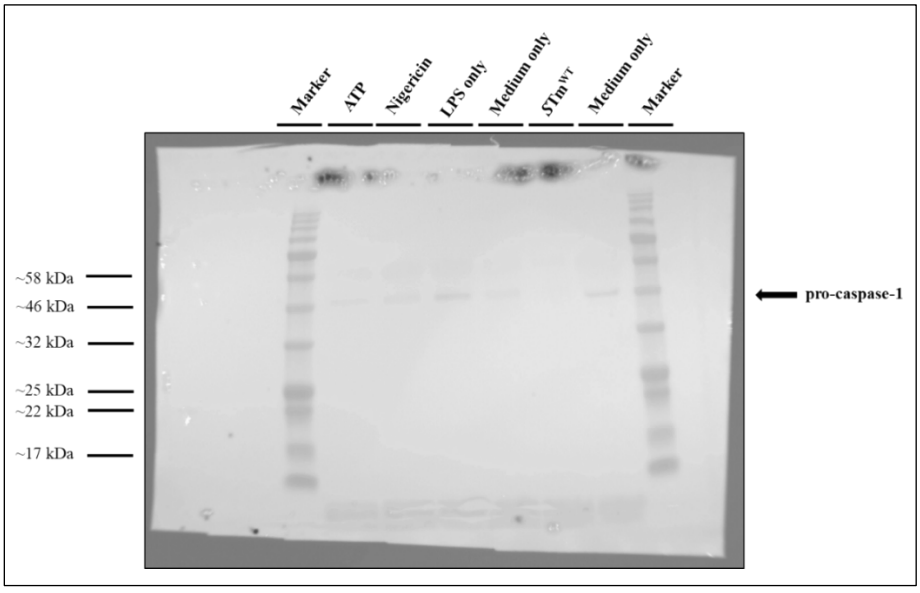


**Appendix 23 Uncropped immunoblot presented in Figure 7.3.4, caspase-1 immunoprecipitation.** Western blotting analysis of caspase-1 protein shows constitutive expression of the protein.

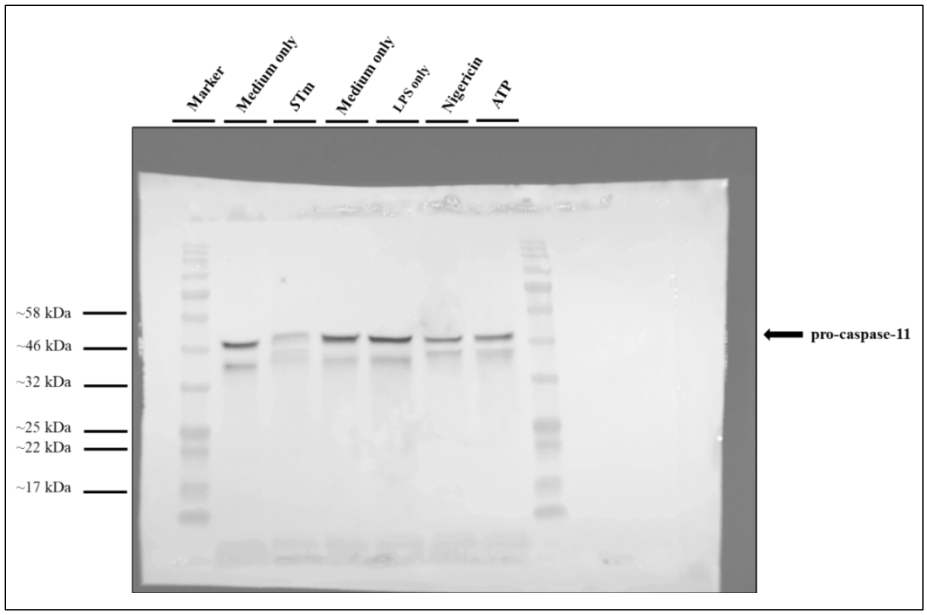


**Appendix 24 Uncropped immunoblot presented in Figure 7.3.5, caspase-11 immunoprecipitation.** Western blotting analysis of DogMo hybrid caspase-1/4/11 protein shows constitutive expression similar that of wild-type caspase-1 protein.

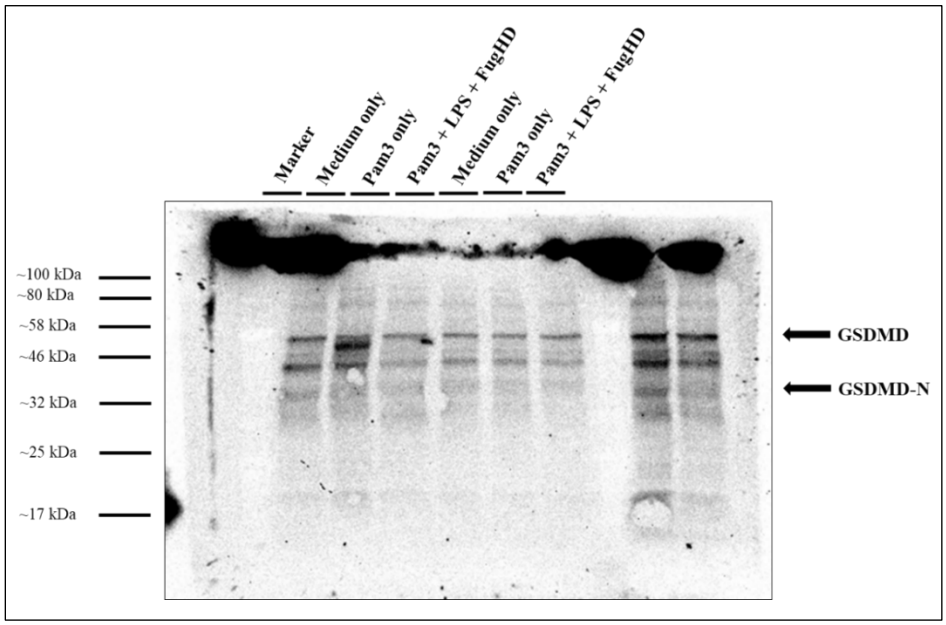


**Appendix 25 Uncropped immunoblot presented in. Figure 7.4.2, GSDMD immunoprecipitation.** Constitutive expression of GSDMD in murine wild-type and DogMo cells.

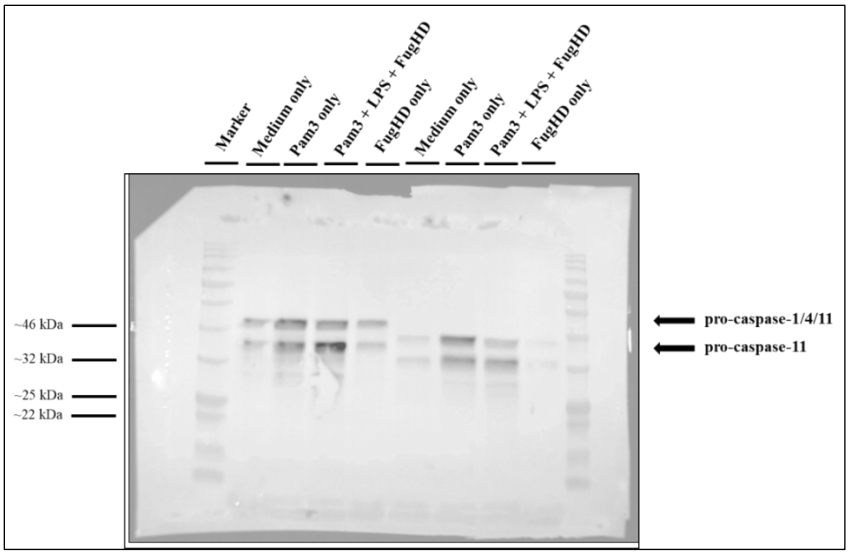


**Appendix 26 Uncropped immunoblot presented in Figure 7.4.3, caspase-11 immunoprecipitation.** Western blotting analysis showed the presence of full length wild-type caspase-1 and hybrid caspase-1/4/11 proteins.

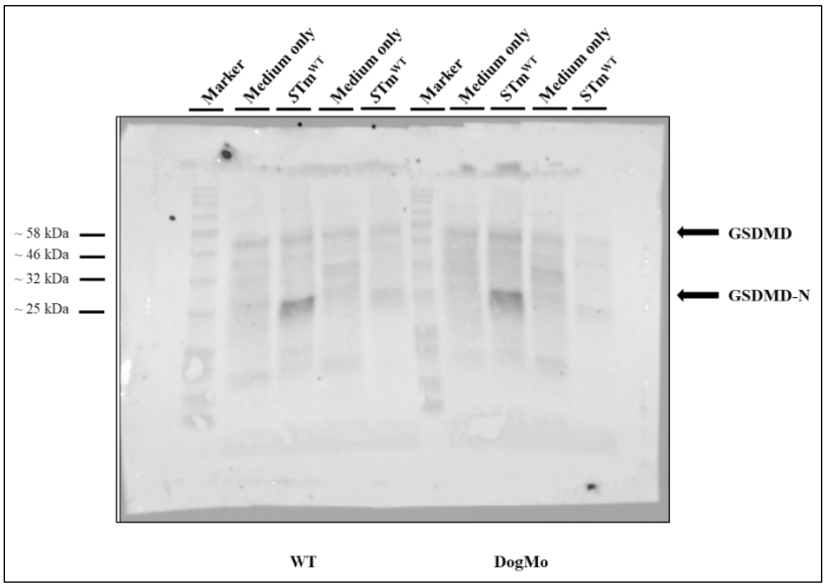


**Appendix 27 Uncropped immunoblot presented in Figures 7.5.3 and 7.5.4, GSDMD immunoprecipitation.** GSDMD is cleaved in wild-type murine macrophages in response to *S.* Typhimurium infection while mouse macrophages containing the hybrid caspase-1/4/11 protein can cleave GSDMD following *S.* Typhimurium infection.

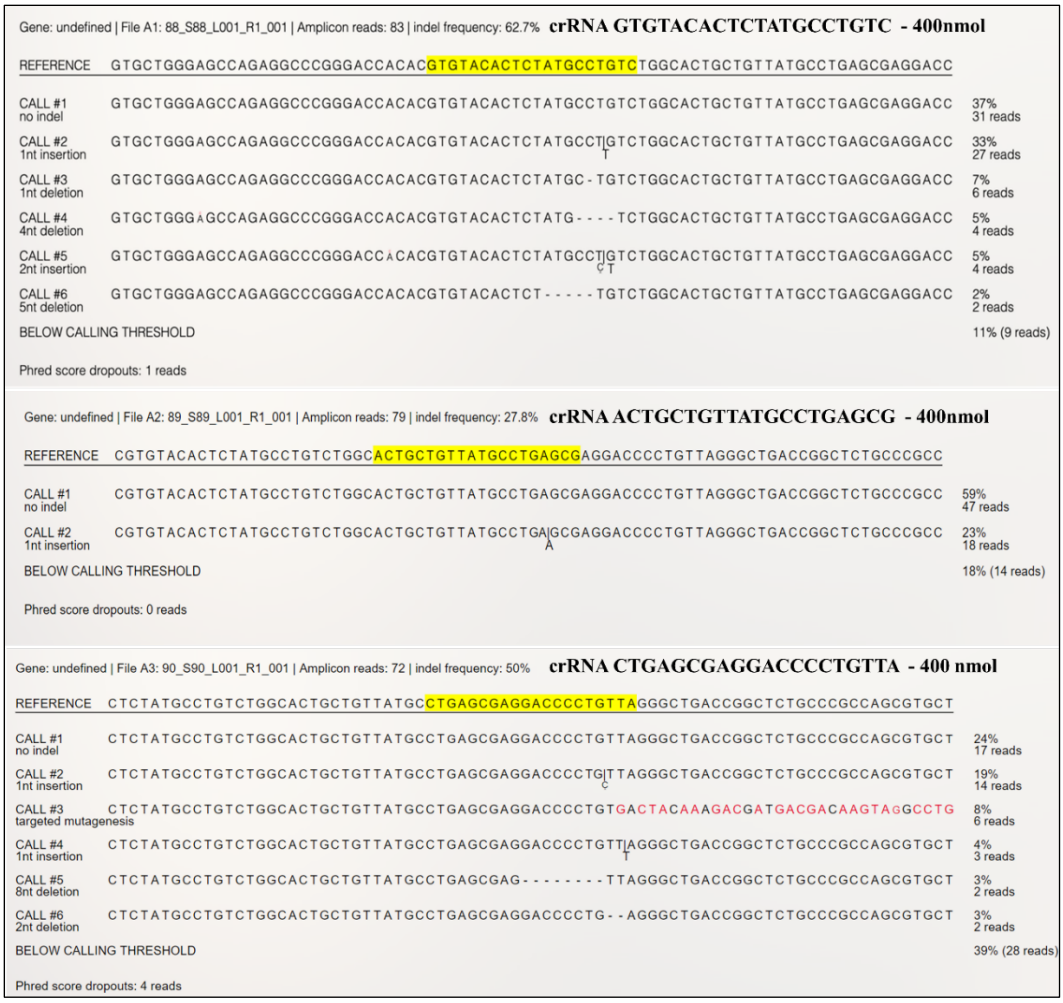


**Appendix 28 OutKnocker sequence analysis identified the FLAG-tag sequence inserted in CRISPR edited DH82 cells using CTGAGCGAGGACCCCTGTTA crRNA for the canine *GSDMD* gene.** DH82 cells were electroporated with RNP complexes at 400nmol final concentrations. CrRNAs and HDR templates were designed to be near the STOP codon of the canine *GSDMD* gene. The underscored nucleotide sequence represents the wild-type reference sequence, while nucleotides highlighted in yellow show CRISPR crRNA target site. Information including total percentage and total number of reads corresponding to each identified indel are shown underneath the reference sequence. Nucleotides shown in smaller font sizes are less confident calls based on the sequencing data, while nucleotides replaced with hyphens represents the position of nucleotides deleted by CRISPR Cas9. The software also provides information on the percentage and total number of reads that could not be aligned to the reference sequence and the number of reads that were excluded from analysis (Phred score dropouts).

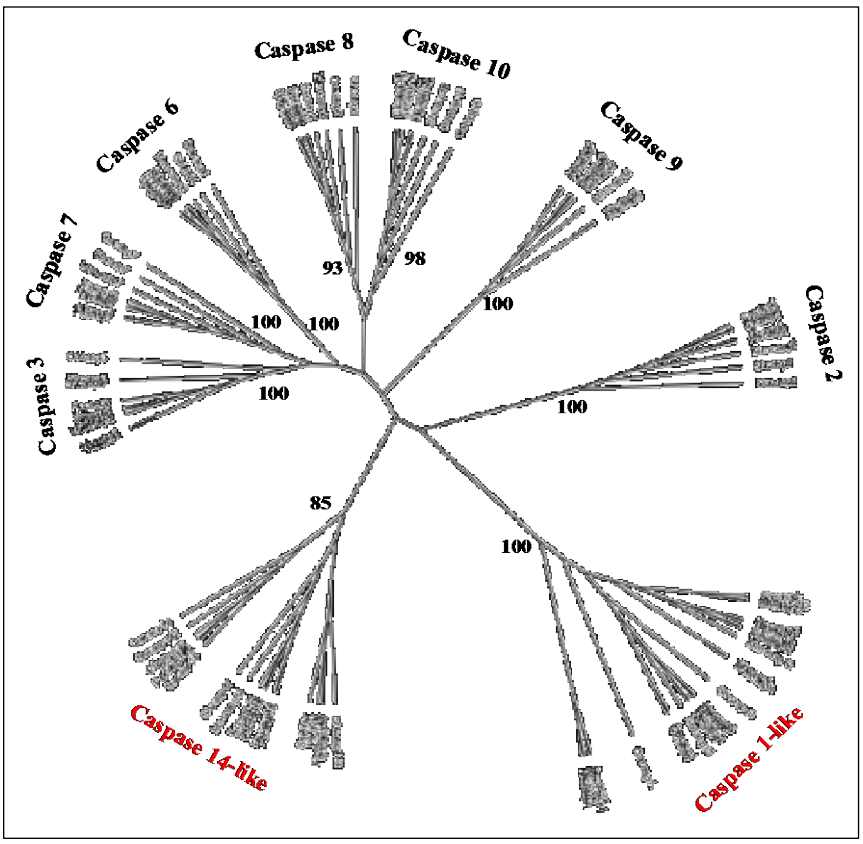


**Appendix 29 Phylogenetic analysis of putative and confirmed caspases identified differences in the caspase-1-like and caspase-14-like evolutionary branches.** The phylogenetic tree was generated using neighbour-joining clustering method. Bootstrapping was used to estimate the confidence of the branches within the phylogenetic tree. The resulting value provided a level of confidence of the branches in the phylogenetic tree, where the higher value represented more confident relationships.

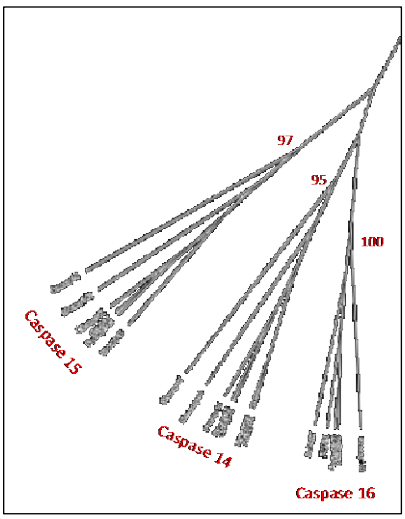


**Appendix 30 Caspase-14 like evolutionary branch contains caspase-14, -15 and 16 genes.** The phylogenetic tree was generated using neighbour-joining clustering method. Bootstrapping was applied to estimate the confidence of the branches within the phylogenetic tree. The resulting value provided a level of confidence of the branches in the phylogenetic tree, where the higher value represented more confident relationships. Close up image of the caspase-14-like cluster showed strong species-based differences.

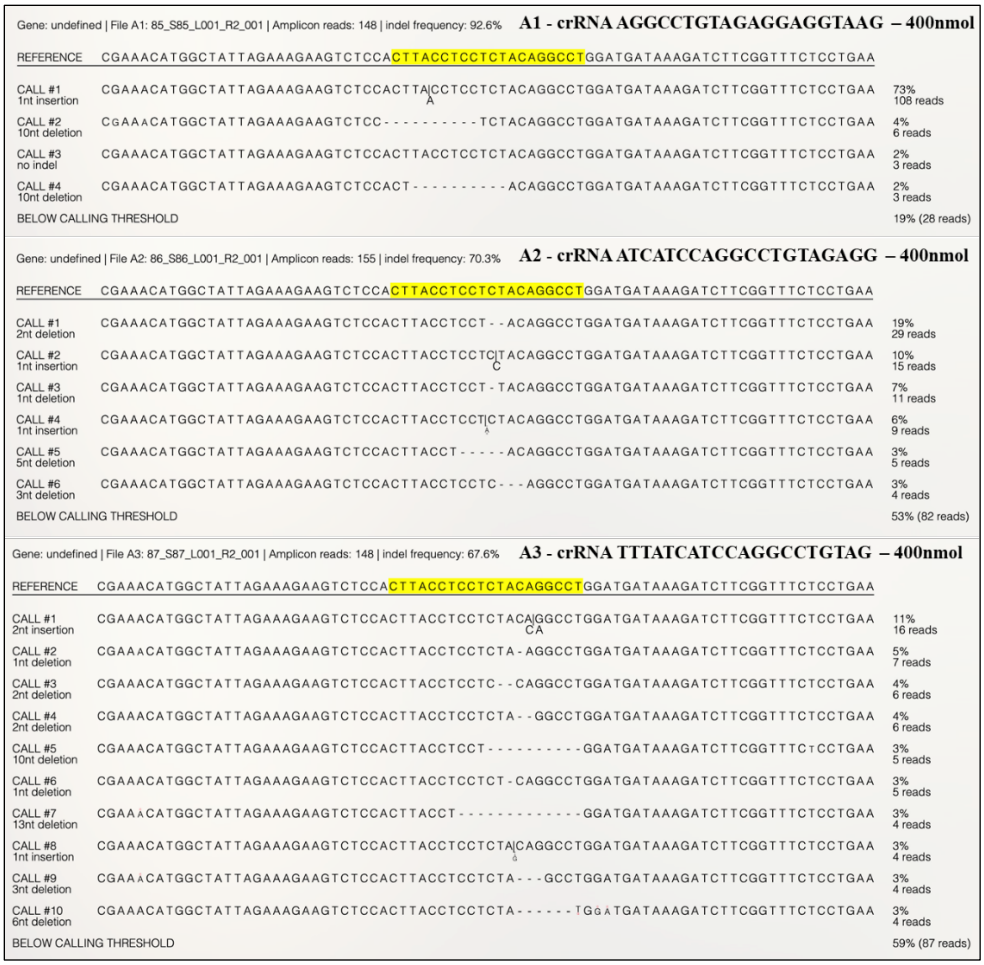


**Appendix 31 List of indels identified by sequence analysis in CRISPR-Cas9 edited DH82 cells for caspase-15.** DH82 cells were electroporated with RNP complexes at 400 nmol final concentration. CrRNAs were designed to be near the catalytic site of caspase-15. Cas9 edited cells yielded amplicon reads that contained a mixture of in-frame and out-of-frame mutations. The underscored nucleotide sequence represents the wild-type reference sequence, while nucleotides highlighted in yellow show CRISPR crRNA target site. Information including total percentage and total number of reads corresponding to each identified indel are shown underneath the reference sequence. Nucleotides shown in smaller font sizes are less confident calls based on the sequencing data, while nucleotides replaced with hyphens represents the position of nucleotides deleted by CRISPR Cas9. The software also provides information on the percentage and total number of reads that could not be aligned to the reference sequence and the number of reads that were excluded from analysis (Phred score dropouts).